

# Characterisation of Vanadium-Based Oxidation Catalysts

*Karakterisering van oxidatie katalysatoren  
op basis van vanadium*

(met een samenvatting in het Nederlands)

Proefschrift

ter verkrijging van de graad van doctor aan de Universiteit Utrecht  
op gezag van de rector magnificus, Prof. Dr. H.O. Voorma,  
ingevolge het besluit van het College voor Promoties  
in het openbaar te verdedigen  
op maandag 19 april 1999 des middags te 2.30 uur

door

**Matthijs Ruitenbeek**

Geboren op 2 februari 1972, te Doorn

Promotoren: Prof. Dr. Ir. J.W. Geus  
Prof. Dr. Ir. D.C. Koningsberger

Copromotor: Dr. A.J. van Dillen

Verbonden aan de Faculteit Scheikunde van de Universiteit Utrecht

Het in dit proefschrift beschreven werk is uitgevoerd in het Debye Instituut van de Universiteit Utrecht bij de sectie Anorganische Chemie en Katalyse en in samenwerking met NIOK, het Nederlands Instituut voor Onderzoek in de Katalyse.

CIP-GEGEVENS KONINKLIJKE BIBLIOTHEEK, DEN HAAG

Ruitenbeek, Matthijs

Characterisation of Vanadium-Based Oxidation Catalysts / Matthijs Ruitenbeek.-

Utrecht: Universiteit Utrecht, Faculteit Scheikunde

Thesis Universiteit Utrecht. - With ref. - With summary in Dutch.

ISBN 90-393-2051-9

Subject headings: heterogeneous oxidation catalysts / vanadium-phosphorus-oxide

© Matthijs Ruitenbeek, 1999

*To search for perfection is all very well  
But to look for heaven is to live here in hell*

Gordon Matthew Sumner

# CONTENTS

---

1. General Introduction	1
2. Experimental Procedures	11
3. Evidence for a new type of vanadyl pairs in $(VO)_2P_2O_7$ ; an ESR and magnetisation study	25
4. Determination of the surface composition of V-P-O catalysts; An XPS and LEIS study	41
5. Comparison of bulk and supported V-P-O catalysts; new insights in the active phase in C4 oxidation to MA	57
6. The structure of (supported) V-P-O catalysts; quantitative analysis of the EXAFS spectra	71
7. The structure of (sub)monolayer $V_2O_5$ on $\gamma-Al_2O_3$ ; An <i>in-situ</i> X-ray absorption study during catalytic oxidation	89
8. An <i>in-situ</i> study of supported V-P-O catalysts during butane oxidation to maleic anhydride	119
9. Summary and concluding remarks	133
Samenvatting	141
Dankwoord	149
Curriculum Vitae	153
List of Publications	155

# 1

---

## GENERAL INTRODUCTION

### **A short introduction to catalysis**

Although nowadays we know that catalytic processes have already been applied for a long period of time, it was not until 1836 that Berzelius introduced the term 'catalysis' [1]. He derived it from the Greek words *kata*, which stands for down, and *lusein*, which means to split or break. Later, in 1895, William Ostwald was the first to write down a definition of a catalyst: 'A catalyst is a substance that changes the rate of a chemical reaction without itself appearing in the products'.

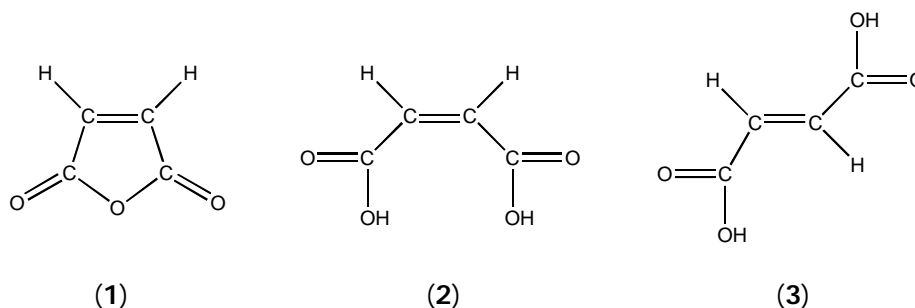
It is important to note that a catalyst does not influence the thermodynamic equilibrium of reactants and products. Therefore, the current definition is slightly better, though close to Ostwald's description: 'A catalyst is a substance that increases the rate of approach to thermodynamic equilibrium of a chemical reaction without being substantially consumed' [2].

Today, almost 70% of all chemicals that are produced have been in contact with a catalyst somewhere in their synthesis process. This number stresses the importance of the role of catalysis in the chemical industry. Without a catalyst, processes are less clean and sometimes impossible to perform. In principle catalysis can be used to abate environmental pollution in two ways: **A**) for cleaning of outgoing waste gases or waste water (end-of-pipe catalysis), and **B**) for improvement or replacement of existing processes in such a way that less or less harmful waste is produced (process-incorporated catalysis).

With regard to **A**, two well known examples are the three-way catalyst, which is used to reduce the levels of CO, NO<sub>x</sub> and VOC's in automotive exhaust gases, and the Claus catalyst utilised to convert sulphur (H<sub>2</sub>S) from industrial exhaust gases. The subject of this thesis is closely related to catalysis of type **B**, *i.e.* improvement of an existing process to achieve a higher product yield, and thus fewer by-products. The process involved is the selective oxidation of *n*-butane to maleic anhydride (MA). The catalyst used for this well studied reaction consists of vanadium-phosphorus-oxide (V-P-O).

### Selective oxidation of *n*-butane to maleic anhydride

Maleic anhydride (**1**) and its derivatives maleic acid (**2**) and fumaric acid (**3**) are produced with an annual world-wide capacity of over 1·10<sup>6</sup> tons [3,4].



These multifunctional chemical intermediates find applications in almost any field of industrial chemistry [3]. The principal use of these compounds is in the manufacture of unsaturated polyester resins (68%) [5]. Minor applications are lubricating oil additives, agricultural chemicals, textile chemicals, paper reinforcement, food additives, and pharmaceuticals [5,6]. Furthermore, due to its double bond and anhydride function, maleic anhydride is a versatile intermediate for the production of co-polymers of MA and, for example, ethylene glycol and vinyl monomer [7]. Recently, potential new uses of MA have been found in its conversion to 1,4-butanediol [8] and the manufacturing of tetrahydrofuran (THF) and butyrolactone via hydrogenation [7].

Maleic anhydride and the two di-acid isomers were first prepared in the 1830's [9,10], but it took about 100 years before commercial manufacture was performed. In 1933 the National Aniline and Chemical Company Inc. started a process for the production of maleic anhydride based on benzene oxidation using a vanadium oxide catalyst [11]. Smaller amounts of maleic acid were also formed as a by-product in the production of phthalic anhydride. The use of benzene as a feedstock for the production of maleic anhydride was dominant in the world until the late 1980's.

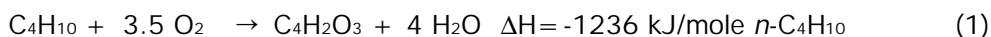
Benzene, although easily oxidised to maleic anhydride with high selectivity, is an inherently inefficient feedstock, since only four out of six carbon atoms are recovered in the product. Various C<sub>4</sub> compounds have therefore been evaluated as raw material substitutes for benzene. In 1966, Bergman and Frisch were the first to observe that the selective oxidation of *n*-butane to maleic anhydride could

### General introduction

be catalysed by vanadium-phosphorus mixed oxides [12]. However, *n*-butane was not competitive due to the comparatively lower yields that could be obtained.

Rapid increases in the price of benzene and the imposition of strict pollution control measures on atmospheric benzene emissions in the USA intensified the search for alternative processes in the USA. These factors led to the first commercial production of maleic anhydride from butane by Monsanto in 1974. The large-scale exploitation of natural gas in the USA and northern Europe brought about that large economic supplies of *n*-butane as a natural gas liquid are readily available. This, together with the rapid advances in catalyst technology, resulted in the maleic anhydride production in the USA to be based for 100% on *n*-butane as a feedstock [3].

The butane oxidation reaction to produce maleic anhydride is very exothermic. The main reaction by-products are carbon monoxide and carbon dioxide. Stoichiometry and heat of reaction of the three principal reactions are as follows:



It is obvious that carbon monoxide and carbon dioxide are the thermodynamically more favoured products. Only kinetic control by a catalyst will enhance the formation of maleic anhydride. In practice, the process is operating at a yield of approximately 60% to the desired product. Carbon monoxide and carbon dioxide are the sole carbon-containing by-products in a ratio of about unity.

Suppression of the unselective and very exothermic oxidation to carbon oxides requires sufficient heat transfer capacities of the reactor. Nonetheless, hot spots are frequently met in MA production plants.

#### Processes for the production of MA from *n*-butane

In general, three different types of processes can be distinguished in commercial production of maleic anhydride from *n*-butane, *i.e.* fixed-bed processes, fluidised-bed processes and the recirculating-solids process.

The fixed-bed process is schematically represented in Figure 1. The reactor consists of a number of tubes that are packed with coarse catalyst bodies. The reactants flow through these tubes. As a result of the obstruction of the gas flow by the catalyst bodies, a pressure drop across the bed is exhibited. Therefore, pressure has to be applied at the inlet to ensure an adequate flow rate. The magnitude of the pressure drop is depending on the flow rate, the length of the catalyst bed and the size of the catalyst bodies.

Since the selective oxidation of *n*-butane to MA is highly exothermic, fixed-bed reactors must contain a facility to remove the reaction heat. This can be done in various ways. The bed can be split into different sections, with provision for cooling the gas in between the sections or the reactor contains a large number of tubes, along which a cooling gas or liquid is recirculated. However, hot spots can

occur easily in fixed-bed reactors. These can be prevented by using larger catalyst bodies, a less active catalyst, or by dilution of the catalyst with an inert solid. In view of the explosion limits and the flammability of mixtures of *n*-butane and air, only low concentrations of *n*-butane can be applied (< 2%). Furthermore, the gases must be mixed and pre-heated before entering the reaction zone. In a fixed-bed reactor, the concentration of *n*-butane will decrease when moving to the end of the tube. To maintain a sufficiently high selectivity at the exit of the reactor a less active catalyst is installed at the entrance and a very active catalyst at the end of the reactor. Palmer and Holzhauser have described other techniques to provide the desired activity gradient through the catalyst bed [13]. Three fixed-bed processes, from Huntsman [14], Pantochim [15], and Scientific Design [16] are currently offered for license.

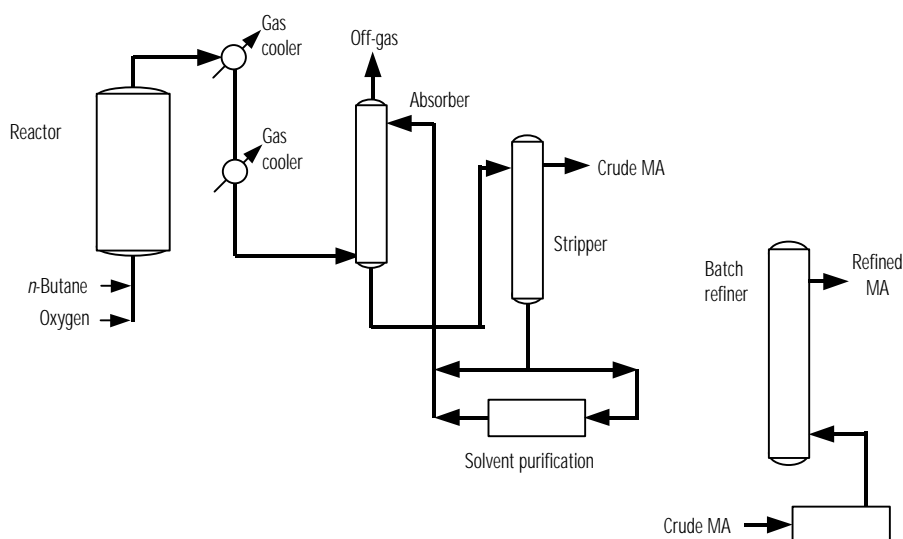


**Figure 1** Schematic flow diagram of the Huntsman fixed-bed maleic anhydride process (MA= maleic anhydride) [3].

Co-incident with the rapid development of the butane-based fixed-bed processes, several companies have developed fluidised-bed processes. In a fluidised-bed process, reaction gases flow upward through a bed of catalyst particles. When the force of the gas flow on the catalyst bed is equal to the weight of the bed, the catalyst bed expands significantly and the catalyst bodies are brought in continuous motion. Because of this motion, better heat transfer characteristics are established and, hence, hot spots cannot occur in a fluidised-bed reactor. Other advantages over fixed-bed reactors comprise the fact that reaction gases can be used without pre-mixing and pre-heating before entering the reactor. Furthermore, higher *n*-butane concentrations can be used due to a decreased explosion risk compared to the fixed-bed process [7].



Several different ways have been developed to produce bulk V-P-O catalyst particles of the right size and the attrition resistance for fluidised-bed purposes [17,18]. When the catalyst bodies are too small, they will be blown out of the reactor. Large bodies, on the other hand, call for extremely high linear gas flow rates. Therefore, the particle size of fluidised-bed catalysts usually ranges from 10 to 150 microns. ABB Lummus Global (ALMA) [19] and BP Chemicals [20] currently offer fluidised-bed processes. The flow diagram for fluidised-bed processes is comparable to that of the fixed-bed process (Figure 1).

DuPont commercially operates the third type of process in their recirculating-solids reactor [21,22]. In this case, oxidation of *n*-butane and regeneration of the catalysts are carried out in two separate reaction zones (see Figure 2).

The selectivity to MA is increased, because the oxidation of *n*-butane is carried out in absence of di-oxygen [21,22]. In the first step, *n*-butane reacts with lattice oxygen from the catalyst. In this stage, the catalyst is reduced by *n*-butane resulting in the selective formation of MA, which is removed in a stripper. Regeneration of the reduced catalyst with di-oxygen takes place in the second reactor zone. In principle, the oxidation state of the catalyst can be controlled optimally in this way.

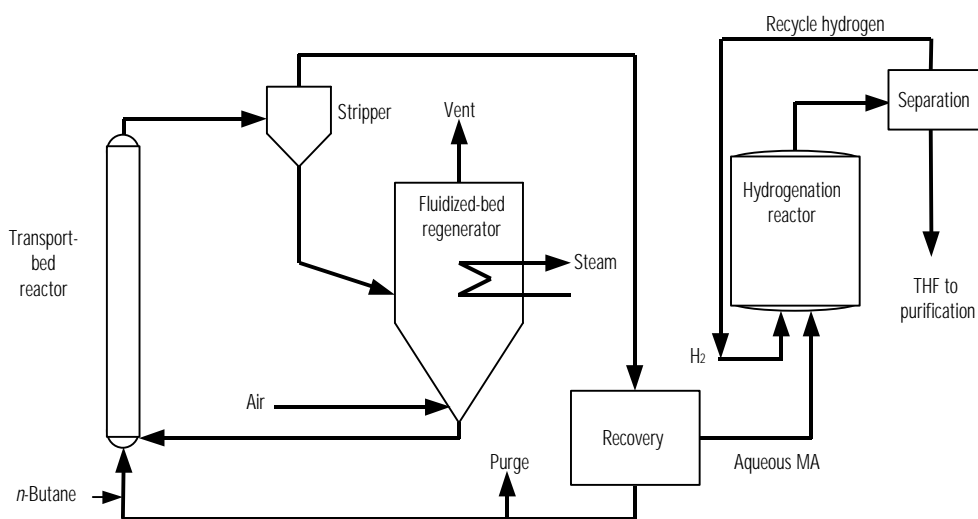


**Figure 2** DuPont recirculating-solids process for the production of THF from *n*-butane via maleic anhydride [3, 7].

A plant for the production of THF by the hydrogenation of MA from a recirculating-solids reactor has been started-up in Spain in 1996 [23]. However, it is more difficult to control the re-oxidation process of the V-P-O catalyst on a large scale and therefore, the predicted performance of the plant has not been realised as yet [24]. In principle, the bulk catalysts used in a fluidised-bed reactor and in a recirculating solids reactor are the same. Table 1 shows the 1993 and 1995

world-wide MA production capacity for the different processes [3]. As can be seen from this table, both fixed-bed and fluidised-bed butane-based processes are growing at the expense of benzene-based processes. Furthermore, it seems that production of MA with fluidised-bed technology will not surpass production with fixed-bed technology. This is probably caused by catalyst restrictions, such as attrition, and difficulties to find an optimum catalyst composition for the fluidised-bed conditions. For this reason, fixed-bed technology is still operated at higher yields to maleic anhydride.

Table 2 represents the long-term maleic anhydride production-consumption balance [25]. The average annual demand growth is estimated to be about 4% [5]. By the year 2004, total world-wide consumption will be increased by about 30% as compared to 1998.

**Table 1** World Maleic anhydride capacity (in metric tons) by reactor type [3].

Reactor (feed)	1993		1995	
	10 <sup>3</sup> t/y	%	10 <sup>3</sup> t/y	%
Fixed-Bed				
<i>Butane</i>	369	43.0	474	50.0
<i>Benzene</i>	325	37.9	244	25.8
Fluidised-Bed				
<i>Butane</i>	127	14.8	192	20.3
<i>Phtalic anhydride co-product</i>	37	4.3	37	3.9
<b>Total</b>	858	100.0	947	100.0

**Table 2** Total world production and consumption of maleic anhydride (\*1000 metric tons). Data taken from reference [25].

	1994	1995	1996	1997	1998	2001	2004
Capacity to produce							
<i>From butane</i>	551.3	647.6	657.1	702.6	767.6	1019.2	1088.7
<i>From benzene</i>	301.0	302.0	300.0	300.0	311.0	289.5	289.5
<i>From PA recovery</i>	23.5	20.5	22.5	24.5	24.5	28.5	28.5
<b>Total</b>	875.8	970.1	979.6	1027.1	1103.1	1337.2	1406.7
Utilisation (%)	81.9	79.4	82.1	83.4	83.8	79.6	85.9
Production	717.1	770.4	803.9	856.4	924.8	1064.1	1207.7
Consumption							
<i>UPE resins</i>	355.3	372.3	383.4	399.7	416.7	471.0	532.9
<i>BDO chemicals</i>	27.0	36.1	40.0	54.2	86.8	120.4	145.4
<i>Other uses</i>	330.2	361.2	380.5	402.5	421.3	472.7	529.4
<b>Total</b>	712.5	769.6	803.9	856.4	924.8	1064.1	1207.7

These numbers, together with the fact that the current yield to maleic anhydride of an equilibrated catalyst only amounts to about 58%, indicate that improvement of the process is of great economic and environmental interest. To this end,

several developments can be considered. First, the bulk V-P-O catalyst should exhibit a higher attrition resistance in order to be more suitable for fluidised-bed purposes. Secondly, the activation period for the bulk catalyst should be shortened. This will result in an earlier achievement of optimum performance. Furthermore, the catalyst formulation can be changed, resulting in better properties and an improved catalytic performance. There is also a demand for a cheaper and more reproducible preparation procedure for the currently applied bulk V-P-O catalysts. However, these improvements can never be achieved without a thorough investigation of the catalytic and structural properties of the active V-P-O phase.

#### **Development of supported V-P-O catalysts**

In a fluidised-bed, where the catalyst particles will continuously collide with each other and with the reactor internals, the catalyst must have a high attrition resistance. To enhance this attrition of a bulk V-P-O catalyst, various methods have been developed. Suciu *et al.*, for instance, have found that treatment of the catalyst precursor with acid results in an agglomeration of catalyst particles [26]. The larger agglomerates showed an increased resistance to attrition. However, the catalytic performance of the system suffered from this treatment, probably because of diffusion limitation in the large conglomerates of catalyst particles.

Another method to improve the attrition resistance of V-P-O catalysts is the incorporation of silica into the fluidised-bed catalyst by addition of a colloidal silica sol. However, this method results in a decreased selectivity to maleic anhydride as well [27,28]. Therefore, DuPont has developed a new method of imparting attrition resistance of the bulk V-P-O catalyst without loss of selectivity to maleic anhydride [29]. Instead of large quantities of colloidal silica, they use 5-10 wt% of polysilicic acid, which is spray-dried in the presence of the catalyst precursor. This technique results in the formation of a thin layer of porous silica at the periphery of the spray-dried bodies. The layer is very durable and porous to reactants and products and does not lead to a detectable degradation of catalytic properties in micro-reactor experiments [29]. However, the other disadvantages of the bulk V-P-O catalyst, such as the expensive preparation and the long equilibration time are not solved by this method.

At Utrecht University much effort has been devoted to the development of supported V-P-O catalysts [30,31]. The supported V-P-O catalysts have superior characteristics over bulk V-P-O, such as, a cheap and reproducible preparation procedure, a large number of active sites per unit surface area, a short activation period and a high mechanical strength. These properties compensate for many of the earlier described disadvantages of the currently applied bulk V-P-O catalysts. Therefore, application of supported V-P-O catalysts in a fluidised-bed process is very promising. Furthermore, the application of a well-dispersed V-P-O phase onto a support material opens new opportunities for characterisation, since no interfering bulk contributions are expected in the various spectra. Moreover, when reasonable catalytic performance is achieved, the supported V-P-O catalysts can serve as model systems for the surface of bulk V-P-O catalysts.

Overbeek *et al.* performed pioneering work concerning the development of a suitable preparation procedure for the supported V-P-O catalysts [32,33]. To this end, bulk V-P-O catalysts were studied first [33,34]. As a result of these studies, a synthesis procedure for the production of supported V-P-O catalysts was developed, based on well-defined and fully controlled conditions. A series of supported samples was screened for their activity and selectivity in the *n*-butane to maleic anhydride reaction [30,31].

### Scope of this thesis

Despite the elaborate research of Overbeek *et al.*, still little is known about the nature of the active sites in the (supported) V-P-O catalyst. Overbeek remarkably increased the yield to maleic anhydride, but never exceeded 24%. Further improvement is desired, but can only be achieved when a detailed structural investigation of the supported V-P-O phase is combined with a synthetic procedure that is well-defined, and that results in a catalyst with controllable and reproducible properties.

This thesis is concerned with the structural characterisation of the active sites of supported V-P-O catalysts. The relation between structure and catalytic activity and selectivity is of crucial importance for further improvement of supported and bulk V-P-O catalysts. The study is based on various characterisation techniques. It has been shown that the structure of the V-P-O catalyst is different under catalytic conditions as compared to ambient conditions [33]. Therefore, many of the adopted characterisation techniques have been applied *in-situ*, *i.e.* at reaction temperature and in the presence of reactants.

(*In-situ*) X-ray absorption spectroscopy has been applied as the major characterisation tool to investigate the mechanism of the *n*-butane oxidation reaction over supported V-P-O catalysts. To support this study, a more fundamental investigation was dedicated to the C<sub>4</sub> and CO oxidation reaction over an alumina-supported V<sub>2</sub>O<sub>5</sub> catalyst.

For all subjects, emphasis will be on the relation between catalyst structure, as studied by spectroscopic techniques and temperature-programmed reduction, and catalytic activity. In chapter 2 a detailed description of the experimental techniques is presented. Chapter 3 deals with the characterisation of the reference phase, VPO/bulk, with ESR spectroscopy and magnetisation experiments. In chapter 4, a study of the surface composition of bulk and supported V-P-O catalysts by means of X-ray Photoelectron Spectroscopy and Low-Energy Ion Scattering is described. In chapter 5, the structure of the supported V-P-O phase is compared with the structure of bulk V-P-O. Qualitative analyses of the Extended X-ray Absorption Fine-structure Spectroscopy (EXAFS) data is represented in chapter 6. Chapter 7 involves a study of the mechanism of CO and butane oxidation over a 17.5 wt% V<sub>2</sub>O<sub>5</sub>-on- $\gamma$ -Al<sub>2</sub>O<sub>3</sub> catalyst by means of *in-situ* X-ray absorption spectroscopy. The results of the *in-situ* characterisation of supported V-P-O catalysts with Raman spectroscopy and X-ray absorption spectroscopy are presented in chapter 8. In chapter 9, finally, a summary of the work of this thesis will be presented, as well as the conclusions of this investigation and suggestions for further research.

## References

- 1 G.C. Bond in: *Heterogeneous Catalysis: Principles and Applications*, Clarendon Press, Oxford, 1987
- 2 B.C. Gates in: *Catalytic Chemistry*, John Wiley & Sons Inc., New York, 1992
- 3 T.R. Felthouse, J.C. Burnett, S.F. Mitchell, M.J. Mummey in: *Kirk-Othmer Encyclopaedia of chemical technology*, 4th edition volume 15, John Wiley & Sons Inc., New York, 1995, 893
- 4 L. Barnes, Huntsman Corporation, *personal communication*
- 5 *Chem. Week*, June 4 1997, 37
- 6 <http://www.huntsman.com/products/chemicals/pch40002.html>
- 7 P.L. Mills, M.P. Harold, J.J. Lerou, in: *Catalytic oxidation, principles and applications*, R.A. Sheldon & R.A. van Santen (eds.), World Scientific, London, 1995, 291
- 8 *Chem. Week*, May 7 1997, 37
- 9 J. Pelouze, *Ann.* **11** (1834), 263
- 10 R. Winckler, *Ann.* **4** (1832), 230
- 11 J.R. Skeen, *Chem. Eng. News* **26** (1948), 3684
- 12 R.I. Bergman, N.W. Frisch, *US Patent* **3,293,268** (1966)
- 13 D.A. Palmer, J.K. Holzhauer, *US Patent* **4,342,699** (1982)
- 14 *Hydrocarbon Process* **70** (1991), 164
- 15 *Eur. Chem. News* **60** (1993), 24
- 16 M. Malow, *Environ. Prog.* **4** (1985), 151
- 17 J.X. McDermott, *US Patent* **4,151,116** (1979)
- 18 P.R. Blum, M.L. Nicholas, E.C. Milberger, P.A. Zock, *Eur. Patent* **0 084 706** (1982)
- 19 C. Fumagalli, G. Golinelli, G. Mazzoni, M. Messori, G. Stefani, F. Trifirò, *Stud. in Surf. Sci. and Catal.* **55** (1990), 537
- 20 J. Haggin, *Chem. Eng. News* **69** (1991), 34
- 21 R.M. Contractor, *US Patent* **5,021,588** (1991)
- 22 R.M. Contractor, *US Patent* **4,668,802** (1987)
- 23 S. Shelly, K. Fouhy, S. Moore, *Chem. Eng.* **100** (1993), 61
- 24 J.J. Lerou, *personal communication*
- 25 R. Lee, Tecnon (UK) Ltd., *personal communication*
- 26 G.D. Suciu, G. Stefani, C. Fumagalli, *UK Patent Application* **2145010A** (1985)
- 27 H. Taheri, *US Patent* **5,011,945** (1991)
- 28 G.J. Hutchings, *Applied Catalysis* **72** (1991), 1
- 29 R.M. Contractor, H.E. Bergna, H.S. Horowitz, C.M. Blackstone, B. Malone, C.C. Torardi, B. Griffiths, U. Chowdry, A.W. Sleight, *Catalysis Today* **1** (1987), 49
- 30 R.A. Overbeek, P.A. Warringa, M.J.D. Crombag, L.M. Visser, A.J. van Dillen, J.W. Geus, *Applied Catalysis A: General* **135** (1996), 209
- 31 R.A. Overbeek, A.R.C.J. Pekelharing, A.J. van Dillen, J.W. Geus, *Applied Catalysis A: General* **135** (1996), 231
- 32 J.W. Geus, R.A. Overbeek, *Eur. Patent* **94201177.6** (1994)

Chapter 1

- 33 R.A. Overbeek, *New aspects of the selective oxidation of n-butane to maleic anhydride: The development of a novel catalyst*, Thesis, Utrecht University, 1994
- 34 R.A. Overbeek, M. Versluijs-Helder, P.A. Warringa, E.J. Bosma, J.W. Geus, *Stud. Surf. Sci. Catal.* **82** (1994), 183

# 2

---

## EXPERIMENTAL PROCEDURES

### **INTRODUCTION**

Most of the chapters of this thesis are based on papers that have been published or submitted for publication to various journals. In these papers, the experimental set-up is not be described in detail. The contents of this chapter should overcome this deficiency. In this chapter the preparation of the catalysts, the experimental set-up for the catalytic test reactions and the applied characterisation techniques are described.

## CATALYST PREPARATION

Various V-P-O catalysts have been prepared in the framework of this research project. These catalysts can be divided into two groups. The first group consists of bulk vanadyl phosphate (VPO/bulk) and was used as a reference phase for the different characterisation techniques and the catalytic experiments. Supported V-P-O catalysts constitute the second group. The latter will comprise the most important part of this thesis.

### Preparation of VPO/bulk

Bulk V-P-O was prepared in organic solvents according to a method described by Katsumoto *et al.* [1]. 14.98 gram (82 mmol) of  $V_2O_5$  (Riedel de Haen, p.a.) was suspended in a mixture of 30 ml *i*-butanol (Merck, p.a.) and 30 ml cyclohexanol (Merck, z.s.). The suspension was refluxed for 16 hours. During this period of time, the colour changed from orange to green. After cooling down to room temperature (RT), 20.80 gram (212 mmol) of 85% *o*- $H_3PO_4$  in 30 ml *i*-butanol was added to obtain a P/V ratio of 1.1:1. Subsequently, the suspension was refluxed for another 5 hours. The resulting mint-green suspension was filtered and washed with cyclohexanol. The thus obtained precursor was dried at 393 K in nitrogen and identified as  $(VO)HPO_4 \cdot \frac{1}{2}H_2O$  with XRD.

Another method to prepare bulk V-P-O, described by Centi *et al.* [2], is performed in hydrochloric acid. 13.12 gram (72 mmol)  $V_2O_5$  (Riedel de Haen, p.a.) was dissolved in 175 ml 37% HCl-solution (Lamers & Pleuger, p.a.) and refluxed for 16 hours. The dark-green solution was cooled to room temperature and 18.23 gram (186 mmol) 85% *o*- $H_3PO_4$  was added. After two more hours of refluxing, the solution was concentrated by evaporation of the water. A blue, viscous syrup was obtained, which was dried in  $N_2$  at 393 K for one night.

Finally, the V-P-O catalysts were obtained by thermal pre-treatment of the hemihydrate phase in a micro-reactor (50 ml/min  $N_2$ , 723 K, 16 hours). They will be referred to as VPO/bulk-org and VPO/bulk-aq for the first and second of the above mentioned preparation procedures, respectively.

### Preparation of supported V-P-O catalysts

Supported V-P-O catalysts have been prepared according to two different methods. Overbeek *et al.* developed the first method [3]. According to this procedure vanadium(V) oxide was reduced electrochemically to V(III)-ions. Subsequently, the resulting V(III) species were deposited onto the support in the presence of a phosphate precursor. After drying and calcination, the supported V-P-O catalyst resulted. With this method it is possible to prepare supported V-P-O catalysts with a broad range of loadings and P/V ratios.

Because of the poor interaction of the V-P-O phase and silica this method had to be adapted to prepare silica-supported V-P-O catalysts [4,5]. To this end, V(III) was deposited onto the silica without a phosphate precursor. After drying, the supported vanadium oxide was impregnated with diluted phosphoric acid. Drying and thermal pre-treatment resulted in silica-supported V-P-O catalysts of various loadings and P/V ratios.



### Experimental procedures

The second method was developed to be able to prepare silica-supported V-P-O catalysts in one step. To this end, the support material was impregnated with a solution of vanadium oxide, oxalic acid and a phosphate precursor. After drying and decomposition of the precursor, the silica-supported V-P-O catalysts were obtained. ICP analysis with a number of supported V-P-O catalysts revealed that the intended V-P-O loading was obtained for all samples that were analysed.

#### Support materials

The support materials used for this study were Al<sub>2</sub>O<sub>3</sub>, TiO<sub>2</sub> and SiO<sub>2</sub>.  $\gamma$ -Al<sub>2</sub>O<sub>3</sub> (Degussa alumina C) has a surface area of 100 m<sup>2</sup>/gram. TiO<sub>2</sub> (Degussa P25) has a surface area of 50 m<sup>2</sup>/gram and an anatase-to-rutile ratio of 9:1. Pre-shaped silica spheres (Engelhard C500-series, 30  $\mu$ m <  $\phi$  < 120  $\mu$ m) were used to prepare tailor-made fluidized-bed catalyst. The specific surface areas as well as the average pore-size of these support materials are mentioned in Table I.

**Table 1** Textural properties of the applied fluidised-bed silicas.

	surface area (m <sup>2</sup> /gram)	pore-volume (ml/gram)	average pore-size (nm)
C500-18	300	0.87	10
C500-19	100	0.73	20
C500-20	80	0.64	30

#### Electrochemical reduction of vanadium (V) to vanadium (III)

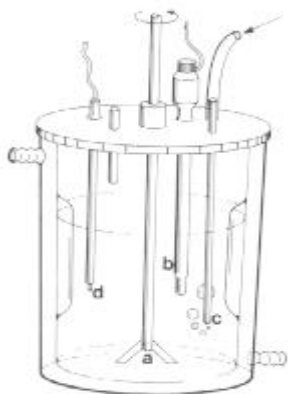
Because of the possibility of re-oxidation, all experiments have been performed in an oxygen lean environment. To this end the experimental set-up was purged with nitrogen. Overbeek *et al.* have optimised the experimental set-up extensively [6]. In a typical experiment, about 20 gram of NH<sub>4</sub>VO<sub>3</sub> (Merck, p.a.) was dissolved in 800 ml 1.5 N HCl-solution (Merck, p.a.). The orange solution was stirred with a magnetic stirrer and purged with N<sub>2</sub>. After complete dissolution of the vanadium precursor, a porous ceramic body, filled with 1.5 N HCl-solution was inserted and Pt electrodes were used in the anode (gauze) and cathode (smooth) compartment. Subsequently, a standard current circuit was applied including an Amperometer and a Voltmeter.

The applied potential was 2-5 V, sufficiently high to obtain an acceptable current (~0.1 A) and sufficiently low to avoid evolution of H<sub>2</sub> gas. Electrolysis was stopped when the V-solution was showing the characteristic blue-green colour of V(III) ions in a hydrochloric acid solution.

The actual vanadium concentration of the electrolyte solution as well as the average valence-state (AV) of the vanadium ions was determined using a titration procedure described by Niwa *et al.* [7]. Typically, the vanadium concentration of the electrolyte solution was *ca.* 0.25 mol/l and the AV was *ca.* 3.0.

**Homogeneous Deposition Precipitation (HDP)**

The precipitation of the vanadium precursor onto the support materials was performed in a standard precipitation set-up as described by Geus [8]. Figure 1 represents the precipitation vessel.



The vessel was equipped with a stirring motor (a) (Heidolph, model RZR-1, 1500 rpm) and baffles to ensure homogeneity of the contents. A pH electrode (b) (Knick model 761) was submerged below the surface of the liquid in order to enable us to monitor the pH during the precipitation. Nitrogen (c) was led into the vessel to prevent oxidation of trivalent vanadium species. Injection of ammonia below the liquid surface was accomplished by insertion of a capillary tube with an internal diameter of 2 mm (d). A surgical peristaltic pump (Gilson minipulse) induced flow of the liquid.

**Figure 1** Precipitation vessel (letters are explained in the text).

The support material (~ 10 gram) was suspended into 1500 ml demineralised water. The pH of the solution was decreased to a value of ~1 with a concentrated HCl-solution. The suspension was vigorously stirred for several minutes, after which the desired amount of V(III) solution was added with a pipette. For the preparation of titania-supported V-P-O catalysts an appropriate amount of  $\text{NH}_4\text{H}_2\text{PO}_4$  (Merck, p.a.) was added as a phosphate source. The phosphate source was omitted in case of silica-supported V-P-O catalysts (*vide infra*). Then precipitation was brought about by slow injection of ammonia (5% solution, Merck, p.a.) at a rate of 0.1 mmol OH<sup>-</sup>/min. During this process, the pH was continuously monitored. Precipitation was stopped when the pH had reached a value of about 7. Subsequently the precipitate was filtered, washed carefully with demineralised water and dried in air at 393 K. A typical precipitation procedure as described takes about 6 hours.

Vogt has shown that this procedure works well for the preparation of supported  $\text{V}_2\text{O}_5$ , which was obtained after oxidation of the deposited precursor [9]. Overbeek, however, has reported that precipitation of vanadium-phosphate precursors onto various supports is suffering from a poor interaction between the precursor and the support material [4,5]. Only with titania, V-P-O can be deposited in one step by adding an appropriate amount of  $\text{NH}_4\text{H}_2\text{PO}_4$  before addition of ammonia. Alumina, on the other hand, acts as a phosphate sponge, resulting in the formation of aluminium-phosphate supporting a poorly selective VPO phase of a very low P/V ratio [6].

**Incipient Wetness Impregnation**

The dried silica-supported vanadium oxide catalysts were impregnated according to the incipient wetness method. Depending on the intended V-P-O loading and

### *Experimental procedures*

the desired P/V ratio an amount of 85% *o*-H<sub>3</sub>PO<sub>4</sub> (Merck, p.a.) was diluted in demineralised water. The impregnated sample was left at RT for 4 hours and subsequently dried in air at 393 K for 12 hours.

#### ***Thermal pretreatment***

All catalyst samples have been thermally pre-treated. To avoid re-oxidation of vanadium, this procedure was performed in N<sub>2</sub> (50 ml/min) at 723 K (heating rate 300 K/h) for 16 hours.

## **CATALYTIC TESTING**

#### ***Testing equipment***

For catalytic test reactions a quartz micro-reactor was positioned in an automated microflow apparatus, which is represented in Figure 2.

The ceramic oven was controlled with a West 3810 temperature controller. Glass pearls were used to pre-heat the gas flow before entering the catalyst bed. The temperature in the middle of the catalyst bed was measured with a Hastalloy-C shielded thermocouple. Available gases were argon (Hoekloos, 99.999%), oxygen (Hoekloos, 99.5%), *n*-butane (Linde, 99.8%), helium (Hoekloos, 99.999%) and carbon monoxide (Hoekloos, 99.992%).

Analysis of non-converted reactants and products is performed on an on-line Balzers QMS-420 quadrupole mass spectrometer, operated with the Quadstar software code (version 1.11). Detected *m/z* values were 18 (H<sub>2</sub>O), 26 (MA), 27 (C<sub>4</sub>H<sub>10</sub>), 28 (CO, CO<sub>2</sub>, MA, C<sub>4</sub>H<sub>10</sub>), 32 (O<sub>2</sub>), 43 (*n*-C<sub>4</sub>H<sub>10</sub>), 40 (Ar), 44 (CO<sub>2</sub>, C<sub>4</sub>H<sub>10</sub>), and 54 (MA).

To avoid condensation of products, all tubing behind the reactor zone, as well as the analysis compartment of the mass spectrometer was kept at 423 K.

#### ***Testing procedure and conditions***

Catalyst samples were tested in the selective oxidation of *n*-butane to maleic anhydride in a broad temperature range. In a typical experiment 1.5 ml (~0.9 gram) of catalyst was placed in the micro-reactor.

In general, catalysts were activated in synthetic air at 653 K for 1 hour prior to catalytic testing. The applied flow was 50 ml/min resulting in a GHSV of 2500 h<sup>-1</sup>. During a catalytic experiment, the gas flow consisted of 1.5 % *n*-C<sub>4</sub>H<sub>10</sub>, 20% oxygen, and 78.5 % argon. Temperature was increased in steps of 10-20 K, and at every temperature 60 data points were collected in 2 hours.

#### ***Calculation of conversion and selectivity***

Calibration of the QMS-420 was performed by measuring the intensity of the various product peaks as a function of concentration in the feed at room temperature without catalyst in the reactor. Corrections were made for fragment ions appearing at *m/z* values other than the molecular ions. For this reason, [CO] was less reliably measured due to interference of N<sub>2</sub>, CO<sub>2</sub>, *n*-C<sub>4</sub>H<sub>10</sub> and MA fragment ions at *m/z* 28.

## Chapter 2

The conversion of *n*-butane and the selectivity to the various products was calculated by the following equations:

$$\text{Conversion of } n\text{-butane} = \frac{[\text{C}_4\text{H}_{10}]_{\text{feed}} - [\text{C}_4\text{H}_{10}]_{\text{products}}}{[\text{C}_4\text{H}_{10}]_{\text{feed}}} \cdot 100\% \quad (1)$$

$$\text{Selectivity towards product X} = \frac{[\text{X}]}{[\text{CO}] + [\text{CO}_2] + [\text{MA}] \cdot 4} \cdot 100\% \quad (2)$$

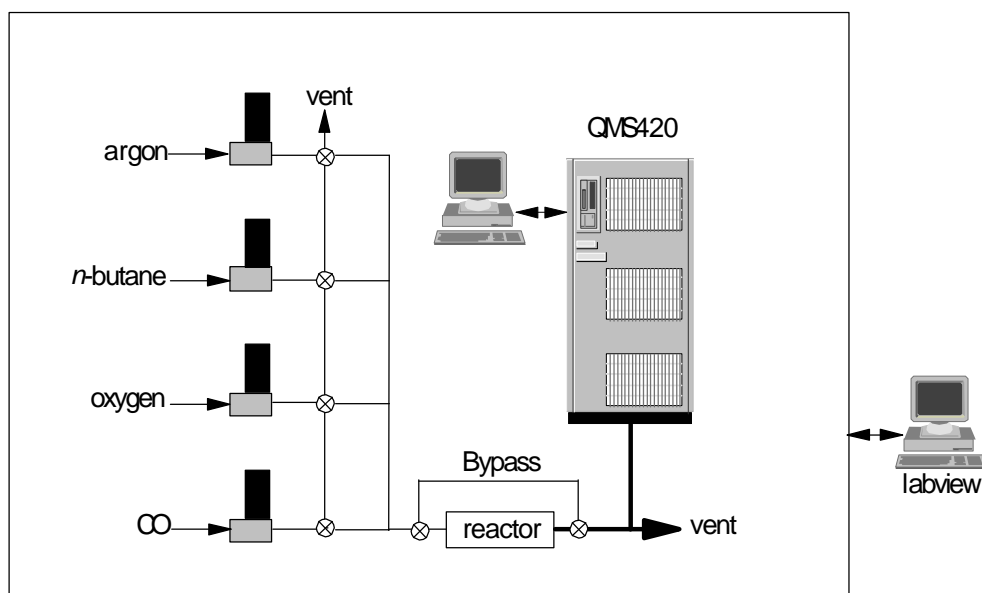


**Figure 2** Experimental set-up of *n*-butane oxidation experiments. Flows are regulated with mass flow controllers and three-way valves. Thick lines represent tubing that is traced at 423 K.

## CHARACTERISATION TECHNIQUES

### Textural analysis

Nitrogen sorption isotherms were recorded to determine the specific surface area and the pore-size distribution of the bare support materials and the V-P-O catalysts. Isotherms were recorded with a Micromeritics ASAP 2400 apparatus. The specific surface areas were calculated from the extent of nitrogen sorption according to the BET theory [10], assuming that the surface area of an adsorbed N<sub>2</sub> molecule is 0.162 nm<sup>2</sup>.

### Inductively Coupled Plasma

The chemical composition of catalyst samples was examined with Inductively Coupled Plasma (ICP). The technique comprises dissolving a known quantity of sample in a solution containing hydrofluoric acid and boric acid, which was carried out in a teflon pressure vessel. After addition of the solution the vessel was closed to prevent the escape of SiF<sub>4</sub> vapours. The vessel was subsequently placed in a stainless steel container and kept at 393 K for one hour. The container and vessel were cooled down to room temperature, after which the dissolved catalyst sample was diluted to appropriate concentrations. Standard solutions for the elements to be determined were used to calculate the concentration of the elements in the V-P-O samples. The ICP measurements were performed in the Department of Earth Sciences of Utrecht University.

### X-ray Diffraction

Powder X-ray diffraction (XRD) experiments were performed with an ENRAF-NONIUS PDS 120 diffractometer, equipped with a position-sensitive ENRAF-NONIUS CPS120 detector. The applied radiation was Co K<sub>α1</sub> ( $\lambda = 1.78897 \text{ \AA}$ ).

### Raman spectroscopy

Raman experiments (LRS) were performed at the Zettlemoyer Center for Surface, Studies which is part of Lehigh University in Bethlehem PA (USA).

### Ambient LRS

Ambient Raman spectra were obtained with a Spectra-Physics Ar<sup>+</sup> laser (model 171) by using *ca.* 25-50 mW of the 514.5 nm line for excitation. About 100-200 mg of the powdered solid was pressed into a thin wafer about 1 mm thick with KBr backing for support. The sample was then mounted onto a spinning sample holder and rotated at *ca.* 2000 rpm to avoid local heating effects. A 90° collection geometry was employed to collect the scattered light. Raman spectra were obtained with a Spex Triplemate spectrometer (model 1877) coupled to an EG and GOMA III optical multi channel analyser (model 1463).

### In-situ LRS

The *in-situ* laser Raman spectra were obtained with an Ar<sup>+</sup> laser (Spectra Physics, model 2020-50). The incident laser line delivered 1-20 mW of power measured at the sample and tuned to 514.5 nm. The scattered radiation from the sample was

## Chapter 2

directed into an OMA III (Princeton Applied Research, Model 1463) optical multi-channel analyser with a photodiode array detector thermo-electrically cooled to 238 K.

About 100-200 mg of pure catalyst were pressed into wafers and placed in the *in-situ* cell. The *in-situ* cell consisted of a stationary sample holder, which has been described elsewhere [11].

### Thermal Analysis

The decomposition and/or dehydration behaviour of the V-P-O precursors were studied with two different thermal analysis techniques. Thermogravimetric (TGA) analyses were performed in a Stanton Redcroft thermobalance (Model STA-780). Differential Scanning Calorimetric (DSC) experiments were carried out in a Setaram DSC 92. For the DSC and TGA experiments typically 20-50 mg of sample was used. Heating rates were 300 K/h.

### Electron Microscopy

The size of the deposited V-P-O particles and their distribution over the support were investigated with Transmission Electron Microscopy (TEM). The samples were ground in a mortar, suspended in ethanol and submerged in an ultrasonic bath for about 1 minute to ensure homogeneity of the suspension. Drops of this suspension were applied to holey carbon films supported on a copper grid. The samples were investigated in a Philips EM 420 electron microscope or a Philips CM 200 microscope equipped with an EDAX elemental analysis system able to analyse the atomic composition of the specimens by means of line-scans, mapping or spot-analysis. Both bright field and dark field images were recorded.

The model catalysts, prepared with the spin-coating technique, have been characterised using Scanning Electron Microscopy (SEM). To render the samples electrically conducting, a thin layer of carbon/tungsten was vapour deposited onto the samples. The micrographs were investigated with a Philips XL30 microscope equipped with a field emission gun and EDAX for elemental analysis.

### X-ray Photoelectron Spectroscopy

X-ray Photoelectron spectra (XPS) spectra were recorded on a VG Microtech XP Clam 2 analyser using a Mg-source operating at 10 mA. The base pressure of this system was less than  $1 \times 10^{-8}$  mbar. Finely ground samples were mounted on a sample holder with double-sided adhesive tape. All measured binding energies were calibrated at the position of the silicon 2p peak at 103.4 eV ( $\text{SiO}_2$ ) or the carbon 1s peak at 284.6 eV when no silica was present in the samples.

### Low-Energy Ion Scattering

Low-Energy Ion Scattering (LEIS) has been applied to obtain information about the composition of the outermost surface layer of the V-P-O catalysts. LEIS experiments were performed in the Section Physics of Surfaces and Interfaces at the Technical University of Eindhoven, using the Energy Resolved Ion Scattering Spectrometer (ERISS), allowing static LEIS. Experimental details are found in chapter 7, which is completely dedicated to the LEIS experiments.

### X-ray Absorption Spectroscopy

To study the structure of the active component in the supported vanadium-based catalysts, X-ray absorption spectroscopy was applied. X-ray Absorption Near Edge Structure (XANES) provides information about the oxidation state of the vanadium and the local geometry of vanadium in the samples. EXAFS provides information about the structural parameters of the specimen, *i.e.* kind of neighbours, coordination numbers, bond distances and disorders (Debye-Waller factor). Furthermore, the characterisation can be performed *in-situ*, and under well-defined reaction conditions. Since the supported V-P-O catalysts are well dispersed, the contribution of the (active) surface to the total spectrum is large. Therefore, the surface reactivity of supported V-P-O catalyst can be assessed with this technique.

When X-rays hit a sample, absorption of radiation takes place when the photon energy reaches the binding energy of a core-electron. In case of the K-edge, this is a 1s electron. If the photon energy is sufficient for excitation of the electron ( $h\nu \geq E_{\text{binding}}$ ), the absorption will sharply increase, resulting in the observation of an absorption edge, while creating a photoelectron. The ejected photoelectrons can be considered as outgoing spherical waves with a wavelength of  $\lambda = 2\pi/k$ , in which  $k$ , the photoelectron wave factor is equal to:

$$k = \left[ \frac{2m}{\hbar^2} \cdot (E - E_b) \right]^{\frac{1}{2}} \quad (3)$$

In this expression,  $E$  is the energy of the incident photons,  $E_b$  is the electron's binding energy,  $m$  is the mass of an electron, and  $\hbar$  is Planck's constant divided by  $2\pi$ .

Neighbouring atoms will reflect the spherical outgoing wave. The outgoing wave can be either in phase or out of phase with the backscattered waves. This will cause modulation of the wave at different incident photon energies. This modulation of the wave will result in fine structure on the absorption spectrum and can be explained by examining the transition probability,  $P$ , for the electrons, which is given by

$$P \propto C \left| \langle \Psi_f | \mathbf{r} | \Psi_i \rangle \right|^2 \quad (4)$$

In this equation,  $C$  is a constant,  $|\Psi_i\rangle$  is the wave function of the initial unexcited state and  $|\Psi_f\rangle$  is the wave function of the final, excited state. The latter is modulated with the interference pattern. Since the transition probability,  $P$ , is directly proportional to the X-ray absorption, a modulated absorption is observed. The backscattering amplitude  $F(k)$  is different for all elements and dependent on  $k$ . Furthermore, a  $k$ -dependent phase shift function has to be taken into account. Each absorber-scatterer pair has its own phase shift function  $\phi(k)$ . These functions can be theoretically derived. The total absorption of the sample as a function of  $k$ , can be described by the EXAFS function,  $\chi(k)$ :

$$\chi(k) = \sum A_j(k) \sin[2kR + \phi_j(k)] \quad (5)$$

## Chapter 2

In which the amplitude function  $A_j(k)$  can be described by:

$$A_j(k) = \frac{N_j}{kR_j^2} \cdot F_j(k) \cdot S_0^2(k) \cdot e^{-2k^2\sigma^2} \cdot e^{-2R_j/\lambda_e(k)} \quad (6)$$

The amplitude function is dependent on the number of scattering atoms in shell  $j$  ( $N_j$ ), the interatomic distance between absorber and scatterer ( $R$ ), the Debye-Waller factor,  $\Delta\sigma^2$ , which accounts for static and thermal disorder in the short-range order of the sample, the phase shift function,  $\phi_j(k)$ , the backscattering amplitude function,  $F_j(k)$ , the mean electron free path,  $\lambda$ , and a factor that corrects for relaxation in the absorber atom and multi-electron excitations,  $S_0^2(k)$ .

The information present in the  $\chi(k)$  function is not readily extracted. Since this function is a superposition of different sine functions, representing the different co-ordination shells, Fourier transformation is used to separate the contributions of the different shells. Data are generally converted from  $k$ -space to  $R$ -space, resulting in radial distribution functions. After correction for phase shifts, these functions show maximums related to coordination distances in the compound.

The Fourier transformation can also be applied to extract contributions from the EXAFS. When a back-transformation is performed on a single co-ordination shell, the  $\chi(k)$  of this single shell can be calculated. Subsequently this can be subtracted from the original  $\chi(k)$ , yielding a new  $\chi(k)$  function, which contains fewer shells and is less complicated to analyse.

It is possible to extract a calculated shell,  $j$ , from  $\chi(k)$  using:

$$\chi(k)_j = \frac{N_j}{kR_j^2} \cdot F_j(k) \cdot e^{-2k^2\sigma^2} \cdot \sin[2kR_j + \phi_j(k)] \quad (7)$$

In this equation,  $F_j(k)$  and  $\phi_j(k)$  are backscattering amplitude and phase shift functions that, in our case, were derived from  $\text{Na}_3\text{VO}_4$  and Ti-foil as experimental reference samples. The strategy of subtracting fitted contributions from the spectrum in order to simplify the data analysis is known as the difference file technique.

The combination of Fourier filtering, and the difference file technique is a powerful approach for EXAFS data analysis and was applied for the data described in this thesis. The complete EXAFS function of the samples that were studied in the framework of this thesis was calculated from the optimised addition of known or expected contributions. A criterion for evaluating the obtained fit is the comparison between the experimental and calculated EXAFS in  $k$ -space and  $R$ -space, using  $k^1$  and  $k^3$  weight factors. Mojet has written an excellent overview of the physical background of XAFS, as well as the strategy for data analysis [12].



## Experimental procedures

### Data collection

V K-edge absorption spectra were taken at station 8.1 of the SRS in Daresbury (UK), using a Si (111) double crystal monochromator. The measurements were generally performed in transmission mode using ion chambers filled with Ar to have a  $\mu x$  of 20% and 80% in the first and second ionisation chamber, respectively. The monochromator was detuned to 50% of maximum intensity at the V K-edge (5465 eV) to minimise the presence of higher harmonics.

To minimise high and low frequency noise the counting time per data point was 1000 ms and at least 4 scans were averaged. A vanadium metal foil of 5  $\mu\text{m}$  was used for calibration of the edge position. Absorption spectra were calibrated at the position of the main-edge jump of vanadium at 5465 eV according to Wong *et al.* [13,14].

The sample was pressed into a self-supporting wafer and mounted in an *in-situ* EXAFS cell [15,16], equipped with beryllium windows. The thickness of the wafer was chosen to give an absorption ( $\mu x$ ) of 2.5 at the absorption edge for optimal signal-to-noise ratio. To prevent thickness effects for the highly loaded samples  $\mu x$  was set to yield of a step of 1.0 in absorption in the edge region. Typically, about 20 mg of catalyst was used, accompanied with 40 mg of BN in order to have a manageable amount.

### Data analysis

Data reduction and data analysis was performed with the XDAP code developed by Vaarkamp *et al.* [17]. Standard procedures were used to extract the EXAFS data from the measured absorption spectra. The pre-edge was subtracted using a modified Victoreen curve [18] and the background was subtracted using cubic spline routines [19,20]. Normalisation was performed by dividing the data by the height of the absorption edge at 50 eV.

Averaging 3-4 scans of the individual background-subtracted and normalised data attained the final EXAFS function.

Phase shifts and backscattering amplitudes from reference compounds were used to calculate the EXAFS contributions:  $\text{Na}_3\text{VO}_4$  for the V-O contribution and Ti-foil for the V-V contribution. The co-ordination in vanadium metal is bcc, which implies that there is considerable overlap between the first two co-ordination shells. Therefore, the metal is not suitable for use as a reference compound for the V-V scatterer pair. We have used Ti-foil as a replacement. Titanium is adjacent in the periodical table, and it is assumed that the backscattering amplitude and the phase shift will not differ to a great extent from those of vanadium.

The fit parameters were determined by multiple shell fitting in R-space [9,12]. Backscatterers were identified by applying the difference file technique using phase-corrected Fourier transformations [9,20,21]. The final fit parameters were obtained after a full optimisation of all parameters in both  $k^1$  and  $k^3$  weighting in the Fourier transformations. Variances were calculated according to the methods described by Mojet [12]. The inaccuracies in the fit parameters were estimated to be 20% in co-ordination number (N), 1% in distance (R), 5% in Debye-Waller Factor ( $\Delta\sigma^2$ ), and 10% in inner potential correction ( $\Delta E_0$ ).

## ACKNOWLEDGMENTS

Most of this work could not have been performed without the outstanding help of many people. Therefore, the following persons are kindly acknowledged:

- Christina van Eck, Evert Zwaan and Gerrit Langezaal (Technical Service Department)
- Willem Nieuwenhuis (Glass Instrument Department)
- Henk Erkelens, Lou Louwerse<sup>‡</sup> and Victor van den Hoek Oostende (Electronics Department)
- Ellart de Wit, Roland Blaauw and Roger Eijkhoudt (Labview)
- Elwin de Wolf, Johan Jansen, Mathieu Meeuwsen, Pim de Jong and Rob Kreiter (practical work)
- Aarnoud Roest, Jos Kleinen and Ageeth Bol (literature reviews)
- John Raaymakers and Piet Elberse (N<sub>2</sub> physisorption)
- Marjan Versluijs-Helder (SEM/XRD/HTXRD)
- Ad Mens (XPS)
- John Geus, Marjan Versluijs-Helder and Roland Tabor (SEM/TEM)
- Antonio Barbon and Ernst van Faasen (ESR)
- J. Keijzer (Magnetisation experiments)
- Chun-Bao Wang and Israel Wachs (Raman spectroscopy)
- Ed Vlietstra and Xingtao Gao (UV-VIS-NIR DRS)
- Arno Kentgens and Gerda Nachtegaal (<sup>31</sup>P MAS NMR)
- Arnoud Dernier van der Gon, Hidde Brongersma, Leon Coulier, and Wim Jansen (LEIS/XPS)
- Liesbeth van Steensel (AFM)
- Ad van der Eerden, Andrea Russell, Barbara Mojet, Bob Leliveld, Diek Koningsberger, Frank de Groot, Fred Mosselmans, Gert van Dorssen, Guus Ijpelaar, Jeroen van Bokhoven, Lorry Murphy, Marius Vaarkamp, Marc Garriga Oostenbrink, Miguel Angel Cauqui Lopez and Sylvain Lemaux (XAFS)

## REFERENCES

- 1 K. Katsumoto, D.M. Marquis, US Patent **4,132,670** (1970)
- 2 G. Centi, C. Garbassi, I. Manenti, A. Riva, F. Trifiro, in: *Preparation of Catalysts III*, B. Delmon, P.A. Jacobs, P. Grange (eds.), Elseviers, Amsterdam, 1983, 543
- 3 R.A. Overbeek, P.A. Warringa, M.J.D. Crombag, L.M. Visser, A.J. van Dillen, J.W. Geus, *Applied Catalysis A: General* **135** (1996), 209
- 4 R.A. Overbeek, A.R.C.J. Pekelharing, A.J. van Dillen, J.W. Geus, *Applied Catalysis A: General* **135** (1996), 231
- 5 R.A. Overbeek, E.J. Bosma, D.H.W. de Blauw, A.J. van Dillen, H.G. Bruil, J.W. Geus, *Applied Catalysis A: General* **163** (1997), 129

Experimental procedures

- 6 R.A. Overbeek, *New Aspects of the Selective Oxidation of n-Butane to Maleic Anhydride, the Development of a Novel Catalyst*, Thesis, Utrecht University, 1994
- 7 M. Niwa, Y. Murakami, *J. Catal.* **76** (1982), 9
- 8 J.W. Geus, *Studies in Surface Science and Catalysis* **16** (1983), 1
- 9 E. Vogt, *Preparation and Properties of Catalysts Supported on Modified Silica*, Thesis, Utrecht University, 1988
- 10 S. Brunauer, P.H. Emmet, E. Teller, *J. Am. Chem. Soc.* **60** (1938), 309
- 11 M.A. Vuurman, A.M. Hirt, I.E. Wachs, *J. Phys. Chem.* **95** (1991), 9928
- 12 B.L.Mojet, *Metal Support Interactions, a step closer to the origin*, Thesis, Utrecht University, 1997
- 13 J. Wong, F.W. Lytle, R.P. Mesmer, and D.H. Maylotte, *Phys. Rev. B* **30** (1984), 5596
- 14 J. Wong, D.H. Maylotte, F.W. Lytle, R.B. Gregor, and R.L.St. Peters, in *EXAFS and near edge structure*, A. Bianconi, L. Inocchia, and S. Stipcich, eds., Springer Verlag, Berlin, 1983, 206
- 15 F.W.H. Kampers, T.M.J. Maas, J. van Grondelle, P. Brinkgreve, D.C. Koningsberger, *Rev. Sci. Instrum.* **60** (1989), 2635
- 16 M. Vaarkamp, B.L.Mojet, F.S. Modica, J.T. Miler, D.C. Koningsberger, *J. Phys. Chem.* **99**, (1995), 16067
- 17 <http://www.xs4all.nl/~xsi/>
- 18 M. Vaarkamp, I. Dring, R.J. Oldman, E.A. Stern, D.C. Koningsberger, *Phys. Rev. B* **50** (1994), 7872
- 19 J.W. Cook Jr, D.E. Sayers, *J. Appl. Phys.* **52** (1981), 5024
- 20 J.B.A.D. van Zon, D.C. Koningsberger, H.F.J. van 't Blik, D.E. Sayers, *J. Chem. Phys.* **82** (1985), 5742
- 21 F.W.H. Kampers, *EXAFS in catalysis, instrumentation and applications*, Thesis, TU Eindhoven, 1988

*Chapter 2*

# 3

---

## EVIDENCE FOR A NEW TYPE OF VANADYL PAIRS IN $(VO)_2P_2O_7$ AN ESR AND MAGNETISATION STUDY

### **ABSTRACT**

ESR and magnetisation experiments have identified a new type of antiferromagnetic pairing of vanadyl groups in the *n*-butane oxidation catalyst vanadylpyrophosphate. This pairing is an order of magnitude weaker than the coupling predominantly found in crystalline  $(VO)_2P_2O_7$ , and can be ascribed to the presence of a hydrated V-P-O phase, which is formed under reaction conditions. However, the presence of an amorphous V-P-O phase with a decreased exchange coupling between vanadyl groups cannot be excluded.

## INTRODUCTION

Bulk catalysts based on Vanadium-Phosphorus-Oxide (V-P-O) are industrially used for the production of maleic anhydride (MA) from *n*-butane. Although the V-P-O system has been under intense investigation for the last three decades, still little is known about the exact nature of the active site [1,2,3]. Nonetheless, it is widely accepted that vanadyl-pyrophosphate,  $(VO)_2P_2O_7$ , is the main component of the active catalyst upon exposure to atmospheric air at room temperature [1,2,3].

In the literature, the catalytic activity of the V-P-O catalysts has been related to the local structure of vanadyl groups in vanadylpyrophosphate. The structure of crystalline vanadylpyrophosphate consists of pairs of edge-sharing pseudo octahedrally co-ordinated vanadium ions at a distance of 3.23 Å which are isolated by pyrophosphate groups [4]. This structural unit is often used to model the active sites in V-P-O catalysts [2,5,6,7,8]. However, various other models have been proposed, *viz.* interfaces between different  $VOPO_4$  phases and  $(VO)_2P_2O_7$  [9],  $V^{5+}$  sites on the surface of  $(VO)_2P_2O_7$  [2],  $V^{5+}$  species in interaction with  $VO(PO_3)_2$  [10], and amorphous  $V^{4+}$  and/or  $V^{5+}$  phases supported on crystalline  $(VO)_2P_2O_7$  [11,12]. To study the amorphous phase we have applied ESR spectroscopy and magnetisation measurements to gain more insight in the magnetic interactions between  $VO^{2+}$  ions in a possibly different environment in an equilibrated bulk V-P-O catalyst. Both, ESR and magnetic measurements are selective for (amorphous)  $V^{4+}$  ( $d^1$ ) ions and do not detect non-magnetic  $V^{5+}$  species.

In principle, a single isolated  $VO^{2+}$  ion ( $S = 1/2$ ,  $L = 7/2$ ) has a characteristic octet ESR spectrum showing the hyperfine coupling to the  $^{51}V$  nuclear magnetic moment. Upon pairing of two vanadyl ions, the two electron spins may combine to a non-magnetic spin singlet ( $S = 0$ ) or a paramagnetic spin triplet state ( $S = 1$ ). Only the latter is ESR detectable. The superexchange interaction between the two vanadium ions leads to a configuration in which the two electron spins have an antiferromagnetic character, *i.e.* the singlet state is energetically favoured. The hyperfine interactions with the  $^{51}V$  ( $I = 7/2$ ) nucleus, being orders of magnitude weaker than the exchange interaction, are averaged out and do not manifest themselves in the ESR spectrum of the spin triplet state. Therefore the ESR spectrum of strongly coupled pairs has the form of a single broad line with inhomogeneous broadening due to *g*-tensor anisotropy.

The probability ( $P_t$ ) that a given pair exists in the paramagnetic triplet state depends on temperature and is given by equation 1.

$$P_t(T) = \frac{3e^{2J/kT}}{1+3e^{2J/kT}} \quad (1)$$

In this equation  $2J = E_s - E_t < 0$  is the energy difference between the spin singlet and triplet states of the pair. For temperatures below  $2J/k$  this factor decreases to zero rapidly and the population of the triplet-state is thermally depleted.

To study the exchange interactions between pairs of vanadyl ions in a bulk V-P-O catalyst we have applied ESR spectroscopy and magnetisation experiments at low temperatures.

### EXPERIMENTAL

The catalyst used in this study was prepared [13] in organic environment (*i*-butanol/cyclohexanol) according to a well-known procedure [14]. This procedure results in the formation of  $VO(HPO_4) \cdot 0.5H_2O$ , which was transformed into V-P-O during thermal pre-treatment in a flow of nitrogen. This VPO/bulk catalyst was tested and equilibrated in the *n*-butane oxidation reaction for more than 100 hours. Results of the catalytic performance testing as well as a detailed description of the extensive characterisation ( $N_2$ -physisorption/XPS/TGA/DSC/(HT)XRD/DRIFTS) have been published elsewhere [13,15].

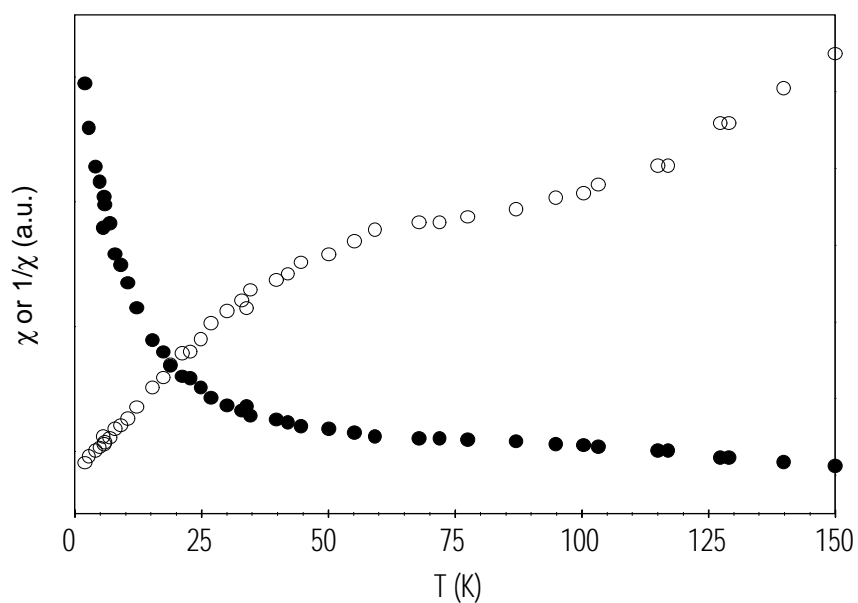
The ESR experiments were performed on an X-band Bruker ESP300 spectrometer equipped with an EN801 resonator (operating in TM110 cylindrical mode with unloaded  $Q=1000$ ). The microwave power was 1 mW, far below saturation levels for the samples considered here. The magnetic field was modulated with a frequency of 12.5 kHz and an amplitude of 1 Gauss. The sample temperature was adjusted in the range of 3.7-300 K with an Oxford ESR900 helium flow cryostat under control of an Oxford ITC503 temperature controller (temperature stability of 0.5 K).

The magnetisation experiments were performed on a vibrating sample magnetometer (Princeton Applied Research model 155) using a Janis Research helium bath cryostat (model 153). After a temperature change sufficient time was taken for temperature equilibration. No indications for thermal or magnetic hysteresis have been observed in the ESR or magnetisation data.

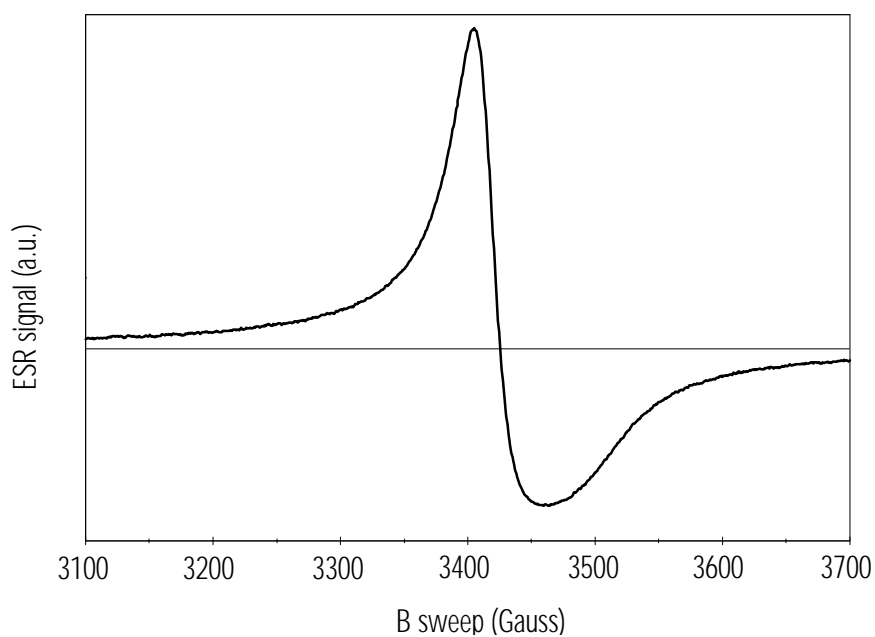
### RESULTS

Figure 1 shows the magnetic susceptibility  $\chi$  (open circles) of the equilibrated bulk catalyst as measured with the magnetometer as a function of temperature between 2 K and 150 K. The filled circles show  $1/\chi$  (same data) on an inverted scale. The data show a clear deviation from the Curie-Weiss law,  $\chi(T) \propto 1/(T-\theta)$ , for temperatures near 80 K. This deviation is indicative of a substantial quantity of V-P-O complexes existing as pairs with a strong antiferromagnetic coupling, which favours anti-parallel alignment of the electronic spins into a nonmagnetic spin singlet state (*vide infra*). The coupling originates from spin exchange interactions with  $J/k = -65.7$  K, and has been reported in the literature before [16,17]. In the following we will refer to these pairs as strongly interacting pairs.

Between 4 and 30 K, the strongly interacting pairs contribute only very little to the total  $\chi$ , as the spin triplet state is thermally depleted. In this temperature range the magnetisation data show a typical Curie-Weiss behaviour for antiferromagnets with a Curie-Weiss temperature  $\theta = 7$  K. For antiferromagnetically coupled pairs this temperature is related to the coupling parameter  $J$  as  $k\theta = -(3/2) J$ .



**Figure 1** Magnetic susceptibility from magnetisation experiments as a function of temperature (open circles) and inverse susceptibility (filled circles).

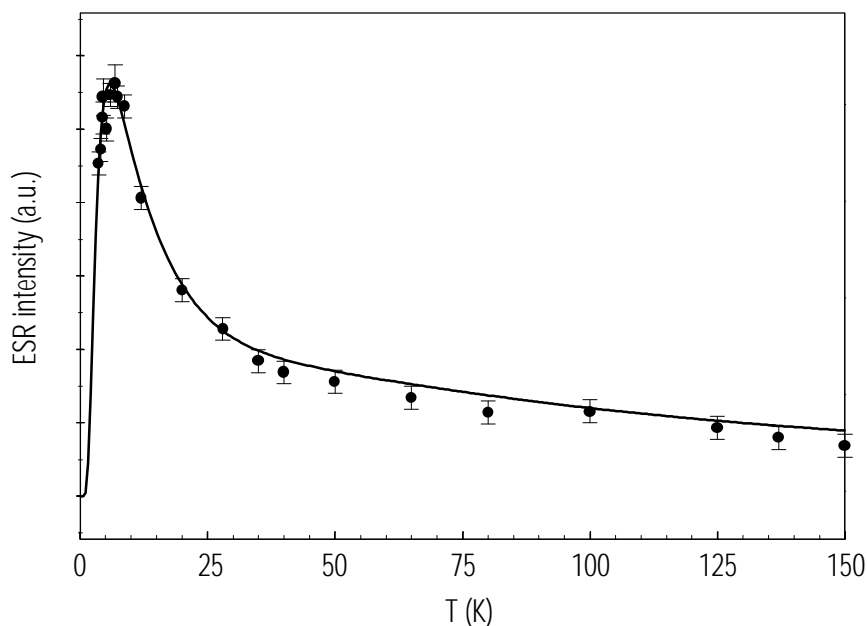


**Figure 2** X-band ESR spectrum of the equilibrated organic bulk V-P-O catalyst at room temperature. The magnetic field is centred at 3400 Gauss, and swept over 600 G. The spectrum has been taken at a microwave frequency of 9.437 GHz.



Figure 2 shows the room temperature ESR spectrum of the equilibrated bulk V-P-O catalyst. It consists of a single asymmetric line centred around  $g=1.96$ , without resolved hyperfine structure. In particular, the hyperfine coupling with the nearby  $^{51}\text{V}$  ( $I=7/2$ ) nucleus is not observed. The absence of V hyperfine coupling is common in solid state V-P-O samples [18] and is attributed to the simultaneous flipping of neighbouring electron spins [19], which averages out the interaction with the nuclei.

The shape of the ESR spectrum corresponds to the powder spectrum of a paramagnetic species with axially symmetric  $g$ -tensor. A fit of the line shape gives axial  $g$ -tensor parameters of  $g_{\parallel}=1.935\pm 0.008$  and  $g_{\perp}=1.970\pm 0.005$ . These values agree with the  $g$ -tensor parameters reported for isolated  $\text{VO}^{2+}$  ions [20,21]. Figure 3 shows the total integrated ESR intensity as a function of temperature (points). Just as with the magnetisation data, the ESR intensity exhibits a slight shoulder around 80 K, which is caused by the presence of a substantial number of pairs with a strong antiferromagnetic exchange coupling ( $J/k=-65.7$  K). At even lower temperatures, the ESR intensity does not exhibit Curie-Weiss behaviour, but shows a well defined maximum near 7 K. This behaviour is not manifest in the magnetisation data and proves that a substantial number of vanadyl groups must



exist as pairs with a weaker antiferromagnetic exchange coupling.

**Figure 3** ESR intensity as a function of temperature (dots). The solid curve represents a fit of the data according to equation 2. The fit parameters are given in the text.

### Chapter 3

Therefore, we have fitted the ESR intensity as the superposition of signals originating from strongly and weakly interacting vanadyl pairs. Within the accuracy of the ESR measurements, one strong interaction is sufficient to mimic the behaviour of strongly interacting pairs. The ESR intensity  $I(T)$  has been fitted with equation 2, which is derived in the appendix of this chapter.

$$I(T) \propto \frac{w_1}{T} \cdot \frac{4e^{\frac{2J_1/kT}{1+3e^{\frac{2J_1/kT}}}}}{1+3e^{\frac{2J_1/kT}}} + \frac{w_2}{T} \cdot \frac{4e^{\frac{2J_2/kT}{1+3e^{\frac{2J_2/kT}}}}}{1+3e^{\frac{2J_2/kT}}} \quad (2)$$

The factors  $(w/T)$  give the Curie approximation to the ESR intensity  $I(T)$  for a given triplet state, the other factors give the Boltzmann probability to find a vanadyl pair in the spin triplet state as defined in equation 1.

The solid line in Figure 3 shows the results from a fit with  $w_1/w_2 = 1.5 \pm 0.3$ , and two types of pairs, *i.e.* strongly interacting ( $J_1/k = -65.7$  K, fixed), and weakly interacting ( $J_2/k = -4.7 \pm 0.5$  K).

### DISCUSSION

We will discuss our results for two different temperature ranges separately, *i.e.* 3-40 K and 40-150 K. Furthermore, we will follow the suggestion of Johnston *et al.*, who supposed that their magnetisation data include two separate contributions [16,17]. The first contribution is originating from strongly interacting pairs

( $J/k = -65.7$  K), and passes through a maximum at around 80 K. The other contribution comes from defects in the vanadylpyrophosphate structure and is monotonously increasing as the temperature is lowered. Although these paramagnetic defects account for just a few percent of the total amount of vanadyl groups in the sample only, they dominate the magnetic susceptibility at low temperature [16].

For comparison, it is interesting to note that the ESR data on the hydrated precursor,  $\text{VO}(\text{HPO}_4) \cdot 0.5\text{H}_2\text{O}$  can be explained without invoking the presence of defects [22]. Powder diffraction data [9,16,17,22] have revealed that the hydrated precursor contains fewer defects than the dehydrated catalyst. The amount of defects in the final catalyst depends on the details of the pre-treatment (heating rate, final temperature and annealing time).

Analogous to Johnston *et al.* we also find a contribution to the magnetisation originating both from weakly interacting vanadium atoms and from strongly interacting pairs [16,17]. This holds for our results measured with both the magnetometer and ESR spectroscopy.

Starting from 150 K and going down in temperature (Figure 1), the magnetic susceptibility initially slightly increases down to 100 K, whereas the susceptibility hardly varies with the temperature between 100 K and 70 K, where the strongly interacting pairs increasingly populate the singlet state. Below 70 K, the contribution from the strongly interacting pairs rapidly falls to zero as the triplet-state is substantially depleted. The dominant part of the susceptibility is now due

to weakly interacting vanadium atoms and the total susceptibility starts to increase again at decreasing temperatures. The weak interactions are still sufficiently strong to average out the hyperfine structure and no structural change in the ESR spectrum is observed. In principle the ESR spectrum of a single isolated spin triplet state ( $S=1$ ) should have characteristic weak  $\Delta m = \pm 2$  transitions at reduced magnetic field values (forbidden half-field transitions). In our sample, the half-field transitions were unobservable, which suggests the presence of additional magnetic interactions between the pairs in the sample [22].

In the temperature range of 3-40 K, the strongly interacting pairs contribute very little to the total susceptibility; at 40 K the contribution from these pairs is 15%, which falls rapidly to zero as the temperature is decreased. The susceptibility follows very well a Curie-Weiss law for an antiferromagnetic compound with a Weiss temperature  $\theta$  of 7 K. The agreement is good for both the ESR intensity measurements and the magnetisation measurements.

However, the two different techniques show discrepancies at lower temperatures. At around 6 K the ESR intensity starts falling off rapidly, whereas the magnetisation data show a monotonous increase of the susceptibility  $\chi(T)$ . We consider the rapid drop of the ESR intensity to be a manifestation of the thermal depopulation of the triplet state of weakly interacting vanadyl pairs. The antiferromagnetic coupling of these pairs is estimated at  $J/k = -4.7$  K. In contrast to the ESR data, the magnetic susceptibility follows the Curie-Weiss law at temperatures below 7 K. A possible explanation for this observation is the fact that ESR selects only those paramagnetic species that obey the conditions for microwave resonance. Therefore, the contribution of the weakly interacting pairs with a narrow ESR spectrum can be identified at low temperatures. Magnetisation measurements, on the contrary, will also reflect the contribution from the rapidly relaxing paramagnetic defects, which are broadened beyond detection in the ESR background.

Both ESR and magnetisation data are assumed to be compatible, and therefore the magnetic susceptibility as a function of temperature was fitted with equation 3 (for a deduction of this formula, see the appendix at the end of this chapter). In this equation the strong pairs ( $w_1$ ,  $J/k = -65.7$  K), the weak pairs ( $w_2$ ,  $J/k = -4.7$  K) and the antiferromagnetic defects ( $w_3$ ) are included.

$$\chi(T) \propto \frac{w_1}{T} \cdot \frac{4e^{2J_1/kT}}{1+3e^{2J_1/kT}} + \frac{w_2}{T} \cdot \frac{4e^{2J_2/kT}}{1+3e^{2J_2/kT}} + \frac{w_3}{T} \quad (3)$$

The defects are supposed to be isolated  $VO^{2+}$  ions having spin  $S=1/2$ . The weight factors ( $w_i$ ) are directly proportional to the number of vanadyl ions involved and result in a calculated ratio  $w_1:w_2:w_3$  of 10:7:2. The weak pairs have not been reported in literature for vanadylpyrophosphate [17,23]. Interpretation of the nature of this feature is therefore difficult.

Without a well-defined structure being available, any sensible interpretation of magnetic behaviour at the molecular level is necessarily speculative. Therefore,

many studies have focussed on the systematic magnetic characterisation of vanadium compounds with known structures. Examples include oxovanadium(IV) hydrogen phosphate hydrates, metal-intercalated layered vanadyl phosphates and organometallic vanadium complexes. The results of these studies will be discussed below.

Oxovanadium(IV) hydrogen phosphates show a large structural diversity, which results in a very rich experimental magnetic behaviour [24,25,26]. Moreover, they are all pyrolytic precursors of vanadylpyrophosphate,  $(VO)_2P_2O_7$  [1].

Various hydrogen phosphate hydrates of the general formula  $VO(HPO_4)_n \cdot nH_2O$ , with  $n = 1, 2$  or  $3$  have been isolated [25]. Although these structures are all based on linking of  $VO_6$  octahedra and  $PO_4$  tetrahedra, they are actually very different. The magnetic properties depend not only on the type of interactions (dimers, single or double chains), but also on the strength of the interaction. The observed exchange constants  $J$ , vary from  $-2K$  to  $-65.7K$ , as mentioned in Table 1 [27].

**Table 1** Magnetic parameters for  $VO(H_xPO_4)_x \cdot yH_2O$ ,  $VO(H_2AsO_4)_2$  and  $(VO)_2P_2O_7$ . **Dm** indicates (non)observed half-field transitions (Data taken from references [27,28]).

Solid	Best fit model <sup>a</sup>	-J(K)	g-tensor	Dm = 2	Reference
x = 1, y = 0.5	HD	43.0	1.966	yes	[28]
x = 1, y = 1.5	HLMC	7.0	1.965	no	[28]
x = 1, y = 2 ( $\alpha$ )	HD	23.0	1.965	yes	[25,28]
x = 1, y = 2 ( $\beta$ )	HLMC	5.0	1.965	no	[28,29]
x = 1, y = 4	HLMC	4.7	1.961	yes	[28,30]
x = 2, y = 0	HLMC	2.0	1.968	no	[28]
$VO(H_2AsO_4)_2$	HLMC	3.0	1.967	no	[28,31]
$(VO)_2P_2O_7$	HAMC ( $\alpha = 0.7$ )	65.7	1.960	yes <sup>b</sup>	[28]

<sup>a</sup>Hamiltonians used to model experimental magnetic behaviour: HD  $H = -2JS_1 \cdot S_2$  (isotropic Heisenberg dimer), HLMC  $H = -2JS_i(S_i \cdot S_{i+1})$  (Heisenberg linear magnetic chain), HAMC  $H = -2J_i S_i(S_{2i} \cdot S_{2i+1} + a S_{2i} \cdot S_{2i-1})$  (Heisenberg alternating magnetic chain).

<sup>b</sup>Weak signal detected at  $T < 15K$ .

The value of  $-4.7 K$ , observed in our VPO/bulk sample, nicely agrees with the exchange integral reported for  $VO(HPO_4) \cdot 4H_2O$  or  $\beta$ - $VO(HPO_4) \cdot 2H_2O$  (Table 1). It is known that the V-P-O samples are hygroscopic. According to equations 4 and 5 dehydration of these hydrated V-P-O phases results in a weight loss of 35 or 23 wt%, respectively [24]. The results of the thermal analysis (TGA) of our sample are represented in Figure 4.

Evidence for a new type of vanadyl pairs in  $(VO)_2P_2O_7$

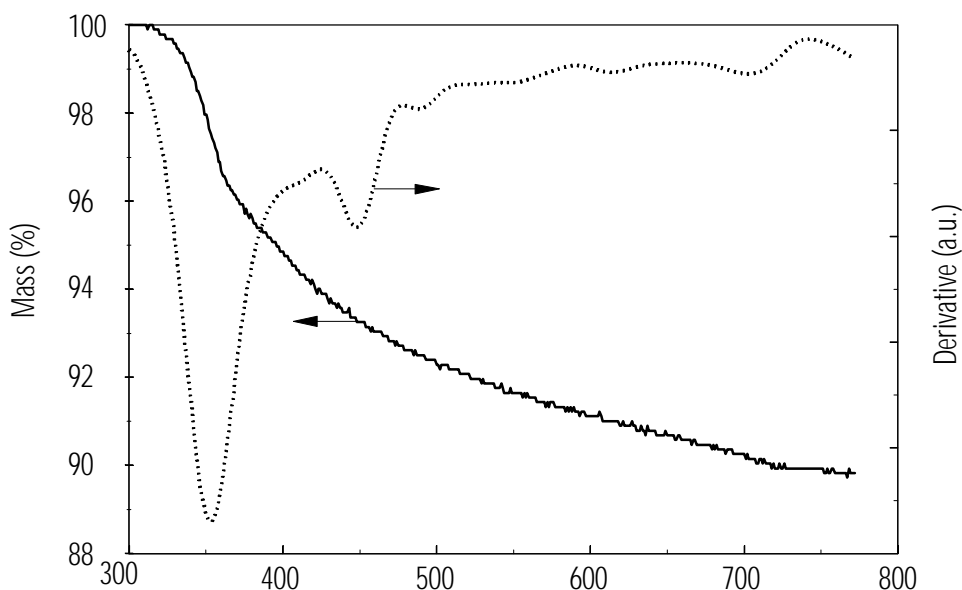


**Figure 4** Thermal analysis data of the equilibrated bulk V-P-O catalyst.

The water content of our V-P-O sample was determined to be 10 wt%. Taking into account that 37 % of the  $VO^{2+}$  ions in our sample exist as weakly interacting pairs, one cannot exclude the presence of one of the hydrated phases as the origin of the  $-4.7$  K feature. A weight loss of 13 or 9% is expected for a 37% content of  $VO(HPO_4) \cdot 4H_2O$  or  $\beta\text{-}VO(HPO_4) \cdot 2H_2O$ , respectively. Furthermore, the shape of the dehydration curve (TGA) resembles the dehydration curve of  $VO(HPO_4) \cdot 4H_2O$  to  $(VO)_2P_2O_7$  via  $\beta\text{-}VO(HPO_4) \cdot 2H_2O$  [24].

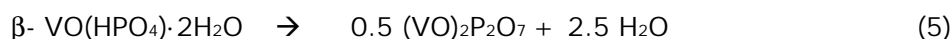
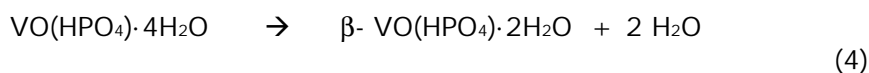
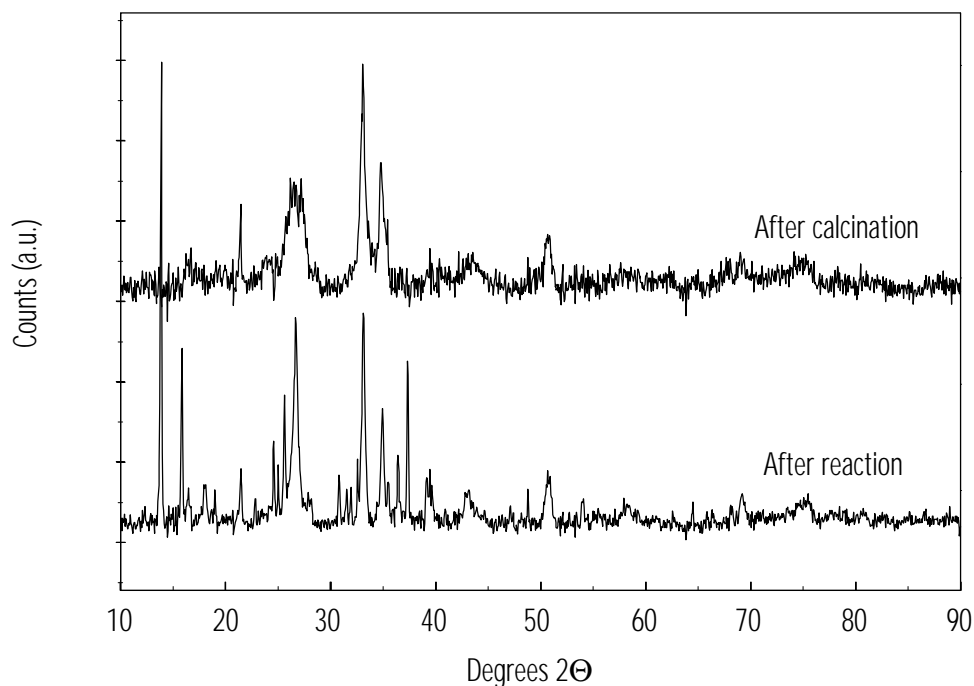


Figure 5 shows that after reaction, a distinct number of additional peaks are present in the XRD pattern of the sample. The extra peaks can be assigned to  $VO(HPO_4) \cdot 4H_2O$ , which structure has been described by Zazhigalov *et al.* [32]. However, Amoros and co-workers have found that dehydration of  $VO(HPO_4) \cdot 4H_2O$  and  $\beta\text{-}VO(HPO_4) \cdot 2H_2O$  is irreversible [24], and, therefore, rehydration to a phase with only physisorbed water is to be expected. Apparently, rehydration has taken place under or after reaction conditions, since steam is one of the reaction products.



**Figure 5** XRD patterns of VPO/bulk after calcination and after reaction.

To study this behaviour in more detail, we have saturated a freshly pre-treated bulk catalyst with water at room temperature in a humid atmosphere and collected the XRD and TGA data. We found that under the above mentioned conditions, no rehydration to a crystalline hydrated phase took place. The XRD pattern of the sample was equal to that of the freshly pre-treated sample. Only physisorbed water was evolved upon heating during TGA (not shown here).

Although we cannot exclude the presence of a hydrated phase as the origin of the -4.7 K feature, there are more possible explanations for this weak exchange interaction. Beltran *et al.* have shown that the diversity of magnetic behaviour of V-P-O compounds cannot be explained by their respective structural features only. Based on the temperature dependence of their magnetic susceptibility and ESR spectroscopic measurements and the results of their  $^{31}\text{P}$  NMR experiments, as well as semi-quantitative calculations, they proposed a model that accounts for phosphate groups involved in the spin density transfer between antiferromagnetically coupled vanadium ions [27]. A series of consistent sets of magnetic orbitals was applicable to explain the diversity of the experimental magnetic behaviour and the magnitude of the superexchange interactions in a great number of oxovanadium(IV) phosphates [26,27].

Evidence for a new type of vanadyl pairs in  $(VO)_2P_2O_7$

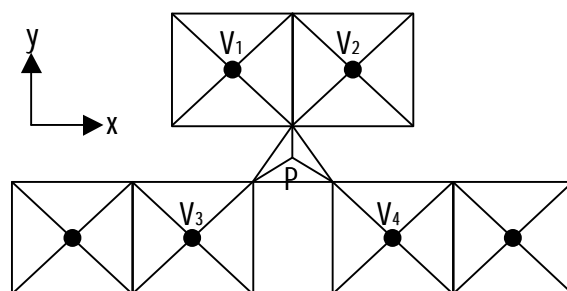


**Figure 6** Fragment of the crystal structure of  $(VO)_2P_2O_7$  projected in the  $xy$  plane. The idealised scheme shows  $\mu(O,O')$  and  $\mu(O)$  phosphate bridges (vide supra).

Figure 6 represents an idealised projection of the relevant fragment of the crystal structure of vanadylpyrophosphate [4]. Besides from the  $\mu$ -(oxo) bridges, which connect vanadium atoms of adjacent layers along the (001) direction, di- $\mu$ -(O) phosphate ( $V_1$ - $V_2$ ) bridges and two topological different types of di- $\mu$ -( $O,O'$ ) phosphate bridges ( $V_3$ - $V_4$  and  $V_1$ - $V_3$ ) can be distinguished [27].

The spin density of vanadium is mainly localised in the  $d_{xy}$  orbitals [33]. Consequently, the only phosphorus or oxygen atomic orbitals that might be involved in exchange pathways are those able to hold electronic density in the  $xy$  plane. These are the  $d_{xy}$ ,  $d_{x^2-y^2}$ ,  $p_x$  and  $p_y$  atomic orbital pairs of phosphorus and the symmetry adapted linear combinations of  $p$  atomic orbitals from the three equivalent oxygen atoms [27].

Maximum  $\pi$  overlap resulting from this atomic orbital set, and consequently the strongest magnetic interaction, is obtained when the  $VO_6$  octahedra in the different dimeric moieties ( $V_1$ - $V_2$ ,  $V_3$ - $V_4$  and  $V_1$ - $V_3$ ) are arranged in such a way that the vanadium  $d_{xy}$  orbitals are coplanar and share a lobe axis [27]. This situation is observed in  $(VO)_2P_2O_7$  (Figure 6). Any deviation from this optimal topology will result in weaker magnetic interactions. For instance, in the case of  $VO(HPO_4) \cdot 0.5H_2O$ , the 'equatorial'  $xy$  planes of the edge-sharing  $VO_6$  octahedra ( $V_1$ - $V_2$ ) define a dihedral angle of  $60^\circ$  resulting in a poorer overlap of the magnetic orbitals through the  $\mu$ -(O) phosphate bridge ( $J = -43K$ ). The inter-chain ( $V_1$ - $V_3$ ) and intra-chain ( $V_1$ - $V_4$ ) di- $\mu$ -( $O,O'$ ) phosphate bridges even become ineffective [34].

Amoros *et al.* concluded that, because of the in-plane displacement of the respective  $VO_6$  octahedra, magnetic interaction through di- $\mu$ -( $O,O'$ ) phosphate inter-chain bridges ( $V_1$ - $V_3$ ) in  $(VO)_2P_2O_7$  is also negligible [27].

The only phosphate bridges present in the structure of  $\alpha$ - $VO(HPO_4) \cdot 2H_2O$ ,  $\beta$ - $VO(HPO_4) \cdot 2H_2O$  and  $VO(HPO_4) \cdot 4H_2O$  are of the  $\mu$ -( $O,O'$ ) type [28]. Apparently, the  $VO_6$  octahedra are only adequately arranged in the case of  $\alpha$ - $VO(HPO_4) \cdot 2H_2O$ , resulting in an exchange coupling of  $-23 K$  (Table 1). The relative displacement of the  $VO_6$  octahedra along the  $z$  axis in the case of  $VO(HPO_4) \cdot 4H_2O$  [35], and the twisting of the  $VO_6$  equatorial planes in  $\beta$ - $VO(HPO_4) \cdot 2H_2O$  [36] obviously yield less effective exchange pathways through phosphate groups. Finally, Amoros *et*

*al.* state that the super-exchange through PO<sub>4</sub> groups is much more effective than through simple oxo bridges. The magnetic activity of  $\mu$ -oxo bridges would only become apparent in the absence of a suitable path involving PO<sub>4</sub> groups [27].

Other systems applied to study magnetic exchange through PO<sub>4</sub> bridging entities are layered vanadyl phosphates [37]. These structures can be generated upon the reduction of V<sup>5+</sup> centres of the native layered VOPO<sub>4</sub>·2H<sub>2</sub>O compounds by intercalation of metal ions [28]. The soft hydrothermal synthesis conditions (473 K, 2 days) [37,38] usually result in open frameworks (generally of lamellar morphology), including hydration water molecules, of a general composition described by the formula M(VOPO<sub>4</sub>)<sub>2</sub>·nH<sub>2</sub>O, (n= 4, M= Na, Ca, Sr, Pb, Co, Ni, Cu; n= 3, M= K, Rb, Pb, Ni) [39,40,41]. Furthermore, intercalation of 'Mo<sub>2</sub>O<sub>8</sub>' complex ions [42] and Cu(en)<sub>2</sub> or Ni(en)<sub>2</sub> (en= ethylenediamine) [28] have been reported in literature. These systems have all been studied with magnetic measurements and <sup>31</sup>P NMR experiments [37]. Magnetic interactions between the V<sup>4+</sup> centres in these compounds are of the order of J/k= -2K and vary from ferromagnetic to antiferromagnetic [41,42].

Roca *et al.* have defined several building blocks that were found for the various intercalated layered vanadyl phosphates [37]. In terms of these molecular building blocks, which are represented in Figure 7, there is no reason to expect alternative behaviour for the layered oxo vanadium phosphates.

Building blocks DI, DIV, and DVIII are found in (VO)<sub>2</sub>P<sub>2</sub>O<sub>7</sub>; DII, DIII, and DVIII in VO(HPO<sub>4</sub>)·0.5H<sub>2</sub>O; DV in  $\alpha$ -VO(HPO<sub>4</sub>)·2H<sub>2</sub>O; DVII in VO(HPO<sub>4</sub>)·4H<sub>2</sub>O; DX in Ba<sub>2</sub>VO(PO<sub>4</sub>)<sub>2</sub>·H<sub>2</sub>O; DXII in Ca(VOPO<sub>4</sub>)<sub>2</sub>·4H<sub>2</sub>O; and DXIII in Ba(VOPO<sub>4</sub>)<sub>2</sub>·4H<sub>2</sub>O. Chair-like V(OPO<sub>2</sub>)V links in M(VOPO<sub>4</sub>)<sub>2</sub>·nH<sub>2</sub>O vary between those of type DXII (Ca(VOPO<sub>4</sub>)<sub>2</sub>·4H<sub>2</sub>O) and DXIII (Ba(VOPO<sub>4</sub>)<sub>2</sub>·4H<sub>2</sub>O) and are similar to those found in VO(HPO<sub>4</sub>)·4H<sub>2</sub>O (DVII) [26,35].

Correlation between the <sup>31</sup>P NMR line shifts ( $\delta$ ) and the exchange constants (J) allowed Roca *et al.* to discuss the contribution of phosphate molecular orbitals to the magnetic orbitals [37]. The J vs.  $\delta$  correlation was found to be independent of the dimensionality of the magnetic interactions [37]. This supports the idea that topological parameters of the phosphate bridges in the building blocks determine the nature of the active magnetic exchange pathways. Extended Hückel calculations of the overlap potential as a function of geometry have shown that the effective orbital overlap, and consequently, the magnitude of the magnetic interaction are depending on three structural parameters, *i.e.* (i) d(Å), in-plane relative displacement of the medium basal planes of the VO<sub>6</sub> octahedra; (ii)  $\theta$ (°), out-of-plane relative displacements of the VO<sub>6</sub> medium basal planes; and (iii)  $\phi$ (°), tilting of the PO<sub>4</sub> groups relatively to the VO<sub>6</sub> octahedra [37]. For example, Papoutsakis *et al.* reported an antiferromagnetic coupling (J/k= -4.7K) accompanied by a 6.7° dihedral angle between the VO<sub>6</sub> basal planes in VO(HPO<sub>4</sub>)·4H<sub>2</sub>O [41].



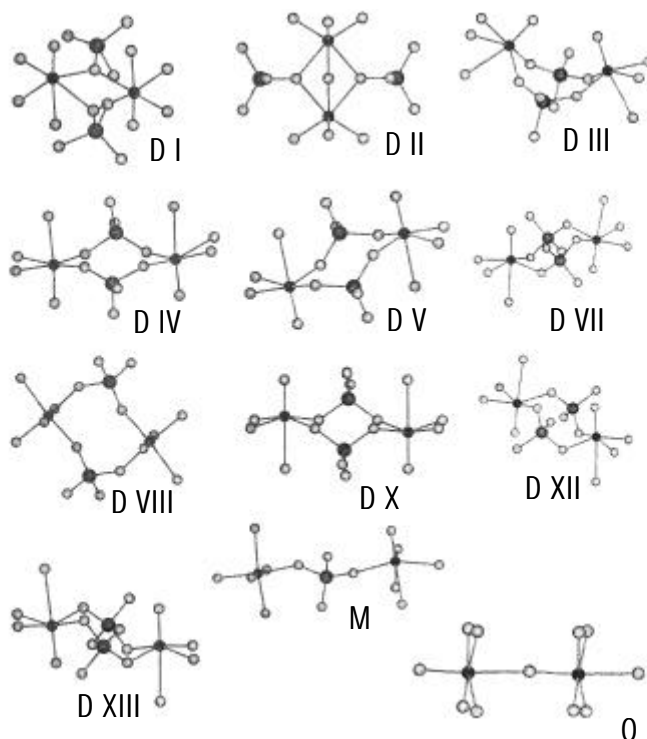


**Figure 7** Representative building blocks ( $PO_4$  and  $VO_6$ ) observed in several known structures of oxovanadium phosphates. D corresponds to di- $\mu$ -( $O,O'$ ) $PO_4$   $V(OPO)_2V$  chair-like type or di- $\mu$ -( $O$ ) $PO_4$  bridges. M and O labels refer to the magnetically less effective  $\mu$ -( $O,O'$ ) $PO_4$  and oxo ( $V=O$ ) bridges, respectively. Figure taken from ref. [37].

Intramolecular antiferromagnetic exchange has also been reported for a broad range of organometallic oxovanadium(IV) complexes, including Schiff bases, carboxylic acids and porphyrins [43]. For these compounds, the J parameter only slightly depends on the nature of substituents on the various ligands. However, the role of bridging moieties has already been recognised in the 1970s for dimeric  $V^{4+}$ ,  $Cu^{2+}$ ,  $Cr^{3+}$  and  $Fe^{3+}$  complexes [43,44]. Recently, le Bideau *et al.* have correlated the exchange integral (J) with the Hammett parameter ( $\sigma$ ) for different layered vanadyl phosphonates [45]. In these complexes, the electronic effect of substituents to the ' $V(OPO)_2V$ ' chair-like sub-units is clearly evident. The reported J/k values are  $-5.5$ ,  $-4.5$ ,  $-3.3$  and  $0$  K for  $C_6H_5$ ,  $C_6H_4$ -*p*-F,  $C_6H_4$ -*m*-F and  $C_6H_4$ -*p*- $NO_2$ , respectively [45]. Unfortunately, the authors did not specify the structural differences of these compounds.

Summarising, a broad diversity in magnetic behaviour has been reported in literature for dimeric oxovanadium(IV) compounds with J/k values ranging from  $-2$  to  $-252$  K. In general, the absolute value of the spin-spin coupling in these compounds is decreasing when the geometry of the ' $V(OPO)_2V$ ' units shows

increased deviation from the ideal octahedral geometry. Furthermore,  $J$  is smaller when the bridging unit becomes larger ( $J_{V-O-V} > J_{V-OP-O-V}$ ). Empirical data have been confirmed by quantum mechanical calculations [37].

Based on this model, we expect that the weakly interacting vanadyl groups ( $J/k = -4.7$  K) we have observed in our bulk V-P-O catalysts are located in a distorted V-P-O phase. The small exchange coupling between the  $VO^{2+}$  ions makes this distorted V-P-O phase characteristically different from vanadylpyrophosphate. This assumption was already predicted by López-Granados *et al.* who found an increased line width in ESR spectra of bulk V-P-O catalysts with an increased disorder [46]. However, these authors did not determine the exchange interactions.

### CONCLUSIONS

Combining the results from ESR and magnetisation experiments, the relative numbers of  $VO^{2+}$  ions existing in strong pairs ( $J/k = -65.7$  K), weak pairs ( $J/k = -4.7$  K), and defects in our sample are estimated to be 10:7:2, respectively.

In conclusion, this work has revealed the presence of substantial contributions of a  $V^{4+}$  phase, different from vanadylpyrophosphate in an equilibrated organic bulk V-P-O catalyst. This contribution would not have been observed with magnetisation experiments only, but manifests itself prominently in low-temperature ESR data. There are strong indications that the extra contribution is the result of the presence of  $VO(HPO_4) \cdot 4H_2O$ . This phase must be formed under reaction conditions, since steam is one of the major reaction products. At room temperature, in agreement with literature, no rehydration to any crystalline hydrated V-P-O phase was observed.

### APPENDIX

The formulae for the ESR intensity can be deduced according to the following procedure. The ESR intensity of  $N$  particles with spin  $S$ :

$$I = \frac{N}{V} \cdot \frac{(g\mu)^2}{3kT} \cdot S(S+1) \quad (6)$$

For a system with  $N_d$  ions as defects ( $S = 1/2$ ),  $N_{wp}$  ions as weak pairs ( $\frac{N_{wp}}{2}$  pairs,  $S = 1$ ,  $J/k = -4.7$  K), and  $N_{sp}$  ions as strong pairs ( $\frac{N_{sp}}{2}$  pairs,  $S = 1$ ,  $J/k = -65.7$  K) the ESR intensity equals:

$$I = \frac{(g\mu)^2}{V3kT} \cdot \left\{ \frac{3}{4} \cdot N_d + 2 \cdot \frac{N_{sp}}{2} \cdot \frac{3e^{-131.4/kT}}{1+3e^{-131.4/kT}} + 2 \cdot \frac{N_{wp}}{2} \cdot \frac{3e^{-9.4/kT}}{1+3e^{-9.4/kT}} \right\} \quad (7)$$

$$= \frac{(g\mu)^2}{V3kT} \cdot \frac{3}{4} \cdot \left\{ N_d + N_{sp} \cdot \frac{4e^{-131.4/kT}}{1 + 3e^{-131.4/kT}} + N_{wp} \cdot \frac{4e^{-9.4/kT}}{1 + 3e^{-9.4/kT}} \right\} \quad (8)$$

## REFERENCES

- 1 B.K. Hodnett, *Catal. Rev. -Sci. Eng.* **27**(3) (1985), 373
- 2 G. Centi, F. Trifirò, J.R. Ebner, V.M. Franchetti, *Chem. Rev.* **88** (1988), 55
- 3 G. Centi, *Catal. Today* **16**, (1993), 5
- 4 P.T. Nguyen, R.D. Hoffman, A.W. Sleight, *Mater. Res. Bull.* **30** (1995), 1055
- 5 P.A. Agaskar, L. De Caul, R.K. Graselli, *Catal. Lett.* **23** (1994), 339
- 6 B. Schiott, K.A. Jorgensen, *Catal. Today* **16** (1993), 79
- 7 D. Ye, A. Satsuma, T. Hattori, Y. Murakami, *J. Chem. Soc., Chem. Commun.* (1990), 1337
- 8 A. Satsuma, Y. Tanaka, A. Hattori, T. Hattori, Y. Murakami, *J. Chem. Soc., Chem. Commun.* (1994), 1073
- 9 E. Bordes, *Catal. Today* **1** (1987), 499
- 10 M.T. Sananes, A. Tuel, J.C. Volta, *J. Catal.* **145** (1994), 251
- 11 N. Harrouch Batis, H. Batis, A. Ghorbel, J.C. Vedrine, J.C. Volta, *J. Catal.* **128** (1991), 248
- 12 G. Bergeret, M. David, J.P. Broyer, J.C. Volta, G. Hecquet, *Catal. Today* **1** (1987), 37
- 13 R.A. Overbeek, M. Versluijs-Helder, P.A. Warringa, E.J. Bosma, J.W. Geus, *Stud. Surf. Sci. Catal.* **82** (1994), 183
- 14 K. Katsumoto, D.M. Marquis, US Patent **4,132,670** (1970)
- 15 R.A. Overbeek, *New aspects of the selective oxidation of n-butane to maleic anhydride: The development of a novel catalyst*, Thesis, Utrecht University, 1994
- 16 D.C. Johnston, J.W. Johnson, D.P. Goshorn, A.J. Jacobsen, *Phys. Rev B* **35** (1987), 219
- 17 D.C. Johnston, J.W. Johnson, *J. Chem. Soc. Chem. Commun.* (1985), 1720
- 18 Y. Zhang-Lin, M. Forissier, J.C. Vedrine, J.C. Volta., *J. Catal.* **145** (1994) 267
- 19 A. Bencini, D. Gatteschi, *EPR of exchange coupled systems*, Springer-Verlach, Berlin, 1990
- 20 C.J. Ballhausen, H.B. Gray, *Inorg. Chem.* **1** (1962), 111
- 21 M. Nakamura, K. Kawai, Y. Fujiwara, *J. Catal.* **34** (1974), 345
- 22 B. Scott, D.A. Cleary, *Mater. Res. Bul.* **26** (1991), 857
- 23 D.C. Johnston, J.W. Johnson, D.P. Goshorn, A.J. Jacobson, *Phys. Rev. B.* **35** (1987), 219
- 24 P. Amoros, R. Ibanez, A. Beltran, D. Beltran, A. Fuertes, P. Gomez, E. Hernandez, J. Rodriguez, *Chem. Mater.* **3** (1991), 407
- 25 G. Villeneuve, K.S. Suh, P. Amoros, N. Casan, D. Beltran, *Chem. Mater.* **4** (1992), 108

Chapter 3

- 26 D. Beltran, A. Beltran, P. Amoros, R. Ibanez, E. Martinez, A. Le Bail, G. Ferey, G. Villeneuve, *Eur. J. Solid State Inorg. Chem.* **28** (1991), 131
- 27 P. Amoros, A. Beltran, D. Beltran, *J. Alloys and Compounds* **188** (1992), 123
- 28 D. Beltran, P. Amoros, R. Ibanez, E. Martinez, A. Beltran, A. Le Bail, G. Ferey, G. Villeneuve, *Solid State Ionics* **32** (1989), 57
- 29 A. Le Bail, G. Ferey, P. Amoros, D. Beltran, G. Villeneuve, *J. Solid State Chem.* **79** (1989), 169
- 30 J. Wroblewski, *Inorg. Chem.* **27** (1988), 946
- 31 P. Amoros, A. Beltran, D. Beltran, G. Villeneuve, *Eur. J. Solid State Inorg. Chem.* **29** (1992), 257
- 32 V. Zazhigalov, V. Belousov, G. Ludwig, G. Komashko, A. Pyatnitskaya, *Sov. Prog. Chem.* **54** (1988), 36
- 33 P. Amoros, R. Ibanez, A. Beltran, D. Beltran, *J. Chem. Soc. Dalton Trans.* (1988), 1665
- 34 C.C. Torardi, J.C. Calabrese, *Inorg. Chem.* **23** (1984), 1308
- 35 M.E. Leonowicz, J.W. Johnson, J.F. Brody, H.F. Shanson, J.M. Newsam, *J. Solid State Chem.* **56** (1985), 370
- 36 A. Le Bail, G. Ferey, P. Amoros, D. Beltran, G. Villeneuve, *J. Solid State Chem.* **79** (1989), 169
- 37 M. Roca, P. Amoros, J. Cano, M.D. Marcos, J. Alamo, A. Beltran, D. Beltran, *Inorg. Chem.* **37** (1998), 3167
- 38 M. Roca, M.D. Marcos, P. Amoros, J. Alamo, A. Beltran, D. Beltran, *Inorg. Chem.* **36** (1997), 3414
- 39 S.L. Wang, H.Y. Kang, C.Y. Cheng, K.H. Lii, *Inorg. Chem.* **30** (1991), 3496
- 40 H.Y. Kang, W.C. Lee, S.L. Wang, K.H. Lii, *Inorg. Chem.* **31** (1992), 4743
- 41 D. Papoutsakis, J.E. Jackson, D.G. Nocera, *Inorg. Chem.* **35** (1996), 800
- 42 Y. Shin, D.G. Nocera, *J. Am. Chem. Soc.* **114** (1992), 1264
- 43 A. Syamal, *Coord. Chem. Rev.* **16** (1975), 309
- 44 D.J. Hodgson, *Prog. Inorg. Chem.* **19** (1975), 173
- 45 J. Le Bideau, D. Papoutsakis, J.E. Jackson, D.G. Nocera, *J. Am. Chem. Soc.* **119** (1997), 1313
- 46 M. López-Granados, J.C. Conesa, M. Fernández-García, *J. Catal.* **141** (1993), 671

# 4

## DETERMINATION OF THE SURFACE COMPOSITION OF V-P-O CATALYSTS AN XPS AND LEIS STUDY

---

### ABSTRACT

The surface P/V ratio of various V-P-O catalysts has been investigated using X-ray Photoelectron Spectroscopy (XPS) and Low-Energy Ion Scattering (LEIS). XPS data showed that the surface of bulk V-P-O catalysts was only slightly enriched with phosphate, with calculated surface P/V ratios ranging from 1.03 to 1.21. The average oxidation state of the surface vanadium atoms was determined to be  $+4.0 \pm 0.1$  and a significant amount of carbon appeared to be present.

Interpretation of the LEIS data of the bulk V-P-O catalysts is severely complicated due to the presence of these carbonaceous surface species. The surface of the organic bulk V-P-O catalyst contained about the same amount of carbon as the aqueous VPO/bulk catalyst. This amount of carbon was large enough to complicate the LEIS analyses due to the shielding of other surface elements.

After removal of the carbon layer by a combustion treatment in air (200 mbar O<sub>2</sub>) at 573 K, a surface P/V ratio of  $1.5 \pm 0.5$  was determined for the aqueous bulk catalyst. Quantification of the P/V ratio of the supported V-P-O catalysts is less impeded by the presence of carbon, due to the larger specific surface area of the samples. However, the peaks of the <sup>31</sup>P and the <sup>30</sup>Si isotopes are too poorly resolved to enable one to establish the P/V ratio of the silica-supported catalyst. Nevertheless, it is shown that after more than 100 hours time-on-stream, less phosphate was present on the surface of the spent catalyst.

## INTRODUCTION

It is generally mentioned in the literature that a prerequisite for optimum catalytic performance of V-P-O catalysts is the addition of an overstoichiometric amount of phosphate during the preparation. The best catalytic performance has been reported for catalysts of a preparative P/V ratio of 1.1 [1]. The extra phosphate is believed to be present at the surface of the V-P-O catalyst. Chapters 5 and 6 of this thesis, however, will show that the actual structure and composition of the surface layers of the bulk V-P-O catalyst are still very poorly known. One of the frequently applied characterisation techniques is X-ray Photoelectron Spectroscopy (XPS), which in principle can be used to determine the average oxidation state of the vanadium ions in the surface layers, as well as the surface P/V ratio.

Though several groups have employed XPS, univocal results have not been obtained [2,3,4,5,6,7,8,9,10,11]. Generally, the experimental P/V ratio ranges from 1.5 to 3, which is much higher than the stoichiometric bulk value of vanadyl phosphates, *i.e.* 1.0.

In our opinion, it is not surprising to observe relatively high surface P/V ratios. The bulk V-P-O catalysts usually show specific surface areas ranging from 5 to 35 m<sup>2</sup>/g. Generally, about 10% of extra phosphate is added during the preparation [12]. Assuming that the bulk indeed consists of stoichiometric vanadyl phosphate (P/V=1.0), the excess phosphate must either be present at the surface as terminal (pyro)phosphate groups, or be poorly bound to the surface and be removed during the synthesis procedure. In the first case, the surface P/V ratio is dependent on the specific surface area of the sample, which is not reported in literature [10].

However, Coulston and co-workers have calculated the dependency of the P/V ratio on the morphology of vanadylpyrophosphate [11]. Their results indicate that exposure of the different crystal planes of vanadylpyrophosphate will result in maximum surface P/V ratios of 1.015 (021 plane), 0.986 (001 plane), 1.098 (100 plane, phosphate termination), and 1.136 (100 plane, pyrophosphate termination) [11]. These numbers indicate that only a limited amount of excess phosphate can be bound at the surface of vanadylpyrophosphate. Consequently, all phosphate exceeding the above mentioned limits has to be poorly bound and might be removed during synthesis.

More phosphate could be present at the surface when different surface V-P-O phases are formed. Morishige *et al.* proposed that the high experimentally observed P/V ratio is the result of the presence of an amorphous metaphosphate phase on the surface [7]. VO(PO<sub>3</sub>)<sub>2</sub> would be formed upon thermal pretreatment of VO(H<sub>2</sub>PO<sub>4</sub>)<sub>2</sub>, present in the VO(HPO<sub>4</sub>)·0.5H<sub>2</sub>O precursor as a contaminant [4,7]. Sananes and co-workers have shown that this poorly active VO(PO<sub>3</sub>)<sub>2</sub> phase has a surface P/V ratio of 4.0, which is much higher than the generally observed values for vanadium phosphates [13,14].

Delichere *et al.* have argued that the high experimental P/V ratios are the result of vanadium vacancies in the (amorphous) surface layers of vanadylpyrophosphate [10]. For this reason, they proposed a model in which the composition of the V-P-O catalysts is described by the general formula: [(V<sup>IV</sup><sub>(1-5x)</sub>V<sup>V</sup><sub>4x</sub>⋄<sub>x</sub>)O]<sub>2</sub>P<sub>2</sub>O<sub>7</sub>. In this formula, ⋄ is a vanadium vacancy. Nevertheless, this is not sufficient to explain

the reported experimental P/V ratios of 1.5-1.9, and other effects have to be taken into account as well.

The quantitative XPS analysis makes use of the photo-ionisation cross sections, which have been calculated for a very large number of metal oxides by Scofield [15]. However, these values have proven to be inadequate for the analysis of V-P-O XPS data [10,11]. Therefore, several authors determined experimental sensitivity factors for vanadium and phosphorus using V-P-O glasses [16,17,18]. For these compounds, it is assumed that the surface P/V ratio is the same as that of the bulk. With this approach, experimental surface P/V ratios of 1.1 to 1.4 were determined for bulk V-P-O catalysts [16,17,18]. Nevertheless, the surface P/V ratio of V-P-O glasses might also be the result of phosphorus segregation from the bulk. Therefore, the assumption that the surface P/V ratio is equal to the bulk P/V ratio is not obvious.

To overcome this problem, Coulston *et al.* have used five organometallic complexes containing vanadium and phosphorus atoms as standard materials [11]. Phosphorus segregation is not to be expected in these clusters, however it has not been proven that the ligands are stable under UHV conditions. Nevertheless, an experimental P/V ratio of 1.1 was found for a bulk V-P-O catalyst with 10% excess phosphorus [11]. This amount is in agreement with the predictions of Coulston, based on a model of phosphate groups termination the vanadylpyrophosphate surfaces [11].

Since the P/V ratios which have been determined with XPS are not satisfactory, we have applied Low-Energy Ion Scattering (LEIS) to establish the surface composition of our bulk and supported V-P-O catalysts. In contrast to XPS, which has a penetration depth of 1-5 nm (3-20 monolayers), LEIS is a technique that selectively probes the outermost atomic layer of a (catalyst) surface. This offers the opportunity to study the surface P/V ratio of V-P-O catalysts more precisely than with XPS, which averages out the surface and bulk composition of the samples.

### Low-Energy Ion Scattering

For an introduction to LEIS, we would like to mention some excellent references [19,20]. For using LEIS for composition analysis of oxidic surfaces, we refer to reference [21]. In short, a beam of mono-energetic noble gas ions (0.1-10 keV) is scattered by atoms of the target surface. These collisions can be considered as binary elastic scattering events as represented in Figure 1. Therefore, LEIS data are independent of the chemical environment of the scattering element, which is another advantage compared to XPS.

During a collision, the incident ion loses kinetic energy. The final energy ( $E_f$ ) depends on the energy of the ion before the collision ( $E_i$ ), on the mass of the ion ( $m_1$ ), on the mass of the surface atom ( $m_2$ ) that is scattered from and on the scattering angle ( $\Theta$ ):

$$E_f = E_i K^2(\Theta, \gamma) \quad (1)$$

## Chapter 4

Under the condition that the mass of the incident ion is smaller than the mass of the surface atom, the kinematic factor  $K$  depends on the scattering angle and the mass ratio  $\gamma = m_1/m_2$  according to:

$$K = \frac{\cos\Theta + \sqrt{\gamma^2 - \sin^2\Theta}}{1 + \gamma} \quad (2)$$

In a typical LEIS experiment, the mass and the kinetic energy of the incident ions are known and the scattered ions are detected at a fixed scattering angle ( $\Theta = 145^\circ$  in our experiments). Therefore, the energy spectrum of the scattered ions represents the mass spectrum of the surface.

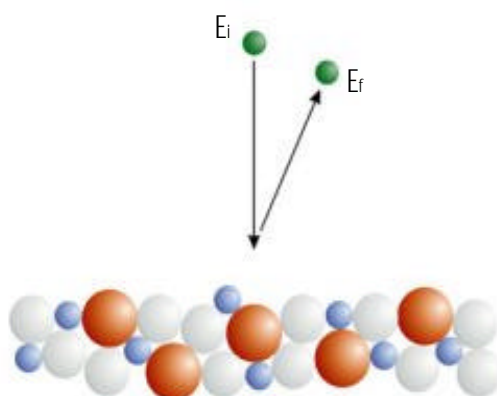


**Figure 1** Schematic representation of the binary collision model.

The technique is surface-sensitive, since almost all ions penetrating the first atomic layer will be neutralised and, therefore, are not detected. Because of the ion bombardment, atoms are sputtered from the target surface. For helium ions, a sputter dose of  $10^{16}$  ions/cm<sup>2</sup> equals about one monolayer. This allows determination of the in-depth distribution of the elements in the sample. Based on a model proposed by Matsunami and co-workers [22], we have calculated a sputter rate of 0.3 atoms/ion and 0.5 atoms/ion for vanadium and phosphorus in our samples, respectively.

### Quantification of LEIS experiments

In a LEIS experiment, the intensity of the signal,  $S$ , for scattering by element  $i$  can be expressed as:

$$S_i = I_p \cdot N_i \cdot \sigma_i \cdot P_i^+ \cdot c \quad (3)$$

In this equation,  $I_p$  represents the primary ion current,  $N_i$  the surface atomic density,  $\sigma_i$  the differential scattering cross section and  $P_i^+$  the fraction of back



scattered ions. The instrumental factor,  $c$ , includes the acceptance angle  $\Delta\Omega$  and the transmission of the energy analyser. The differential scattering cross section depends on the energy, the scattering angle and the nuclear mass and charge numbers of the collision partners.  $\sigma_i$  can be calculated with reasonable precision from the interaction between two atoms,  $Z_1$  and  $Z_2$ , and can be written in the form of a screened Coulomb potential using  $\chi$  as the screening function [19,23]:

$$V(r) = \frac{Z_1 Z_2 e^2}{r} \cdot \chi \cdot \left( \frac{r}{a} \right) \quad (4)$$

The Molière potential can be used as screening function [23]:

$$\chi = 0.35 \cdot e^{-0.3x} + 0.55 \cdot e^{-1.2x} + 0.10 \cdot e^{-6.0x} \quad (5)$$

In this equation,  $x = r/a$ , in which  $a$  equals the Thomas-Fermi screening radius for the collision:

$$a = \frac{0.885 \cdot a_0}{\left( \sqrt{Z_1} + \sqrt{Z_2} \right)^{2/3}} \quad (6)$$

The values of  $a$  usually are between 0.1 Å and 0.2 Å for most interactions. However, quantification is difficult because in equation 4,  $P_i^+$  usually is poorly known as the sensitivity of LEIS varies with the probed element. Best standards are single-crystal faces of pure elements or alloys, of which the surface atomic density,  $N_i$  is exactly known. For elements, such as vanadium and phosphorus, standard samples exposing stable and well-defined surface structures are not available. For this reason, quantitative analysis is usually performed using the dual isotope surface composition (DISC) method, described by Ackermans *et al.* [24]. The DISC method is based on the comparison of LEIS spectra recorded with  $^3\text{He}^+$  and  $^4\text{He}^+$  to determine the experimental  $P^+$  factor.

## EXPERIMENTAL

### XPS

XPS spectra were obtained with a VG Clam 2 spectrometer equipped with a Mg  $K\alpha$  source and a hemispherical analyser connected to a single-channel detector. Measurements were done at 20 eV pass energy. The background pressure during data acquisition was kept below  $10^{-8}$  mbar. The samples were crushed and mounted on an iron stub carrying an indium film.

In general, XPS averages the surface and bulk contributions in the spectra. Therefore, our experiments were performed at two different positions of the X-ray source, *i.e.* at angles of  $0^\circ$  and  $60^\circ$ , respectively. This will result in different

## Chapter 4

penetration depths of the applied X-rays and, consequently, a different sensitivity for the surface of the sample.

Peak areas were determined using Gauss-Lorentz curves and a Shirley background subtraction procedure [25]. The applied atomic sensitivity factors were 2.116 (V), 0.486 (P) and 0.296 (C), respectively [26]. The average oxidation state (AV) of the surface vanadium atoms was calculated with an empirical formula reported by Coulston *et al.* [11]:

$$AV = 13.82 - 0.68 \cdot [O(1s) - V(2p_{3/2})] \quad (7)$$

In this formula, O(1s) and V(2p<sub>3/2</sub>) are the absolute values of the electron binding energies. With this method, correction of the peak positions for charging of the sample is not necessary.

### LEIS

LEIS experiments were performed in the Section Physics of Surfaces and Interfaces at the Technical University of Eindhoven, using the Energy Resolved Ion Scattering Spectrometer (ERISS), allowing one to perform static LEIS. A disadvantage is that ion bombardment in the LEIS process modifies the surface structure and/or the surface composition. Therefore, it is important to execute LEIS experiments under static conditions, *i.e.* with no detectable sputter damage. Static conditions require that the ion dose is thus low ( $10^{13}$ - $10^{14}$  ions/cm<sup>2</sup>) that subsequent LEIS spectra are identical. The effect of sputter damage can be reduced by scanning the beam over a larger sample area and using a more effective analyser of the backscattered ions, as applied in the ERISS. The base pressure of this system was  $1 \cdot 10^{-9}$  mbar.

Different ions, *i.e.* <sup>3</sup>He<sup>+</sup> and <sup>4</sup>He<sup>+</sup>, were used with an energy, E<sub>i</sub>, of 3 keV. Prior to the experiments, the samples were kept for 30 minutes at 373 K in He to remove physisorbed water and other contaminants.

### Catalyst preparation

In this investigation, we used various different samples, *viz.* VPO/bulk-org and VPO/bulk-aq, and VPO/SiO<sub>2</sub>. Sample preparation has been described in chapter 2 of this thesis. VPO/bulk-org and VPO/bulk-aq have been used to study the differences between the two preparation procedures. VPO/bulk-org was prepared with two different P/V ratios, *i.e.* 1.0 and 1.1, and the results on these catalysts are compared. Furthermore, a comparison is made between LEIS results on the VPO/SiO<sub>2</sub> and on the VPO/bulk catalysts. Finally, the results with the VPO/SiO<sub>2</sub> catalysts before and after use in the catalytic reaction are compared for more than 100 hours time-on-stream.

## RESULTS and DISCUSSION

### XPS

Tables 1 and 2 represent the XPS data for the VPO/bulk samples at two different incident angles of the X-rays ( $0^\circ$  and  $60^\circ$ , respectively). The data in Table 2 are more sensitive for surface contributions.

**Table 1** XPS data of the VPO/bulk catalysts. Data were collected with an incident beam angle of  $0^\circ$ .

Sample	P/V	V/C	AV
VPO/bulk-org P/V 1.0	1.06	0.80	4.0
VPO/bulk-org P/V 1.1	0.89	1.83	4.1
VPO/bulk-aq P/V 1.1	1.12	1.57	4.0

Table 1 indicates that all samples mainly consist of  $V^{4+}$ . However, in the VPO/bulk-org samples a small amount of  $V^{5+}$  is present too. This is in agreement with the literature, where AV-values of 4.02-4.3 have been reported for V-P-O catalysts [27]. Moreover, the data found with VPO/bulk-org P/V 1.1 are in agreement with the results reported in chapter 3 of this thesis, where we have shown that about 10% of the vanadyl groups in this catalyst exist as  $V^{5+}$  defects. Nevertheless, one should be careful with drawing conclusions from these values. A difference of 0.1 eV in the peak positions already results in a difference in the AV values of 0.07. In general, the resolution of an XPS spectrometer amounts to 0.25 eV and, hence, the differences in AV could be within the experimental error of the XPS measurements.

The observed P/V ratios are smaller than those reported in the literature for bulk V-P-O catalysts, which are ranging from 1.5 to 3.0 [1,27]. For VPO/bulk-org P/V 1.1, we even observed a P/V ratio smaller than the stoichiometric value of 1.0. This indicates that vanadium enrichment of the surface has taken place. Coulston and co-workers were the first to report similar results for  $\beta$ -VOPO<sub>4</sub> [11]. In literature, it is argued that an over-stoichiometric amount of phosphorus at the surface stabilises the  $V^{4+}$  oxidation state [1]. Our data are in agreement with this idea; the higher the P/V ratio, the lower the average vanadium oxidation state.

A large amount of carbon is observed in the VPO/bulk samples, regardless of the preparation procedure (organic or aqueous). This indicates that not only residual carbon from the organic solvents used, but also traces (ppm) of organic contamination from the aqueous preparation result in the formation of 1-2 monolayers of carbon. This has consequences for the interpretation of our LEIS data (*vide infra*).

The penetration depth with these XPS experiments was rather high and this might be the reason that the measured P/V ratios and the average oxidation states are close to the bulk values. Therefore, we have carried out additional XPS experiments with a different incident angle in order to obtain XPS data that are more sensitive to the surface composition. The results of these experiments are represented in Table 2. From this table, two general trends can be observed for all

samples, *i.e.* the experimental P/V ratio is higher and the contribution of carbon to the spectra has increased. The calculated AV values of Tables 1 and 2 are comparable within the experimental error. When surface phosphate enrichment and carbon deposition on the surface of the V-P-O catalysts are assumed, these observations are in line with the idea that with a decreased incident angle more surface sensitivity is obtained. However, the penetration depth at this incident angle is still several monolayers and, hence, the real surface P/V ratio is averaged with the bulk P/V ratio.

**Table 2** XPS data of the VPO/bulk catalysts. Data were collected with an incident beam angle of 60°.

Sample	P/V	V/C	AV
VPO/bulk-org P/V 1.0	1.19	0.53	3.9
VPO/bulk-org P/V 1.1	1.21	1.47	4.0
VPO/bulk-aq P/V 1.1	1.03	0.83	4.0

The VPO/SiO<sub>2</sub> sample, which was prepared in aqueous media, contains much less carbon. In our opinion, this is the result of the much larger specific surface area of this catalyst as compared to the bulk catalysts, *i.e.* 9 m<sup>2</sup>/g for VPO/bulk-org and 54 m<sup>2</sup>/g for VPO/SiO<sub>2</sub>, respectively [28]. Therefore, the carbon is spread over a much larger surface area for VPO/SiO<sub>2</sub>, and consequently less shielding of the V-P-O contributions is to be expected. However, we were not able to determine the V 2p peak area because of a strong interference with the O 1s satellite peak. Due to the complex peak pattern, we were not able to determine the P/V ratio and the average vanadium oxidation state for the VPO/SiO<sub>2</sub> samples.

### LEIS

Figure 2 represents a typical LEIS spectrum that was obtained with a VPO/bulk-aq catalyst (left) and a silica-supported V-P-O catalyst (right). In the spectrum of VPO/bulk (<sup>3</sup>He<sup>+</sup>), the peaks arising from carbon, vanadium, phosphorus and oxygen are clearly visible and nicely separated. When <sup>4</sup>He<sup>+</sup> was employed, no carbon was observed in the spectra of the VPO/bulk catalysts and of VPO/SiO<sub>2</sub>. This does not mean that no carbon is present at the surface, but it is the result of the fact that elements of a relatively low atomic number are not probed by <sup>4</sup>He<sup>+</sup>. In the spectra of the supported V-P-O catalysts, the presence of silicon at the surface is clearly visible. This indicates that the V-P-O phase was present as clusters and not as a thin surface layer completely covering the silica surface, resulting in the exposition of bare silica. The peaks of <sup>29</sup>Si, <sup>30</sup>Si and <sup>31</sup>P overlap, because the loading of this sample was about 20%, and hence the Si/P ratio was quite high. For this reason, we were not able to quantify the data of the VPO/SiO<sub>2</sub> catalyst, and we used the (P + Si)/V ratio instead.

Determination of the surface composition of V-P-O catalysts

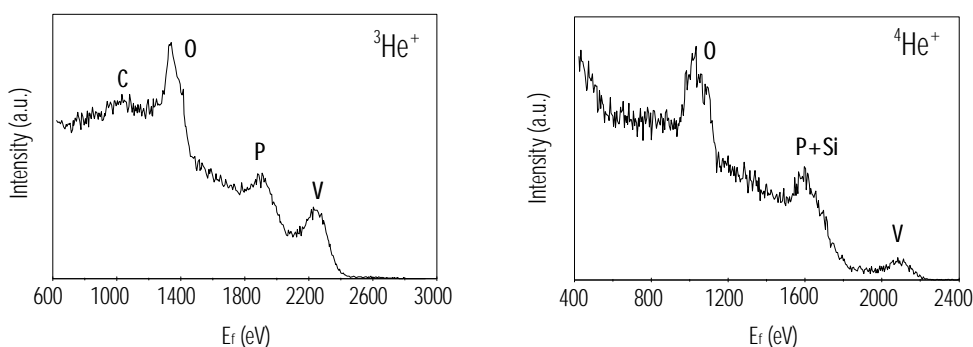


**Figure 2** Typical LEIS  ${}^3\text{He}^+$  spectrum of VPO/bulk-aq (left) and  ${}^4\text{He}^+$  spectrum of VPO/SiO<sub>2</sub> (right).

In the literature, only one LEIS study on V-P-O compounds has been reported [10]. Delichere and co-workers have reported a LEIS investigation on various bulk V-P-O catalysts with different P/V ratios, different pre-treatments and different times-on-stream in the *n*-butane oxidation reaction [10]. However, the intensity of their ion beam was relatively high. Consequently, the surface of their samples must have been severely damaged by sputtering already within the first minutes of their analyses. In agreement with our results, Delichere and co-workers have observed a large amount of carbon on the surface of their bulk V-P-O catalysts. However, it is not clear whether they considered the shielding effects of these carbon contaminants with the quantification of their LEIS data.

We have taken several spectra after a certain period of time under the He<sup>+</sup> beam and the peak areas were determined. Due to sputtering effects, depth profiles of the samples have been obtained in this way. Figures 3 and 4 represent the vanadium, phosphorus and oxygen signals as a function of the ion dose for the VPO/bulk-org catalysts. In these figures, the major contribution in the spectra is originating from surface oxygen atoms, followed by that of vanadium. The intensity of the phosphorus signal is relatively low, which can be attributed to shielding effects. We expect that the surface is terminated by (pyro)phosphate groups and, hence, relatively more oxygen is assumed to be present.

Furthermore, the surface phosphate species are terminated by P=O or P-OH groups and, consequently, the phosphorus atoms are shielded by oxygen atoms. This explains the low P intensity. Surface vanadium atoms are generally expected to be terminated by V-OH groups, V=O (vanadyl) groups or Lewis acid V- $\delta$  (vacancy) sites. Vanadium is already observed after an ion dose of 10<sup>13</sup> ions/cm<sup>2</sup>, which is about 5% of the amount of ions necessary to remove one monolayer. This means that free Lewis-acid vanadium sites, which are not shielded by phosphate or contaminants, must be present at the surface. This, together with the higher atomic mass of vanadium, can explain the relatively high intensity of vanadium in the LEIS spectra.

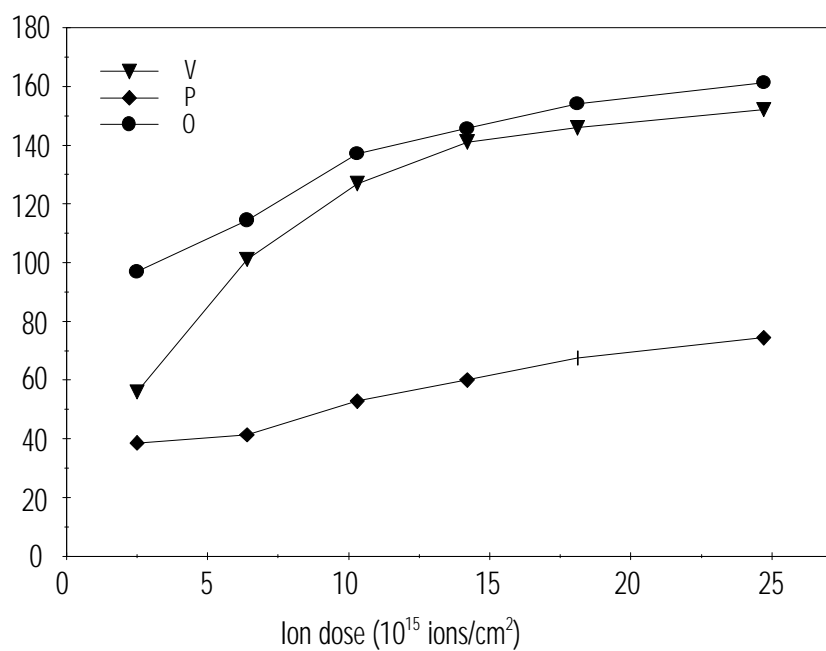


**Figure 3** V, P, O peak areas as a function of ion dose for VPO/bulk-org with a P/V ratio 1.0 ( $^4\text{He}^+$ )

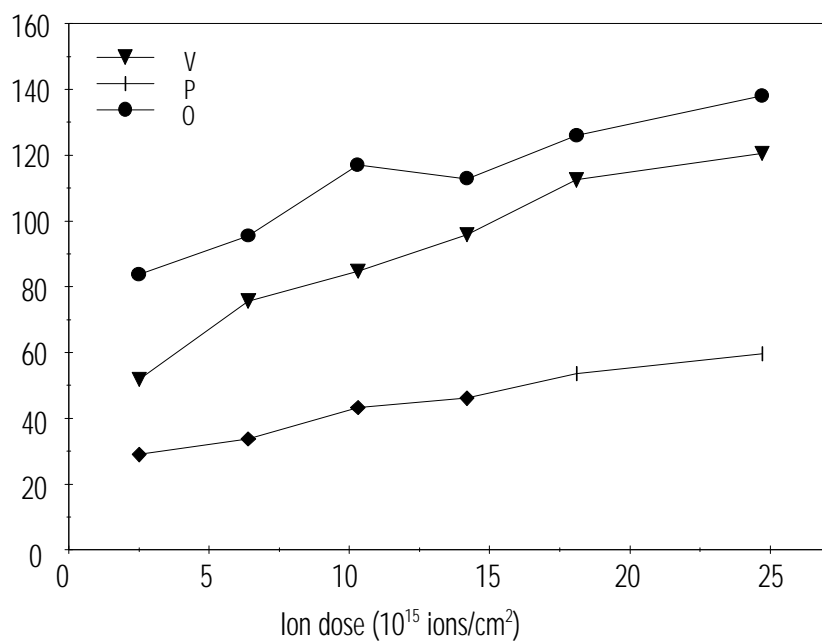


**Figure 4** V, P and O peak areas as a function of ion dose for VPO/bulk-org with a P/V ratio 1.1 ( $^4\text{He}^+$ ).

For all VPO/bulk catalysts the intensity of the signals arising from the surface components increases according to the sequence phosphorus < vanadium < oxygen. In chapter 3 of this thesis, we have shown that the VPO/bulk-org sample contains only 63% vanadylpyrophosphate,  $(VO)_2P_2O_7$ , of which a stoichiometric ratio for V:P:O of 1:1:4.5 is calculated. Due to the possible presence of other phases, a deviating surface composition and mass differences between the various surface components, the experimental ratio is far from the stoichiometric ratio. Furthermore, a significant amount of the surface of the V-P-O samples is covered by carbonaceous species. Since we don't know whether the carbon is equally spread over the surface or preferentially adsorbed on a specific element or type of surface-terminating group, it is hard to draw any conclusions from these data.

The changes in the intensities of the V, P, and O signals with time under the ion beam are the result of sputtering effects. The LEIS spectra exhibit a definite evolution with a growth of the vanadium and oxygen signals and a smaller increase of the phosphorus signal as shown in Figures 3 and 4. This behaviour is very typical of the initial sputtering of a contaminating surface layer, such as water or hydrogen and/or carbon containing species [29]. The increase is most pronounced for vanadium, which would indicate that this element is preferably covered with contaminants [10]. The same trends were observed with the VPO/bulk-aq sample, but these data are not shown here.

The presence of strongly adsorbed water molecules that were not removed during the drying procedure or hydrogen atoms from terminating OH groups could be the explanation for the increase of the oxygen signal. The intensity of the P signal is less dependent on the ion dose and, therefore, the decreasing P/V ratio (Figure 5) can be ascribed to an increasing V signal with time.

The presence of a significant excess of phosphorus on the surface, which is screening the vanadium ions, would show a P signal decreasing and a V signal increasing in time. This is not observed. The sharp increase of the vanadium signal must be the result of the selective sputtering of contaminants deposited on vanadium. Delichere and co-workers have found the same trends and argued that the carbonaceous contaminant is preferentially adsorbed on the Lewis-acid vanadium sites [10]. Another explanation could be that the surface layer of the VPO/bulk samples is very vanadium-deficient, resulting in a sharp increase of the signal at larger depth. As indicated in Figure 5, a steady P/V ratio is observed beyond an ion dose of about  $6 \cdot 10^{15}$  (~0.6 ML). However, we can not draw any conclusions from this, because carbon is shielding at least part of the surface and we do not know to what extent the different elements are shielded. Therefore, attributing a P/V ratio to the measured values is not straightforward.

The data of the two VPO/bulk-org catalysts showed similar trends, although their P/V ratio was installed differently (1.0 and 1.1, respectively). Furthermore, both samples showed a large amount of carbon on the surface (XPS/LEIS). Consequently, quantification of our LEIS data is difficult.

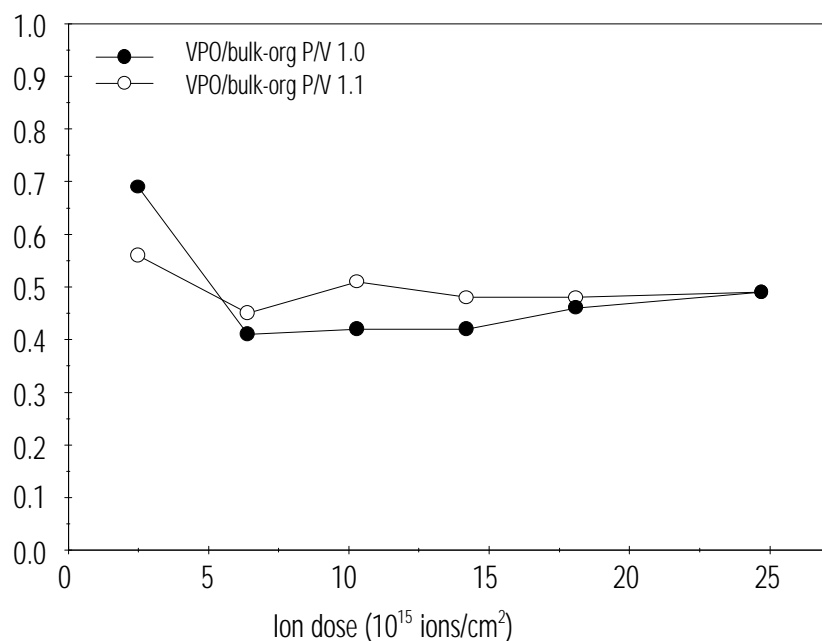


**Figure 5** Experimental P/V ratio of the two VPO/bulk-org catalysts as a function of the ion dose ( $^4\text{He}^+$ ).

Generally, quantification of LEIS spectra is still restricted to metal and alloy samples, where calibration against standards is possible. Best standards are single crystal faces, of which the surface atomic density is well known. For elements, such as vanadium and phosphorus, standard samples, which expose a stable and well-defined surface structure of a known surface atomic density, are difficult to obtain. For this reason, quantitative analysis is usually performed using the dual isotope surface composition (DISC) method [24]. Delichere *et al.* used this method to determine a relative sensitivity factor of vanadium with respect to phosphorus [10]. However, their measurements have been obstructed by the presence of carbon as well (*vide supra*).

To solve the problem of the carbonaceous surface contamination we have tried to remove the carbon by a mild oxidation of a sample (573 K in air). From the data obtained with this sample, it can be concluded that the amount of carbon had dramatically decreased as a result of the pre-treatment. However, the oxidation could also have modified the sample slightly. This change can be accompanied by structural changes of the surface or the bulk of the sample and consequently, results are not comparable to the results with the fresh samples [30].

The clean sample was used to establish the relative sensitivity factor according to the DISC method. In our investigation, this factor was determined to be  $1.5 \pm 0.5$ . Overbeek determined the surface P/V ratio of various supported V-P-O catalysts with XPS [31,32,33] and found values in the range of 1.9 to 2.9. However, Overbeek has used the standard atomic sensitivity factors, which have proven to



be less satisfactory [10,11]. Unfortunately, we were not able to perform an acceptable fit of the XPS data to obtain a reliable P/V ratio. However, LEIS is not suffering from this disadvantage. As mentioned before, the LEIS data of the supported V-P-O samples are much less affected by the presence of carbon on the surface. Nonetheless, the LEIS data of the silica-supported V-P-O catalyst are complicated by the overlap of the  $^{30}\text{Si}$  and the  $^{31}\text{P}$  signals, as can be seen in Figure 2. We would be able to separate these signals by curve fitting of the silicon and phosphorus peaks. However, to do so, appropriate phosphorus-containing reference compounds are necessary.

Figure 6 represents the V, P and O signal as a function of the ion dose of VPO/SiO<sub>2</sub> after reaction. The fresh sample shows the same trends. It is clear that the most intense signal is arising from oxygen. This can be either oxygen from the V-P-O phase, or from the silica support material. Due to the extra contribution from Si, the (P + Si) signal is more intense than the V signal.

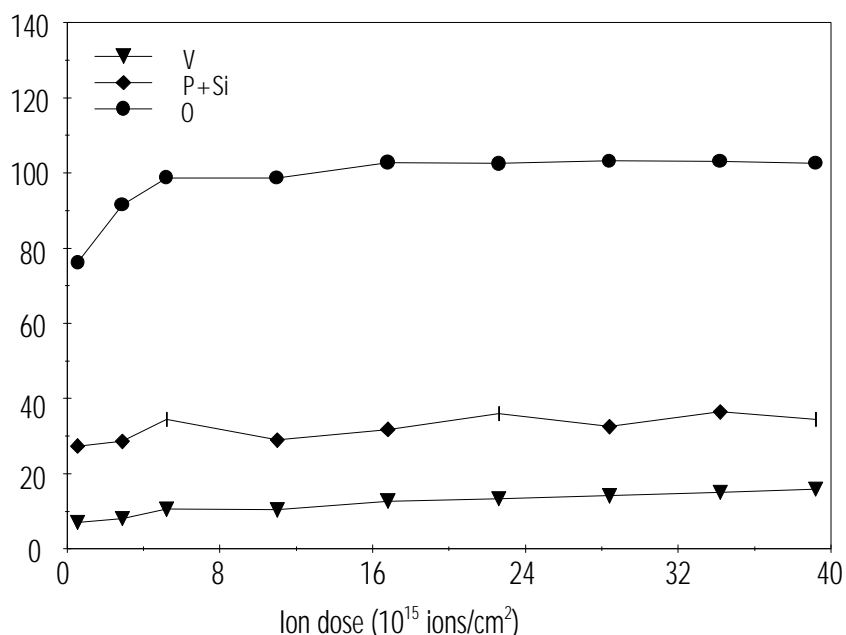


**Figure 6** V, P and O peak areas as a function of ion dose for VPO/SiO<sub>2</sub> with a P/V ratio 1.1 ( $^4\text{He}^+$ ).

Figure 7 represents the LEIS intensities of the various elements in the spectra of a fresh VPO/SiO<sub>2</sub> and the same VPO/SiO<sub>2</sub> catalyst, which had been applied in the *n*-butane oxidation reaction for more than 100 hours. One of the important problems of the commercial operation of V-P-O catalysts is the loss of phosphate during the reaction. Therefore, we expected that the surface P/V ratio should have decreased after 100 hours time-on-stream. Although we determined the (P + Si)/V ratio instead of the P/V ratio, it is clear that this ratio is larger for the fresh sample. To

our opinion, this can only occur when the surface concentration of phosphorus atoms has decreased under reaction conditions. The depth profile shows that after removal of a few surface layers, a constant  $(P+Si)/V$  is observed for the fresh as well as for the spent sample. This ratio will equal the composition of the deeper layers of the supported V-P-O phase.

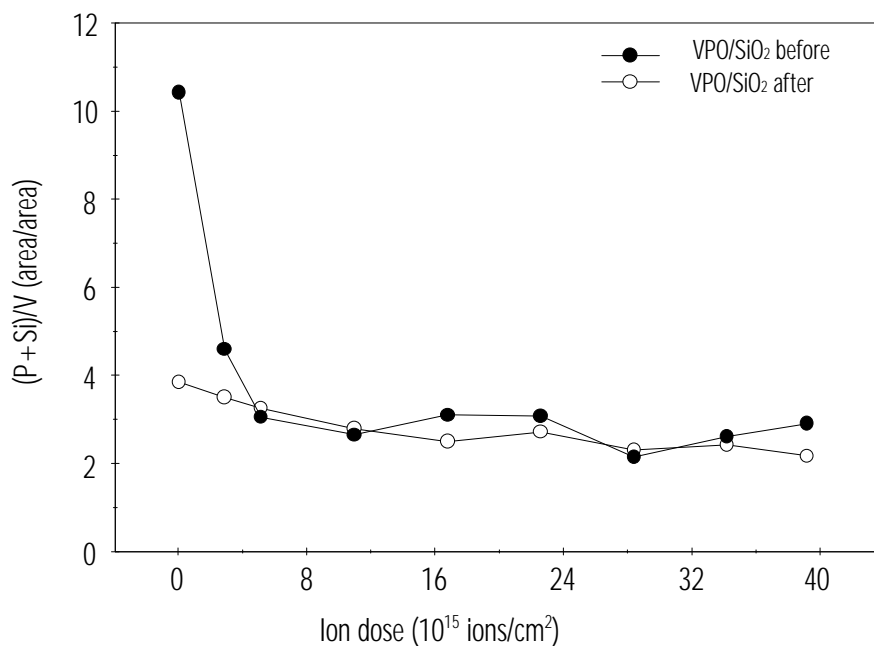


**Figure 7** Experimental  $(P+Si)/V$  ratio of  $VPO/SiO_2$  with a  $P/V$  ratio 1.1 (before and after reaction).

## CONCLUSIONS

We have applied XPS and LEIS experiments to study the surface composition of V-P-O catalysts. XPS data appeared to be inadequate because surface and bulk contributions are averaged in the spectra. Furthermore, the atomic sensitivity factors for vanadium and phosphorus have proven to be not satisfactory to enable one to quantify the XPS results. However, with experiments at different incident angles we were able to establish that surface phosphate enrichment has occurred in all VPO/bulk samples.

We have also tried to quantify indisputably the surface  $P/V$  ratio with LEIS. This technique is only sensitive for the outermost atomic layer of the specimen. However, the presence of a large amount of carbonaceous species on the surface impeded a quantitative determination of the surface  $P/V$  ratio. The amount of carbon turned out to be independent of the preparation method of the samples (aqueous or organic).

Silica-supported V-P-O catalysts showed much less carbon deposition per m<sup>2</sup> because of a larger specific surface area. However, with the supported catalysts, overlap of the silicon and phosphorus peaks complicated the analysis of the data. Nevertheless, in combination with the results in chapter 5, we have found that a spent catalyst shows a decreased surface (P+Si)/V ratio, which indicates that phosphate is lost under reaction conditions.

To overcome the observed drawbacks, we recommend performing LEIS experiments on pre-cleaned V-P-O catalysts. By choosing an appropriate and careful pre-treatment procedure, the carbonaceous contaminants can be removed without structural changes of the V-P-O surface.


Furthermore, peak-fitting procedures based on Si and P signals of reference compounds will make separation of the P and Si peaks in the spectra of the silica-supported V-P-O samples possible. As a phosphorus reference compound, InP could be used.

## REFERENCES

- 1 G. Centi, F. Trifirò, J.R. Ebner, and V.M. Franchetti, *Chem. Rev.* **88** (1988), 55
- 2 N. Harrouch Batis, H. Batis, A. Ghorbel, J.C. Vedrine, J.C. Volta, *J. Catal.* **128** (1991), 248
- 3 M. Abon, K.E. Béré, A. Tuel, P. Delichere, *J. Catal.* **156** (1995), 28
- 4 L.M. Cornaglia, C. Caspani, E.A. Lombardo, *Appl. Catal.* **74** (1991), 15
- 5 F. Garbassi, J. Bart, R. Tassinari, G. Vlaic, P. Labarde, *J. Catal.* **98** (1986), 317
- 6 A. Satsuma, A. Hattori, A. Futura, A. Miyamoto, T. Hattori, Y. Murakami, *J. Phys. Chem.* **92** (1988), 2275
- 7 H. Morishige, J. Tamaki, N. Miura, N. Yamazoe, *Chem. Lett.* (1990), 1513
- 8 G. Stefani, F. Budi, C. Fumagalli, G.D. Succiu, in: G. Centi, F. Trifirò (eds.), *New developments in Selective Oxidation*, Elsevier, Amsterdam, 1990, 537
- 9 P. Bastians, M. Genet, L. Daza, D. Acosta, P. Ruiz, B. Delmon, in: P. Ruiz, B. Delmon (eds.), *New developments in selective oxidation by heterogeneous catalysts*, Elsevier, Amsterdam, 1992, 267
- 10 P. Delichere, K.E. Béré, M. Abon, *Appl. Catal. A: General* **172** (1998), 295
- 11 G.W. Coulston, E.A. Thompson, N. Herron, *J. Catal.* **163** (1996), 122
- 12 G. Centi, F. Trifirò, J.R. Ebner, V.M. Franchetti, *Chem. Rev.* **88** (1988), 55
- 13 M.T. Sananes, G.J. Hutchings, J.C. Volta, *J. Chem. Soc. Chem. Commun.* (1995), 243
- 14 M.T. Sananes, G.J. Hutchings, J.C. Volta, *J. Catal.* **154** (1995), 253
- 15 J.H. Scofield, *J. Electron Spectrosc. Rel. Phen.* **8** (1976), 129
- 16 T. Shimoda, T. Okuhara, M. Misono, *Bull Chem. Soc. Jpn.* **58** (1985), 2163
- 17 T. Okuhara, M. Misono, *Catal. Today* **16** (1993), 61
- 18 B. Kubias, F. Richter, H. Papp, A. Krepel, A. Kretschmer, in: R.K. Graselli, S.T. Oyama, A.M. Gaffney, J.E. Lyons (Eds.), *Proceedings of the third world congress on oxidation catalysis*, Elsevier, Amsterdam, 1997, 461

#### Chapter 4

- 19 G.C. van Leerdam, *Surface Analysis of Catalysts by Low-Energy Ion Scattering*, Thesis, TU Eindhoven, 1991
- 20 H. Niehuis, W. Heiland, E. Taglauer, *Surf. Sci. Rep.* **17** (1993), 213
- 21 H.H. Brongersma, P.A. Groenen, J.-P. Jacobs, in: *Science of Ceramic Interfaces II*, ed. J. Nowotny, Elseviers, Amsterdam, 1994, 113
- 22 N. Matsunami, Y. Yamamura, Y. Itakawa, N. Itoh, Y. Kazumata, S. Miyagawa, K. Morita, R. Shimizu, Tawara, *At. Dat. Nucl. Dat. Tab.* **31** (1984), 1
- 23 J.F. van der Veen, *Surface Science Reports* **5** (1985), 199
- 24 P.A.J. Ackermans, M.A.P. Creuwels, H.H. Brongersma, P.J. Scanlon, *Surf. Sci.* **227** (1990), 361
- 25 D.A. Shirley, *Phys. Rev. B* **5** (1972), 4709
- 26 J.F. Moulder, W.F. Stickle, P.E. Sobol, K.D. Bomben, *Handbook of X-ray Photoelectron Spectroscopy*, J. Chastain (ed.), PE Corporation, Eden Prairie, 1992
- 27 M. Abon, J.C. Volta, *Applied Catalysis: A General* **157** (1997), 173
- 28 Chapter 5 of this thesis, and references therein
- 29 H.H. Brongersma, G.C. van Leerdam, in: H.H. Brongersma, R.A. van Santen (Eds.), *Fundamental aspects of heterogeneous catalysts studied in particle beams*, 1991, 283
- 30 R.A. Overbeek, M. Versluijs-Helder, P.A. Warringa, E.J. Bosma, J.W. Geus, *Stud. Surf. Sci. Catal.* **82** (1994), 183
- 31 R.A. Overbeek, *New aspects of the selective oxidation of n-butane to maleic anhydride: The development of a novel catalyst*, Thesis, Utrecht University, 1994
- 32 R.A. Overbeek, A.R.C.J. Pekelharing, A.J. van Dillen, J.W. Geus, *Applied Catalysis A: General* **135** (1996), 231
- 33 R.A. Overbeek, P.A. Warringa, M.J.D. Crombag, L.M. Visser, A.J. van Dillen, J.W. Geus, *Applied Catalysis A: General* **135** (1996), 209



---

## COMPARISON OF BULK AND SUPPORTED V-P-O CATALYSTS NEW INSIGHTS IN THE ACTIVE PHASE IN C4 OXIDATION TO MA

### ABSTRACT

V-P-O catalysts supported on the surface of silica and titania particles were studied and results are compared with those obtained from bulk V-P-O. The catalytic performance was tested in the *n*-butane oxidation reaction to maleic anhydride and the structure of the (equilibrated) catalysts after the catalytic reaction was characterised with X-ray absorption spectroscopy (XAFS) and (low-temperature) Electron Spin Resonance spectroscopy (ESR).

Our results show considerable differences in catalytic performance between VPO/TiO<sub>2</sub>, on the one, and VPO/SiO<sub>2</sub> and VPO/bulk, on the other hand. The yield to maleic anhydride is comparable for VPO/bulk and VPO/SiO<sub>2</sub>.

The differences in catalytic behaviour are attributed to differences in the local structure around vanadium (XAFS). Furthermore, different spin exchange interactions between vanadium atoms in the three samples have been observed (ESR). The combination of the characterisation methods employed suggests that the structure of the supported V-P-O phase is possibly amorphous and differs considerably from that of bulk crystalline vanadylpyrophosphate.

We therefore propose that the oxidation of *n*-butane to maleic anhydride takes place over a surface V-P-O phase that does not equal vanadylpyrophosphate. This finding has high relevance for our understanding of the catalytic activity of bulk crystalline V-P-O catalysts as well.

## INTRODUCTION

Bulk catalysts based on vanadium-phosphorus-oxide (V-P-O) are industrially used for the production of maleic anhydride (MA) from *n*-butane. The V-P-O system has been under investigation for the last three decades, and although it is widely accepted that vanadylpyrophosphate,  $(VO)_2P_2O_7$ , is the main component in the active catalyst, still little is known about the exact nature of the catalytic active site [1,2,3,4].

At Utrecht University much effort has been devoted to the development of supported V-P-O catalysts, as the supported V-P-O catalysts have superior characteristics over bulk V-P-O, such as a cheap and reproducible preparation procedure, a larger amount of active sites per unit surface area, a short activation period, and a high mechanical strength [5,6,7]. Therefore, application of supported V-P-O catalysts in a fluidised-bed process is very promising.

The newly developed supported catalysts show interesting catalytic properties. For instance, titania-supported V-P-O is already active at moderate temperatures (523 K vs. 673 K for the commercial bulk catalyst), although the selectivity is rather low [5,7]. Silica-supported V-P-O catalysts, on the other hand, show reasonable yields to maleic anhydride [6] and these systems have been further optimised in our laboratory.

In the literature, only a few other examples of deposition of V-P-O on silica [8,9,10], titania [11], alumina [11,12,13,14] and  $AlPO_4$  [15] have been described. Generally, the lack of long-range order of the supported V-P-O moieties compromises a proper characterisation of the supported V-P-O phase with common techniques, such as X-ray diffraction and FTIR spectroscopy. Nevertheless, most supported V-P-O catalysts are reported to consist of a phase that strongly resembles  $V^{5+}$ -phosphate, mostly  $\gamma$ - $VOPO_4$  or  $\alpha$ - $VOPO_4$  [16,17].

Generally, the catalytic activity of V-P-O catalysts has been related to the local structure of surface vanadyl groups in vanadylpyrophosphate. However, with most techniques, no explicit information about the catalytically active surface is obtained. The structure of crystalline vanadylpyrophosphate consists of pairs of edge-sharing pseudo octahedrally co-ordinated vanadium ions at a distance of 3.23 Å, isolated from other pairs by pyrophosphate groups [18]. This structural unit is often used to model the active sites in V-P-O catalysts [2,19,20]. In addition, various other models have been proposed, *i.e.* interfaces between different  $VOPO_4$  phases and  $(VO)_2P_2O_7$  [16,17],  $V^{5+}$  sites on the surface of  $(VO)_2P_2O_7$  [2],  $V^{5+}$  species in interaction with  $VO(PO_3)_2$  [21], and amorphous  $V^{4+}$  and/or  $V^{5+}$  phases supported on crystalline  $(VO)_2P_2O_7$  [22,23].

In this chapter we describe our study on the structure-activity relationship of supported V-P-O catalysts. To this end, we have applied X-ray absorption spectroscopy (XANES/EXAFS) at the vanadium K-edge and ESR spectroscopy. These techniques do not require crystallinity of the sample and provide information on the local micro-structure around the vanadium site.

## EXPERIMENTAL

### **Catalyst preparation**

The catalysts used in this study were bulk V-P-O, titania-supported V-P-O (8.2 wt% V), and silica-supported V-P-O (7.5 wt% V). All catalysts were prepared with an atomic P/V ratio of 1.1. Bulk V-P-O was prepared in *i*-butanol according to a well-known procedure [24] and exhibited a crystalline structure [25].

Supported V-P-O catalysts have been prepared using TiO<sub>2</sub> (Degussa P25) and SiO<sub>2</sub> (Engelhard C500-20) according to a procedure developed by Overbeek *et al.* [5,6,26].

In brief, the method comprises an electrochemical reduction of V<sup>5+</sup> to V<sup>3+</sup> ions in diluted hydrochloric acid solution, followed by homogeneous deposition precipitation (HDP) of the V<sup>3+</sup> species onto the supports in the presence of NH<sub>4</sub>H<sub>2</sub>PO<sub>4</sub>. For the preparation of silica-supported catalysts, this method was slightly adapted, because of the poor interaction of the V-P-O with silica [6,27]. First, an amount of V<sup>3+</sup> precursor was precipitated in the absence of a phosphate precursor. After drying in air at 393 K for 16 hours, the partially oxidised supported vanadium oxide was subsequently impregnated with diluted phosphoric acid to obtain silica-supported V-P-O. The supported catalysts will be referred to as VPO/TiO<sub>2</sub> and VPO/SiO<sub>2</sub>. The applied loadings compare to a calculated monolayer coverage of 2.0 and 2.7 for VPO/SiO<sub>2</sub> and VPO/TiO<sub>2</sub>, respectively.

Catalyst precursors were kept in N<sub>2</sub> at 723 K for 16 hours prior to catalytic tests and subsequent characterisation.

### **Catalyst performance**

After calcination, bulk and supported V-P-O samples (1.5 ml) were tested in the selective oxidation of *n*-butane using a 1.5% *n*-butane, 20.5% O<sub>2</sub>, 78.5% Ar flow (50 ml/min, GHSV = 2000 h<sup>-1</sup>) at atmospheric pressure. Formed gaseous products, as well as unconverted reactants were analysed using an on-line Balzers QMA-420 mass spectrometer operating at 423 K to avoid condensation of products. Carbon mass balances were in the range of 0.98 to 1.02. A detailed description of the experimental conditions has been given in chapter 2 of this thesis [28].

### **Catalyst characterisation**

All catalysts have been characterised with X-ray absorption spectroscopy (XANES/EXAFS) and ESR spectroscopy.

XAS data were collected at Station 8.1 of the SRS facility in Daresbury (UK). The energy of the electron beam was 2 GeV (average current ~ 100 mA). The Si (111) double crystal monochromator was detuned to 50 % intensity to minimise the presence of higher harmonics. The measurements were all carried out in transmission mode using ionisation chambers as detectors. To minimise noise the counting time per data point was taken to be 1000 ms and at least four scans were recorded and averaged. All samples were recorded *ex-situ* in He at 77 K. The energy calibration was performed by means of a V-foil (5µm). The absolute value of the vanadium-edge is 5465 eV.

The catalyst samples were pressed into self-supporting wafers and mounted in an EXAFS cell [29]. The thickness of the wafer was chosen in such a way as to give an absorption ( $\mu x$ ) of 2.5 at the absorption edge for optimal signal-to-noise ratio. To prevent self-absorption by the catalysts the amount of sample was chosen such that a step in absorption of 1.0 in the edge region ( $\Delta\mu x = 1$ ) was obtained. If necessary, samples were diluted with boron nitride (BN). Standard procedures were used to extract the EXAFS data from the measured absorption spectrum. The background was subtracted using Victoreen routines [30].

The ESR experiments were performed on an X-band Bruker ESP300 spectrometer equipped with an EN801 resonator (operating in TM110 cylindrical mode with unloaded  $Q = 1000$ ). The microwave power was 1 mW, far below saturation levels for the supported V-P-O samples. The magnetic field was modulated with a frequency of 12.5 kHz and an amplitude of 1 Gauss. The sample temperature was adjusted in the range of 3.7-300 K with an Oxford ESR900 helium flow cryostat under control of an Oxford ITC503 temperature controller (temperature stability of 0.5 K).

## RESULTS AND DISCUSSION

### *Catalyst performance*

In Figure 1 the conversions as a function of the temperature over VPO/bulk, VPO/TiO<sub>2</sub> and VPO/SiO<sub>2</sub> are represented. It is obvious that VPO/TiO<sub>2</sub> is the most active catalyst, already showing conversion at 473 K. In general, our titania-supported catalysts are even more active at lower loadings [5]. Despite the lower amount of V-P-O present in the silica-supported catalyst, this sample is more active than the bulk catalyst. The higher specific surface areas of the active component in the supported catalysts can explain this difference. The specific surface area (BET method) of the samples was determined to be 9 m<sup>2</sup>/g for VPO/bulk, 54 m<sup>2</sup>/g for VPO/SiO<sub>2</sub> and 44 m<sup>2</sup>/g for VPO/TiO<sub>2</sub>, respectively.

Both VPO/bulk and VPO/SiO<sub>2</sub> show about the same selectivity to maleic anhydride (Figure 2). The optimum yield for VPO/bulk and VPO/SiO<sub>2</sub> is 25-30% at a conversion of 50%. This might indicate that the nature of the active sites of the silica-supported and of the bulk catalyst is the same. However, with VPO/SiO<sub>2</sub> the selectivity decreases much more rapidly when the conversion is raised. The selectivity of VPO/TiO<sub>2</sub> at low conversions is substantially below that of the other catalysts and only a yield of 6% is obtained at a conversion of 30%.

The differences in activity and selectivity between VPO/TiO<sub>2</sub>, on the one, and VPO/SiO<sub>2</sub> and VPO/bulk, on the other hand, have been ascribed to the stronger interaction between V-P-O and titania [5,7]. Therefore, we will focus on the structural characterisation of the various samples in the remaining part of this chapter.



Comparison of bulk and supported V-P-O catalysts

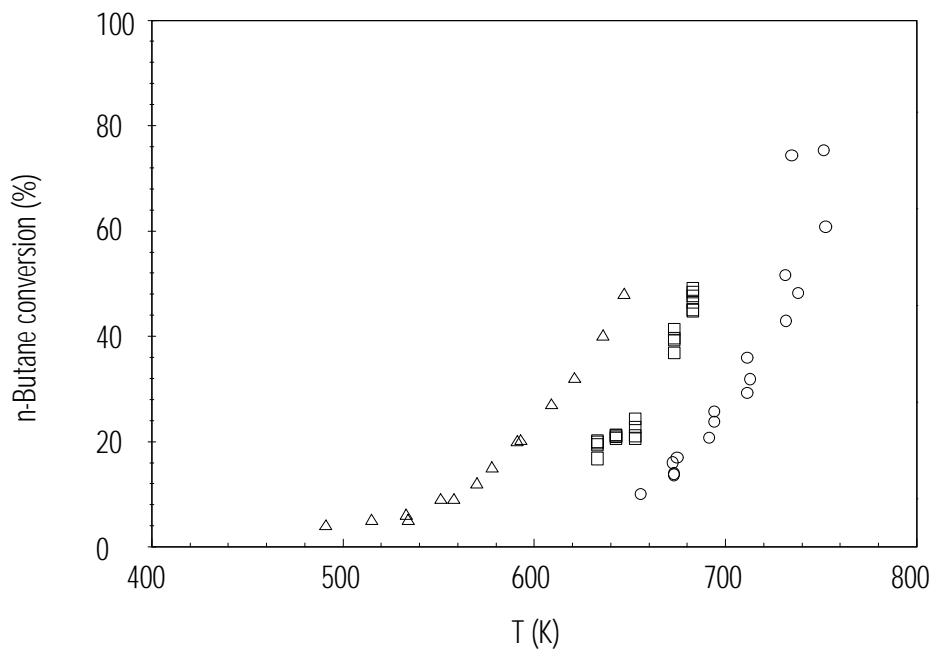


**Figure 1** *n*-Butane conversion as a function of temperature for VPO/Bulk (circles), VPO/SiO<sub>2</sub> (squares) and VPO/TiO<sub>2</sub> (triangles).

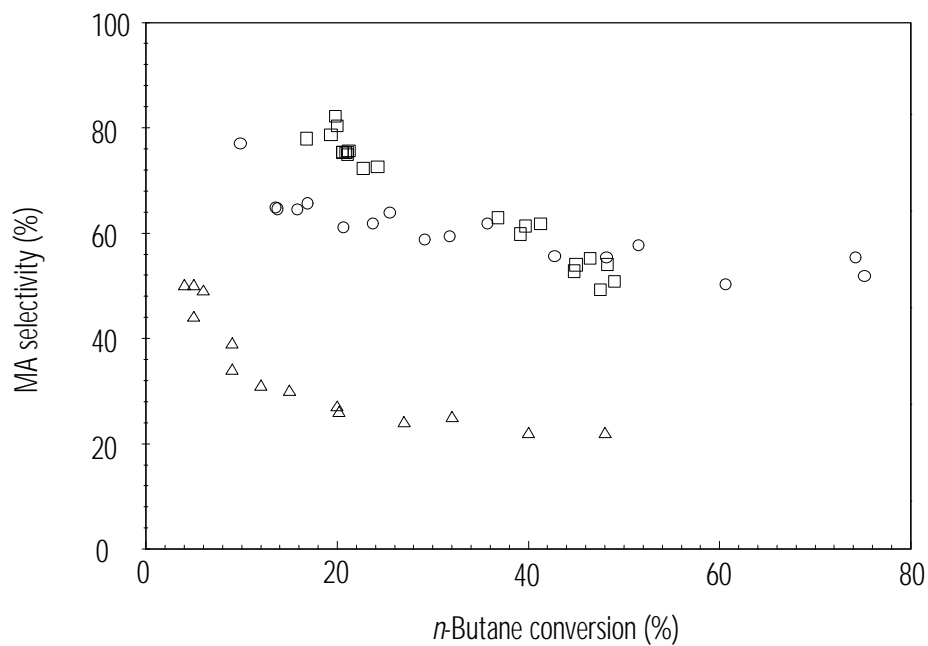
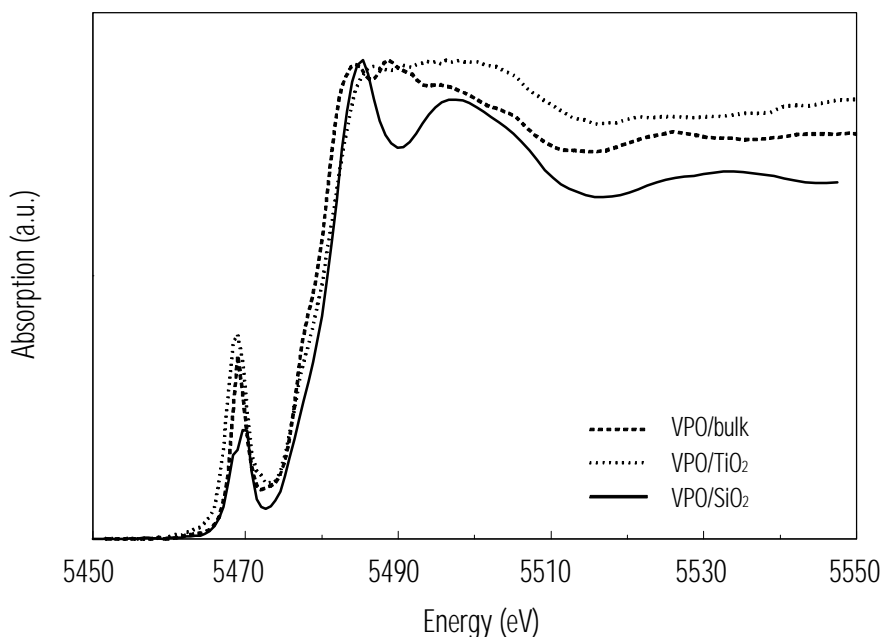


**Figure 2** Selectivity to MA as a function of *n*-butane conversion for VPO/Bulk (circles), VPO/SiO<sub>2</sub> (squares) and VPO/TiO<sub>2</sub> (triangles).

### X-ray absorption spectroscopy

In Figure 3, the XANES spectra of VPO/bulk, VPO/TiO<sub>2</sub> and VPO/SiO<sub>2</sub> after being used in the oxidation of *n*-butane are represented. The three spectra show clearly different features in the positions and shape of the pre-edge and the main



absorption edge.

**Figure 3** Vanadium K-edge XANES spectra of VPO/Bulk, VPO/SiO<sub>2</sub> and VPO/TiO<sub>2</sub> employed in the oxidation of *n*-butane.

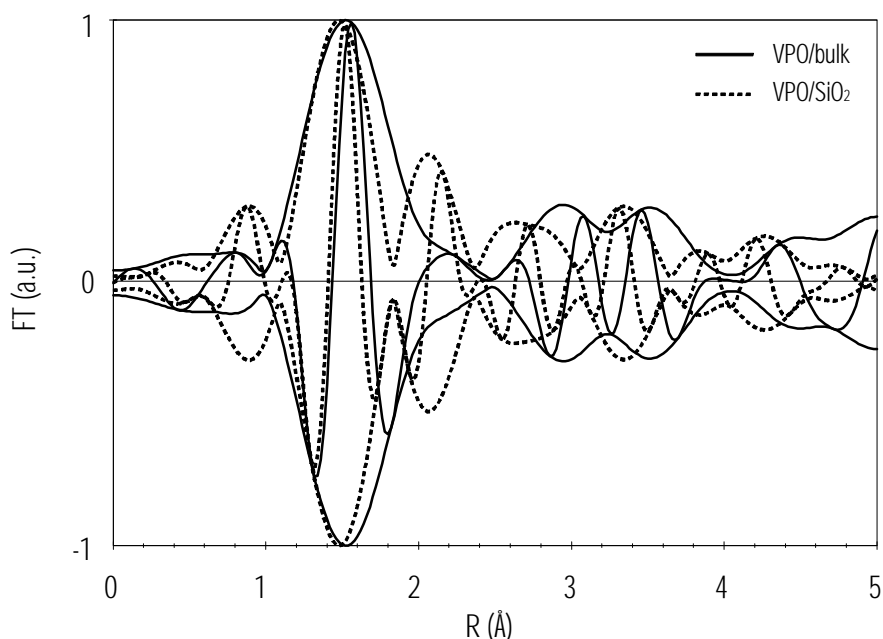
Based on the work of Wong *et al.*, these features can be attributed to different coordination geometries found in various vanadyl compounds, *i.e.* tetrahedral (VO<sub>4</sub>), square pyramidal (VO<sub>5</sub>) or distorted octahedral (VO<sub>6</sub>) [31,32,33]. The XANES spectrum of VPO/bulk agrees well with that reported for VO<sub>5</sub> or distorted VO<sub>6</sub> compounds, as expected from the single crystal XRD data [18,34]. However, the XANES spectra of VPO/TiO<sub>2</sub> and VPO/SiO<sub>2</sub> are clearly different, indicating that VO<sub>4</sub> geometry is present in the titania-supported catalyst and distorted VO<sub>6</sub> geometry in the silica-supported catalyst respectively.

However, the XANES features of the X-ray absorption data must first be confirmed by the EXAFS spectra before conclusions can be drawn.

Figure 4 shows the k<sup>2</sup> Fourier transforms of VPO/bulk and VPO/SiO<sub>2</sub>. It is obvious that the imaginary parts of the two Fourier transforms differ significantly around 1.5 Å. This is the range where the contributions of the first-shell oxygen atoms are located. Furthermore, an important additional contribution at about 2 Å is present in the data of VPO/SiO<sub>2</sub>. For the higher co-ordination shells the spectra of bulk and supported V-P-O differ considerably. A detailed description of the EXAFS data

analysis of the bulk and of the supported V-P-O catalysts will be presented in chapter 6 of this thesis.

Recently, Nguyen and co-workers have revealed the structure of crystalline vanadylpyrophosphate [18]. Our EXAFS data of VPO/bulk could be fitted up to a distance of 3.5 Å with the single crystal X-ray data of Nguyen *et al.* [18]. Above this threshold, too many contributions must be included in the calculations, which results in a low reliability of the final fit. The results of the EXAFS data analysis of



VPO/bulk have been reported elsewhere [35,37].

**Figure 4** Fourier transforms ( $k^2$ ,  $\Delta k = 3.5-10 \text{ \AA}^{-1}$ ) of the EXAFS data of VPO/bulk (solid line) and VPO/SiO<sub>2</sub> (dotted line).

Although an appreciable amount (about 30%) of our VPO/bulk catalyst consists of an amorphous V-P-O phase [34,36], the EXAFS spectrum is dominated by the structure of the ideally crystalline vanadylpyrophosphate phase [35]. This places EXAFS, together with Raman spectroscopy and XRD, in the group of techniques less appropriate or unsuitable to study possible amorphous (surface) contributions in bulk V-P-O catalysts.

Figure 5 represents the  $k^2$  Fourier transforms of the EXAFS data of both supported catalysts. These spectra are markedly different from each other both in the first co-ordination shell and in the higher shells. It is important to note that the spectrum of VPO/TiO<sub>2</sub> also deviates from that of VPO/bulk. This means that the structures of both supported V-P-O catalysts differ from that of bulk crystalline (VO)<sub>2</sub>P<sub>2</sub>O<sub>7</sub>.

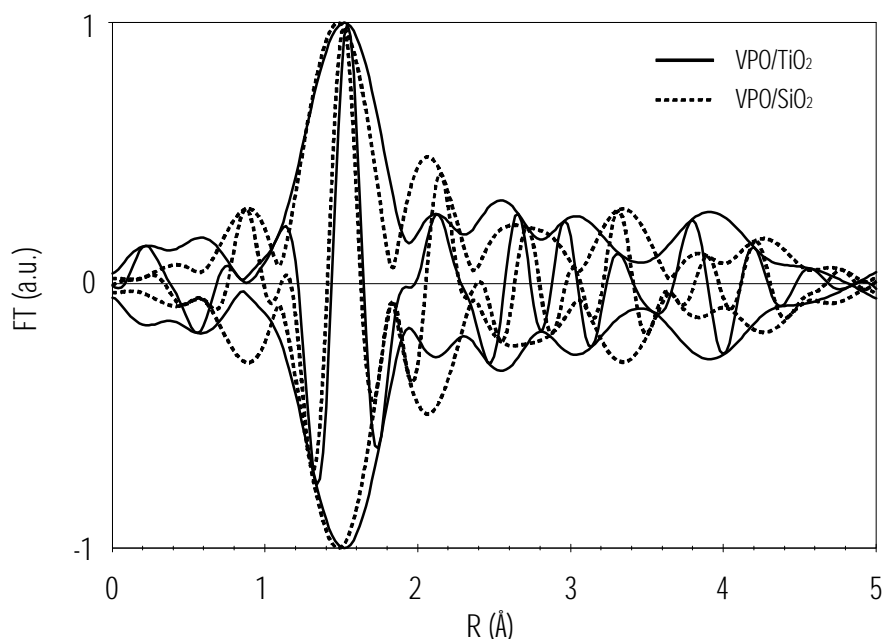


**Figure 5** Fourier transforms ( $k^2$ ,  $\Delta k = 3.5-10 \text{ \AA}^{-1}$ ) of the EXAFS data of VPO/TiO<sub>2</sub> (solid line) and VPO/SiO<sub>2</sub> (dotted line).

As stated above, EXAFS is a technique that can probe the local structure around the central vanadium atom, up to a distance of 4 Å. In principle, the EXAFS spectrum represents the superposition of both bulk and surface contributions. However, the EXAFS spectrum of VPO/SiO<sub>2</sub> is not suffering from interfering dominant bulk contributions and, hence, represents clearly the local structure of the amorphous V-P-O phase at the surface.

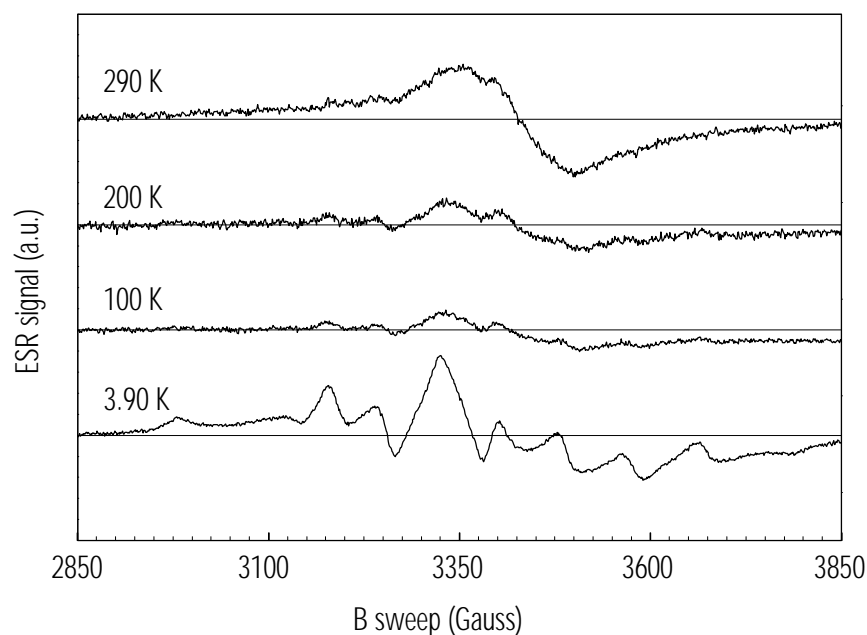
Preliminary analyses of the EXAFS data indicate that VPO/TiO<sub>2</sub> consists of small particles, in which the isolated V atoms are tetrahedrally co-ordinated by oxygen atoms, including oxygen atoms bridging V and Ti [35]. The VPO/SiO<sub>2</sub> catalyst on the other hand, consists of vanadyl groups in an octahedral environment [35,37]. This result raises the question concerning the distance between adjacent V atoms. It is important to note that with both supported V-P-O catalysts no V-V contributions are found in the EXAFS data up to a distance of 3.5 Å. To study the V-V interaction in the supported catalysts we therefore have applied ESR spectroscopy.

#### **ESR spectroscopy**

ESR spectroscopy is a powerful technique to probe paramagnetic centres. The major part of V-P-O catalysts consists of V<sup>4+</sup>-phosphate (d<sup>1</sup>) with electronic spin  $S = 1/2$ . When the supported catalysts contain only isolated vanadyl groups, the ESR spectrum will appear as a characteristic octet of the hyperfine coupling with the <sup>51</sup>V nucleus ( $I = 7/2$ ). In practice, the V hyperfine coupling is often unresolved in solid state V-P-O samples [38].

This absence is attributed to strong exchange interactions between adjacent electron spins [39], which averages out the hyperfine interaction with the vanadium nucleus.

Figure 6 represents the ESR spectra of VPO/TiO<sub>2</sub> at various temperatures. At room temperature the ESR spectra of the two supported catalysts correspond to the spectrum of VPO/bulk [34,36]. However, when the temperature is decreased, the spectrum of VPO/TiO<sub>2</sub> starts revealing the hyperfine coupling with the V nucleus. In contrast to this, with VPO/SiO<sub>2</sub> no hyperfine coupling is visible, resulting in a spectrum that resembles Figure 2 in chapter 3. This indicates that exchange interactions between neighbouring vanadyl groups dominate the hyperfine coupling down to very low temperatures with VPO/SiO<sub>2</sub>. The strength of this interaction can be determined from the temperature dependence of the ESR intensity [34,36]. For bulk V-P-O we have previously found that its ESR spectrum contains three different contributions, *i.e.* strongly interacting vanadyl groups ( $J/k = -65.7$  K), weakly interacting vanadyl groups ( $J/k = -4.7$  K), and



antiferromagnetic defects in a ratio of 10:7:2 [34,36].

**Figure 6** X-band ESR spectra of VPO/TiO<sub>2</sub> at different temperatures, *i.e.* 290 K, 200 K, 100 K and 3.90 K. The magnetic field is centred at 3400 Gauss, and swept over 1000 G. The spectrum has been taken at a microwave frequency of 9.437 GHz.

In the paramagnetic regime ( $T > T_{\text{Neel}}$ ), the ESR intensity,  $I$ , can be described by the Curie-Weiss equation for antiferromagnets:

$$I(T) \propto \frac{1}{T - \theta} \quad (1)$$

The Curie-Weiss temperature,  $\theta$ , can be extracted from a plot of the reciprocal of the total integrated ESR intensity of VPO/SiO<sub>2</sub> as a function of the temperature (Figure 7).

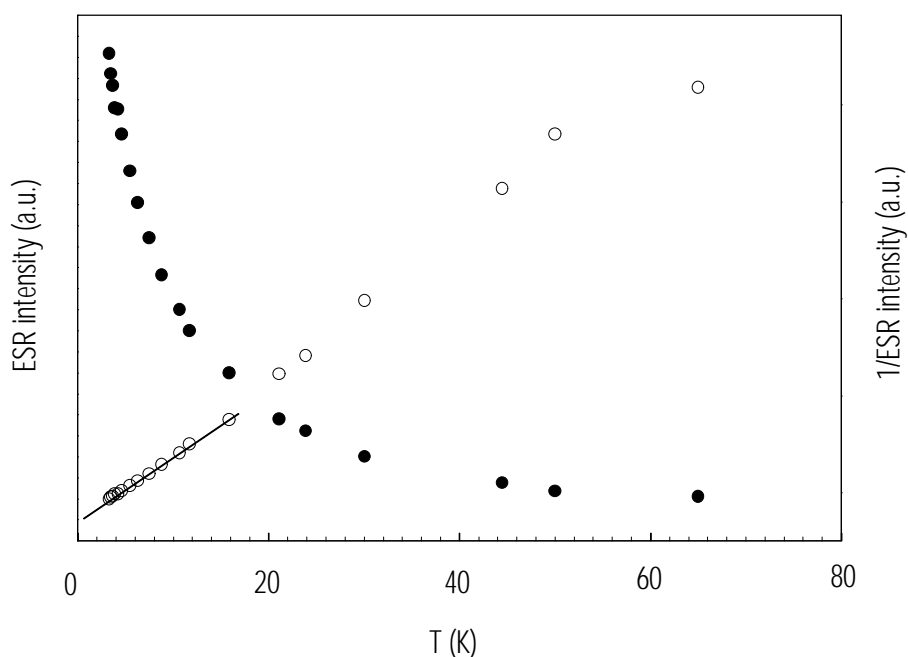


**Figure 7** Total integrated ESR intensity (●) and the reciprocal values (○) of these data of VPO/SiO<sub>2</sub> as a function of temperature. The solid curve represents a fit of the data assuming Curie-Weiss behaviour.

For antiferromagnetically coupled pairs the Curie-Weiss temperature  $\theta$  is related to the coupling parameter  $J$  via the relation  $k\theta = -(3/2)J$ . The linear relation between the reciprocal ESR intensity and  $T$  indicates that the compound is exhibiting Curie-Weiss behaviour at low temperatures. The Curie-Weiss temperature is extrapolated to  $\theta = 2 \pm 1$  K. This value is significantly lower than that measured with the VPO/bulk sample in which, in the amorphous part, an antiferromagnetic coupling between vanadyl groups exists ( $J/k = -4.7$  K, which corresponds to  $\theta = 7.1$  K). However, this interaction is still strong enough to average out the hyperfine coupling in the ESR data down to the lowest temperatures accessible with our equipment (3.7 K).

The small value of the Curie-Weiss temperature in VPO/SiO<sub>2</sub> suggests that the average V-V distance in the amorphous V-P-O phase is considerably larger than 3.23 Å (the V-V distance in crystalline vanadylpyrophosphate), which points to a distance probably too large to be observed with EXAFS.

## CONCLUSIONS

Our results show considerable differences between VPO/TiO<sub>2</sub> and VPO/SiO<sub>2</sub> in the catalytic performance, the local structure around vanadium (XANES/EXAFS) and the spin exchange interactions between vanadium atoms (ESR). The combination of characterisation methods used has revealed that the structure of the supported V-P-O phase does not match that of crystalline vanadylpyrophosphate.

There are three strong indications that the active phase in VPO/SiO<sub>2</sub> could resemble the real active phase of bulk V-P-O catalysts: i) catalytic selectivity, ii) catalytic yield, iii) XANES/EXAFS.

We are convinced that the local structure of our supported V-P-O phase can be considered as a model for the amorphous surface of bulk V-P-O. Our results support the view that the catalytic sites of bulk V-P-O catalysts are located in an amorphous surface phase.

As it may serve as a model for the amorphous component in bulk V-P-O catalysts, it will be interesting to study the structure of the VPO/SiO<sub>2</sub> catalyst in more detail. The analysis of the EXAFS data of this sample as well as application of other characterisation techniques can provide more insight in the nature of the real active site of the bulk V-P-O catalyst.

## REFERENCES

- 1 B.K. Hodnett, *Catal. Rev. -Sci. Eng.* **27**(3) (1985), 373
- 2 G. Centi, F. Trifirò, J.R. Ebner, and V.M. Franchetti, *Chem. Rev.* **88** (1988), 55
- 3 G. Centi, *Catal. Today* **16** (1993), 5
- 4 M. Abon, J.C. Volta, *Applied Catalysis: A General* **157** (1997), 173
- 5 R.A. Overbeek, P.A. Warringa, M.J.D. Crombag, L.M. Visser, A.J. van Dillen, J.W. Geus, *Applied Catalysis A: General* **135** (1996), 209
- 6 R.A. Overbeek, A.R.C.J. Pekelharing, A.J. van Dillen, J.W. Geus, *Applied Catalysis A: General* **135** (1996), 231
- 7 M. Ruitenbeek, R.A. Overbeek, A.J. van Dillen, D.C Koningsberger, J.W. Geus, *Recl. Trav. Chim. Pays-Bas* **115** (1996), 519
- 8 V.A. Zazhigalov, Yu. P. Zaitsev, V.M. Belousov, B. parlitz, W. Hanke, G. Ohlman, *React. Kinet. Catal. Lett.* **32** (1986), 209
- 9 K.E. Birkeland, S.M. Babitz, G. K. Bethke, H.H. Kung, G.W. Coulston, S.R. Bare, *J. Phys. Chem. B* **101** (1997), 6895
- 10 J.M.C. Bueno, G.K. Bethke, M.C. Kung, H.H. Kung, *Catal. Today* **43** (1998), 101

## Chapter 5

- 11 M. Martinez-Lara, L. Moreno-Real, R. Pozas-Tormo, A. Jiminez-Lopez, S. Bruque, P. Ruiz, G. Poncelet, *Can. J. Chem* **70** (1992), 5
- 12 M. Nakamura, K. Kawai, Y. Fujiwara, *J. Catal.* **34** (1974), 345
- 13 N.T. Do, M. Baerns, *Appl. Catal.* **45** (1988), 1
- 14 A. Ramstetter, M. Bearns, *J. Catal* **109** (1988), 303
- 15 P.S. Kuo, B.L. Yang, *J. Catal.* **117** (1989), 301
- 16 E. Bordes, *Catal. Today* **1** (1987), 499
- 17 G.J. Hutchings, A. Desmartin-Chomel, R. Olier, J.C. Volta, *Nature* **368** (1994), 41
- 18 P.T. Nguyen, R.D. Hoffman, and A.W. Sleight, *Mater. Res. Bull.* **30** (1995), 1055
- 19 P.A. Agaskar, L. DeCaul, R.K. Graselli, *Catal. Lett.* **23** (1994), 339
- 20 B. Schiott, K.A. Jorgensen, *Catal. Today* **16** (1993), 79
- 21 M.T. Sananes, A. Tuel, J.C. Volta, *J. Catal.* **145** (1994), 251
- 22 N. Harrouch Batis, H. Batis, A. Ghorbel, J.C. Vedrine, J.C. Volta, *J. Catal.* **128** (1991), 248
- 23 G. Bergeret, M. David, J.P. Broyer, J.C. Volta, G. Hecquet, *Catal. Today* **1** (1987), 37
- 24 K. Katsumoto, D.M. Marquis, US Patent **4,132,670** (1970)
- 25 R.A. Overbeek, M. Versluijs-Helder, P.A. Warringa, E.J. Bosma, J.W. Geus, *Stud. Surf. Sci. Catal.* **82** (1994), 183
- 26 J.W. Geus, R.A. Overbeek, *Eur. Patent* **94201177.6** (1994)
- 27 R.A. Overbeek, E.J. Bosma, D.W.H. de Blauw, A.J. van Dillen, H.G. Bruil, J.W. Geus, *Applied Catalysis* **163** (1997), 129
- 28 Chapter 2 of this thesis, and references therein
- 29 M. Vaarkamp, B.L. Mojet, J.T. Miller, D.C. Koningsberger, *J. Phys. Chem.* **99** (1995), 16067
- 30 J.B.A.D. van Zon, D.C. Koningsberger, H.F.J. van Blik, D.E.J. Sayers, *J. Chem. Phys.* **82** (1985), 5742
- 31 J. Wong, F.W. Lytle, R.P. Mesmer, and D.H. Maylotte, *Phys. Rev. B* **30** (1984), 5596
- 32 J. Wong, R.P. Mesmer, D.H. Maylotte, and F.W. Lytle, , in: *EXAFS and near edge structure*, A. Bianconi, L. Inocchia, and S. Stipcich, eds., Springer Verlag, Berlin, 1983, 130
- 33 J. Wong, D.H. Maylotte, F.W. Lytle, R.B. Gregor, and R.L. St. Peters, in: *EXAFS and near edge structure*, A. Bianconi, L. Inocchia, and S. Stipcich, eds., Springer Verlag, Berlin, 1983, 206
- 34 Chapter 3 of this thesis, and references therein
- 35 M. Ruitenbeek, R.A. Overbeek, D.C. Koningsberger, J.W. Geus, in: *Catalytic Activation and Functionalisation of Light Alkanes*, E.G. Derouane et al. (eds.), Kluwer Academic Publishers, Dordrecht, 1998, 423
- 36 M. Ruitenbeek, A. Barbon, E.E. van Faassen, J.W. Geus, *Catalysis Letters* **54** (1998), 101
- 37 Chapter 6 of this thesis, and references therein



*Comparison of bulk and supported V-P-O catalysts*

- 38 Y. Zhang-Lin, M. Forissier, J.C. Vedrine, J.C. Volta., *J. Catal.* **145** (1994) 267
- 39 A. Bencini, D. Gatteschi, *EPR of exchange coupled systems*, Springer-Verlach, Berlin, 1990

*Chapter 5*

## THE STRUCTURE OF (SUPPORTED) V-P-O CATALYSTS QUANTITATIVE ANALYSIS OF EXAFS SPECTRA

---

### **ABSTRACT**

EXAFS data of VPO/bulk-org and VPO/bulk-aq catalysts and two supported V-P-O catalysts were collected in helium atmosphere at 77 K after more than 100 hours time-on-stream. The EXAFS data of the bulk samples could be fitted with the single crystal XRD parameters of vanadylpyrophosphate. The EXAFS spectra of the supported catalysts, VPO/SiO<sub>2</sub> and VPO/TiO<sub>2</sub> were different from that of the bulk V-P-O catalysts.

EXAFS data analysis showed that VPO/TiO<sub>2</sub> consists of isolated tetrahedral vanadyl units, bonded to the titania support via three bridging oxygen atoms. In this sample, phosphate is directly bonded to the support, and not to the vanadium units. These results are in agreement with our ESR measurements.

It was possible to fit VPO/SiO<sub>2</sub> with two different models. The first model showed a slightly better fit, although the structural parameters were not in agreement with the ESR data of this sample. In the second model, the silica-supported catalyst has octahedral co-ordinated vanadium sites, which are corner-shared. Co-ordination numbers indicate that these clusters would consist of six vanadium units.

## INTRODUCTION

As indicated in the previous two chapters, many authors have reviewed the nature of the active sites in V-P-O catalysts [1,2]. The analysis of characterisation data is usually complicated due to the presence of many different crystalline V-P-O phases [3], some of which are included in Table 1.

Some authors have put forward the idea that only specific crystalline V-P-O phases are active and selective in the butane to MA reaction [4,5,6]. Vanadylpyrophosphate is most frequently reported to be the sole active and selective phase [4,7,8,9,10]. Others claim that combinations of crystalline V-P-O phases are responsible for the special catalytic properties [3,11,12,13]. Furthermore, the presence of amorphous V-P-O phases supported on a  $V^{4+}$  matrix has been discussed by Hodnett and Delmon [14,15,16].

We have shown with ESR spectroscopy and magnetisation measurements that a hydrated vanadium(IV)phosphate is present in the bulk catalysts [1,17]. However, *in-situ* XRD results indicate that this phase is not present under reaction conditions [18]. Yamazoe *et al.* [19] and Sananes *et al.* [20,21] claim that this should be a phosphorus-rich (P/V ~ 2) surface layer.

**Table 1** Different crystalline (dehydrated) V-P-O phases that have been reported in the literature.

Valence	Reported phases
$V^{3+}$	$V(PO_3)_3$ [22,23]
$V^{4+}$	$(VO)_2P_2O_7$ [24,25], $VO(PO_3)_2$ [26]
$V^{5+}$	$\alpha_1$ -VOPO <sub>4</sub> [3], $\alpha_2$ -VOPO <sub>4</sub> [27], $\beta$ -VOPO <sub>4</sub> [28], $\gamma$ -VOPO <sub>4</sub> [29], $\delta$ -VOPO <sub>4</sub> [29], T-VOPO <sub>4</sub> [18]

The techniques mostly applied to reveal the structure of the active sites in V-P-O catalysts are X-ray diffraction (XRD) [4,7,8] and Laser Raman Spectroscopy (LRS) [4,8,30,31,32]. However, XRD requires long-range order in the specimen and is, hence, restricted to crystalline samples. Inherently, LRS is a bulk-technique too, due to its typical penetration depth of 1  $\mu\text{m}$  [33]. Moreover, information about the surface of the bulk cannot be obtained with LRS, because of the significantly stronger Raman scattering from crystalline oxide phases (typically orders of magnitude greater) [33]. For this reason, these techniques are less suitable to study the nature of the active phase in bulk V-P-O catalysts.

However, well dispersed supported catalysts can be used as model systems for the surface of bulk catalysts [2,33,34], because they are not suffering from interfering bulk contributions in the spectra. We have applied EXAFS spectroscopy for analysis of the surface structure of these model-supported catalysts and have presented the raw-data in a previous paper [2,35]. The XANES part of the data revealed that the co-ordination geometry of vanadium in VPO/bulk (distorted  $VO_6$ ), VPO/TiO<sub>2</sub> ( $VO_4$ ) and VPO/SiO<sub>2</sub> (distorted  $VO_5$  or  $VO_6$ ) differs considerably. Furthermore, the EXAFS data of both supported catalysts, VPO/SiO<sub>2</sub> and VPO/TiO<sub>2</sub> show striking differences with the EXAFS spectrum obtained with the

VPO/bulk catalyst. In this chapter, the results of the quantitative analysis of the EXAFS data will be discussed. The XANES data and the ESR results, which have been presented in chapter 5 of this thesis, will form the basis for the structural models, which have been used to fit the EXAFS data.

## EXPERIMENTAL

### **Catalysts**

The catalysts used in this study were bulk V-P-O, titania-supported V-P-O (8.2 wt% V), and silica-supported V-P-O (7.5 wt% V) [2,36]. For use as reference compounds, bulk V-P-O was prepared following two different methods, *i.e.* in *i*-butanol/cyclohexanol (VPO/bulk-org) according to Katsumoto *et al.* [37], and in 37% HCl-solution (VPO/bulk-aq) according to Centi *et al.* [38]. A detailed description of the procedures can be found in chapter 2 of this thesis [36]. All catalysts were prepared with an atomic P/V ratio of 1.1 and characterised after more than hundred hours time-on-stream in the *n*-butane oxidation reaction [2].

### **X-ray absorption spectroscopy**

EXAFS data were collected at Station 8.1 of the SRS facility in Daresbury (UK) using a Si(111) double crystal monochromator. The measurements were performed in transmission mode under a static helium atmosphere at 77 K as described in chapter 2 of this thesis [2,36].

Data for phase shifts and backscattering-amplitudes were obtained from reference compounds. Ti-foil was used for V-V scattering, and Na<sub>3</sub>VO<sub>4</sub> was taken for V-O contributions. The characteristics of V-P scatterer pair were derived from theoretical calculations (FEFF 3.1).

The fit parameters were determined by multiple shell fitting in R-space, a procedure which is explained in chapter 2 of this thesis and in detail by Mojet [39].

## RESULTS

### **VPO/bulk catalysts**

Figure 1 represents the EXAFS data of the two bulk reference catalysts. In this figure, it is shown that the data of both bulk V-P-O catalysts are very similar. Only small differences in the amplitude can be observed.

The structure of vanadylpyrophosphate consists of edge sharing distorted octahedral VO<sub>6</sub> units, which are connected by pyrophosphate groups [24,25]. For the VO<sub>6</sub> unit, four different oxygen neighbours can be discriminated. First, one short vanadyl bond (1.59 Å) is present. Furthermore, the VO<sub>6</sub> units consist of two bridging O atoms between the edge-sharing VO<sub>6</sub> units (1.94 Å) and two O neighbours at the corners of the VO<sub>6</sub> dimers (2.07 Å). Finally, one oxygen neighbour is present at 2.36 Å. This is the vanadyl oxygen in the opposite plane of the layered structure.

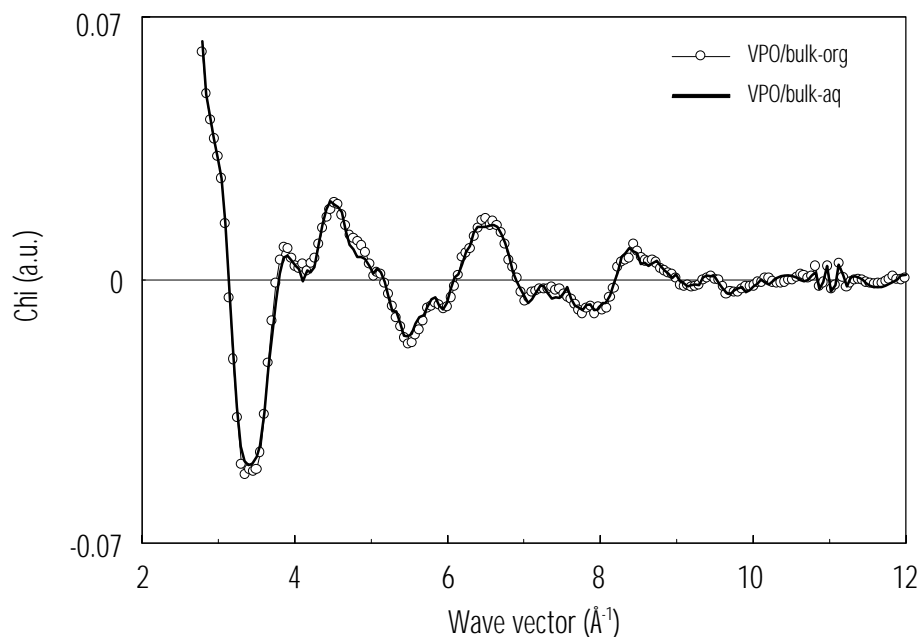


**Figure 1** EXAFS functions of VPO/bulk-org (open circles) and VPO/bulk-aq (solid line). Spectra were taken in He at 77K.

The parameters (co-ordination numbers and bond distances) were taken from the single crystal data of vanadylpyrophosphate [24,25]. Co-ordination numbers (CN) and distances (R) of the first shells were first fixed, while the Debye-Waller factors and inner potential corrections were adjusted. In a final fit, also the co-ordination numbers and distances were optimised using the difference file technique in R-space [36]. These final co-ordination parameters slightly deviate from the single-crystal vanadylpyrophosphate structure. In Figure 2, the Fourier transform of these data and the best fits are shown for VPO/bulk-org and VPO/bulk-aq respectively. The final fit parameters of the two bulk catalysts are included in

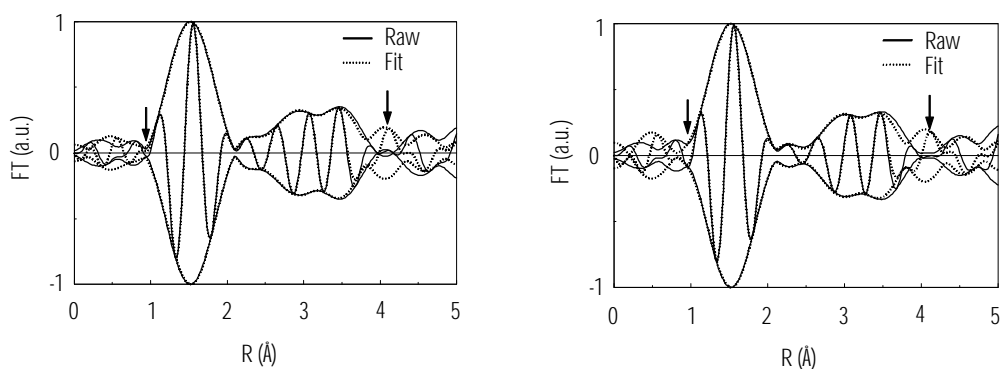


Table 2.

**Figure 2** Fourier transforms ( $k^2$ ,  $\Delta k = 3.5-10 \text{ \AA}^{-1}$ ,  $\Delta R = 1-4 \text{ \AA}$ ) of VPO/bulk-org (left) and VPO/bulk-aq (right); The spectra represent raw data (solid lines) and best fits (dotted lines). The arrows indicate the fitting range.

**Table 2** Fitted atomic distances, co-ordination numbers, Debye-Waller factors and inner potential corrections of the two VPO/bulk catalysts. In this table, single crystal XRD parameters and our EXAFS data analysis results are represented.

<i>organic</i>	XRD		FIT		$Ds^2$	$E_0$
	$R (\text{\AA})$	CN	$R (\text{\AA})$	CN		
V-O <sub>1</sub>	1.59	1	1.59	1.0	0.00262	10.47
V-O <sub>2</sub>	1.94	2	1.94	2.1	-0.00087	4.88
V-O <sub>3</sub>	2.07	2	2.07	2.0	0.00733	-5.68
V-O <sub>4</sub>	2.36	1	2.37	1.0	0.00014	-10.24
V-V	3.23	1	3.22	1.0	-0.00145	-3.64
V-P	3.33	4	3.39	4.0	0.00756	-1.31
<i>aqueous</i>	$R (\text{\AA})$	CN	$R (\text{\AA})$	CN	$Ds^2$	$E_0$
V-O <sub>1</sub>	1.59	1	1.59	1.0	0.00169	10.85
V-O <sub>2</sub>	1.94	2	1.94	2.0	-0.00211	1.87
V-O <sub>3</sub>	2.07	2	2.07	2.0	0.00465	2.25
V-O <sub>4</sub>	2.36	1	2.36	1.1	0.01167	0.24
V-V	3.23	1	3.29	1.1	-0.00608	4.58
V-P	3.33	3	3.33	3.9	0.01368	-2.06

### Supported V-P-O catalysts

In chapter 5, we have presented the Fourier transforms of the EXAFS data of VPO/bulk-org, VPO/SiO<sub>2</sub> and VPO/TiO<sub>2</sub>. It was shown that the Fourier transforms of VPO/SiO<sub>2</sub> and of VPO/TiO<sub>2</sub> do not resemble that of VPO/bulk. Figure 3 compares the EXAFS functions of the two supported V-P-O catalysts of this investigation. From this figure, it is clear that the structure of VPO/TiO<sub>2</sub> and VPO/SiO<sub>2</sub> are also different. We will first present the EXAFS analysis parameters of the silica-supported V-P-O catalyst.

### Silica-supported V-P-O

The major differences between the EXAFS data of VPO/bulk and VPO/SiO<sub>2</sub>, which are shown in Figure 4 of chapter 5 are the much smaller contribution at 1.5 Å and an additional contribution at 2.0 Å in the uncorrected Fourier transforms [2]. Furthermore, the contributions beyond 2.0 Å in the uncorrected Fourier transforms are located at different positions [2].

Two different structural models could be obtained for the VPO/SiO<sub>2</sub> catalyst. In Figures 4 and 5, the Fourier transforms ( $k^2$ ,  $\Delta k = 3.5-10 \text{ \AA}^{-1}$ ,  $\Delta R = 1-3.5 \text{ \AA}$ ) of the EXAFS data and the best fits are represented for model 1 and 2, respectively. The accompanying structural parameters are represented in Table 3.

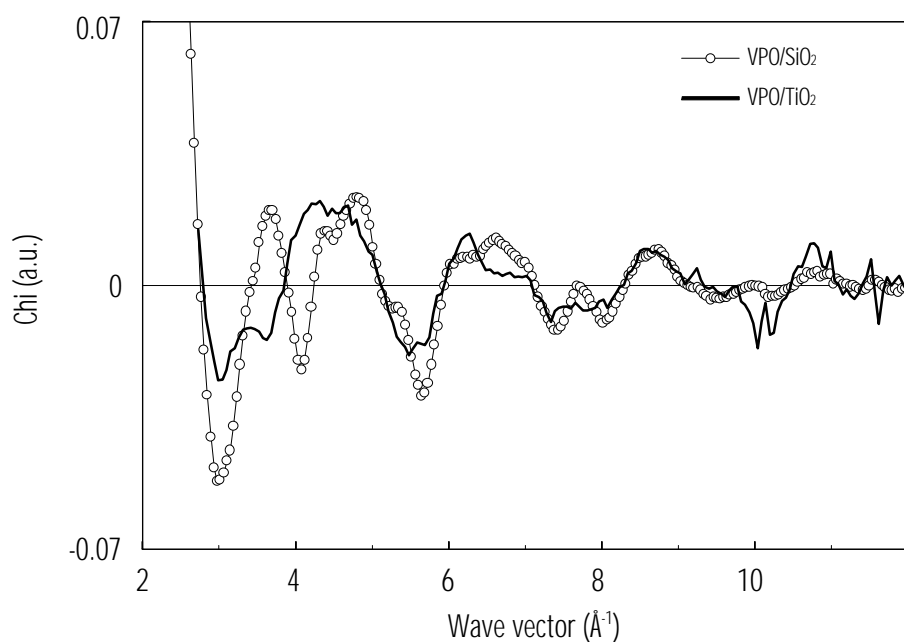


**Figure 3** EXAFS functions of VPO/SiO<sub>2</sub> (open circles) and VPO/TiO<sub>2</sub> (solid line). Spectra were taken in He at 77 K.

**Table 3** Fitted atomic distances, co-ordination numbers, Debye-Waller factors and inner potential corrections of the two models for the VPO/SiO<sub>2</sub> catalysts.

Model 1	$R$ (Å)	CN	$Ds^2$	$E_0$
V-O <sub>1</sub>	1.59	1.0	0.00078	-4.96
V-O <sub>2</sub>	2.00	2.0	-0.00335	-9.15
V-O <sub>3</sub>	2.74	2.0	-0.00378	-14.19
V-V	3.20	1.1	-0.00234	-15.00
V-P	4.05	2.4	0.00200	-8.79
Model 2	$R$ (Å)	CN	$Ds^2$	$E_0$
V-O <sub>1</sub>	1.62	1.0	0.00008	-8.07
V-O <sub>2</sub>	1.98	2.0	-0.00230	-9.08
V-O <sub>3</sub>	2.07	1.9	0.01497	0.65
V-O <sub>4</sub>	2.70	2.1	-0.00044	-13.00
V-P	3.56	2.1	0.00652	1.88
V-V	4.32	2.4	-0.01071	2.55



The structure of the supported V-P-O phase

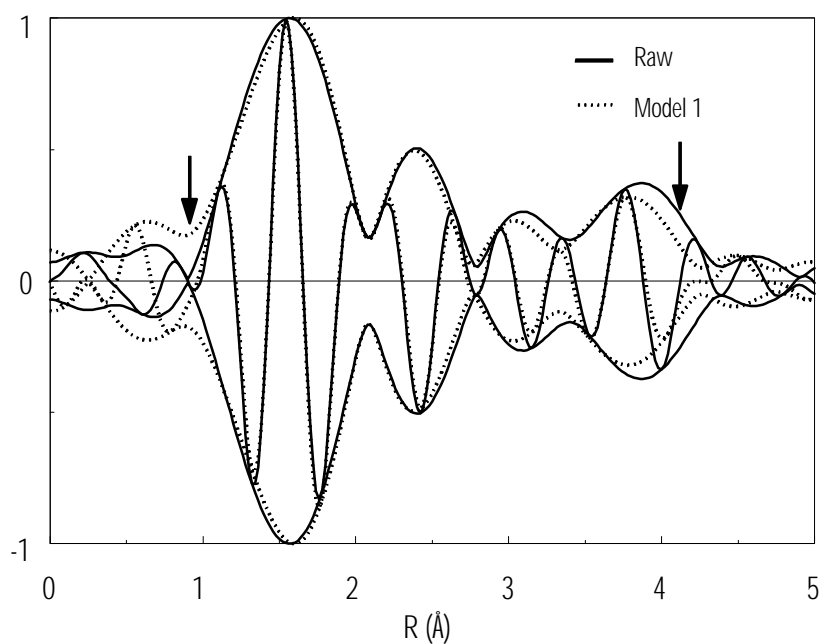


**Figure 4** Fourier transforms (solid line) and best fit (dotted line) of model 1 for the VPO/SiO<sub>2</sub> catalyst ( $k^2$ ,  $\mathbf{Dk} = 3.5-10 \text{ \AA}^{-1}$ ,  $\mathbf{DR} = 1-4 \text{ \AA}$ ). The arrows

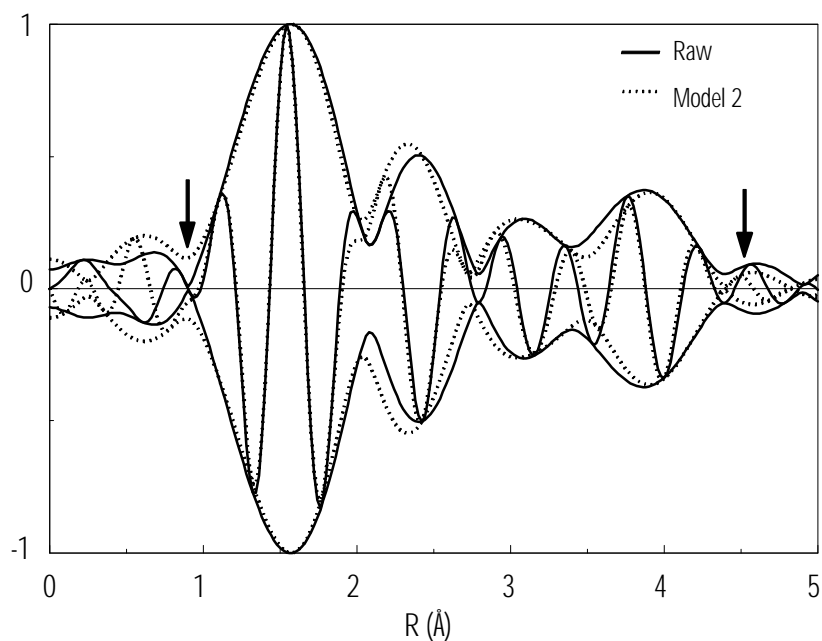


**Figure 5** Fourier transforms (solid line) and best fit (dotted line) of model 2 for the VPO/SiO<sub>2</sub> catalyst ( $k^2$ ,  $\mathbf{Dk} = 3.5-10 \text{ \AA}^{-1}$ ,  $\mathbf{DR} = 1-4.5 \text{ \AA}$ ). The arrows indicate the fitting range.

Model 1 shows a best fit with one short vanadyl bond at 1.59 Å. Two vanadyl groups are bridged by two oxygen atoms at 2.00 Å resulting in a vanadium-vanadium distance of 3.20 Å. Furthermore, two oxygen neighbours are observed at 2.74 Å. Finally, several phosphorus neighbours are detected at 4.05 Å (CN=2.4). In this model, all  $E_0$  corrections are negative. The very negative  $E_0$  for V-V cannot be understood. Furthermore, most Debye-Waller factors are negative, which is unlikely when these values are compared to the values for VPO/bulk.

The second model was fitted with the vanadium neighbours at 4.32 Å (CN=2.4) and the phosphorus neighbours at 3.56 Å (CN=2.1). Furthermore, four oxygen neighbours are found at 1.98 Å (CN=2.0) and 2.07 Å (CN=2.0) respectively. The co-ordination number of the contribution at 2.70 Å is equal to that in model 1.  $E_0$  values are reasonable, except for the V-O<sub>4</sub> contribution at 2.70 Å. Moreover, the Debye-Waller factors seem to be reasonable.

#### ***Titania-supported V-P-O***

The EXAFS data of VPO/TiO<sub>2</sub> were more difficult to fit. In Table 4, the results of our best fit for this sample are represented. The accompanying Fourier transforms are represented in Figure 6.

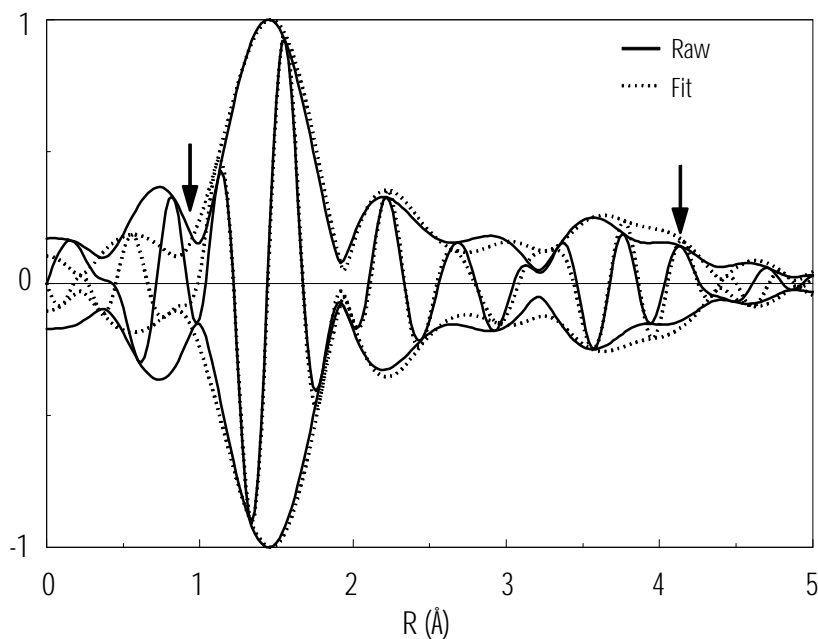


**Figure 6** Fourier transforms (solid line) and best fit (dotted line) for the VPO/TiO<sub>2</sub> catalyst ( $k^2$ ,  $\Delta k = 3.5-10 \text{ \AA}^{-1}$ ,  $\Delta R = 1-4.2 \text{ \AA}$ ). The arrows indicate the fitting range.

**Table 4** Fitted atomic distances, co-ordination numbers, Debye-Waller factors and inner potential corrections of the VPO/TiO<sub>2</sub> catalyst.

	<i>R</i> (Å)	CN	<i>Ds</i> <sup>2</sup>	<i>E</i> <sub>0</sub>
V-O <sub>1</sub>	1.61	1.0	-0.00185	-7.75
V-O <sub>2</sub>	1.99	3.0	0.00441	-7.75
V-O <sub>3</sub>	2.59	2.4	-0.00197	14.45
V-P	3.38	2.3	0.02454	-1.51
V-V or V-Ti	4.06	0.6	-0.0150	-14.90

The structural parameters of the VPO/TiO<sub>2</sub> sample indicate one short vanadyl at 1.61 Å. Furthermore, three oxygen neighbours are found at 1.99 Å and several more oxygen neighbours at 2.58 Å. In the model, two phosphorus neighbours could be fitted at 3.38 Å and a small amount of vanadium or titanium neighbours is present at 4.06 Å.

## DISCUSSION

### VPO/bulk catalysts

In the literature, only a few examples of EXAFS studies on bulk vanadium(IV)-phosphate catalysts are known [40,41,42,43]. Generally, only a qualitative description of the spectra has been presented. This is probably due to the complexity of the V-P-O catalyst system, which results in a very complicated data analysis.

López-Granados *et al.* have studied bulk catalysts that were prepared according to the same methods that were employed in this investigation [40]. For catalysts with a high P/V ratio (> 1), only a single shell was observed in the Fourier transform. Second shell contributions were found for catalysts with a P/V ratio of 0.7 and for bulk crystalline (VO)<sub>2</sub>P<sub>2</sub>O<sub>7</sub> [40]. However, due to the disorder in their V-P-O samples, López-Granados and co-workers were not able to fit the filtered oscillations of the V-O shell in (VO)<sub>2</sub>P<sub>2</sub>O<sub>7</sub> nor in the other samples.

Better results were obtained by Centi and co-workers, who found that the aqueous VPO/bulk is more ordered than its organic counterpart [41]. For the organic bulk catalyst, a two-dimensional structure is suggested, whereas for the aqueous bulk catalyst a three-dimensional structure is assumed [41].

Vlaic and Garbassi have also studied a VPO/bulk-aq catalysts with different P/V ratios, and have compared the data with the spectra of VO<sub>2</sub>, V<sub>2</sub>O<sub>5</sub>, and VO(acac)<sub>2</sub> [42]. They concluded that at low phosphorus contents, vanadium tends to coordinate five oxygen atoms in the first shell. One at a short distance (1.57 ± 0.02 Å), and four at a long distance (1.96 ± 0.01 Å) [42]. In the presence of an excess of phosphorus (P/V > 1), the distances do not change, but the coordination numbers decrease from 5 (1+4) to 4 (1+3). This is an indication that the structure changes from distorted octahedral to square pyramidal upon addition of more phosphate [42].

Our samples have been prepared with a P/V ratio of 1.1, according to well-known preparation procedures. We have studied these samples with EXAFS after a long time-on-stream (> 100 hours). The EXAFS and XRD [1] results are in agreement with the results in the literature, for both the P/V ratio, and the preparation method. Moreover, the Fourier transforms of Centi *et al.* closely resemble our data.

In this study, we have carried out a quantitative EXAFS data analysis of these VPO/bulk catalysts. To our knowledge, such results have not been reported in the literature. A good fit was obtained when the co-ordination numbers and distances were fixed and taken from single-crystal XRD data [25]. This procedure works well for distances up to 3.5 Å. However, at larger distances too many scatterers are present in the co-ordination shell [24,25]. This complicates the data analysis severely, resulting in deviations between raw data and fit beyond a distance of 3.5 Å. These deviations could, however, also be the result of disorder in the samples. Consequently, the optimised fit parameters are average values and this may explain the deviations from the ideal structural parameters of vanadylpyrophosphate. Taking into account that EXAFS is a bulk technique, which is not specific sensitive for the surface of the samples, this surface contribution should also result in deviations from the single-crystal data. These deviations are not observed in our data at distances smaller than 3.5 Å, which can be an indication that the additional (surface) contribution is highly disordered and averaged out in the EXAFS background. Nevertheless, the results for the VPO/bulk samples show that our approach of EXAFS-data analysis, which makes use of experimental and theoretical references for V-O, V-V and V-P scatterer pairs is viable for the analysis of V-P-O EXAFS data. The analysis data of both VPO/bulk catalysts show that the distorted VO<sub>6</sub> unit resembles the structure of vanadylpyrophosphate. Furthermore, the V-P and V-V contributions are close to the ideal values of 3.30 - 3.37 Å (V-P) and 3.23 Å (V-V) [24,25].

Besides the co-ordination numbers and bond distances, also the Debye-Waller factors ( $\Delta\sigma^2$ ) and inner potential corrections ( $E_0$ ) are important parameters in the EXAFS data analysis. For both VPO/bulk catalysts, a systematic decrease of the  $E_0$  values is found for the V-O contributions. These trends can be assigned to differences in nature (ionic vs. covalent) of the V-O bonds and could provide information about the V-O bond strength in our catalysts [44]. The Debye-Waller factors are a measure for the disorder in the samples, compared to the reference compounds. In general, these values are positive. For our VPO/bulk samples, the Debye-Waller factors of V-O<sub>2</sub> and V-V are negative. The oxygen atoms of the V-O<sub>2</sub> contribution are the bridging oxygen atoms of the edge-sharing VO<sub>6</sub> units. Consequently, they are more tightly bound, which results in a negative Debye-Waller factor. The rigid framework of the edge-sharing VO<sub>6</sub> dimers and the temperature at which the VPO/bulk EXAFS data were collected (77 K) probably account for the negative Debye-Waller factor compared to the reference (Ti-foil), which was measured at room temperature.

### Supported V-P-O catalysts

In chapter 5 of this thesis, we already showed that the structure of the supported V-P-O catalysts is different from the structure of VPO/bulk. This is now confirmed by the quantitative analysis of the EXAFS data, since no acceptable fit was obtained when the structural parameters of vanadylpyrophosphate were used as starting values for the fit. It must be noted that homogeneity of the samples is a prerequisite for a reliable quantitative approach with EXAFS. In the following sections, we will discuss the structural parameters obtained for the supported V-P-O catalysts and propose different models for the V-P-O phase supported on SiO<sub>2</sub> and TiO<sub>2</sub>.

### **Silica-supported V-P-O**

For VPO/SiO<sub>2</sub>, two different models were obtained. Model 1 showed the best fit. However, the structural parameters of this model are not in agreement with the XANES data of this sample. The XANES part of the X-ray absorption data revealed that the co-ordination geometry of vanadium in bulk V-P-O (VO<sub>6</sub>), titania-supported V-P-O (VO<sub>4</sub>) and silica-supported V-P-O (distorted VO<sub>6</sub> or VO<sub>5</sub>) differs considerably [2,35]. Based on the structural parameters the total oxygen coordination number in the first shell around vanadium is five for the VPO/SiO<sub>2</sub> catalyst. However, the two oxygen neighbours at 2.74 Å are too far away to be considered as chemically bonded to vanadium and, hence, a square pyramidal or distorted octahedral configuration is not easily visualised in this model. Furthermore, the presence of a vanadium neighbour at 3.20 Å is in disagreement with the ESR results of this sample [2,35]. The very weak exchange interaction that we have found for VPO/SiO<sub>2</sub> ( $\theta = 2 \pm 1$  K) excludes a model in which the orbitals of vanadium overlap as is the case when the interatomic distance would be 3.20 Å. In vanadylpyrophosphate, where the V-V distance is 3.23 Å, overlap of the vanadium 3d<sub>xy</sub> orbitals results in an exchange interaction of -65.7 K. Other criteria to reject model 1 are the very negative E<sub>0</sub> value for the V-V contribution compared to VPO/bulk (Table 2) and the negative Debye-Waller factors for the V-O<sub>2</sub> and V-O<sub>3</sub> contributions that cannot be understood.

Therefore, we have been looking for a model that is in agreement with our XANES and ESR results. The results of this fit are represented in model 2. In this model, a square pyramidal configuration is met by the presence of one short vanadyl bond at 1.61 Å and four V-O bonds around 2 Å. Furthermore, two oxygen neighbours are present at 2.70 Å. We tentatively assign this contribution to oxygen atoms from the silica support. The vanadium-phosphorus distance of 3.56 Å that was obtained with model 2 is rather large compared to the values generally found for vanadylpyrophosphate (3.33 Å). However, when the phosphorus atom is considered to be bonded to vanadium via a bridging oxygen atom, this distance is depending on the V-O-P angle. In vanadylpyrophosphate, V-O-P angles are ranging from 122° to 154°, and consequently V-P distances range from 3.10 to 3.45 Å [24,25]. A distance of 3.56 Å would mean that the V-O-P angle is about 180°, which is extraordinary. Finally, a V-V distance of 4.32 Å is fitted. This value is significantly more than twice the V-O distance in the plane of the VO<sub>5</sub> units. However, when the VO<sub>5</sub> units are corner-sharing and the V-O-V angle is about 180°, multiple scattering effects play an important role. These effects could

account for the relatively large V-V distance that we have calculated. The distance of 4.32 Å is much larger than the V-V distance in vanadylpyrophosphate and, therefore, model 2 is in agreement with the ESR data of VPO/SiO<sub>2</sub>, since the overlap of the vanadium orbitals is expected to be poor. The fractional co-ordination numbers of the V-V and V-P contributions in model 2 can easily be explained. Considering a corner-sharing geometry of the VO<sub>5</sub> units, each of the four corners of the base units can be terminated by another VO<sub>5</sub> unit or a phosphate group, as represented in Figure 7. Consequently, the sum of the V-P and V-V co-ordination numbers is not allowed to exceed the value of four, which is the case for model 2 within the experimental error.

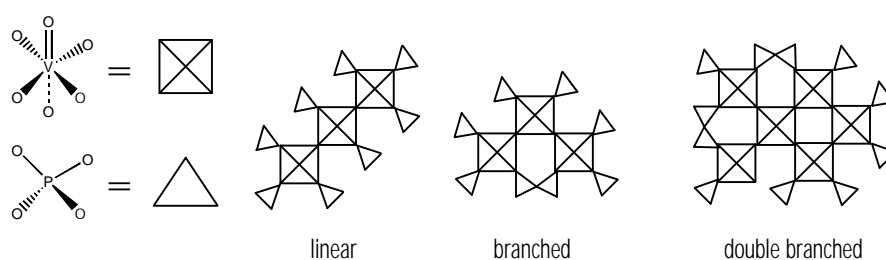


**Figure 7** Possible structures formed upon connection of several structural units of model 2 for VPO/SiO<sub>2</sub>.

**Table 5** Average co-ordination numbers of V-V and V-P for different geometries of the structural units of model 2.

Number of VO <sub>x</sub> units	Geometry	Average CN <sub>V-V</sub>	Average CN <sub>V-P</sub>
1	-	0	4
2	-	1	3
3	linear	1.3	2.7
4	linear + branched	1.5	2.5
5	linear + branched	1.6	2.4
6	linear + branched	1.7	2.3
6	double branched	2.0	2.0

Based on the geometries represented in Figure 7, the average co-ordination numbers of V-V and V-P depend on the number of VO<sub>5</sub> units that is present in the cluster. We have calculated the average V-V and V-P co-ordination numbers for a number of clusters and geometries (linear, branched or double branched) and the results of these calculations are represented in Table 5. From this table, it is apparent that the average V-V and V-P co-ordination numbers mainly depend on the size of the clusters and much less on the geometry. The co-ordination numbers that were obtained for model 2 indicate that the clusters in our VPO/SiO<sub>2</sub> catalyst consist of three to four VO<sub>5</sub> units.

The structural parameters of model 2 indicate that the selective oxidation of *n*-butane to maleic anhydride does not necessarily proceed via the vanadyl dimer

that is present in *e.g.* vanadylpyrophosphate. This is in agreement with Raman results of Wachs and co-workers [45].

#### ***Titania-supported V-P-O***

The structure of VPO/TiO<sub>2</sub> is deviating from both vanadylpyrophosphate and VPO/SiO<sub>2</sub> [2,35]. However, it was difficult to obtain a good fit for the EXAFS data. Nevertheless, the best fit for this sample shows structural parameters that are quite reasonable. Furthermore, they are in agreement with our XANES and ESR results [2,35].

The best fit of the EXAFS data of VPO/TiO<sub>2</sub> shows bond distances which are almost equal to those found for model 2 (VPO/SiO<sub>2</sub>), except for the long V-O contribution, which is located at 2.59 Å instead of 2.70 Å. However, the co-ordination numbers are significantly different, and hence a different structure is assumed.

Based on XANES, ESR and the best fit of the EXAFS data of VPO/TiO<sub>2</sub> we therefore propose that the sample consists of isolated tetrahedral vanadyl units. These units consist of one short vanadium-oxygen bond (1.61 Å) and three vanadium-oxygen bonds of 1.99 Å (V-O-Ti). Phosphate is present in the sample, but not chemically bound to the VO<sub>4</sub> units. Overbeek has shown that phosphate has a high affinity for adsorption on titania during the precipitation of V-P-O onto this support material, and consequently direct anchoring of phosphate to titania should be possible [46]. Wachs and co-workers also showed that anchoring of phosphate species to titania is possible [33]. However, they claim the formation of HO-P(-O-Ti)<sub>3</sub> species instead of a configuration in which one Ti-O-P bond is present. The V-O contribution at 2.59 Å could be an oxygen atom from a neighbouring phosphate group. However, the negative Debye-Waller factor for this contribution could not be explained this way, because it is expected to be positive and very high due to the fact that PO<sub>4</sub> groups are relatively free to move. On the other hand, it is possible that hydrogen bonding between the OH groups of the phosphate and the vanadyl oxygen atom occurs, resulting in a negative Debye-Waller factor. This might also explain the slightly elongated V=O bond length compared to the V=O bond length in VPO/bulk and VPO/SiO<sub>2</sub> (1.61 Å vs. 1.59 Å). Finally, a very small V-V contribution is found, which should be originating from neighbouring vanadyl units. However, it is more obvious to assign this contribution to titanium neighbours of the support. The Ti-O bond length in titania (rutile) is 1.947 Å [47], and hence the distance of 4.06 Å for V-Ti in our sample seems reasonable. Furthermore, the negative Debye-Waller factor for the V-Ti can now be explained by the very rigid (Ti-O)<sub>3</sub>-V=O unit. However, the V-Ti co-ordination number is very low. A co-ordination number of 3 is expected for the proposed structure, whereas a co-ordination number of 0.6 is found. A possible explanation for this feature could be that more V-O contributions should be taken into account within a distance of 4.0 Å which are originating from the neighbouring phosphate groups. These extra oxygen scatterers could have interference with the V-Ti scattering pair, resulting in deviating co-ordination numbers. Molecular modelling may provide more information about the validity of

the proposed structural model for VPO/TiO<sub>2</sub>. The proposed structure of the V-P-O sites in the VPO/TiO<sub>2</sub> sample is visualised in Figure 8.

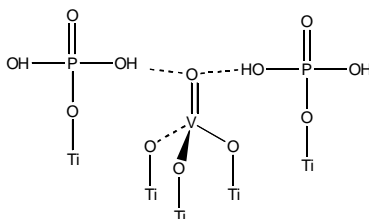


**Figure 8** Proposed model for the structure of VPO/TiO<sub>2</sub> as deduced from EXAFS data analysis, XANES and ESR experiments.

#### V-P-O structure in relation to catalytic properties

It is very interesting to correlate the structural parameters found with our EXAFS data analysis for the various V-P-O catalysts with their catalytic. In chapter 5 of this thesis, we have shown that VPO/bulk and VPO/SiO<sub>2</sub> show comparable selectivity to MA at equal conversion levels, whereas VPO/TiO<sub>2</sub> is very active, but much less selective.

The vanadyl oxygen atom is found at an almost equal distance of 1.59 Å, 1.62 Å and 1.61 Å for VPO/bulk, VPO/SiO<sub>2</sub> and VPO/TiO<sub>2</sub>, respectively. However, the Debye-Waller factors for this V-O<sub>1</sub> contribution are positive for VPO/bulk and VPO/SiO<sub>2</sub> and negative for the VPO/TiO<sub>2</sub> catalyst, which indicates that the vanadium oxygen bond is much stronger in the latter. Nevertheless, the role of the vanadyl group in the *n*-butane oxidation reaction is still not clear [7] and a more systematic approach with various vanadium oxide based catalysts is necessary to provide more knowledge on this subject.

Another interesting observation is the relative geometry of the vanadium units in the three catalysts. XANES and EXAFS indicate that the local geometry of vanadium is distorted octahedral for VPO/bulk and VPO/SiO<sub>2</sub> and tetrahedral for VPO/TiO<sub>2</sub>. It is, however, interesting to note that the octahedrons are edge-sharing in VPO/bulk and corner-sharing in the VPO/SiO<sub>2</sub> catalyst. Nevertheless, the surface structure of VPO/bulk is not selectively probed with EXAFS and consequently it is not obvious that the active sites in VPO/bulk are edge-sharing VO<sub>6</sub> units. The high selectivity of the VPO/SiO<sub>2</sub> catalyst indicates that an edge-sharing geometry is not a prerequisite for optimal catalytic performance in the *n*-butane oxidation reaction.

Furthermore it is important to note that the selective catalysts, VPO/bulk and VPO/SiO<sub>2</sub>, contain V-O-P bonds, which are most probably absent in the VPO/TiO<sub>2</sub> catalyst. These V-O-P bonds apparently play a crucial role in the selective oxidation of *n*-butane to maleic anhydride.



## **CONCLUSIONS**

We have performed the quantitative analysis of the EXAFS data of VPO/bulk-org, VPO/bulk-aq, VPO/SiO<sub>2</sub> and VPO/TiO<sub>2</sub> catalysts, of which the Fourier transforms of the EXAFS data have been presented in chapter 5 of this thesis.

The structure of the two VPO/bulk catalysts nicely matches the single-crystal XRD data of vanadylpyrophosphate. Only small differences in the contributions of V-P and V-V have been observed for the samples, but these are within the limits of accuracy of our fitting procedure. These results indicate that the applied difference file technique, which makes use of experimental references, is suitable for the analysis of the complex V-P-O system. However, the results of the analysis of the VPO/bulk samples also show the limitations of X-ray absorption spectroscopy as a (bulk) characterisation tool. Despite the fact that only 63 % of the VPO/bulk-org sample consists of vanadylpyrophosphate [1,17], the EXAFS data were almost perfectly fitted with the single-crystal XRD data of vanadylpyrophosphate. This indicates that the minor (surface) components are apparently invisible in the EXAFS background.

The spectra of VPO/SiO<sub>2</sub> and VPO/TiO<sub>2</sub> are not suffering from this drawback, since the applied active phase is highly dispersed over the support surface and no dominating bulk contributions are expected in the spectra. However, we are not certain about the homogeneity of the sample and therefore we can only speculate about the structure of the supported V-P-O phases. For VPO/SiO<sub>2</sub>, two models were deduced from the EXAFS data analysis. The best fit was obtained with a model that had no chemical significance, *i.e.* no realistic chemical structure could be created from the EXAFS parameters. The second model was in agreement with XANES and ESR data and showed a distorted octahedral geometry. The VO<sub>5</sub> units were corner-sharing and the average V-P and V-V co-ordination numbers indicated that the clusters consisted of six units, terminated by phosphate groups.

For VPO/TiO<sub>2</sub>, the structural model that was derived from the EXAFS data analysis indicates that this catalysts consists of isolated tetrahedral vanadyl groups, which are tightly bound to the support via three Ti-O-V bridging bonds. In the VPO/TiO<sub>2</sub> catalyst, phosphate is not directly bound to the VO<sub>4</sub> units, but rather directly to the titania surface. The P-OH groups of these phosphate moieties are likely co-ordinated to the vanadyl bond of the VO<sub>4</sub> tetrahedrons via hydrogen bonds. This model is in agreement with XANES and ESR data as well.

The obtained models are of great importance for the understanding of the essential structural parameters that determine the optimal catalytic performance of V-P-O catalysts in the selective oxidation of *n*-butane to maleic anhydride.

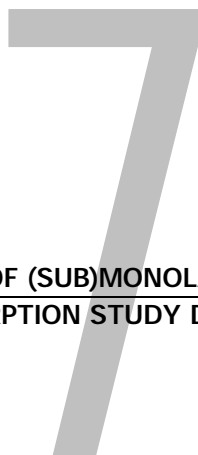
## REFERENCES

- 1 Chapter 3 of this thesis, and references therein
- 2 Chapter 5 of this thesis, and references therein
- 3 E. Bordes, *Catal. Today* **1** (1987), 499
- 4 T.P. Moser, G.L. Schrader, *J. Catal.* **92** (1985), 216
- 5 M.E. Lashier, *An investigation of active and selective oxygen in vanadium phosphorus oxide catalysts for n-butane oxidation to maleic anhydride*, Thesis, Iowa State University, 1989
- 6 E. Bordes, *Proc. Shell Conference on Oxidation Catalysts*, Wolfheze, 1990
- 7 G. Centi, *Catal. Today* **16** (1993), 5
- 8 V.V. Gulians, J.B. Bensiger, S. Sundaresan, I.E. Wachs, J.M. Jehng, J.E. Roberts, *Catal. Today* **28** (1996), 275
- 9 T. Shimoda, T. Okuhara, M. Misono, *Bull. Chem. Soc. Jpn.* **58** (1985), 2163
- 10 G. Busca, F. Cavani, G. Centi, F. Trifiro, *J. Catal.* **99** (1986), 400
- 11 N. Harrouch-Batis, H. Batis, A. Ghorbel, J.C. Vedrine, J.C. Volta, *J. Catal.* **128** (1991), 248
- 12 G.J. Hutchings, A.D. Chomel, R. Olier, J.C. Volta, *Nature* **368** (1994), 41
- 13 E. Bordes, P. Courtine, *J. Chem. Soc. Chem. Commun.* (1985), 294
- 14 B.K. Hodnett, B. Delmon, *J. Catal.* **88** (1984), 43
- 15 B.K. Hodnett, B. Delmon, *Ind. Eng. Chem. Fundam.* **23** (1984), 465
- 16 B.K. Hodnett, B. Delmon, *Appl. Catal.* **15** (1985), 141
- 17 M. Ruitenbeek, A. Barbon, E.E. van Faassen, J.W. Geus, *Catalysis Letters* **54** (1998), 101
- 18 R.A. Overbeek, *New aspects of the selective oxidation of n-butane to maleic anhydride: The development of a novel catalyst*, Thesis, Utrecht University, 1994
- 19 H. Morishige, J. Tamaki, N. Miura, N. Yamazoe, *Chem. Lett.* (1990), 1513
- 20 M.T. Sananes, G.J. Hutchings, J.C. Volta, *J. Chem. Soc., Chem. Commun.* (1995), 243
- 21 M.T. Sananes, G.J. Hutchings, J.C. Volta, *J. Catal.* **154** (1995), 253
- 22 G. Ladwig, *Z. Chem.* **19** (1979), 386
- 23 A. Brückner, A. Martin, B. Kubias, B. Lücke, *J. Chem. Soc. Faraday Trans.* **94** (1998), 2221
- 24 Y.E. Gorbunova, S.A. Linde, *Sov. Phys. Dokl.* **24** (1979), 138
- 25 P.T. Nguyen, R.D. Hoffman, and A.W. Sleight, *Mater. Res. Bull.* **30** (1995), 1055
- 26 A.V. Lavrov, L.S. Guzeeva, P.M. Fedorov, *Inorg. Mat.* **10** (1974), 1869
- 27 R. Gopal, C. Calvo, *J. Solid State Chem.* **5** (1972), 432
- 28 B. Jordan, C. Calvo, *Can. J. Chem.* **51** (1973), 2621
- 29 E. Bordes, J.W. Johnson, A. Raminosona, P. Courtine, *Mater. Sci. Monogr.* **25B** (1985), 887
- 30 M.E. Lashier, T.P. Moser, G.L. Schrader, *Stud. Surf. Sci. Catal.* **55** (1990), 573
- 31 M.E. Lashier, G.L. Schrader, *J. Catal.* **128** (1991), 113

*The structure of the supported V-P-O phase*

- 32 F. Ben Abdelouahab, R. Olier, N. Guilhaume, F. Lefèbre, J.C. Volta, *J. Catal.* **134** (1992), 151
- 33 I.E. Wachs, J.M. Jehng, G. Deo, B.M. Weckhuysen, V.V. Guliants, J.B. Benziger, *Catal. Today* **32** (1996), 47
- 34 M. Ruitenbeek, R.A. Overbeek, A.J. van Dillen, D.C. Koningsberger, J.W. Geus, *Recl. Trav. Chim. Pays-Bas* **115** (1996), 519
- 35 M. Ruitenbeek, A.J. van Dillen, A. Barbon, E.E. van Faassen, D.C. Koningsberger and J.W. Geus, *Catal. Letters* **55** (1998), 133
- 36 Chapter 2 of this thesis, and references therein
- 37 K. Katsumoto, D.M. Marquis, US Patent **4,132,670** (1970)
- 38 G. Centi, C. Garbassi, I. Manenti, A. Riva, F. Trifiro, in: *Preparation of Catalysts III*, B. Delmon, P.A. Jacobs, P. Grange (eds.), Elseviers, Amsterdam, 1983, 543
- 39 B.L.Mojet, *Metal Support Interactions, a step closer to the origin*, Thesis, Utrecht University, 1997
- 40 M. López-Granados, J.C. Conesa, M. Fernández-García, *J. Catal.* **141** (1993), 671
- 41 G. Centi, F. Trifiro, G. Busca, J. Ebner, J. Gleaves, *Faraday. Discuss. Chem. Soc.* **87** (1989), 215
- 42 G. Vlaic, F. Garbassi, *J. Catal.* **122** (1990), 312
- 43 G. Koyano, T. Okuhara, M. Misono, *J. Am. Chem. Soc.* **120** (1998), 767
- 44 S. Lemaux, A. Bensaddik, J.H. Bitter, D.C. Koningsberger, to be published
- 45 I.E. Wachs, J.M. Jehng, G. Deo, B.M. Weckhuysen, V.V. Guliants, J.B. Benziger, *Catalysis Today* **32** (1996), 47
- 46 R.A. Overbeek, E.J. Bosma, D.W.H. de Blauw, A.J. van Dillen, H.G. Bruil, J.W. Geus, *Applied Catalysis A: General* **163** (1997), 129
- 47 T.M. Sabine, C.J. Howard, *Acta Crystallographica B* **24** (1982), 1968

*Chapter 6*



**THE STRUCTURE OF (SUB)MONOLAYER V<sub>2</sub>O<sub>5</sub> ON ALUMINA**  
**AN *IN-SITU* X-RAY ABSORPTION STUDY DURING CATALYTIC OXIDATION**

**ABSTRACT**

The mechanism of catalytic oxidation reactions was studied using X-ray Absorption spectroscopy (XAFS) over a 17.5 wt% V<sub>2</sub>O<sub>5</sub>/Al<sub>2</sub>O<sub>3</sub> catalyst under reaction conditions. It was found that X-ray Absorption Near-Edge Structure (XANES) is a powerful tool to study changes in the local environment and the oxidation state of the vanadium centres during catalytic oxidation. At 623 K, the catalyst follows the associative mechanism in CO oxidation. XAFS revealed that the Mars-Van-Krevelen mechanism is operative at 723 K for both CO, and *n*-butane oxidation.

The Extended X-ray Absorption Fine Structure (EXAFS) results showed that the structure of the supported V<sub>2</sub>O<sub>5</sub> phase consists of monomeric tetrahedral (Al-O)<sub>3</sub>-V=O units after dehydration in air at 623 K. However, the residuals of the EXAFS analysis indicate that an extra contribution has to be accounted for. This contribution probably consists of polymeric vanadate species. The structure remains unchanged during steady-state *n*-butane and CO oxidation at 623 K and 723 K. Furthermore, when oxygen was removed from the feed at 623 K, no changes in the spectra occurred. However, when oxygen is removed from the feed at 723 K, reduction of the vanadium species was observed, *i.e.* the vanadyl oxygen atom is removed. The V<sup>3+</sup> ion subsequently migrates into the  $\gamma$ -Al<sub>2</sub>O<sub>3</sub> lattice, where it is positioned at an Al<sup>3+</sup> octahedral position. This migration process appears to be reversible; so the (Al-O)<sub>3</sub>-V=O units are thus restored by re-oxidation.

## INTRODUCTION

Supported vanadium oxide catalysts are widely used for catalytic partial oxidation of hydrocarbons [1,2], photo-oxidation [3,4], selective catalytic reduction of  $\text{NO}_x$  [5] and the oxidation of benzene to phenol with  $\text{N}_2\text{O}$  [6]. The reaction path of these kinds of reactions is often related to the Mars-Van-Krevelen mechanism (*vide infra*).

One can distinguish several different reaction steps in catalytic oxidation reactions. Besides redox reactions, such as reduction and oxidation of the catalyst surface, acid-base reactions between reactants and products, on the one, and the catalyst, on the other hand, can take place. Combinations of such steps lead to different overall-reaction mechanisms. Golodets has divided these possible mechanisms in four different groups, which are schematically represented in Figure 1 [7].

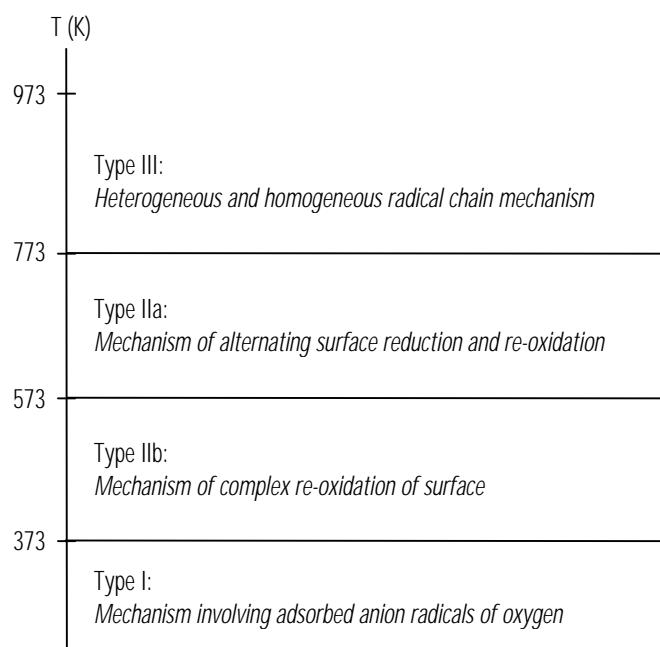


**Figure 1** Different types of mechanisms of oxidation reactions as a function of temperature, according to Golodets [7].

At elevated temperatures ( $T > 773$  K), reactions with the participation of free radicals in the gas phase take place. At moderate temperatures ( $573 \text{ K} < T < 773$  K), mostly the Mars-Van-Krevelen mechanism proceeds. At low temperatures ( $T < 373$  K), reactions generally occur through a peroxidic mechanism in which adsorbed radicals are involved.

The most studied mechanism is the above type IIa mechanism. Mars and Van Krevelen were the first to have demonstrated this two-step consecutive mechanism for the oxidation of naphthalene [8]. This so-called Mars-Van-Krevelen

or redox mechanism is operative at moderate temperatures. It is schematically represented in Figure 2.

The mechanism can best be defined as: "a mechanism in which one of the products leaves the surface, containing one of the constituents of the lattice". With this definition, not only oxidation, reduction, de-oxygenation and oxidative dehydrogenation can be described, but also e.g. chlorination, dechlorination and hydrodesulphurisation. The latter reactions frequently obey the Mars-Van-Krevelen kinetics without consumption of oxygen from the lattice of the catalyst.

First, the reactant to be oxidised is adsorbed on the surface of the catalyst resulting in the formation of an adsorbed complex. Subsequently a reaction takes place between the adsorbate and oxygen from the lattice of the catalyst, resulting in the formation of a (partially) oxidised product, which after desorption leaves an oxygen vacancy at the surface. Re-oxidation of this vacancy takes place via gas phase oxygen, as represented in Figure 2. If diffusion of lattice oxygen is sufficiently fast, the  $O^{2-}$  surface species will migrate into the lattice. This process can continuously take place as long as reactants are present to reduce the catalyst and oxygen to re-oxidise the surface. The presence of metal ions of which the lower oxidation state is relatively stable is a prerequisite for the development of this mechanism.

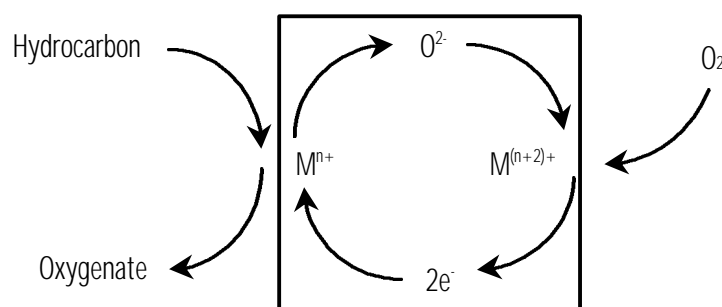


**Figure 2** Schematic representation of the redox or Mars-Van-Krevelen oxidation mechanism (type IIa).

In general, the Mars-Van-Krevelen mechanism is assumed to be operative for selective oxidation reactions. At the same time, the complex surface re-oxidation mechanism (type IIb) can play an important role. In this mechanism, formation of the final oxidation products occurs simultaneously with re-oxidation of the surface in a single concerted step. This mechanism is responsible for the formation of total oxidation products [7].

The surface of a metal oxide catalyst is likely to contain an amount of metal ions of a lower oxidation state. Up to a certain concentration, these metal sites can be considered as defects in the metal oxide matrix. However, when the oxygen vacancy concentration becomes too high, a new solid phase can form. Formation of a new solid phase generally calls for a nucleation step, which usually proceeds too slowly to give rise to a marked catalytic activity. If the redox mechanism is to be operative, it is undesirable that (part of) the catalyst becomes crystalline.

Catalysts exhibiting the Mars-Van-Krevelen mechanism therefore should be able to contain a certain amount of lattice defects without recrystallising into a metal suboxide.

Van Dillen has shown that a marked concentration of oxygen vacancies is attained only at elevated temperatures [9]. Lowering of this temperature by modification of the catalyst results in a more favourable catalytic performance. This suggests that the catalytic activity can be predicted from the thermodynamic stability of non-stoichiometric oxides. In general, however, transition metal oxides also exhibit a significant activity at temperatures where non-stoichiometry is thermodynamically less favoured. Under these conditions, the so-called associative mechanism (type IIb) is believed to be operating.

As indicated in Figure 3, oxygen vacancies are assumed to be present at the surface of the catalyst together with localised metal ions of a lower oxidation state according to the associative mechanism. After adsorption of molecular oxygen, an electron is transferred from a neighbouring metal ion to the oxygen molecule, resulting in the formation of an adsorbed superoxide anion,  $O_2^-$ . Dissociation of this ion into two  $O^-$  species is followed by a rapid oxidation of the reactant. Because this oxygen sequence is not in equilibrium, the rate of reaction with the reactant is sufficiently high to prevent formation of  $O^{2-}$  and subsequent exchange with the lattice.

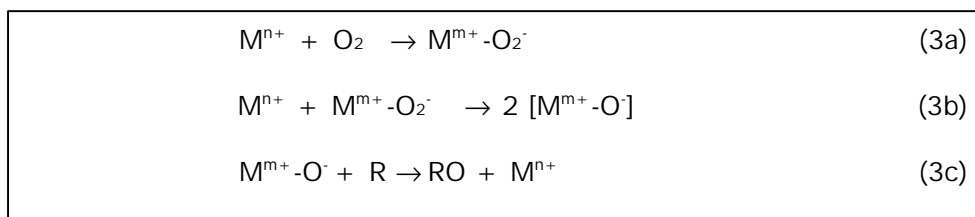


**Figure 3** Detailed scheme of the associative mechanism (type IIb).

X-ray absorption near-edge structure (XANES) has long been known to be rich in chemical and structural information [10]. For instance, it provides information about the oxidation state of vanadium. The main indication of the oxidation state of the vanadium atoms is the position of the K-edge in the spectrum. A higher valence state implies a lower energy of the core electron levels and, consequently, the presence of the K-edge at a higher energy [11,12,13,14].

Also the pre-edge of the spectrum, which reflects transitions from the K-shell to empty bound d-levels, provides information about the oxidation state of vanadium. Oxidation generally brings about an increase in the intensity of the pre-edge peak, though an effect of the surroundings of the vanadium ions has to be taken into consideration too [11,12,13]. Therefore, X-ray absorption spectroscopy has proven to be very suitable to study the oxidation state and the local atomic geometry of the vanadium sites in our catalysts *in-situ*, i.e. at reaction temperatures and in the presence of reactants.

In the past, we have studied the mechanism of *n*-butane oxidation to maleic anhydride over a titania-supported V-P-O catalyst with *in-situ* X-ray absorption



spectroscopy (XANES) in the presence of *n*-butane and air at 553 K [15]. It was found that the average oxidation state of the vanadium atoms in the catalyst did not change any more after several reduction/re-oxidation cycles [15]. This strongly indicates that the generally assumed Mars-Van-Krevelen mechanism is not operating with this catalyst system. However, it was under debate whether XANES is a proper tool to study the mechanism of oxidation reactions in detail. We realise that the investigation of oxidation reaction mechanisms should not be performed without additional  $^{18}O/^{16}O$  scrambling experiments and kinetic measurements. Therefore, we have used a  $V_2O_5$ -on-alumina catalyst to proof the principle of mechanistic research with XAFS spectroscopy. This catalyst system is well known for activity in  $H_2$  and CO oxidation [16] and *n*-butane oxidation [17] and has been extensively characterised [17]. The catalyst was proven to consist of a highly dispersed supported vanadium oxide phase [17]. This is an important condition for the use of X-ray absorption spectroscopy in catalysis, since this technique monitors all vanadium atoms including possible not-active bulk structures.

Van den Berg has determined the activity of a 7.94 wt%  $V_2O_5$ -on-alumina catalyst for oxidation of carbon monoxide [16]. Data were corrected for the activity of the support, because it was found that the activity of the support was not negligible. The results of Van den Berg are represented in Figure 4.

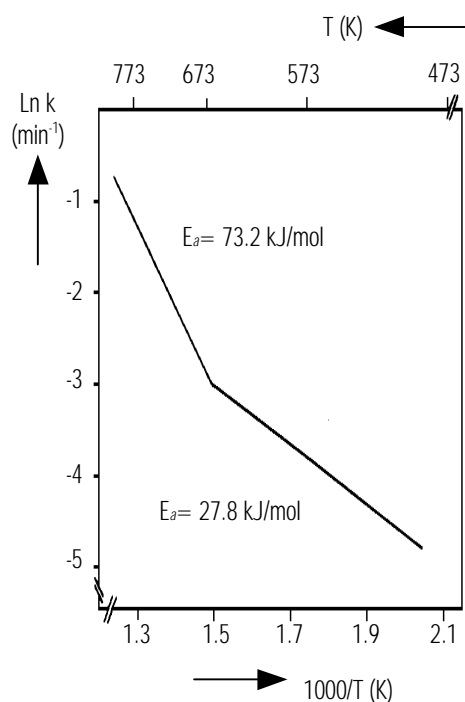


**Figure 4** Catalytic data of 7.94 wt%  $V_2O_5/Al_2O_3$ . Data and figures were taken from reference [16].

The data show that the Arrhenius plot for the oxidation of CO consist of two straight lines [16]. Below about 657 K, the activation energy was found to be 28 kJ/mol, whereas at higher temperatures a value of 73 kJ/mol was calculated. The latter activation energy agrees well with the value measured with defect-rich  $V_2O_5$  [16]. Furthermore, Van den Berg showed that the two different sets of activation energies and pre-exponential factors were not accompanied by different reaction orders [16], which implies that indeed two different mechanisms are operative.

The present chapter deals with the *in-situ* characterisation of a 17.5 wt%  $V_2O_5$ -on- $Al_2O_3$  catalyst. The sample was studied with *in-situ* X-ray absorption spectroscopy after different pre-treatment procedures and during catalytic oxidation of CO and  $n-C_4H_{10}$ .

Furthermore, the structure of the catalyst was studied after removal of oxygen from the feed. When the associative mechanism is viable, removal of oxygen should have no or only little impact on the spectra. However, when the Mars-Van-Krevelen mechanism is operating, these oxygen-free conditions should result in reduction of the sample. Consequently, structural changes of the  $VO_x$  phase are expected and these should be observable in both the XANES and EXAFS part of the XAFS spectra of the catalyst.

Additional TPR/TPO experiments and principal component analysis (PCA) were performed to support the X-ray absorption spectroscopy results. It will be shown that the structure of the supported  $VO_x$  species strongly depends on the employed conditions (dehydration, oxidation and reduction). The structural changes upon reduction of the specimen will be dealt with, and a model of the reduced  $VO_x$  structure will be presented. As far as we know, no characterisation of the reduced vanadium oxide phase has been reported in the literature [50].

## EXPERIMENTAL

### Sample preparation

Deo and Wachs of the Zettlemoyer Centre for Surface Studies of Lehigh University (USA) kindly supplied the sample we used for this study. 17.5 wt%  $V_2O_5$ -on-alumina (Harshaw,  $\sim 180\text{ m}^2/\text{g}$ ) was prepared by incipient-wetness impregnation. A vanadium(III)*iso*-propoxide (Alfa, 95-99% purity) in methanol (Fisher, 99.9% purity) solution was used to impregnate the oxide support in a nitrogen environment. The sample was first dried in  $N_2$  at room temperature for 2 hours to remove excess methanol and further dried at 393 K for 16 hours under flowing  $N_2$ . The samples were finally kept at 773 K for 1 hour under flowing  $N_2$  and an additional 15 hours under flowing dry air to form surface vanadium oxide species.

### XANES/EXAFS experiments

Vanadium K-edge spectra were collected at Station 8.1 of the Synchrotron Radiation Source in Daresbury (UK). A detailed description of the sample preparation and the equipment used for this study is found in chapter 2 of this thesis.

The structure of  $V_2O_5$  on alumina during catalytic oxidation

Samples have been studied after several treatments, which are specified in Table 1. Prior to these treatments, the sample was prepared and treated as described above. After treatment 1, the sample will be denoted as the fresh catalyst. Treatments 2 and 3 were dehydration experiments in helium and in air, respectively. The mechanistic studies were started with the dehydration procedure in air (treatment 3). The mechanism of the CO oxidation reaction was studied at two different temperatures, *i.e.* at 623 K and 723 K. The first temperature is well below the temperature corresponding with the kink in the Arrhenius curve (670 K) as observed by Van den Berg and 723 K is above this temperature [16]. Finally, we repeated the experiment at 723 K for the *n*-butane oxidation reaction in treatments 8 and 9. A detailed description of the data reduction and data analysis procedures is found in chapter 2 of this thesis [18].

**Table 1** Conditions after and during which the X-ray absorption data were collected. All flows were set to about 100 ml/min.

Treatment	Pre-treatment	Measuring conditions
1	15 min He flush at RT	He, 77K
2	a) 15 min He flush at RT b) RT to 723 K (300 K/h) in He c) Cooldown to RT in He	He, 77 K
3	a) 15 min He flush at RT b) RT to 723 K (300 K/h) in air c) Cooldown to 623 K in air	air, 623 K
4	a) Treatment 3 b) RT to 623 K (300 K/h) in He c) 30 <sup>+</sup> min 1% CO, 5% O <sub>2</sub> in He at 623 K	CO, O <sub>2</sub> , He, 623 K
5	a) Treatment 4 b) 30 <sup>+</sup> min 1% CO in He at 623 K	CO, He, 623 K
6	a) Treatment 5 b) 60 <sup>+</sup> min 1% CO, 5% O <sub>2</sub> in He at 723 K	CO, O <sub>2</sub> , He, 723 K
7	a) Treatment 6 b) 30 <sup>+</sup> min 1% CO in He at 723 K	CO, He, 723 K
8	a) Treatment 3 b) RT to 723 K (300 K/h) in He c) 30 <sup>+</sup> min 1% C <sub>4</sub> H <sub>10</sub> , 20% O <sub>2</sub> in He at 723 K	C <sub>4</sub> H <sub>10</sub> , O <sub>2</sub> , He, 723 K
9	a) Treatment 8 b) 30 <sup>+</sup> min 1% C <sub>4</sub> H <sub>10</sub> in He at 723 K	C <sub>4</sub> H <sub>10</sub> , He, 723 K

### Principal Component Analysis

Principal component analysis (PCA) is a numerical technique that can indicate the number of spectral components that contribute to a series of spectra consisting of different components. The use of PCA is especially valuable in the analysis of EXAFS data, since the distorted nature of oxides makes analysis of the EXAFS data difficult when using traditional curve fitting methods. Furthermore, it has been applied with XPS data, where the lack of proper reference spectra makes curve fitting difficult [19,20,21]. A nice introduction to PCA is outlined by Hercules *et al.* [19,22]. The requirements for PCA are: *i)* the measured spectra are linear sums of the individual components; *ii)* the components vary independently; *iii)* the data matrix contains more spectra than components [19].

PCA was carried out on  $\chi(k)$  spectra using a procedure outlined by Malinowski [23]. First, a data matrix, [D], was constructed from the  $\chi(k)$  spectra such that the columns correspond to the individual  $\chi(k)$  spectra and the rows to the  $\chi(k)$  spectral elements (the data points). The next step usually is to obtain the correlation or covariance values,  $r_0$ , by multiplying [D] with its transpose. In general, it is not mandatory for PCA that the spectral elements of  $\chi(k)$  occur at identical abscissa intervals [22]. Subsequently, a symmetric square matrix, [Z], is constructed. The [Z] matrix is then decomposed into eigenvectors using an iterative procedure, according to Malinowski [23]. The eigenvectors or abstracted principal components, which represent the signal data in the matrix, can be separated from those which account for random noise. The indicator function (IND) and the F-test are usually chosen as criteria for selecting the number of abstract principal components [22]. IND is an empirical function proposed by Malinowski, which should reach a minimum when the correct number of abstract principal components are considered [23]. The F-test requires evaluation of the F statistics to test two variances [24,25]. The probability that F-values higher than the evaluated F-statistic exist is given by  $\alpha$ . The null hypothesis is that a given factor is a member of the pool of factors, which are considered as noise. Hence, if  $\alpha$  is  $\leq$  P%, then the associated eigenvector is accepted as an abstract principal component. Generally, the P% test level is 10% [22].

### TPR/TPO experiments

Reduction and re-oxidation of the sample was studied using Temperature-Programmed reduction and Temperature-Programmed Oxidation. TPR/TPO experiments were carried out with a TPD/R/O 1100 apparatus (Thermoquest/CE instruments). 91.6 mg of the sample (as synthesised) was placed in a quartz tubular reactor and dehydrated by heating at 623 K in air. Subsequently, TPR was performed with a mixture of 5% H<sub>2</sub> in argon (20 ml/min, heating rate 10 K/min). After the first TPR experiment, the sample was cooled down to room temperature and TPO was performed with a mixture of 5% O<sub>2</sub> in He (20 ml/min, heating rate 10 K/min). Subsequently, a second TPR experiment was performed (conditions equal to the first TPR).

## RESULTS

We will present the results of this investigation in separate sections. These sections are distinguished by the four different types of experiments that we have performed, *i.e.* dehydration, CO oxidation at 623 K, CO oxidation at 723 K and *n*-C<sub>4</sub>H<sub>10</sub> oxidation at 723 K.

### Dehydration experiments

Figure 5 represents the V K-edge spectra of the fresh 17.5 wt%  $V_2O_5/Al_2O_3$  sample and after the two different thermal pre-treatment procedures, *i.e.* in He and in air.

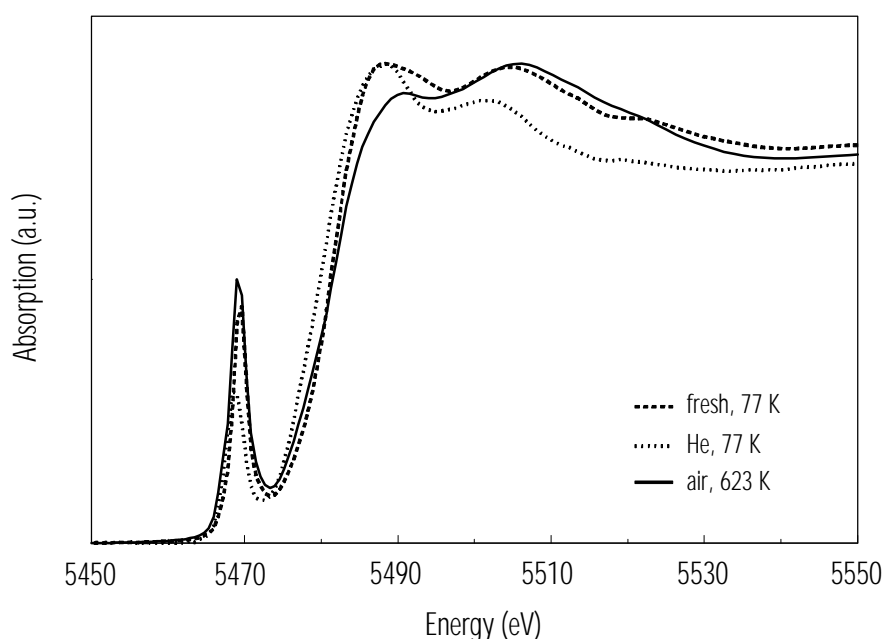


**Figure 5** V K-edge spectra of the 17.5 wt%  $V_2O_5/Al_2O_3$  catalyst after different dehydration procedures (for conditions see Table 1).

The spectrum of the fresh catalyst shows the typical vanadium K-edge spectrum, *i.e.* a pre-edge peak (5470 eV) peaks at the absorption edge (5480 eV) and peaks at energies more than 10 eV higher than the edge position. It is obvious that the two pre-treatment procedures result in different spectra. The changes of the edge positions as well as the relative intensity of the pre-edge are represented in Table 2. Besides the differences in position and intensity of the pre-edge, also the peaks around and beyond the absorption edge show clear differences. Pre-treatment in helium resulted in a shift of the pre-edge to lower energy and a decrease of the pre-edge intensity. During the pre-treatment in air, however, the pre-edge slightly shifted to higher energy and the relative intensity increased.

Figure 6 represents the raw EXAFS functions after or during the different treatments. It is obvious that differences between the three samples are also visible in the EXAFS data. From the spectra in Figures 5 and 6, it can be concluded that the dehydration method had a tremendous impact on the final structure of the catalyst sample. Dehydration in helium does not result in the same structure as dehydration in air.

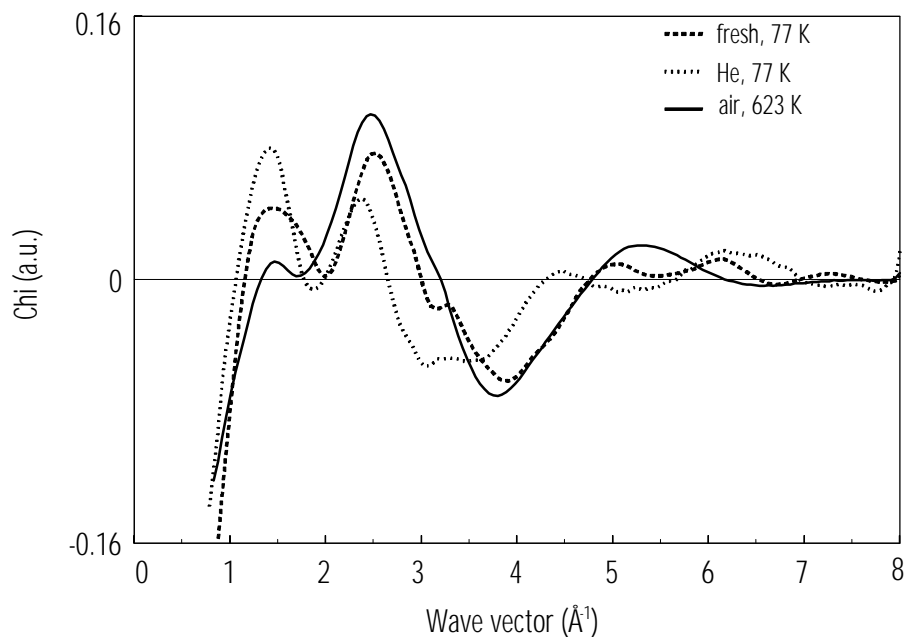


**Figure 6** EXAFS spectra of the 17.5 wt%  $V_2O_5/Al_2O_3$  catalyst after different pre-treatment procedures (for conditions see Table 1).

We have determined the structural parameters of the 17.5 wt%  $V_2O_5/Al_2O_3$  sample during the different treatments using a  $k^2$  R-space fit with the difference file technique. This was performed using the XDAP code [18]. The accompanying structural fit parameters are included in Table 3.

EXAFS analysis of the hydrated sample (treatment 1) showed one short vanadyl bond at 1.55 Å and a second V-O bond at 1.74 Å. Furthermore, two oxygen neighbours located at 1.90 Å have been found. The  $k^2$  Fourier Transform of the raw data and of the best fit of this sample are represented in Figure 7. The structure of the sample that was dehydrated in helium (treatment 2) is more complicated. It was not possible to obtain a reliable fit with parameters known from the literature.

After dehydration in air (treatment 3), we observe one short bond of 1.62 Å and three longer bonds of 1.82 Å. This distorted tetrahedron is in agreement with the shape of the XANES for this specimen. The  $k^2$  Fourier Transform of the raw data and of the best fit of this sample are represented in Figure 8. The sample that had been dehydrated in air has been used for the mechanistic studies.

The structure of V<sub>2</sub>O<sub>5</sub> on alumina during catalytic oxidation

**Table 2** Pre-edge positions and relative intensities of the 17.5 wt% V<sub>2</sub>O<sub>5</sub>/Al<sub>2</sub>O<sub>3</sub> sample after/during the different treatments.

Treatment	Conditions	Pre-edge position(eV)	I <sub>pre-edge</sub> /I <sub>edge</sub>
1	Fresh, 77 K	5469.4	0.49
2	He, 77 K	5468.6	0.31
3	air, 623 K	5469.2	0.55
4	CO, O <sub>2</sub> , He, 623 K	5469.2	0.54
5	CO, He, 623 K	5469.2	0.53
6	CO, O <sub>2</sub> , He, 723 K	5469.4	0.48
7	CO, He, 723 K	5468.4	0.18
8	C <sub>4</sub> H <sub>10</sub> , O <sub>2</sub> , He, 723 K	5469.4	0.54
9	C <sub>4</sub> H <sub>10</sub> , He, 723 K	5468.4	0.21

**Table 3** Structural parameters of the 17.5 wt% V<sub>2</sub>O<sub>5</sub>/Al<sub>2</sub>O<sub>3</sub> sample after different treatments. R= distance, CN= co-ordination number, Δσ<sup>2</sup>= Deviation of Debye-Waller factor from Na<sub>3</sub>VO<sub>4</sub> reference compound, E<sub>0</sub>= Inner-potential correction.

Treatment	Description	Scatterer	R (Å)	CN	Ds <sup>2</sup>	E <sub>0</sub>		
1	fresh	O	1.55	1.0	-0.01738	-1.21		
		O	1.74	1.0	-0.01892	4.57		
		O	1.90	2.0	0.00184	2.01		
3	Air, 623 K	O	1.62	1.0	-0.00989	0.49		
		O	1.82	3.0	0.01463	0.84		
		O	1.62	1.0	-0.00693	2.43		
4	CO, O <sub>2</sub> , He, 623 K	O	1.82	3.1	0.02309	2.16		
		O	1.62	1.0	-0.00651	1.17		
		O	1.82	3.1	0.02457	2.77		
6	CO, O <sub>2</sub> , He 723 K	- <sup>a</sup>	- <sup>a</sup>	- <sup>a</sup>	- <sup>a</sup>	- <sup>a</sup>		
		7	CO, He, 723 K	O	1.97	3.0	-0.00100	-4.85
				O	2.10	3.1	0.00138	5.46
		Al	2.73	2.9	0.02300	5.71		
		Al	3.79	1.0	0.00361	1.22		
8	C <sub>4</sub> H <sub>10</sub> , O <sub>2</sub> , He, 723 K	O	1.62	1.0	-0.01181	-0.15		
		O	1.82	3.1	0.00590	2.89		
9	C <sub>4</sub> H <sub>10</sub> , He, 723 K	- <sup>a</sup>	- <sup>a</sup>	- <sup>a</sup>	- <sup>a</sup>	- <sup>a</sup>		

a: No acceptable fit of data obtained

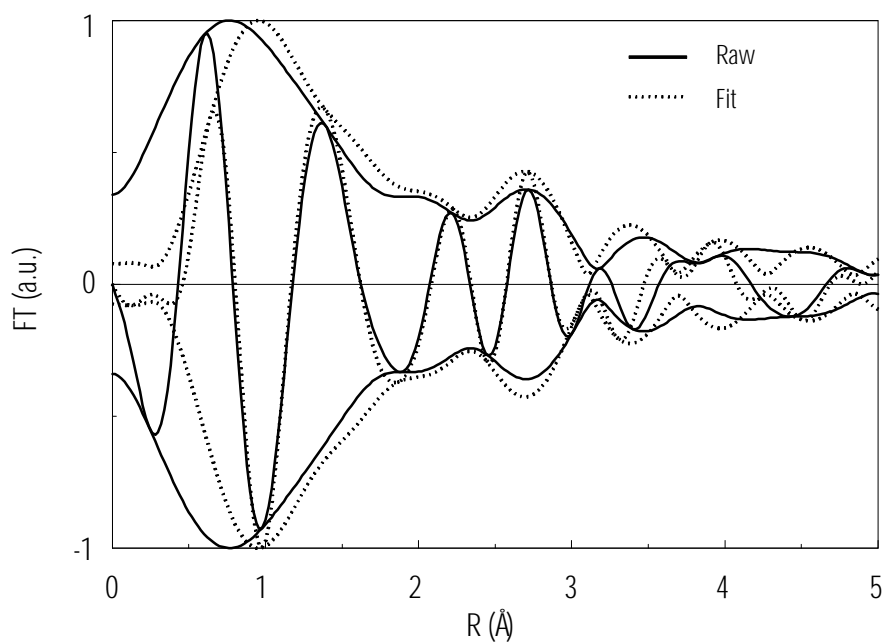
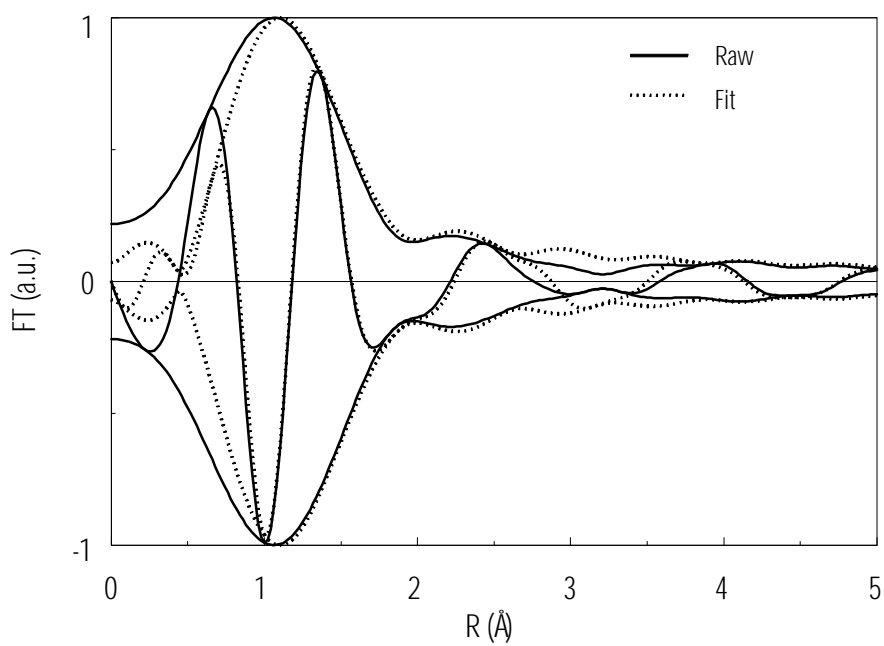


**Figure 7** Fourier transforms ( $k^2$ ,  $\mathbf{D}k = 2.5\text{-}8.0 \text{ \AA}^{-1}$ ,  $\mathbf{D}R = 1.0\text{-}3.0 \text{ \AA}$ ) of the EXAFS spectrum (solid line) and the best fit (dotted line) of the fresh sample



(treatment 1).



*The structure of V<sub>2</sub>O<sub>5</sub> on alumina during catalytic oxidation*

**Figure 8** *Fourier transforms ( $k^2$ ,  $\mathbf{Dk} = 2.5\text{-}8.0 \text{ \AA}^{-1}$ ,  $\mathbf{DR} = 1.0\text{-}3.0 \text{ \AA}$ ) of the EXAFS spectrum (solid line) and the best fit (dotted line) of the sample that was dehydrated in air (treatment 3).*

**CO oxidation at 623 K**

In Figure 9, the different *in-situ* V K-edge spectra of the catalyst during CO oxidation with and without oxygen at 623 K are represented. The spectra show that there are only small differences between the spectra of the dehydrated sample (treatment 3) and the sample during CO oxidation at 623 K (treatments 4 and 5). Moreover, minor changes in the first peaks around the absorption edge are observed. There is almost no difference between the spectra taken during the steady state experiment or after removal of oxygen from the feed at 623 K.

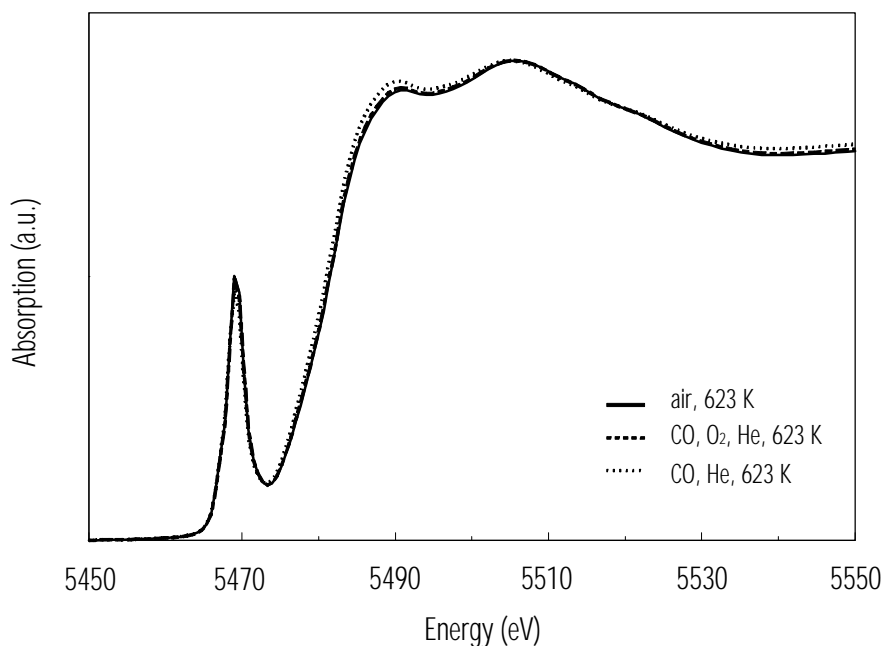


**Figure 9** V K-edge spectra of the 17.5 wt.%  $V_2O_5/Al_2O_3$  catalyst before and during CO oxidation at 623 K (for conditions see Table 1).

The sample that was dehydrated in air was used for all further *in-situ* experiments. During CO oxidation at 623 K, almost no changes in the spectrum can be observed as represented in Figure 10. Bond distances and coordination numbers remained the same within the experimental error. However, for both V-O contributions, at 1.62 Å and 1.82 Å, respectively, increased Debye-Waller factors are observed. In the absence of oxygen at 623 K (treatment 5), the catalyst showed a further increase of the Debye-Waller factors, but again, no changes in distance and co-ordination number.

The structure of  $V_2O_5$  on alumina during catalytic oxidation

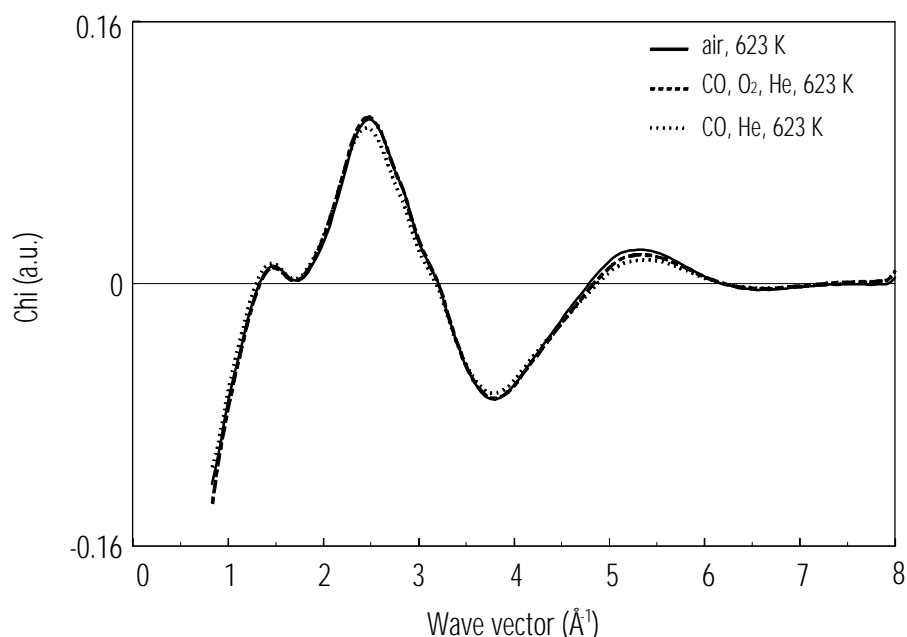


**Figure 10** EXAFS spectra of the 17.5 wt%  $V_2O_5/Al_2O_3$  catalyst before and during CO oxidation at 623 K (for conditions see Table 1).

Figures 6, 10 and 12 indicate that the structure of the supported  $V_2O_5$  phase is closely analogous for several differently pre-treated samples. The air-dehydrated sample (treatment 3) and of the samples of the steady-state experiments with CO and *n*-butane at 623 K and 723 K (treatments 4, 5 and 8) are almost identical. These spectra are assumed to be composed of various distinct  $V_2O_5$  species, *i.e.* monomeric vanadyl species and polymeric vanadate species [17].

However, it appeared possible to fit the data with one major component, the monomeric vanadyl species. Nevertheless, the residuals indicate that for a proper fit also the polymeric species must be taken into account. To establish the number of species and their relative amount, Principal Component Analysis (PCA) was applied.

In Table 4, results of the principle component analysis of a data matrix containing the spectra of treatments 3, 4, 5 and 8, as well as the chi data of the fit of the monomeric species are represented. The spectral window for the analysis was 2.5-8 Å<sup>-1</sup>. The data show a minimum for the indicator function (IND) at the second factor. Furthermore, the Q-test values exceed the 10% margin at the third factor. These results indicate that the spectra of the 17.5 wt%  $V_2O_5/\gamma-Al_2O_3$  consists of two components during or after treatments 3, 4, 5 and 8, *i.e.* the vanadyl monomers and polymeric species, which have not been included in the fit.

**Table 4** Principle Component Analysis of the 17.5 wt% V<sub>2</sub>O<sub>5</sub>/g-Al<sub>2</sub>O<sub>3</sub> before and during CO and n-butane oxidation at 623 and 723 K and the first shell fit of the monomeric species. Analysis range = 2.5-8 Å<sup>-1</sup>.

Factor	<i>r</i> <sub>0</sub>	IND	F	Q (%)
1	0.72169	1.79 x10 <sup>-3</sup>	70.77	0.11
2	0.01794	1.69 x10 <sup>-3</sup>	12.52	3.84
3	0.00158	2.87 x10 <sup>-3</sup>	2.91	23.01
4	0.00051	4.19 x10 <sup>-3</sup>	9.48	19.99
5	0.00003			

#### CO oxidation at 723 K

Figure 11 shows the spectra during CO oxidation at 723 K. At 723 K, the spectrum of the first scan was almost equal to the previous spectrum (623K CO oxidation). However, the two following spectra were already different. This indicates that the sample is changing under the applied conditions. Furthermore, switching off oxygen at 723 K turned out to have a substantial effect on both the pre-edge and the absorption edge itself (Figure 11). Both edges shifted to lower energies. Furthermore, the relative intensity of the pre-edge decreased from 0.55 ( $I_{\text{pre-edge}}/I_{\text{edge}}$ ) to 0.18 as indicated in Table 2.

In agreement with the XANES spectra, differences were observed between the various scans during the steady-state experiment at 723 K (treatment 6), as indicated in Figure 12. This indicates that the structure of the catalyst changed under these conditions. We have performed a CO oxidation experiment in the *in-situ* EXAFS cell, connected to an on-line Balzers QMS420 mass spectrometer. Although we realise that the experimental set-up in the EXAFS cell did not meet the ideal micro-reactor conditions (plug-flow, etc.) [26], the corrected CO conversion was 4% at 623 K and 23% at 723 K. Consequently, the differences in the spectra could be brought about by the different composition of the gas mixtures at different conversion levels.

The structure of  $V_2O_5$  on alumina during catalytic oxidation

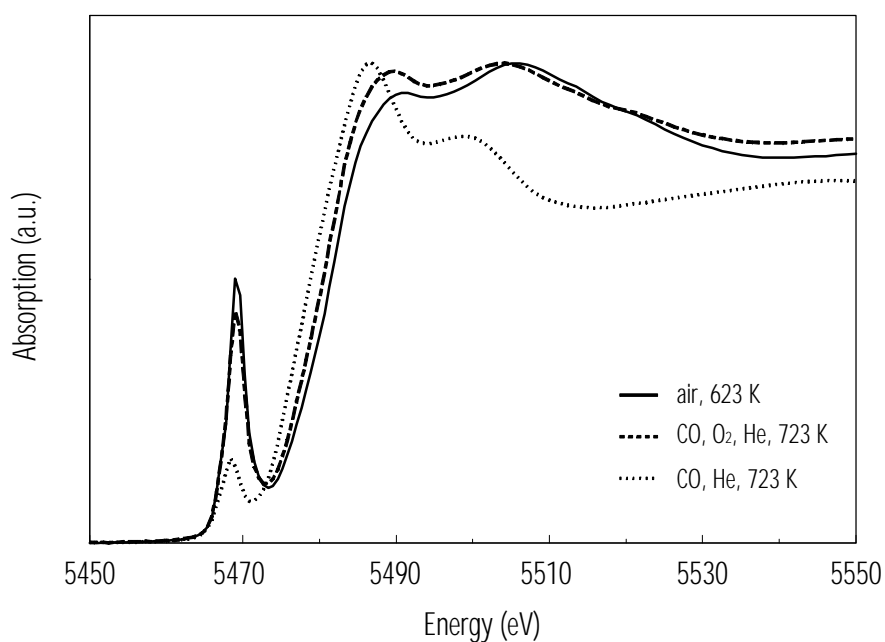


**Figure 11** V K-edge spectra of the 17.5 wt.%  $V_2O_5/Al_2O_3$  catalyst before and during CO oxidation at 723 K (for conditions see Table 1).

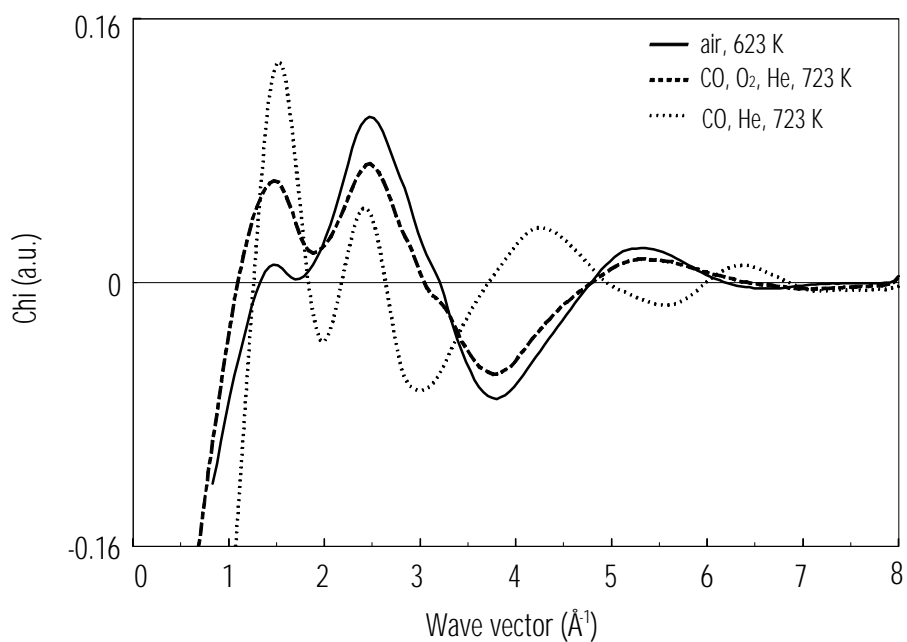
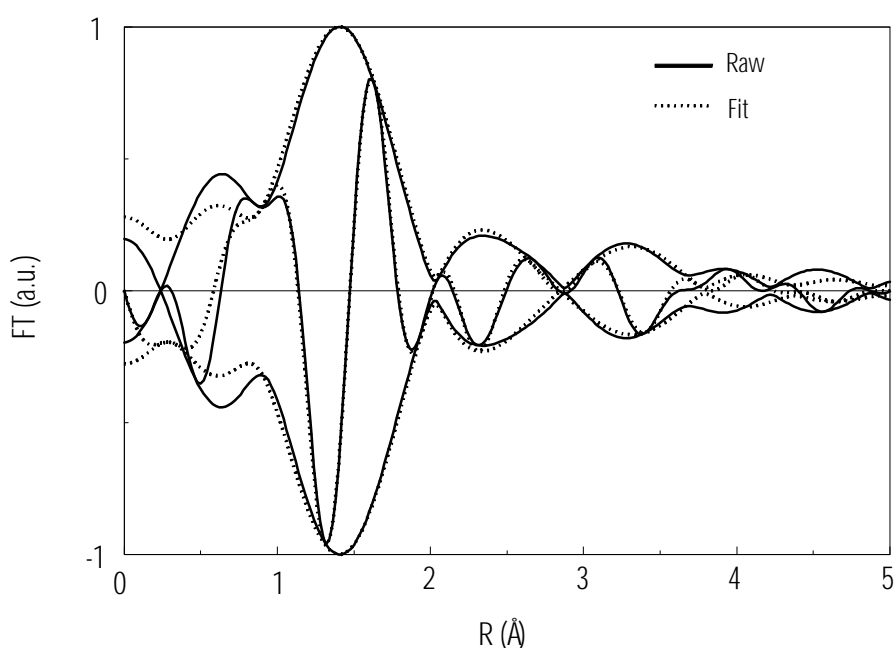


**Figure 12** EXAFS spectra of the 17.5 wt.%  $V_2O_5/Al_2O_3$  catalyst before and during CO oxidation at 723 K (for conditions see Table 1).

When oxygen was removed from the feed at 723 K (treatment 7), a more dramatic change of the catalyst structure was observed. This structural change is probably the result of reduction of the vanadium species in the catalyst. As far as we know, no characterisation of a reduced vanadium oxide phase has been reported in the literature [50]. Therefore, analysis of the EXAFS data of the reduced phase will provide useful new information. We have fitted the structure of the reduced vanadium oxide phase with three oxygen neighbours at 1.97 Å and three oxygen neighbours at 2.10 Å (distorted octahedral geometry). Furthermore, two vanadium-aluminium contributions were included in the fit, *i.e.* at 2.73 Å (CN=3) and at 3.79 Å (CN=1). The  $k^2$  Fourier transforms of the EXAFS data and

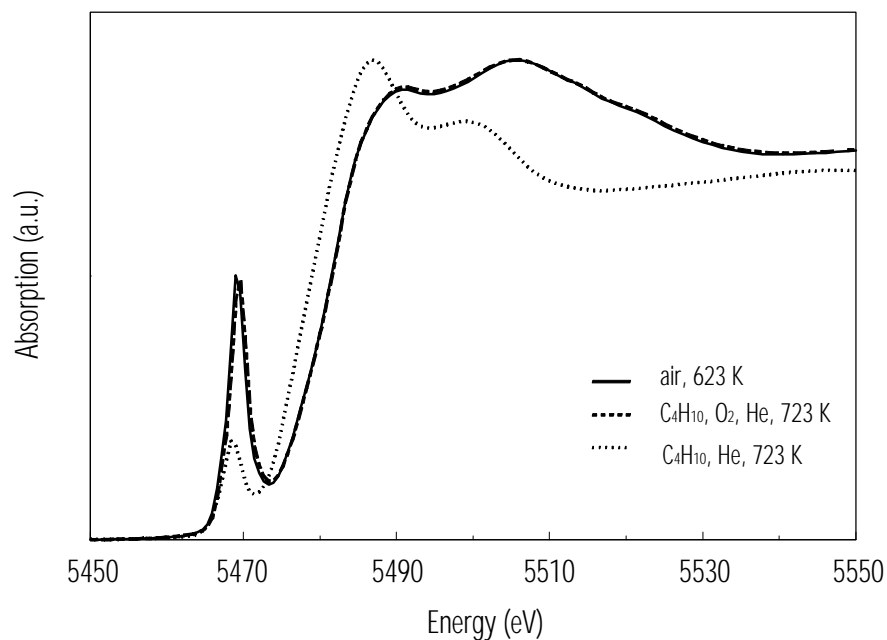


of the best fit of this sample are represented in Figure 13.

**Figure 13** Fourier transforms ( $k^2$ ,  $DK=2.5-8.0 \text{ \AA}^{-1}$ ,  $DR=1.0-3.5 \text{ \AA}$ ) of the EXAFS spectrum (solid line) and the best fit (dotted line) of the sample after reduction in CO at 723 K (treatment 7).

#### **$n\text{-C}_4\text{H}_{10}$ oxidation at 723 K**

Figures 14 and 15 show the *in-situ* results during the *n*-butane oxidation experiments. The results of these *n*-butane oxidation experiments are comparable to the CO oxidation experiments at 723 K. Under steady-state conditions (treatment 8), no changes of the XANES spectrum as compared to that of the dehydrated samples were observed as shown in Figure 14. However, when the oxygen was removed from the feed (treatment 9) a pronounced decrease of the



pre-edge intensity as well as a shift to lower energies took place. These changes are indicative for reduction of the vanadium species.

**Figure 14** V K-edge spectra of the 17.5 wt%  $V_2O_5/Al_2O_3$  catalyst before and during *n*-butane oxidation at 723 K (for conditions see Table 1).

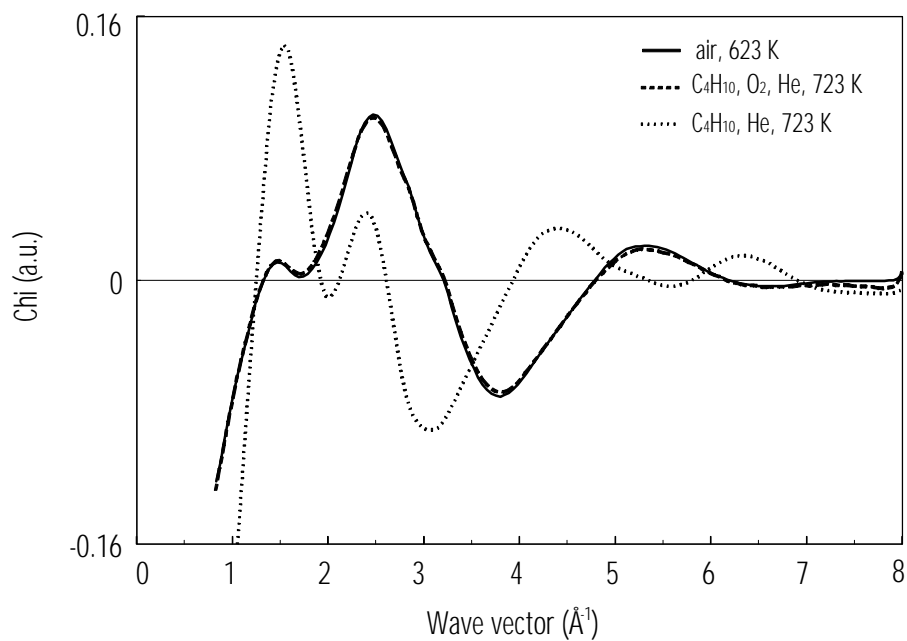


**Figure 15** EXAFS spectra of the 17.5 wt%  $V_2O_5/Al_2O_3$  catalyst before and during *n*-butane oxidation at 723 K (for conditions see Table 1).

The EXAFS data of the *n*-C<sub>4</sub>H<sub>10</sub> oxidation experiments are in agreement with the XANES spectra. Figure 15 shows that the structure of the air-dehydrated sample and the sample under steady-state conditions are almost equal; a dramatic change of this structure after removal of oxygen from the feed occurred. Apparently, *n*-butane is also able to reduce the supported VO<sub>x</sub> phase at this temperature. However, when the spectra of the two 'reduced' catalysts are compared, differences are observed. It is possible that these are brought about by the difference in reducing power of CO and C<sub>4</sub>H<sub>10</sub>.

### Temperature-Programmed Reduction

Temperature-Programmed Reduction (TPR) is a technique that provides information about the reducibility of oxidic materials. We have applied TPR to study the structural changes upon cyclic reduction/re-oxidation experiments. The results could give information about the structure of the reduced vanadium oxide phase as measured with the *in-situ* EXAFS experiments.

Figure 16 represents the results of the TPR experiments of the dehydrated catalyst (first TPR). After this experiment, we re-oxidised the specimen and subsequently, performed a second TPR experiment. During the first TPR, one broad asymmetric peak is observed. The onset temperature is about 600 K and the peak maximum is at 800 K. The total integrated intensity of the peak corresponds nicely to a reduction of V<sup>5+</sup> to V<sup>3+</sup>.

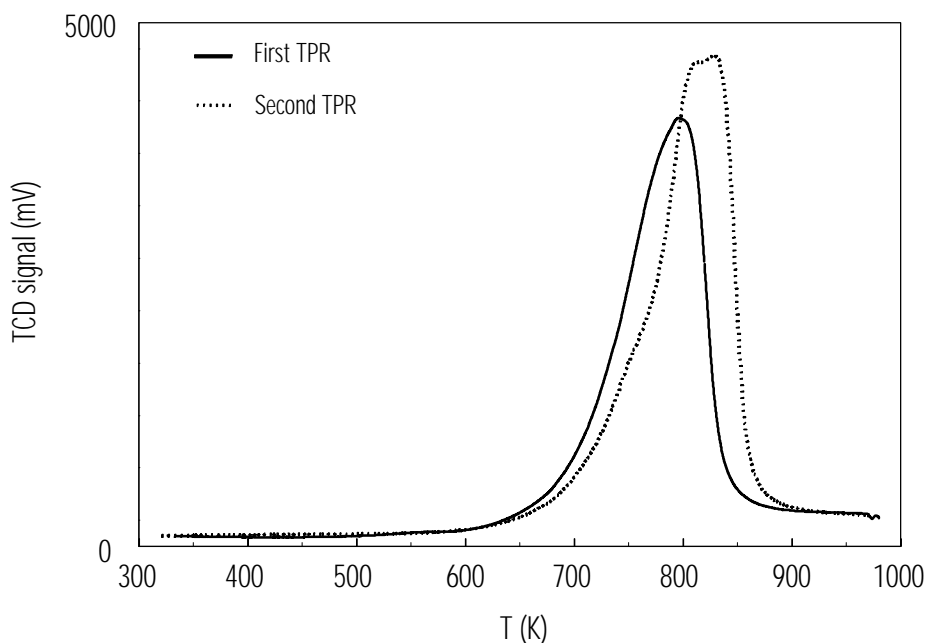




**Figure 16** TPR patterns of the 17.5 wt%  $V_2O_5/Al_2O_3$  sample after dehydration (first TPR) and after re-oxidation (second TPR). Between subsequent TPR/TPO/TPR runs, the sample was not exposed to air.

For the second TPR, the onset temperature is again 600 K, but the  $T_{max}$  has shifted to a higher temperature. The differences between the peak areas of the two TPR experiments were about 7%, which is within the experimental error.

## DISCUSSION

It is well known that the activity and selectivity of supported  $V_2O_5$  catalysts strongly depend on the supports used and the preparation procedures. One of the essential factors in controlling the catalytic performance is the local structure of the vanadium oxide species on the support. The oxygen co-ordination number and the state of aggregation on various supports have been widely studied. For reasons of comparison, we will start the discussion of our results with an overview of what is known in the literature about the structure of supported vanadium(V) oxide. Subsequently we will discuss our results for the different types of experiments (dehydration, CO oxidation at 623 K, CO oxidation at 723 K and  $C_4H_{10}$  oxidation at 723 K) and compare the results with literature data. Finally, we will place our results in the framework of the associative mechanism and the Mars-Van-Krevelen mechanism and propose a model for the structure of the reduced vanadium oxide phase.

### The structure of supported vanadium oxide

The molecular structures of surface vanadia species have been extensively investigated in the past few years with many different spectroscopic methods: Raman [59,27,28,29], IR [27,30,31], XANES/EXAFS [59,32,33,34,35,36,37], solid state  $^{51}V$  NMR [38,39,40,41], UV-VIS DRS [59,42,43,44], chemiluminescence [45,46], and ESR [44,47,48]. The local structure of  $V_2O_5$  supported on silica and  $\gamma$ -alumina has been most intensively studied.

In general, ESR and UV/VIS results are consistent with each other, although ESR results are restricted to paramagnetic  $V^{4+}$  containing species. On silica, vanadium atoms are generally stabilised in an oxygen tetrahedron in the dehydrated state. Hydrated silica-supported  $V_2O_5$  mostly exists in an octahedral configuration.

On alumina, both ESR and UV/VIS studies demonstrated that vanadium is five- or six-fold co-ordinated by oxygen. However, Raman studies revealed the formation of different types of vanadium oxide species: polymeric arrays of octahedral  $VO_6$  units as the main phase and tetrahedral  $VO_4$  species as a minor constituent on both, silica and alumina [29].

Unfortunately, the dynamic nature of the surface vanadia species has resulted in confusion in the published literature, since many studies have compared measurements taken under different experimental conditions (ambient *vs.* *in-situ*, hydrated *vs.* dehydrated) [49,50].

Most of the early studies were performed with samples exposed to atmospheric air. There is considerable evidence that under these conditions monolayer species

react with atmospheric moisture and therefore, hydrated structures are assumed [51,52]. Under hydrous conditions, the  $\text{VO}_x$  species may be properly formulated as structure B or C in Figure 17. On heating in a dry atmosphere, dehydration may take place to structure A and/or to an octahedral polyvanadate species, such as structure D [53,54], or to a simple vanadyl species [55]. *In-situ* Raman experiments generally show a shift of the Raman bands due to dehydration of monolayer species [49,51].

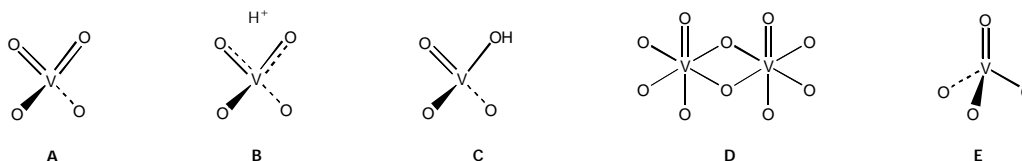


**Figure 17** Possible structures for  $\text{VO}_x$  species in the monolayer phase.

In a recent review, Wachs *et al.* stated that dehydrated surface vanadia species on  $\text{Al}_2\text{O}_3$ ,  $\text{TiO}_2$ ,  $\text{ZrO}_2$ ,  $\text{Nb}_2\text{O}_5$  and  $\text{CeO}_2$  all possess identical molecular structures [49]. On these oxidic supports mainly isolated  $\text{VO}_4$  units would be present. Their  $^{18}\text{O}$  isotopic labelling experiments demonstrated that these surface vanadia species possess only one terminal  $\text{V}=\text{O}$  bond [56,57]. Therefore, Wachs and co-workers tentatively assume that the molecular structures of these surface vanadia species consist of a terminal  $\text{V}=\text{O}$  bond and three bridging  $\text{V}-\text{O}$ -support bonds for the isolated species by (structure E in Figure 17). Furthermore, a small amount of polymerised species are present, which consist of a terminal  $\text{V}=\text{O}$  bond with one bridging  $\text{V}-\text{O}$ -support bond and two bridging  $\text{V}-\text{O}-\text{V}$  bonds [49]. The latter resembles structure D in Figure 17.

#### X-ray absorption spectroscopy with (supported) vanadium oxide

Wong *et al.* have investigated the V K-edge spectra of a broad range of vanadium compounds, including oxides, vanadates, vanadyl compounds and intermetallics in great detail [11,13]. Their study has been of great importance for the interpretation of all later work on V K-edge spectra regarding symmetry, coordination geometry, ligand type (N,O) and bond lengths.

Wong *et al.* distinguished two types of near-edge spectra: i) octahedrally coordinated compounds, such as  $\text{V}_2\text{O}_3$  *etc.*, which exhibit a weak pre-edge absorption peak, and ii) tetrahedrally co-ordinated compounds, such as  $\text{NH}_4\text{VO}_3$ , *etc.*, or compounds with a short vanadyl bond in a square pyramid, all of which exhibit a rather strong pre-edge peak [11].

This pre-edge peak is the result of a transition from the  $1s$  state to the total empty manifold of the compound. For a transition metal atom (like vanadium) in octahedral symmetry, the  $1s$  to  $3d$  transition is dipole forbidden, but it is an allowed quadrupole transition [11]. It is weak, but observable. However, in a distorted octahedral environment, mixing of the  $3d$  orbitals with the  $4p$  orbitals takes place [11]. Therefore, the pre-edge peak can be rather strong, as for instance in the spectrum of bulk  $\text{V}_2\text{O}_5$  [11]. For tetrahedral complexes, the lack of

a centre of inversion permits a dipole transition from 1s to the T<sub>2</sub> orbitals, which can possess 4p character in addition to 3d character. This gives rise to the strong pre-edge usually found with these compounds [11].

Various authors have described the application of XAFS to study supported V<sub>2</sub>O<sub>5</sub> catalysts. Kozłowski *et al.* have studied vanadium oxides supported on silica and  $\gamma$ -alumina [36,37]. They found that the main species on alumina are VO<sub>4</sub> dimers with two short (1.67 Å) and two long (1.82 Å) V-O bonds, whereas on silica mainly V<sub>2</sub>O<sub>5</sub>-like clusters were observed.

Tanaka *et al.* observed polymeric VO<sub>5</sub> square pyramids on silica and monomeric VO<sub>4</sub> tetrahedrons on alumina under ambient conditions [32]. For the dehydrated samples, VO<sub>4</sub> tetrahedrons were also observed with the alumina-supported catalyst. No octahedral species were found with EXAFS [33]. These species could not be completely excluded, because diffuse reflectance UV-VIS experiments revealed a broad, but small band in the 400–500 nm region [33]. This band was assigned to a charge-transfer band of octahedral VO<sub>6</sub> species [58].

Yoshida *et al.* have investigated the structural parameters of alumina-supported V<sub>2</sub>O<sub>5</sub> in the hydrated and dehydrated state with X-ray absorption spectroscopy [32,33,34]. However, no clear information about the dehydration procedure has been provided (air or inert). For the dehydrated sample they reported one short V=O bond of 1.63 Å ( $\Delta\sigma^2 = -0.0050$ ) and three longer V-O-support bonds ( $R = 1.78$  Å,  $\Delta\sigma^2 = 0.0065$ ). They found that in the hydrated sample, the V=O bond is slightly elongated (1.67 Å), and the Debye-Waller factor increased to 0.0022 indicating that the oxygen is less tightly bound (structure B in Figure 17).

Gao *et al.* have reported XANES data of a 10 wt% vanadium oxide-on-silica-catalyst in the hydrated and dehydrated state, of which the pre-edge position and intensity, as well as the XANES are almost equal to our results [59]. Based on their X-ray absorption spectra and UV-VIS DRS spectra, they concluded that the structure of the dehydrated silica-supported V<sub>2</sub>O<sub>5</sub> phase consists of a distorted tetrahedron [59].

### Structure of the supported vanadium oxide phase

Considering our XAFS results, it is obvious that for the 17.5 wt% V<sub>2</sub>O<sub>5</sub>-on-Al<sub>2</sub>O<sub>3</sub> catalyst, a geometry without inversion symmetry is expected in almost all cases. Only the reduced samples, *i.e.* the samples after dehydration in helium or during CO and *n*-C<sub>4</sub>H<sub>10</sub> oxidation in the absence of oxygen at 723 K (treatments 2, 7 and 9), show a decreased pre-edge feature that is shifted to lower energies. These results strongly indicate that the preferred geometry of the sample is tetrahedral in the oxidised state, and (distorted) octahedral in the reduced state [60]. In case of complete inversion symmetry, only the quadrupole contributions to the pre-edge peak are observable. For iron-based compounds, this results in an  $I_{\text{pre-edge}}/I_{\text{edge}}$  ratio of 0.07 [61]. However, for vanadium compounds, this ratio is not known. Therefore, it is difficult to attribute a specific co-ordination geometry to the reduced VO<sub>x</sub> phase. Nonetheless, it is expected that this co-ordination is preferably distorted octahedral.

The results of our *in-situ* experiments show that the tetrahedron at the oxidised state is not affected by the conditions during the steady-state oxidation reactions

at 623 K. However, under CO oxidation conditions at 723 K (treatment 6) the structure of the supported vanadium oxide phase already changes. When oxygen is removed from the feed at 723 K (treatment 7), the pre-edge peak shifts to lower energy and the intensity decreases. Furthermore, the XANES spectrum changes. These changes indicate that the vanadium geometry changes from distorted tetrahedral to distorted octahedral. These findings are in agreement with the structural parameters obtained from the EXAFS data analysis. We will now discuss the EXAFS results during the different treatments of this investigation

### Structure before and after dehydration experiments

The XANES spectra of the fresh 17.5 wt% V<sub>2</sub>O<sub>5</sub>-on-Al<sub>2</sub>O<sub>3</sub> catalyst and the spectra that were obtained after the two different dehydration procedures show differences in co-ordination geometry. The fresh, hydrated sample exhibits the characteristic XANES of a VO<sub>5</sub> compound (square pyramidal configuration as in V<sub>2</sub>O<sub>5</sub>, V<sub>4</sub>O<sub>7</sub> or V-metal) [11,12,13]. After dehydration in helium (treatment 2), the XANES spectrum resembles the spectra reported for octahedral (VO<sub>6</sub>) compounds [11,12,13], whereas after dehydration in air (treatment 3), the characteristic spectrum of a tetrahedrally coordinated vanadium compound (VO<sub>4</sub>) is observed [11,12,13].

The EXAFS data of our dehydration experiments also display remarkable differences between the spectra of the fresh sample (treatment 1) and the dehydrated samples (treatments 2 and 3). The data for the fresh sample do not match the model proposed by Yoshida and co-workers, *i.e.* a tetrahedral monomer with elongated vanadium-oxygen bonds. We obtained better results when a model that resembles structure C in Figure 17 was used. This structure is in agreement with the dehydration model as proposed by Gao *et al.* for a 10 wt% V<sub>2</sub>O<sub>5</sub>-on-SiO<sub>2</sub> catalyst [59].

After dehydration in helium, the vanadium species could have been reduced due to removal of the OH groups from the hydrated structure. This is, however, not resulting in the same reduced phase as with the samples reduced by CO or *n*-butane. We were not able to obtain a good fit of these data, because defect-rich species have been formed after dehydration in helium. This is probably the result of inhomogeneity of the type of species present after dehydration in helium.

Based on the Raman results of Wachs and co-workers, we expect that a tetrahedral species with one short vanadyl bond and three longer vanadium-oxygen bonds is formed after dehydration in air (treatment 3) [17]. This model is in agreement with our XANES data of this sample. The EXAFS data analysis was successfully performed with a fit consisting of one short vanadyl bond (1.62 Å) and three V-O-Al bonds (1.82 Å). However, the Raman data revealed an additional component in the spectra of the dehydrated sample, *i.e.* polymerised vanadyl species. Although we obtained a good fit of our raw EXAFS function with only the monomers in our model, we have applied Principal Component Analysis (PCA) to see whether more components are present in the spectrum of the dehydrated sample (treatment 3).

The results of the PCA clearly indicate the presence of a second component in the spectrum of the dehydrated sample. The IND function shows a minimum for the

second factor and both, the first and the second factor show a Q(%) of less than 10% which was set as the limit. The eigenvectors indicate that the first factor is the dominant species in the sample. This factor is the monomeric (Al-O)<sub>3</sub>-V=O species. The minor component is probably the polymeric type of species (Figure 17D).

#### **Structure during CO oxidation at 623 K**

During CO oxidation at 623 K (treatment 4), the structure of the supported V<sub>2</sub>O<sub>5</sub> phase does hardly change as compared to that of the air-dehydrated sample (treatment 3). Besides small changes in the Debye-Waller factors, spectra are nearly equal. Furthermore, when oxygen was removed from the feed (treatment 5), no changes in the structure of the XANES and EXAFS spectra are observed. These results indicate that the applied conditions have no impact on the structure of the supported vanadium oxide phase at this temperature.

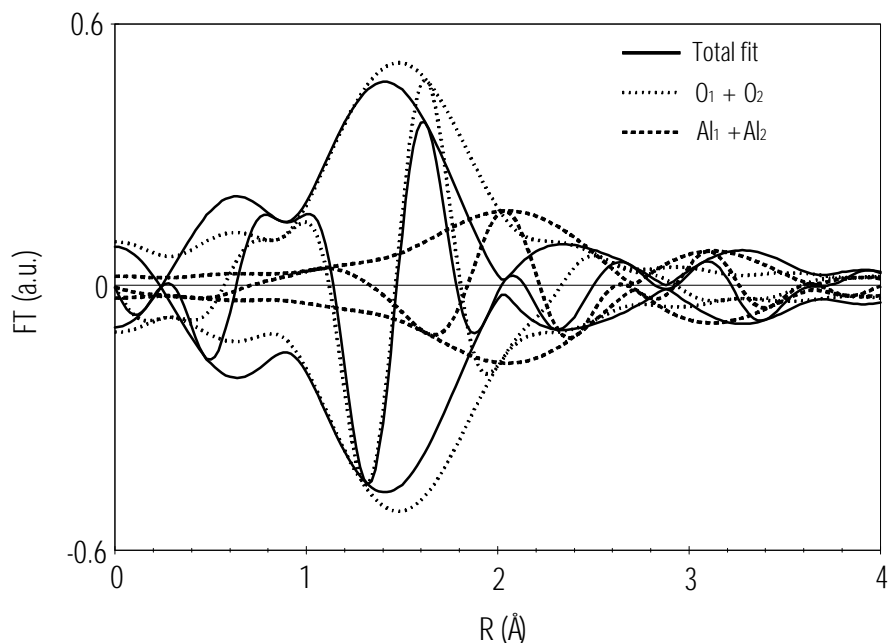
#### **Structure during CO oxidation at 723 K**

During CO oxidation at 723 K, we have already observed changes in the XANES and EXAFS spectra during the steady-state experiment (treatment 6). This indicates that under the steady-state conditions, the structure of the supported vanadium oxide phase is changed by the reactants. However, when oxygen is removed from the feed at 723 K (treatment 6), more pronounced structural changes occurred. These changes indicate that CO is able to remove oxygen from the catalysts. Reduction brings about removal of oxygen. The XANES data, however, show a change of the local geometry around vanadium from tetrahedral (VO<sub>4</sub>) to octahedral (VO<sub>6</sub>), *i.e.* an increased oxygen co-ordination number. This can only be the result of a dramatic structural change of the supported VO<sub>x</sub> phase. As was mentioned before, the structure of the reduced vanadium oxide phase has not been resolved yet.

Based on the XANES of the reduced sample, which are represented in Figure 11, formation of a distorted octahedral configuration upon reduction is expected. However, the pre-edge position clearly indicates that reduction of the sample by CO had taken place. This means that despite the reduction, an increase of the oxygen co-ordination number has occurred. To our opinion, two explanations could be given for the increase of the oxygen co-ordination number upon reduction of the sample, *i.e.* formation of bulk V<sub>2</sub>O<sub>3</sub> or migration of the V<sup>3+</sup> ions into the  $\gamma$ -Al<sub>2</sub>O<sub>3</sub> lattice.

Haber has suggested that the reduced VO<sub>x</sub> phase exists as bulk V<sub>2</sub>O<sub>3</sub> on the surface of the support [62]. The structure of V<sub>2</sub>O<sub>3</sub> is isomorphous with corundum  $\alpha$ -Al<sub>2</sub>O<sub>3</sub>, in which the oxygen positions are hexagonal close-packed (hcp), with the trivalent cations occupying the octahedral interstices [63]. This results in three vanadium-oxygen bonds of 1.96 Å, and three vanadium-oxygen bonds of 2.06 Å [11,63]. The pre-edge feature in the XANES spectra of the reduced samples makes this structure to be a possible candidate for the analysis of the EXAFS data. However, vanadium neighbours should also be taken into account and we were not able to insert V-V contributions in our fitting procedure. Furthermore, the formation of bulk V<sub>2</sub>O<sub>3</sub> upon reduction of the supported vanadium oxide phase

could result in the formation of bulk  $V_2O_5$  after re-oxidation of the sample [62]. However, our TPR/TPO experiments did not give an indication of sintering, providing that the oxidised  $VO_x$  phase does not re-disperse. On the contrary, the



peak maximum of the second TPR has shifted to a higher temperature. Since for  $V_2O_5$  the nucleation-reduction mechanism is operative [64], this is a strong indication that the particles are better dispersed after re-oxidation of the reduced sample.

**Figure 18** V-O and V-Al contributions and total R-space fit of the reduced sample. Without the V-Al contributions, fit results were not acceptable.

The other possibility of obtaining a six-fold coordination of  $V^{3+}$  is migration of the low-valent ions into the  $\gamma$ - $Al_2O_3$  lattice. Various authors have described processes in which low-valent cations have been incorporated in the (sub)surface layers of  $\gamma$ -alumina [65,66]. These ions might occupy the tetrahedral and octahedral sites of  $\gamma$ -alumina with the formation of a 'surface spinel' [65] or  $AlVO_3$  type of compound [67]. We therefore suggest that the  $V^{3+}$  ions have migrated into the  $\gamma$ - $Al_2O_3$  lattice, resulting in the formation of a (surface)  $ABO_3$ -type of compound. In literature, only a few examples of such materials are known [67,68]. Reid and Sabine reported the formation of  $AlVO_3$  as the result of the  $H_2$ -reduction of a physical mixture of  $V_2O_5$  and  $Al_2O_3$  [67]. In this metal-deficient spinel,  $V^{3+}$  cations are positioned preferentially in the octahedral  $Al^{3+}$  positions of the  $Al_2O_3$  lattice, forcing the  $Al^{3+}$  ions into tetrahedral positions [67]. Although in our 17.5 wt%  $V_2O_5$ -on- $Al_2O_3$  catalyst much less vanadium is present, we think that the process

is similar. Therefore, we have used the structural parameters of AlVO<sub>3</sub> to fit the EXAFS spectrum of the reduced VO<sub>x</sub>. The EXAFS data nicely correlate with this model, showing both V-O and V-Al contributions in the spectra. Analysis of the data is complicated, because the V-O and V-Al contributions in the Fourier transforms are strongly interfering and correlated, as can be seen in Figure 18. This might explain the absence of V<sup>3+</sup> EXAFS analysis data in the literature on supported vanadium oxide.

We have also performed molecular modelling (force field) on the reduced vanadium oxide-on-alumina system. Preliminary results reveal that V<sup>3+</sup> ions are not stable on the surface of alumina and that they immediately migrate to an Al<sup>3+</sup> octahedral position after reduction. However, for most ions (Cr<sup>3+</sup>, Ni<sup>2+</sup>), this process is irreversible and re-oxidation of the sample is almost impossible [65,66]. Nevertheless, our TPR/TPO experiments show that it is possible to re-oxidise the reduced vanadium oxide catalyst.

#### **Structure during *n*-butane oxidation at 723 K**

In principle, the XAFS data that were collected under *n*-C<sub>4</sub>H<sub>10</sub> oxidation conditions (treatments 8 and 9) show the same trends as we observed during CO oxidation at 723 K (treatments 6 and 7). When oxygen was removed from the feed, the XANES and EXAFS change dramatically, which is the result of reduction of the vanadium oxide species. However, under steady-state conditions (treatment 8), no differences are observed with the spectrum of the dehydrated sample (treatment 3). This indicates that *n*-butane is less reactive towards the vanadium oxide phase than CO. Another explanation could be that the applied conditions are different for the two experiments, *i.e.* 20 % oxygen for the *n*-butane experiment (treatment 8) and 5 % oxygen for the CO experiment (treatment 6). Nevertheless, in an oxygen-free environment, the *n*-butane reduces the vanadium oxide phase at 723 K.

#### **EXAFS results in relation to the oxidation mechanism**

Our XAFS experiments were performed at two different temperatures, *i.e.* at 623 K and at 723 K. Based on the results of Van den Berg, who studied the CO oxidation reaction with V<sub>2</sub>O<sub>5</sub>-on- $\gamma$ -Al<sub>2</sub>O<sub>3</sub>, we expect that the associative mechanism is operative at 623 K [16]. When the associative mechanism is operating, oxidation of CO and *n*-butane proceeds via adsorbed oxygen anions, and hence the structure of the supported vanadium oxide phase is not affected by the reactants. No lattice oxygen is consumed and, consequently, the structure of the supported vanadium oxide phase does not change when oxygen was removed from the feed at 623 K (treatment 5). The results of our XAFS experiments at 623 K are in full agreement with the associative mechanism.

When the oxidation reaction obeys the Mars-Van-Krevelen mechanism, the reaction consumes lattice oxygen. The lattice is subsequently re-oxidised by gas phase oxygen. Our CO oxidation experiments at 723 K show that the catalyst structure was already changing under steady-state conditions, which indicates that lattice oxygen is involved in the oxidation process under these conditions. Furthermore, when oxygen was removed from the feed, the structure of the supported vanadium oxide phase changed completely. This indicates that the

## *Chapter 7*

reaction proceeds via the Mars-Van-Krevelen mechanism under these conditions, because structural changes can only appear when lattice oxygen is consumed.



## CONCLUSIONS

In this chapter, we have shown that X-ray absorption spectroscopy is a useful tool to monitor the structure of a 17.5 wt%  $V_2O_5$ -on- $\gamma$ - $Al_2O_3$  catalyst. Experiments were performed *in-situ*, i.e. at reaction temperatures and in the presence of reactants. We have used XANES, EXAFS, PCA and TPR/TPO experiments to obtain a better understanding of the structure of the supported vanadium oxide phase and the influence of the reaction conditions on the structure.

The fresh catalyst is hydrated and the vanadium oxide phase consists of a species, which is bound to the support with two oxygen atoms. Furthermore, the vanadium atom is co-ordinated by one vanadyl oxygen atom and one OH group. In agreement with the literature, dehydration to a tetrahedral species occurred during thermal pre-treatment in air. The structure of this  $(Al-O)_3-V=O$  remained stable under steady state CO and *n*-butane oxidation conditions at 623 K and 723 K. However, when oxygen was removed from the feed at 723 K the X-ray absorption spectra dramatically changed. These changes were the result of reduction of the vanadium species. EXAFS data analysis of the reduced species was complicated, but showed that the reduced vanadium ions migrate into the surface layers of  $\gamma$ - $Al_2O_3$ . Figure 19 represents a model for our findings. This process was confirmed by molecular modelling. We think that this process is reversible, and that the  $(Al-O)_3-V=O$  species are restored after re-oxidation. To our knowledge, this is the first time that the structure of the  $V^{3+}$  phase is confirmed by experimental data.

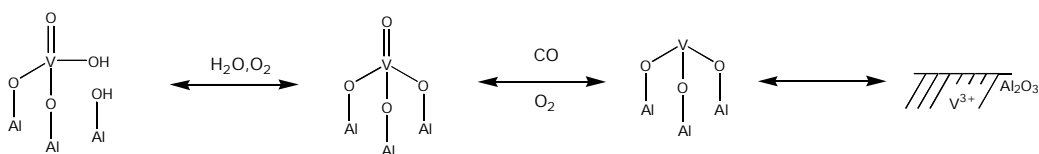


**Figure 19** Model for the structure of the supported hydrated, dehydrated and reduced vanadium oxide phase.

Our results show that the structure of a well-dispersed supported oxide phase is very sensitive for the applied conditions (temperature, type of reactants). Therefore, X-ray absorption spectroscopy is a powerful tool to study these changes in relation with the reaction mechanism *in-situ*, i.e. at reaction temperatures and in the presence of reactants. Although we realise that X-ray absorption spectroscopy cannot be used as a stand-alone mechanistic characterisation technique, the application of XANES and EXAFS to investigate the mechanism of oxidation reactions is an additional tool and catalytic experiments and  $^{18}O/^{16}O$  scrambling experiments will be necessary to complete the picture.

## REFERENCES

- 1 I.E. Wachs, R.Y. Saleh, S.S. Chan, C.C. Chersich, *Appl. Catal.* **15** (1985), 339
- 2 K. Mori, M. Inomata, A. Miyamoto, Y. Murakami, *J. Chem. Soc. Faraday Trans. I* **80** (1984), 2666
- 3 T. Tanaka, Y. Nishimura, S. Kawasaki, M. Oe, T. Funabiki, S. Yoshida, *J. Catal.* **118** (1989), 327
- 4 S.L. Kaliaguine, B.N. Shelimov, B. Kazansky, *J. Catal.* **55** (1978), 384
- 5 A.A. Siddiqi, J.W. Tenini, *Hydrocarbon Process.* **60** (1984), 649
- 6 M. Iwamoto, J. Hirata, K. Matsukami, S. Kagawa, *J. Phys. Chem.* **87** (1983), 903
- 7 G.I. Golodets, *Stud. Surf. Sci. Catal.* **55** (1990), 693
- 8 P. Mars, D.W. van Krevelen, *Chem. Eng. Sci. (Special Suppl.)* **3** (1954), 41
- 9 A.J. Van Dillen, *Catalytic oxidation of carbon monoxide over oxides of indium and vanadium*, Thesis, Utrecht University, 1977
- 10 L.V. Azaroff, D.M. Pease, *X-ray spectroscopy*, L.V. Azaroff ed., McGraw Hill, New York, 1974
- 11 J. Wong, F.W. Lytle, R.P. Mesmer, and D.H. Maylotte, *Phys. Rev. B* **30** (1984), 5596
- 12 J. Wong, R.P. Mesmer, D.H. Maylotte, and F.W. Lytle, , in: *EXAFS and near edge structure*, A. Bianconi, L. Inocchia, and S. Stipcich eds., Springer Verlag, Berlin, 1983, 130
- 13 J. Wong, D.H. Maylotte, F.W. Lytle, R.B. Gregor, and R.L. St. Peters, in: *EXAFS and near edge structure*, A. Bianconi, L. Inocchia, and S. Stipcich eds., Springer Verlag, Berlin, 1983, 206
- 14 I. Davoli, S. Stizza, M. Benfatto, O. Gzowski, L. Murawski, and A. Bianconi, in: *EXAFS and near edge structure*, A. Bianconi, L. Inocchia, and S. Stipcich eds., Springer Verlag, Berlin, 1983, 162
- 15 M. Ruitenbeek, R.A. Overbeek, A.J. van Dillen, D.C. Koningsberger, J.W. Geus, *Recl. Trav. Chim. Pays-Bas* **115** (1996), 519
- 16 J. van den Berg, *Stoichiometry and catalytic activity of vanadia-based oxides for the oxidation of CO and H<sub>2</sub>*, Thesis, Utrecht University, 1984
- 17 I.E. Wachs, J.-M. Jehng, G. Deo, B.M. Weckhuysen, V.V. Guliants, J.B. Benziger, S. Sundaresan, *J. Catal.* **170** (1997), 75
- 18 Chapter 2 of this thesis, and references therein
- 19 J.N. Fiedor, A. Proctor, M. Houalla, D.M. Hercules, *Surf. Interface Anal.* **20** (1993), 1
- 20 S.J. Scierka, A. Proctor, J.N. Fiedor, D.M. Hercules, *Surf. Interface Anal.* **20** (1993), 901
- 21 M. A. Eberhardt, A. Proctor, M. Houalla, D.M. Hercules, *J. Catal.* **160** (1996), 27
- 22 M.J. Fay, A. Proctor, D.P. Hoffmann, M. Houalla, D.M. Hercules, *Mikrochim. Acta* **109** (1992), 281
- 23 E.R. Malinowski, *Factor Analysis in Chemistry*, 2<sup>nd</sup> ed., John Wiley, New York, 1991

- 24 E.R. Malinowski, *J. Chemom.* **3** (1988), 49
- 25 E.R. Malinowski, *J. Chemom.* **4** (1990), 102
- 26 F.M. Dautzenberg, *ACS Symposium Series* **421** (1989), 277
- 27 I.E. Wachs, *Catalysis Today* **27** (1996), 437
- 28 G.T. Went, S.T. Oyama, *J. Phys. Chem.* **94** (1990), 4240
- 29 F. Roozeboom, M.C. Mittelmeijer-Hazeleger, J.A. Moulijn, J. Medema, V.H.J. de Beer, P.J. Gellings, *J. Phys. Chem.* **84** (1980), 2783
- 30 G. Busca, *Mater. Chem. Phys.* **19** (1988), 157
- 31 A.A. Davydov, *Kinet. Katal.* **34** (1993), 951
- 32 T. Tanaka, H. Yamashita, R. Tsuchitani, T. Funabiki, S. Yoshida, *J. Chem. Soc. Faraday Trans I* **84** (1988), 2987
- 33 S. Yoshida, T. Tanaka, Y. Nishimura, H. Mizutani, T. Funabiki, *Proc. ICC IX*, 1988, 1473
- 34 S. Yoshida, T. Tanaka, T. Hanada, T. Hiraiwa, H. Kanai, *Catal. Lett.* **12** (1992), 277
- 35 E. Vogt, *Preparation and Properties of Catalysts Supported on Modified Silica*, Thesis, Utrecht University, 1988
- 36 R. Kozlowski, R.F. Pettifer, J.M. Thomas, *J. Phys. Chem.* **87** (1983), 5176
- 37 J. Haber, A. Kozłowska, R. Kozłowski, *J. Catal.* **102** (1986), 52
- 38 N. Das, H. Eckert, H. Hu, I.E. Wachs, J.F. Walzer, F.J. Feher, *J. Phys. Chem.* **97** (1993), 8240
- 39 H. Eckert, I.E. Wachs, *Mater. Res. Soc. Symp. Proc.* **111** (1988), 455
- 40 H. Eckert, I.E. Wachs, *J. Phys. Chem.* **93** (1989), 6796
- 41 L.R. Le Costumer, B. Taouk, M. Le Meur, E. Payen, M. Guelton, J.M. Grimblot, *J. Phys. Chem.* **92** (1988), 1230
- 42 B.M. Weckhuysen, I.P. Vannijvel, R.A. Schoonheydt, *Zeolites* **15** (1995), 482
- 43 U. Scharf, M. Schraml-Merth, A. Wokaun, A. Baiker, *J. Chem. Soc. Faraday Trans.* **87** (1991), 3299
- 44 G. Catana, R. Ramachandra Rao, B.M. Weckhuysen, P. van der Voort, E. Vansant, R. Schoonheydt, *J. Phys. Chem. B.* **102** (1998), 8005
- 45 M.F. Hazenkamp, G. Blasse, *J. Phys. Chem.* **96** (1992), 3442
- 46 M. Anpo, M. Sunamoto, M. Che, *J. Phys. Chem.* **93** (1989), 1187
- 47 G. Busca, E. Giamello, *Mater. Chem. Phys.* **25** (1990), 475
- 48 B.I. Wittington, J.R. Anderson, *J. Phys. Chem.* **97** (1993), 1032
- 49 J.M. Jehng, G. Deo, B.M. Weckhuysen, I.E. Wachs, *J. Mol. Catal. A: Chemical* **110** (1996), 41
- 50 I.E. Wachs, B.M. Weckhuysen, *Appl. Catal. A: General* **157** (1997), 67
- 51 S.S. Chan, I.E. Wachs, L.L. Murrell, L. Wang, W. Keith Hall, *J. Phys. Chem.* **88** (1984), 5831
- 52 X. Gao, S.R. Bare, B.M. Weckhuysen, I.E. Wachs, *J. Phys. Chem. B.* **102** (1998), 10684
- 53 T. Kataoka, J.A. Dumesic, *J. Catal.* **112** (1988), 66
- 54 G.C. Bond, J. Perez Zurita, S. Flamerz, P.J. Gellings, H. Bosch, J.G. van Ommen, B.J. Kip, *Appl. Catal.* **22** (1986), 361

Chapter 7

- 55 W. Fluhr, M. Schraml-Marth, A. Wokaun, A. Baiker, *Ber. Bundesges. Phys. Chem.* **8** (1989), 852
- 56 I.E. Wachs, G. Deo, B.M. Weckhuysen, V.V. Guliants, J.B. Benziger, *Catal. Today* **32** (1996), 47
- 57 G. Ramis, C. Cristiani, P. Forzatti, G. Busca, *J. Catal.* **124** (1990), 574
- 58 H. Praliaud, M.-V. Mathieu, *J. Chim. Phys.* **73** (1976), 689
- 59 X. Gao, S.R. Bare, B.M. Weckhuysen, I.E. Wachs, *J. Phys. Chem. B* **102** (1998), 10842
- 60 F. Lemoigno, E. Prouzet, Z.Y. Wu, P. Gressier, G. Ouvrard, *J. Phys. IV France* **7** (1997), 263
- 61 W.A. Caliebe, C.-C. Kao, J.B. Hastings, M. Taguchi, A. Kotani, T. Uozumi, F.M.F. de Groot, *Phys. Rev. B* **58** (1998), 13452
- 62 J. Haber, in: *Catalytic Oxidation, Principles and Applications*, R.A. Sheldon, R.A. van Santen (eds.), World Scientific, London, 1995, 17
- 63 R.E. Newnham, Y.M. de Haan, *Z. Kristall.* **117** (1962), 235
- 64 N.W. Hurst, S.J. Gentry, A. Jones, B.D. McNicol, *Catal. Rev. Sci. Eng.* **24** (1982), 233
- 65 W.S. Xia, H.L. Wan, Y. Chen, *J. Mol. Catal. A: Chemical* **138** (1999), 185
- 66 B.M. Weckhuysen, L.M. de Ridder, P.J. Grobet, R.A. Schoonheydt, *J. Phys. Chem.* **99** (1995), 320
- 67 A.F. Reid, T.M. Sabine, *J. Solid State Chem.* **2** (1970), 203
- 68 B. Reuter, R. Aust, G. Collsmann, Ch. Neuwald, *Z. Anorg. Allg. Chem.* **500** (1983), 188



---

**AN *IN-SITU* STUDY OF SUPPORTED V-P-O CATALYSTS  
DURING BUTANE OXIDATION TO MALEIC ANHYDRIDE**

**ABSTRACT**

Silica- and titania-supported V-P-O catalysts were characterised with *in-situ* Raman spectroscopy and *in-situ* X-ray absorption spectroscopy. The measurements were performed at a reaction temperature of 653 K and in the presence of reactants.

Raman spectroscopy showed that, in agreement with the EXAFS data analysis, the active component in VPO/TiO<sub>2</sub> exists as monolayer type species. These species were sensitive for hydration, but catalytic conditions had no impact on the Raman spectra. In agreement with earlier XANES results, this indicates that the Mars-Van-Krevelen mechanism is not operative for the VPO/TiO<sub>2</sub> catalyst.

The Raman data of VPO/SiO<sub>2</sub> showed the presence of micro-crystalline  $\alpha_1$ -VOPO<sub>4</sub>. Consequently, the less-ordered V<sup>4+</sup> phase(s) were not visible. The  $\alpha_1$ -VOPO<sub>4</sub> phase was not affected by the application of catalytic conditions. Furthermore, the  $\alpha_1$ -VOPO<sub>4</sub> phase was not reduced by *n*-butane at 653 K in the absence of oxygen. EXAFS, on the contrary, probes all V-P-O structures present in the catalyst. EXAFS data analysis showed that the Debye-Waller factors of all contributions in the EXAFS spectrum of VPO/SiO<sub>2</sub> severely increased under catalytic conditions. However, bond distances and co-ordination numbers hardly changed. Nonetheless, differences between the XANES spectra taken under steady-state (*n*-butane/air) conditions and under reducing conditions (*n*-butane/helium) at 653 K indicate that with VPO/SiO<sub>2</sub> the Mars-Van-Krevelen mechanism is operating.

## INTRODUCTION

It is highly important to study the structure of V-P-O catalyst *in-situ*, *i.e.* under conditions close or equal to actual *n*-butane oxidation conditions. The main reason for this is that the structure of the V-P-O phase is depending on the conditions under which the sample has been characterised, as was shown by Overbeek *et al.* [1,2]. With *in-situ* XRD, they showed that two different bulk V-P-O catalysts, prepared from *i*-butanol/cyclohexanol and from HCl-solution, developed different X-ray diffraction patterns upon thermal pre-treatment in nitrogen or air [1]. Furthermore, the composition of the catalysts was different under butane oxidation conditions. Various mixtures of known and unknown crystalline V-P-O phases were observed [1]. Most striking, however, was the observation that the mixture of V-P-O phases changed into vanadylpyrophosphate after exposition to air at room temperature. This transformation was reversible and convincingly indicated that single-phase vanadylpyrophosphate, which was only observed *ex-situ*, is not the sole active phase in V-P-O catalysts [1]. The change of the catalyst structure as a result of exposure to air at room temperature was also observed with X-ray absorption spectroscopy for a titania-supported V-P-O catalyst [3].

Another important consideration for the application of *in-situ* characterisation techniques is the fact that they can provide more insight in the mechanism, which is operative under the applied reaction conditions. The mechanism mostly assumed to be operative for selective catalytic oxidation over solid oxides is the Mars-Van-Krevelen mechanism, in which the catalyst is alternately reduced by the compound to be oxidised and re-oxidised by gaseous molecular di-oxygen [4]. It is important to assess whether the oxidation of *n*-butane over the selective V-P-O catalyst also proceeds via a Mars-Van-Krevelen mechanism. When this mechanism is operative with the V-P-O catalyst, re-circulation of the catalyst between a gas-flow in which the catalyst is exposed exclusively to *n*-butane and a flow in which the catalyst is re-oxidised by gaseous oxygen is viable. Recovery of the resulting more concentrated maleic anhydride from the gas flow can be performed more easily and the risk of explosions is lower [5]. Gleaves *et al.* have shown that passing a flow of  $^{18}\text{O}_2$  and *n*-butane over a bulk V-P-O catalyst resulted in  $\text{C}^{18}\text{O}^{18}\text{O}$ , which indicates that oxygen, chemisorbed from the gas phase, leads to a rapid non-selective oxidation [6]. The authors used TAP (Temporal Analysis of Products) in their investigations. This rapid oxidation to carbon dioxide by oxygen chemisorbed from the gas phase suggests that, in the absence of gaseous oxygen, a higher selectivity can be achieved. These considerations have resulted in the development of the recirculating-solids process of DuPont, which is operated commercially since 1996 [5].

Centi *et al.*, however, have observed that exposure of bulk V-P-O catalyst to *n*-butane at more elevated temperatures leads exclusively to desorption of carbon oxides [7]. Reaction of *n*-butane with the catalyst surface in the absence of oxygen, or with a gas flow of an oxygen content too low to achieve oxidation of *n*-butane, causes carbon-containing species to be deposited on the surface of the catalyst. Exposure of the thus covered catalyst surface to molecular oxygen at temperatures of 673 K to 723 K only results in the non-selective formation of gaseous carbon oxides. To investigate whether the adsorbed carbon-containing

species can react with molecular oxygen to maleic anhydride calls for operation at lower temperatures and, hence, for a catalyst being active at lower temperatures. In previous work, we have investigated the mechanism of *n*-butane oxidation using a titania-supported V-P-O catalyst [1,3]. Titania-supported V-P-O catalysts have proven to be considerably more active than bulk or silica-supported V-P-O catalysts [8,9]. It was found that the Mars-Van-Krevelen mechanism is not operative for the titania-supported V-P-O catalyst [3]. Initially, *n*-butane reacted with the active surface without affecting the oxidation-state of vanadium. Subsequent reaction with molecular oxygen led to reaction and desorption of maleic anhydride.

It is desirable that catalysts to be used in assessing the mechanism of the oxidation of *n*-butane exhibit a high surface-to-volume ratio of the active component, since the reduction of the catalyst may involve only (part of) the surface layer. Furthermore, the catalyst should preferably be active at low temperatures. The ability of the titania-supported V-P-O catalyst to activate *n*-butane already at low temperatures leads to the formation of stable adsorbed intermediates, which allow one to perform the subsequent oxidation with gas-phase oxygen at lower temperatures, generating selective oxidation products [3]. Only a few characterisation techniques have proven to be useful for *in-situ* catalyst characterisation. The main constraint being that the interference of gas phase spectra should be negligibly weak. Besides the earlier mentioned XRD and EXAFS experiments of Overbeek *et al.*, examples of successful *in-situ* characterisation are known with ESR spectroscopy [10] and Laser Raman Spectroscopy (LRS) in the V-P-O literature [11,12,13,14,15,16]. However, all the above mentioned techniques have the drawback that they are not particularly sensitive for the surface of the catalyst under investigation. In chapter 7 of this thesis, we have shown that *in-situ* XAFS can provide information about the reaction mechanism when the active oxide phase is well dispersed. Moreover, in chapter 5 of this thesis we have shown that utilisation of supported V-P-O catalysts avoids bulk contributions to dominate in the spectra [17,18] and, hence, supported V-P-O catalysts are very suitable to be employed for *in-situ* characterisation.

In this investigation, we have applied *in-situ* Raman spectroscopy and *in-situ* X-ray absorption spectroscopy to study the structure of a silica-supported and a titania-supported V-P-O catalyst under actual *n*-butane oxidation conditions. Furthermore, we have applied oxidation-reduction experiments to study the nature of the reactive oxygen atoms in these catalysts.

## EXPERIMENTAL

### **Catalyst preparation**

The samples that were used for this investigating were VPO/SiO<sub>2</sub> (7.5 wt% V) and VPO/TiO<sub>2</sub> (2.8 wt% V). Sample preparation has been described in chapter 2 of this thesis. The *ex-situ* XAFS characterisation of VPO/SiO<sub>2</sub> was described in chapters 5 and 6 of this thesis. The VPO/TiO<sub>2</sub> catalysts that was used in this investigation had a different loading as compared to the VPO/TiO<sub>2</sub> catalyst described in chapters 5 and 6 of this thesis. However, the features of the Raman spectra were almost equal and this catalyst showed much less fluorescence (*vide infra*).

### **Raman spectroscopy**

Raman experiments (LRS) were performed at the Zettlemoyer Center for Surface Studies which is part of Lehigh University in Bethlehem PA (USA). Details about the apparatus can be found in chapter 2 of this thesis.

LRS experiments were performed *ex-situ* in ambient and stationary mode. Under ambient conditions, the sample is spun (1500 rpm) to average out possible inhomogeneities of the sample and avoid heating by the laser beam. When rotation is stopped (stationary mode), the laser beam will induce heating of the sample and, consequently, dehydration occurs. In general, this will only have impact on the spectra of monolayer catalysts. Polymeric and crystalline species will not be affected, and consequently application of experiments in the stationary mode can provide additional information about monolayer thickness in the samples [19].

*In-situ* LRS experiments were performed at different reaction temperatures and with different reactant mixtures, *i.e.* in air, in 1% *n*-butane/air and 1% *n*-butane/helium. The experimental circumstances will be mentioned in the various figures throughout this chapter.

### **XAFS measurements**

X-ray absorption spectroscopy experiments were performed at the Synchrotron Radiation Source at Daresbury Laboratories (Station 8.1) in England. The energy of the electron beam amounts to 2 GeV. Further details can be found in chapter 2 of this thesis.

A specially developed high-temperature *in-situ* cell was used, adapted to operate both in vacuum or under flow conditions [20]. Samples were characterised *ex-situ* in He at 77 K after calcination of the fresh precursor in nitrogen at 723 K for 16 h, under steady-state *n*-butane oxidation conditions (1% *n*-butane/air) and in the absence of oxygen, *i.e.* in *n*-butane/helium at 653 K.



## RESULTS and DISCUSSION

### VPO/TiO<sub>2</sub>

#### Raman experiments

Figure 1 represents the *ex-situ* Raman spectra of VPO/TiO<sub>2</sub>. These spectra were collected in the ambient and in the stationary mode. Spectra were cut-off at 700 cm<sup>-1</sup> because of the dominating contributions of TiO<sub>2</sub> below 700 cm<sup>-1</sup> [21].

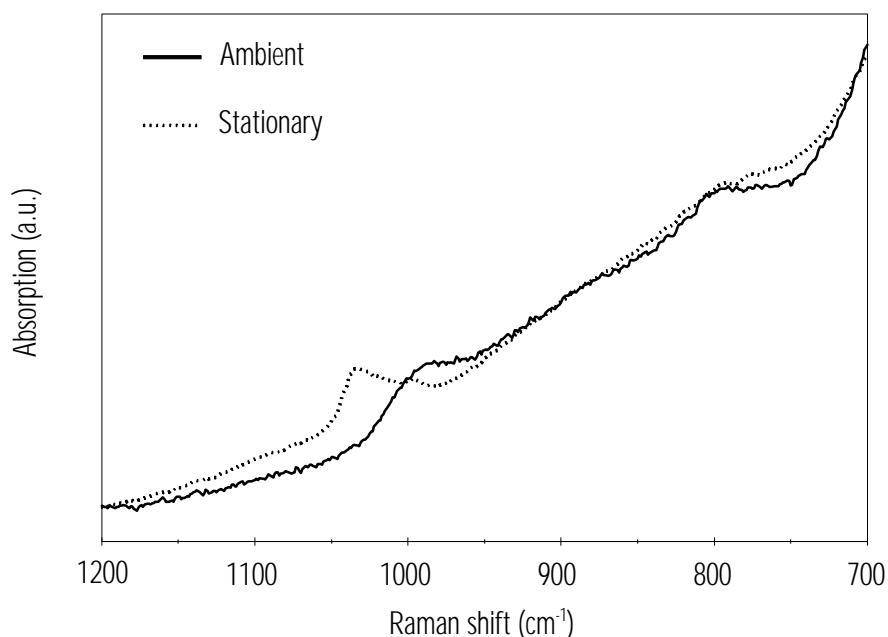


**Figure 1** Ambient Raman spectra of the VPO/TiO<sub>2</sub> catalyst. Spectra were taken at room temperature in air.

The ambient spectrum shows only two small, broad bands at 990 cm<sup>-1</sup> and 800 cm<sup>-1</sup>. The 990 cm<sup>-1</sup> band is shifted to a higher frequency, when the catalyst is dehydrated by the laser beam in the stationary mode. This indicates that this band is originating from a monolayer type V-O bond (*vide supra*). The 800 cm<sup>-1</sup> band broadened and almost disappeared in the stationary mode, but could not be assigned to a certain type of species.

Hardcastle and Wachs have found an empirical correlation between the Raman stretching frequencies of vanadium-oxygen (V-O) bonds and their bond lengths [22]. Based on their formula, a stretching frequency of 990 cm<sup>-1</sup> corresponds to a V-O bond length of  $1.60 \pm 0.017$  Å, which is close to the value of the vanadyl bond obtained from the EXAFS analysis of VPO/TiO<sub>2</sub>.

The Raman band at 800 cm<sup>-1</sup> would be originating from a V-O bond of  $1.71 \pm 0.017$  Å, which is not observed in the EXAFS data analysis of VPO/TiO<sub>2</sub>.

However, we have found a value of  $1.74 \text{ \AA}$  for hydrated vanadyl species in  $\text{V}_2\text{O}_5$  on  $\text{Al}_2\text{O}_3$  [26]. This indicates that the Raman band at  $800 \text{ cm}^{-1}$  could be originating from a hydrated vanadyl species and this is probably the reason for the absence of this band under stationary conditions, *i.e.* after dehydration. Unfortunately, Raman spectroscopy cannot provide direct information about the V-O-support bonds, because these are slightly ionic and, consequently Raman inactive [23].

Figure 2 represents the *in-situ* Raman experiments with  $\text{VPO}/\text{TiO}_2$ . The first spectrum was collected in air at 653 K to decrease the fluorescence of the titania support. Furthermore, the sample was dehydrated during this treatment, which resulted in a shift of the V=O stretching vibration. However, further application of temperature (653 K) and reactants (air, butane/air, *n*-butane) did not affect the spectra of this catalyst.

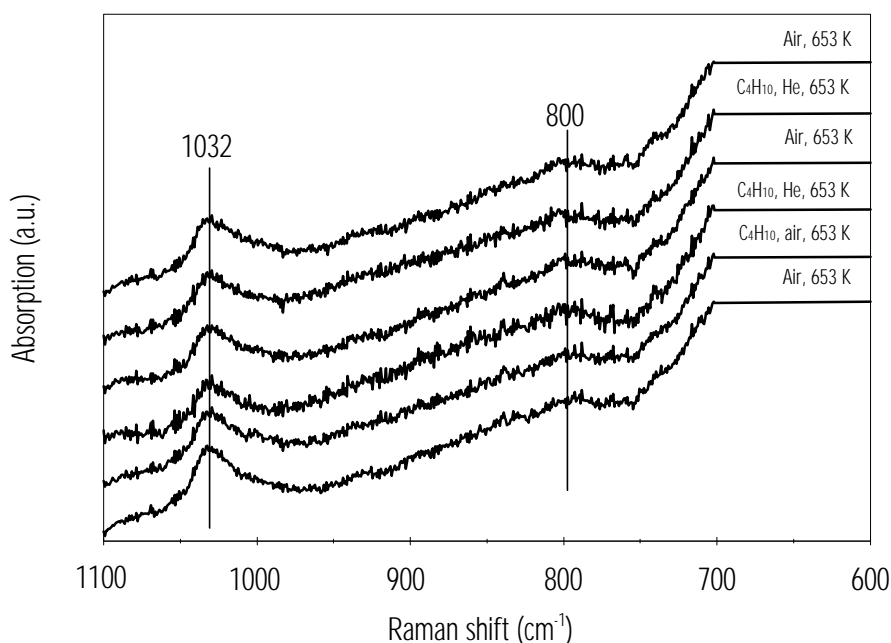


**Figure 2** *In-situ* Raman spectra of  $\text{VPO}/\text{TiO}_2$  ( $1100\text{-}700 \text{ cm}^{-1}$ ). Experiments were consequently performed from bottom to top.

Only very small changes in the intensity of the band at  $1032 \text{ cm}^{-1}$  were observed, showing that a very limited reduction of the catalyst took place upon exposure to butane at 653 K. The original intensity of the spectrum returned after re-oxidation at 653 K. In a second reduction step, the intensity of the band at  $1032 \text{ cm}^{-1}$  showed no more changes.

This is in agreement with the *in-situ* X-ray absorption experiments on a titania-supported V-P-O catalyst of Overbeek *et al.* [1,3]. Summarising their results, the titania-supported V-P-O catalyst was equilibrated after only a few oxidation-reduction cycles. Neither the position of the vanadium K-edge nor the position and

intensity of the pre-edge changed further upon exposure to an atmosphere of O<sub>2</sub>/He or *n*-butane. These observations imply that *n*-butane does not react with lattice oxygen from the V-P-O phase and, consequently, the valence state of vanadium does not change. Our results confirm the XANES results of Overbeek *et al.* and show that the Mars-Van-Krevelen mechanism is not operative for VPO/TiO<sub>2</sub>.

## VPO/SiO<sub>2</sub>

### **Raman experiments**

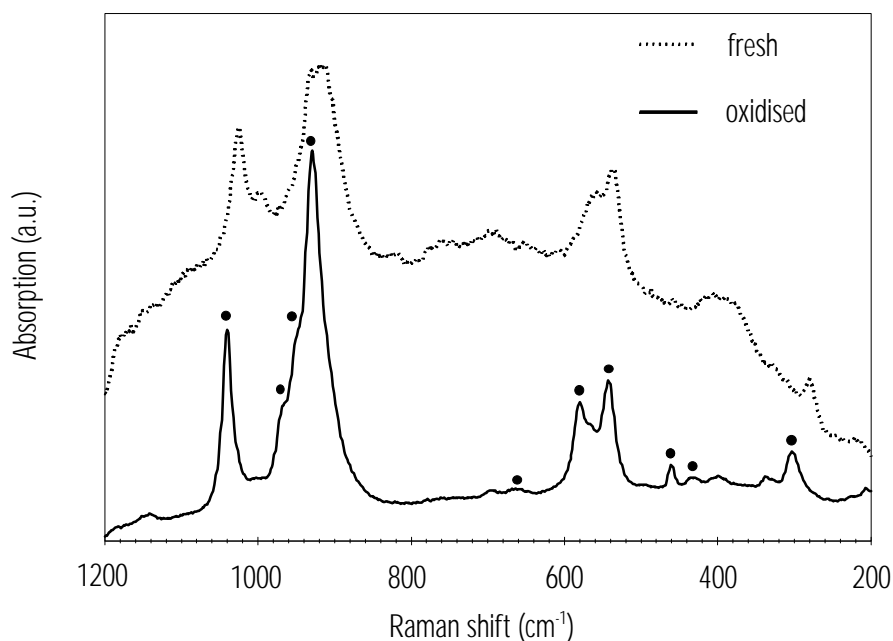
One of the critical problems with Raman spectroscopy is the possible appearance of an intense background, called fluorescence [12]. This can be caused by sample impurities, but also surface hydroxyl groups can give rise to fluorescence [24]. There are several options to cope with fluorescence, but in practice, calcination in air at temperatures of around 773 K is the easiest option. However, with V-P-O catalysts, this is also the most tricky option, since calcination in air at temperatures above 623 K brings about oxidation of V<sup>4+</sup> to V<sup>5+</sup>, which is generally accompanied by structural changes [2].

Figure 3 shows the Raman spectrum of VPO/SiO<sub>2</sub>. Although we only represent the 1200-200 cm<sup>-1</sup> range of the data, the spectrum of the fresh catalyst was superimposed on a large fluorescence contribution. Therefore, we have also taken a spectrum after calcination in air at 653 K for one hour (oxidised). This results in a flat baseline. However, the Raman bands of the calcined catalyst were sharpened and extra bands appeared after the treatment. This indicates that the structure of the sample changed during the calcination, and that calcination to remove the fluorescence background is thus not appropriate for our samples.

All V-P-O compounds exhibit two distinct ranges, *i.e.* between 1200 and 800 cm<sup>-1</sup> and below 700 cm<sup>-1</sup>. The 1200-800 cm<sup>-1</sup> range is characteristic for V-O and P-O stretching modes, while within the range below 700 cm<sup>-1</sup> bending modes, coupled vibrations and collective modes of the crystal lattice can be observed. Raman spectra of V-P-O reference compounds have been reported extensively by Guliants *et al.* [25] and Ben Abdelouahab *et al.* [13].

When the Raman spectrum of the oxidised VPO/SiO<sub>2</sub> is compared to the various reference spectra, it can indisputably be concluded that the only observed phase in the Raman spectrum is  $\alpha_1$ -VOPO<sub>4</sub>. However, the exclusive observation of  $\alpha_1$ -VOPO<sub>4</sub> with Raman spectroscopy does not imply that this is the only V-P-O phase present in the sample. It is well known that the Raman scattering from polymeric and crystalline bulk metal oxide phases is significantly stronger (typically, orders of magnitude greater). Coexisting amorphous phases therefore cannot be detected because of their much weaker Raman scattering [14]. However, the fresh VPO/SiO<sub>2</sub> catalyst has not been oxidised and a significant amount of the VPO/SiO<sub>2</sub> sample constitutes a V<sup>4+</sup> phase. In the fresh sample, only the  $\alpha_1$ -VOPO<sub>4</sub> absorption bands at 929, 579 and 542 cm<sup>-1</sup> are observed, as well as additional absorption bands at 1028 and 913 cm<sup>-1</sup>. However, all absorption bands present in the spectrum after calcination can be assigned to  $\alpha_1$ -VOPO<sub>4</sub>. Therefore, formation

of crystalline  $\alpha_1$ -VOPO<sub>4</sub> is the result of removal of the fluorescence background and of further oxidation of the catalyst. In the fresh sample, both V<sup>4+</sup> and V<sup>5+</sup> probably exhibit the same (lack of) long-range order.



**Figure 3** Ambient Raman spectra of the 'fresh' VPO/SiO<sub>2</sub> catalyst and the catalyst calcined in air at 623 K for 1 hour. The dots indicate bands originating from  $\alpha_1$ -VOPO<sub>4</sub>.

Figure 4 represents the *in-situ* Raman experiments with VPO/SiO<sub>2</sub>. We have tried to perform the anti fluorescence treatment (oxidation) below 423 K to avoid oxidation of the sample as much as possible. The spectrum of the sample prior to the actual *in-situ* conditions (air, RT) is dominated by two very broad bands which maximums at 1038 and 922 cm<sup>-1</sup>. These positions agree with the most intense contributions of  $\alpha_1$ -VOPO<sub>4</sub>.

The bands in the 1050 - 900 cm<sup>-1</sup> range in Figure 4 are seemingly much broader compared to those in Figure 3, but they are represented on a different scale of the x-axis. However, it cannot be excluded that they are a superposition of various contributions. Almost all known V-P-O compounds exhibit a strong absorption band in this region, but at slightly different positions [13].

After taking a spectrum in air at room temperature, we have employed catalytic conditions by flowing a mixture of 1% *n*-butane in oxygen/helium (20/80) and increased the temperature. The sample was kept at 653 K, 703 K and at 703 K and spectra were collected after 1 hour time-on-stream. Subsequently the sample was cooled down to room temperature to change the composition of the gas flow and another room-temperature spectrum was collected. Finally, we increased the temperature in a flow of 1% *n*-butane in helium and spectra were collected at 653 K and at 653 K after 1 hour.

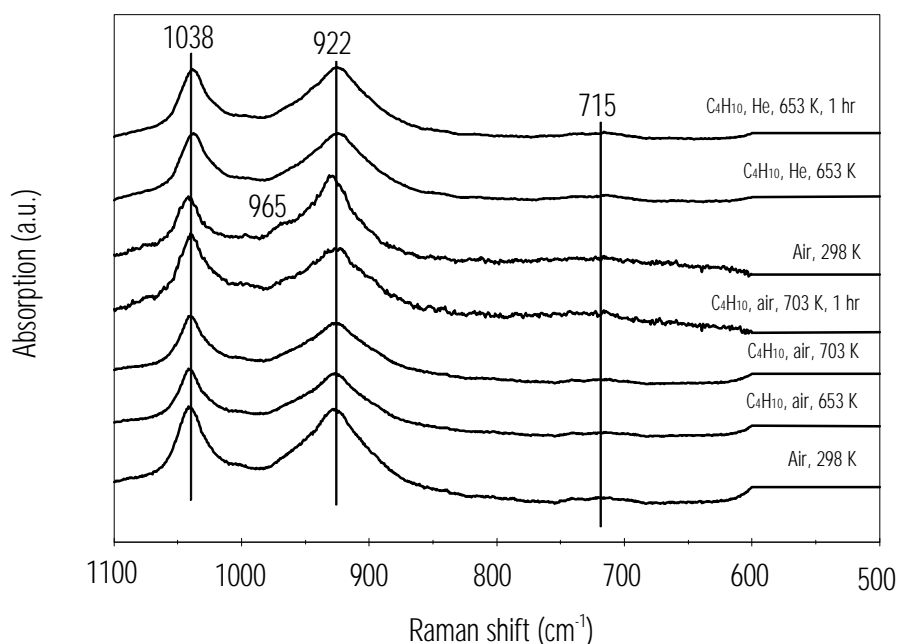


**Figure 4** In-situ Raman spectra of VPO/SiO<sub>2</sub> (1100-600 cm<sup>-1</sup>). Experiments were consequently performed from bottom to top.

All of the above-described treatments had hardly any impact on the positions and intensities of the bands in the Raman spectra of VPO/SiO<sub>2</sub>. This indicates that at least the fraction of the catalyst that is apparent in the Raman spectrum does not change under steady-state *n*-butane oxidation conditions or in the absence of oxygen at these temperatures. However, the catalytic test results of VPO/SiO<sub>2</sub>, which are represented in chapter 5 of this thesis, show that at the applied temperatures a significant conversion of *n*-butane is possible. We do not know the conversion in the *in-situ* Raman cell during our experiment, but we do expect some conversion. This would mean that the  $\alpha_1$ -VOPO<sub>4</sub> part of VPO/SiO<sub>2</sub> does not change into another phase and is not reduced under the applied conditions. This is in agreement with data of  $\alpha_2$ -,  $\beta$ - and  $\gamma$ -VOPO<sub>4</sub> of which no changes at increasing temperature under reaction conditions have been reported [13]. Only the spectrum

of  $\delta$ -VOPO<sub>4</sub> has been reported to change under catalytic conditions, resulting in the formation of  $\alpha_2$ -VOPO<sub>4</sub> [13].

The only spectrum in our data set exhibiting a distinct change is that during the change of gas composition (second air, RT). In this spectrum, the shoulder at 965 cm<sup>-1</sup> is more pronounced and the relative intensity of the two broad bands has changed, but no satisfying explanation can be given for this effect on the spectrum. Unfortunately, the spectra of the sample are dominated by the  $\alpha_1$ -VOPO<sub>4</sub> phase, which does not show changes upon exposure to *n*-butane/air at 653 K. The Raman results would imply that the Mars-Van-Krevelen is not operative for VPO/SiO<sub>2</sub>.

### **XAFS experiments**

Figure 5 represents the XANES spectra of the fresh VPO/SiO<sub>2</sub> sample and the spectra during butane oxidation at 653 K. The third XANES spectrum was taken at 653 K in the absence of oxygen, *i.e.* under reducing conditions. In the little box, a magnification of the pre-edge region is represented. For a detailed description of the interpretation of the physical background of XANES and its implication to the characterisation of vanadium-based compounds, we would like to refer to chapter 7 of this thesis and references therein.

First, we will discuss the pre-edge. In chapter 7 of this thesis, we have shown that the pre-edge feature is sensitive for the valence state of vanadium (energy) and the geometry (intensity) for a V<sub>2</sub>O<sub>5</sub>-on-Al<sub>2</sub>O<sub>3</sub> catalyst [26]. For the VPO/SiO<sub>2</sub> catalyst, two maxima are observed in the pre-edge in all spectra, *i.e.* in the spectrum of the fresh sample and in the *in-situ* spectra.

Gao *et al.* have reported a clear shoulder on the low-energy side of the pre-edge for 10 wt% V<sub>2</sub>O<sub>5</sub> on SiO<sub>2</sub> [27]. This feature was associated with a distortion of the tetrahedral geometry of the sample, resulting in a splitting of the energy levels. However, in our case, it could be an indication for the presence of both V<sup>4+</sup> and V<sup>5+</sup> in the sample. Unfortunately, we cannot quantify the relative amount of these type of species, because the intensity of the pre-edge peaks is also depending on the geometry. Therefore, an increase of the pre-edge intensity at a certain energy does not have to be the result of an increased amount of that specific type of species. Moreover, the intensity is generally increasing according to V<sup>3+</sup> < V<sup>4+</sup> < V<sup>5+</sup> [26]. Consequently, a higher intensity at the high-energy side of the doublet does not necessarily mean a higher amount of V<sup>5+</sup>. The presence of V<sup>5+</sup> is expected because of the observation of  $\alpha_1$ -VOPO<sub>4</sub> in the Raman spectra.

When the pre-edge is considered in more detail, it is obvious that the pre-edge shows the lowest intensity with the fresh catalyst. During *n*-butane oxidation at 653 K, the intensity increases. This indicates that the geometry of the vanadium sites becomes more distorted [26], which is probably the result of thermal disorder. The intensity of the pre-edge decreases significantly when the VPO/SiO<sub>2</sub> is exposed to butane/helium at 653 K. Because this spectrum was also collected at reaction temperature, the thermal disorder is expected to be equal and, hence, the decrease of the intensity must be the result of reduction of the catalyst under these conditions [26]. In analogy with our results on V<sub>2</sub>O<sub>5</sub>-on-Al<sub>2</sub>O<sub>3</sub>, this would indicate that the Mars-Van-Krevelen mechanism is operative for the VPO/SiO<sub>2</sub>

catalyst [26]. In the XANES part of the *in-situ* X-ray absorption data of VPO/SiO<sub>2</sub> clear differences are observed between the fresh sample, on the one, and the *in-situ* treatments on the other hand, which are more analogous. However, the shape of the XANES of all three spectra indicates that vanadium exists in a distorted octahedral or square pyramidal geometry in these samples.

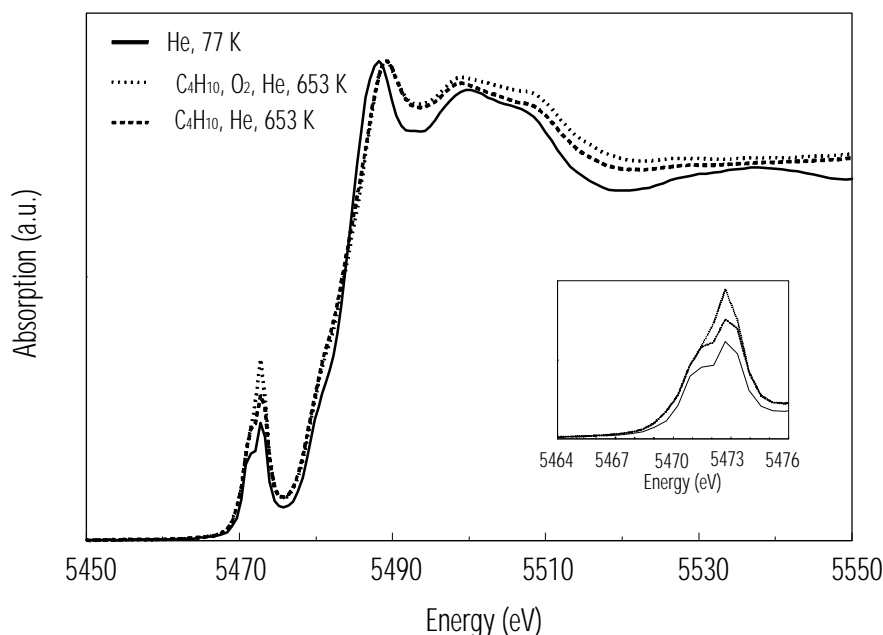


**Figure 5** V K-edge spectra of the VPO/SiO<sub>2</sub> catalyst before and during *n*-butane oxidation, and under reducing conditions at 653 K. The box represents an enlargement of the pre-edge region.

Figure 6 represents the Fourier Transforms of the EXAFS spectra of the three experiments, *i.e.* fresh, during *n*-butane oxidation at 653 K and in the absence of oxygen at 653 K. In this figure, it can be seen that the spectrum during the two *in-situ* experiments, *i.e.* steady-state and in the absence of oxygen at 653 K, is equal. However, both spectra severely differ from the *ex-situ* spectrum, which was taken in helium at 77 K. The difference in amplitude between the *ex-situ* and *in-situ* Fourier transforms can be explained by the different temperatures at which the data collection was performed. Generally, a higher temperature brings about increased thermal vibrations of the lattice and, consequently, an increase of the Debye-Waller factors. This results in dampening of the signal intensity.

The impact of temperature on the Debye-Waller factors of the various scatterer pairs can be different. The first shell V-O contributions [18], which are located around 1.6 Å in the uncorrected Fourier transform only lost some intensity, but the position of these contributions was not affected. This is in agreement with the XANES data in Figure 5, because it means that the distorted VO<sub>5</sub> or VO<sub>6</sub> geometry is not affected by the applied conditions. However, beyond 2 Å dramatic changes

in the imaginary and absolute part of the Fourier transforms occurred upon exposure to the reactants at 653 K. This is the range where V-P, V-V and other V-O contributions are found [18]. Temperature and applied reactants were the same as with the Raman experiments and the Raman results in Figure 4 did not indicate a different structure. However, EXAFS probes all vanadium sites and the spectra are the average of the whole sample, whereas Raman more selectively probes long-range ordered species leaving amorphous part broadened beyond detection in the background. However, it is more likely that the change of the EXAFS spectrum is the result of an increase of the Debye-Waller factors in stead of structural changes of the catalyst. EXAFS data analysis, in which we fixed all parameters except for the Debye-Waller factors, confirmed this assumption. A reasonable fit was obtained, with Debye-Waller factors above 0.0200 for the higher co-ordination shells (V-P, V-V and V-O). The increase of the Debye-Waller factors is not necessarily equal for all shells. Consequently, the interference of these contributions changes and this accounts for the changes in the absolute and the imaginary part of the Fourier transforms above 2 Å.

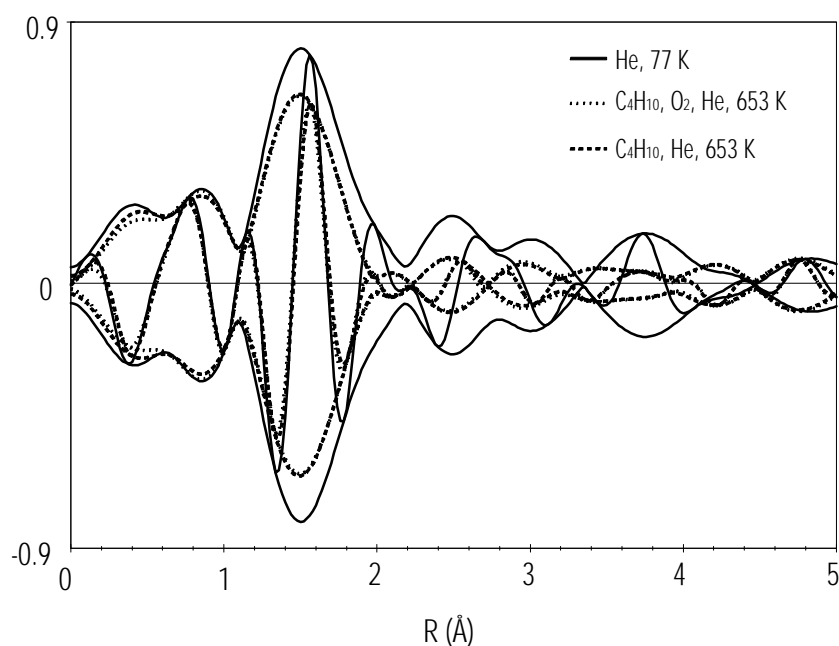


**Figure 6** Fourier transforms ( $k^2$ ,  $Dk=3.5-10 \text{ \AA}^{-1}$ ) V K-edge spectra of the VPO/SiO<sub>2</sub> catalyst before and during *n*-butane oxidation, and under reducing conditions at 653 K.

We have repeated several reduction (*n*-butane/He) and re-oxidation (air) experiments with VPO/SiO<sub>2</sub>, but the spectra were equal to the *in-situ* spectra shown in Figure 6. Therefore, information about redox behaviour (mechanism) and related structural changes cannot be made with the EXAFS data of this catalyst. Unfortunately, EXAFS is less sensitive for possible structural changes in VPO/SiO<sub>2</sub>,



compared to the highly dispersed  $V_2O_5$ -on- $Al_2O_3$  catalyst of which we have reported the results in chapter 7 of this thesis.

## CONCLUSIONS

To establish the mechanism of the butane oxidation reaction to MA over silica- and titania-supported V-P-O catalysts we have applied *in-situ* Raman spectroscopy and *in-situ* XAFS spectroscopy at reaction temperature and in the presence of reactants. Our results show that the Raman spectra of the supported V-P-O catalysts were not affected by application of catalytic conditions to the samples.

In agreement with the results in chapter 6 of this thesis, it was shown that VPO/TiO<sub>2</sub> exist as monomeric monolayer type of species. These species showed characteristic Raman bands at 990 cm<sup>-1</sup> and 800 cm<sup>-1</sup> (hydrated) and at 1032 cm<sup>-1</sup> after dehydration. The band at 1032 cm<sup>-1</sup> did not change upon steady-state butane oxidation at 653K. However, when oxygen was removed from the feed at 653 K a small reduction of the intensity of the band at 1032 cm<sup>-1</sup> occurred. This indicates that the sample is slightly reduced. However, subsequent reduction after re-oxidation did not bring about reduction of the intensity of the 1032 cm<sup>-1</sup> band again. This indicates that the Mars-Van-Krevelen mechanism is not operative for VPO/TiO<sub>2</sub>, which is in agreement with prior EXAFS results with a titania-supported V-P-O catalyst.

However, for VPO/SiO<sub>2</sub> the lack of changes in the *in-situ* Raman spectra does not imply that the catalyst is not changing under these conditions. The Raman spectra of VPO/SiO<sub>2</sub> are dominated by a small amount of  $\alpha_1$ -VOPO<sub>4</sub>, which in agreement with the literature is inert. X-ray absorption spectroscopy does not discriminate between the various vanadium sites and revealed that the structure of VPO/SiO<sub>2</sub> is not affected under butane oxidation conditions at 653 K, *i.e.* the VO<sub>5</sub> units still exist, but the Debye-Waller factors increased due to thermal effects. However, the changes in the pre-edge of the *in-situ* absorption spectra indicate that with VPO/SiO<sub>2</sub>, the Mars-Van-Krevelen mechanism is operative.

## REFERENCES

- 1 R.A. Overbeek, *New aspects of the selective oxidation of n-butane to maleic anhydride: The development of a novel catalyst*, Thesis, Utrecht University, 1994
- 2 R.A. Overbeek, M. Versluijs-Helder, P.A. Warringa, E.J. Bosma, J.W. Geus, *Stud. Surf. Sci. Catal.* **82** (1994), 183
- 3 M. Ruitenbeek, R.A. Overbeek, A.J. van Dillen, D.C Koningsberger, J.W. Geus, *Recl. Trav. Chim. Pays-Bas* **115** (1996), 519
- 4 P. Mars, D.W. van Krevelen, *Chem. Eng. Sci. (Special Suppl.)* **3** (1954), 41
- 5 Chapter 1 of this thesis, and references therein
- 6 J.T. Gleaves, J.R. Ebner, and T.C. Kuechler, *Catal. Rev. Sc. Eng.* **30**(1) (1988), 49

## Chapter 8

- 7 G. Centi, F. Trifiro, G. Busca, J. Ebner, and J. Gleaves, *Disc. Faraday. Soc.* **87** (1989), 215
- 8 R.A. Overbeek, P.A. Warringa, M.J.D. Crombag, L.M. Visser, A.J. van Dillen, and J.W. Geus, *Appl. Catal. A* **135** (1996), 209
- 9 R.A. Overbeek, A.R.C.J. Pekelharing, A.J. van Dillen, and J.W. Geus, *Appl. Catal. A* **135** (1996), 231
- 10 A. Brückner, B. Kubias, B. Lücke, *Catalysis Today* **32** (1996), 215
- 11 M.E. Lashier, G.L. Schrader, *J. Catal.* **128** (1991), 113
- 12 H. Knötzinger, *Catalysis Today* **32** (1996), 71
- 13 F. Ben Abdelouahab, R. Olier, N. Guilhaume, F. Lefebvre, J.C. Volta, *J. Catal.* **134** (1992), 151
- 14 I.E. Wachs, J.M. Jehng, G. Deo, B.M. Weckhuysen, V.V. Guliants, J.B. Benziger, *Catalysis Today* **32** (1996), 47
- 15 J.C. Volta, K. Bere, Y.J. Zhang, R. Olier, *ACS symposium series* **523** (1993), 217
- 16 G.J. Hutchings, A. Desmartin-Chomel, R. Olier, J.C. Volta, *Nature* **368** (1994), 41
- 17 Chapter 5 of this thesis, and references therein
- 18 Chapter 6 of this thesis, and references therein
- 19 J.M. Jehng, G. Deo, B.M. Weckhuysen, I.E. Wachs, *J. Mol. Catal. A: Chemical* **110** (1996), 41
- 20 M. Vaarkamp, B.L. Mojet, M.J. Kappers, J.T. Miller, and D.C. Koningsberger, *J. Phys. Chem.* **99** (1995), 16067
- 21 G. Deo, I.E. Wachs, *J. Catal.* **146** (1994), 335
- 22 F.D. Hardcastle, I.E. Wachs, *J. Phys. Chem.* **95** (1991), 5031
- 23 I.E. Wachs, *Catalysis Today* **27** (1996), 437
- 24 H. Jeziorowski, H. Knötzinger, *Chem. Phys. Lett.* **51** (1977), 519
- 25 V.V. Guliants, J.B. Benziger, S. Sundaresan, I.E. Wachs, J.M. Jehng, J.E. Roberts, *Catalysis Today* **28** (1996), 275
- 26 Chapter 7 of this thesis, and references therein
- 27 X. Gao, S.R. Bare, B.M. Weckhuysen, I.E. Wachs, *J. Phys. Chem. B* **102** (1998), 10842

# 9

---

## SUMMARY AND CONCLUDING REMARKS

### INTRODUCTION

Three main research objectives form the basis of the work described in this thesis: i) preparation of highly active and selective supported V-P-O catalysts for the selective oxidation of *n*-butane to maleic anhydride; ii) characterisation of the structure of the supported V-P-O catalysts and determination of the nature of the active sites and iii) determination of the mechanism of the oxidation reaction. This final chapter deals with a summary of the results described in the preceding chapters of this thesis. Suggestions for further research in this field will be proposed.

## SUMMARY

The vanadium-phosphorus-oxide (V-P-O) catalyst has been applied commercially in the selective oxidation of *n*-butane to maleic anhydride since 1974. Notwithstanding this long period of commercial operation, the currently applied bulk V-P-O catalyst has several drawbacks, such as poor reproduction of the synthesis, high production costs, a long and difficult activation procedure and deactivation under reaction conditions. Furthermore, despite three decades of extensive research, still little is known about the real nature of the active sites in the V-P-O catalyst.

Our idea was to develop a supported V-P-O catalyst in order to overcome the drawbacks of the bulk system. The supported V-P-O catalysts were expected to show superior characteristics over bulk V-P-O, such as a cheap and reproducible preparation procedure, a large number of active sites per unit surface area, a short activation period and a high mechanical strength. Therefore, employment of supported V-P-O catalysts in a fluidised-bed process is very promising. Furthermore, the application of a well-dispersed V-P-O phase onto a support material would open new opportunities for a detailed characterisation of the active phase, since no interfering bulk contributions are expected in the various spectra. Moreover, when a reasonable catalytic performance is achieved, the supported V-P-O catalysts can serve as model systems for the surface of bulk V-P-O catalyst.

In a prior research project, Overbeek has shown that silica- and titania-supported V-P-O catalysts show interesting properties in the *n*-butane oxidation reaction [1]. After a thorough characterisation of the important features of the bulk V-P-O catalysts, Overbeek developed a preparation procedure, which was cheaper and much more controllable than the preparation procedure(s) of bulk V-P-O. However, the newly developed supported V-P-O catalysts did not show reasonable catalytic performance (yield < 20%). In general, titania-supported catalysts are much more active than their silica counterparts. However, silica-supported catalysts are much more selective, resulting in better overall yields [1].

We have prepared several silica-supported V-P-O catalysts and further improved the catalytic performance. Our best silica-supported V-P-O catalyst (7.5 wt% V, P/V 1.1) showed a catalytic yield to maleic anhydride of 26%. The selectivity of these catalysts was comparable to the selectivity of our home made bulk V-P-O catalyst, but the supported catalyst is still more active, probably due to a larger amount of active sites per unit surface area. The catalytic yield of our VPO/bulk catalyst and our silica-supported V-P-O catalyst still does not approach the values obtained with commercially applied V-P-O catalysts, which have been optimised for a long period of time. Nonetheless, we think that comparison of the structure of the silica-supported V-P-O phase with the structure of our VPO/bulk sample can result in a better fundamental understanding of the V-P-O system.

Several chapters of this thesis are dedicated to the comparison of the characterisation results obtained with our VPO/bulk catalyst and with our best VPO/SiO<sub>2</sub> catalyst. Overbeek has shown that the active phase in bulk V-P-O catalysts is probably an amorphous phase [1]. X-ray diffraction and Transmission Electron Microscopy revealed that the VPO/SiO<sub>2</sub> catalyst did not contain crystalline V-P-O components and, hence, we think that we can consider the

### Summary and concluding remarks

supported V-P-O phase as a model system for the amorphous part of the bulk V-P-O catalyst.

In chapter 3 of this thesis, we describe the characterisation the VPO/bulk sample with Electron Spin Resonance spectroscopy (ESR) and magnetisation measurements. We showed that the catalyst contains three different contributions. Combining the results from ESR and magnetisation experiments the relative numbers of  $\text{VO}^{2+}$  ions existing in strong pairs ( $J/k = -65.7$  K), weak pairs ( $J/k = -4.7$  K) and  $\text{V}^{5+}$  defects in our sample is estimated to be 10:7:2, respectively. The contribution of the strongly coupled vanadium ions is originating from vanadylpyrophosphate, which is the major component of this catalyst. However, we detected a significant amount of a formerly not reported  $\text{V}^{4+}$  phase with a weak exchange coupling. Furthermore, our results show that a significant amount of  $\text{V}^{5+}$  defects is present in VPO/bulk. The so-called weak pairs would not have been observed with magnetisation experiments only. However, they manifest themselves prominently in the low-temperature ESR data. X-ray diffraction showed that the additional contribution could be originating from the presence of  $\text{VO}(\text{HPO}_4) \cdot 4\text{H}_2\text{O}$ . This hydrated V-P-O phase must be formed under reaction conditions, since steam is one of the major reaction products. In agreement with the literature, no rehydration to any crystalline hydrated V-P-O phase was observed at room temperature. However, it must be, mentioned that the ESR and magnetisation results have not been obtained *in-situ* and therefore, it is not sure whether the observed phases are present in the catalyst under actual *n*-butane oxidation conditions.

We have chosen to study the surface composition of several bulk V-P-O catalysts with LEIS and XPS and to compare these with the results obtained with VPO/ $\text{SiO}_2$ . The results of this study are represented in chapter 4 of this thesis. One of the important features of the V-P-O catalyst, the surface composition, is still debated in the literature. Interpretation of X-ray Photoelectron Spectra (XPS) is complicated due to the lack of appropriate reference compounds. Low-Energy Ion Scattering is not suffering from this drawback. Quantification of the data can be performed with the samples themselves, using the DISC method. Furthermore, this technique only probes the outermost surface layer of the specimen. XPS showed that a significant amount of carbonaceous contaminant was deposited on the surface of the bulk V-P-O catalysts, regardless of the preparation method (organic or aqueous). This carbon shields the vanadium, phosphorus and oxygen atoms on the surface and severely complicates the quantitative analysis. We were able to combust the carbon in air at 573 K. However, this also brought about oxidation of vanadium (colour change), which could result in structural changes. The supported catalyst contained much less carbon, which is probably caused by the higher specific surface area. For VPO/ $\text{SiO}_2$ , it was shown that phosphate is removed from the surface under reaction conditions. However, overlap of the  $^{30}\text{Si}$  and  $^{31}\text{P}$  peaks in the LEIS spectra of this sample complicated quantitative analysis as well. Nevertheless, we have obtained promising preliminary results with the LEIS experiments.

In chapter 5 of this thesis, we describe the catalytic test results of our supported V-P-O samples and compare these results with the performance of the VPO/bulk

catalyst. In agreement with the results of Overbeek, the titania-supported V-P-O catalysts are most active based on the amount of active phase present in the reactor, followed by VPO/SiO<sub>2</sub> and VPO/bulk. When the yield to maleic anhydride is plotted as a function of conversion, it appeared that the performance of VPO/SiO<sub>2</sub> and VPO/bulk are almost equal. This is a condition to be met for the application of the silica-supported V-P-O catalyst as a model system for the surface of bulk V-P-O catalysts.

Subsequently, we have extensively characterised the supported V-P-O phase with X-ray absorption spectroscopy (XAFS). X-ray Absorption Near Edge Structure (XANES) and the pre-edge region of the vanadium K-edge spectra showed that the titania-supported V-P-O catalysts consist of tetrahedrally co-ordinated vanadium sites, whereas the VPO/SiO<sub>2</sub> and VPO/bulk sample show (distorted) octahedral geometry.

In addition, we have applied ESR spectroscopy to investigate vanadium-vanadium interactions in the supported V-P-O catalysts, analogously to the earlier mentioned experiments with VPO/bulk. For VPO/TiO<sub>2</sub>, we have observed the characteristic octet of the hyperfine coupling of the electron spin ( $S = 1/2$ ) with the <sup>51</sup>V nucleus ( $I = 7/2$ ). This indicates that only isolated vanadyl species are present in this catalyst. For VPO/SiO<sub>2</sub>, no hyperfine coupling was observed. The absence of hyperfine coupling is attributed to exchange interactions between adjacent electron spins, which averages out the hyperfine interaction with the vanadium nucleus. The low-temperature ESR data of VPO/SiO<sub>2</sub> obey the Curie-Weiss law indicating an antiferromagnetic exchange interaction. We have extrapolated a value for the exchange coupling,  $\theta$ , of 2 K, a value much lower than usually reported for V-P-O compounds. We believe that this very weak exchange coupling is originating from an amorphous V-P-O phase or a V-P-O phase in which the vanadium atoms are separated far enough to avoid overlap of the 3d orbitals.

Chapter 6 of this thesis deals with the quantitative analysis of the EXAFS data of VPO/bulk, VPO/SiO<sub>2</sub> and VPO/TiO<sub>2</sub>, which were collected in helium at 77 K. We have shown that a bulk technique as XAS is not adequate for structural investigations of the bulk V-P-O samples, because the surface contribution in the spectra is broadened beyond detection in the background of the bulk contributions. Despite the fact that ESR experiments showed that the VPO/bulk catalyst only consists for 63% of vanadylpyrophosphate, the Extended X-ray Absorption Fine Structure spectrum (EXAFS) of VPO/bulk was nicely fitted with the single-crystal X-ray diffraction data of vanadylpyrophosphate. The EXAFS spectra of the silica- and titania-supported V-P-O catalyst did not agree with the data for VPO/bulk. Therefore, we concluded that the structure of the supported V-P-O phase does not resemble vanadylpyrophosphate. Moreover, the structure of VPO/TiO<sub>2</sub> was not equal to the structure of VPO/SiO<sub>2</sub>. For both supported V-P-O catalysts, no long-range order was observed in the spectra. Quantitative analysis of the EXAFS data of the supported catalysts was difficult, probably due to inhomogeneities in the samples or the existence of a highly disordered and amorphous phase(s). Nevertheless, for both supported V-P-O catalysts, reasonable structural models have been obtained. For VPO/SiO<sub>2</sub>, only one structural model shows acceptable chemical parameters. In this model,

### Summary and concluding remarks

vanadium is arranged in square planar  $\text{VO}_5$  units with one short vanadyl bond (1.59 Å) and four planar V-O bonds of about 2 Å. Based on the observed coordination numbers, the average cluster was calculated to consist of three to four of such corner-sharing  $\text{VO}_5$  units. The resulting V-V distance of 4.32 Å is in agreement with the ESR results of  $\text{VPO/SiO}_2$ . Phosphate groups fill the remaining  $\text{VO}_5$  corner positions, resulting in a relatively long V-P distance of 3.56 Å. In agreement with the ESR data,  $\text{VPO/TiO}_2$  consists of isolated vanadyl units in which the tetrahedral  $\text{VO}_4$  units are connected to the titania support material via three V-O-Ti bridging bond. In this model, phosphate is not directly bound to the  $\text{VO}_4$  units, but rather to the support material. However, the V-P distance is probably close enough to cause hydrogen bonding between the phosphate terminating P-OH groups and the vanadyl oxygen atom. The catalytic performance of  $\text{VPO/SiO}_2$ , combined with the structural characterisation of this sample has brought us to the conclusion that vanadylpyrophosphate is not necessarily present in the active phase of the V-P-O catalyst. The poor selectivity of  $\text{VPO/TiO}_2$ , as compared to  $\text{VPO/bulk}$  and  $\text{VPO/SiO}_2$  can most probably be explained by the absence of V-O-P bonds in this catalyst. The presence of V-O-P bonds seems to be a prerequisite for optimal catalytic selectivity to MA. Another interesting observation is the difference in geometry of the vanadium units in the three catalysts. XANES and EXAFS indicate that the local geometry of vanadium is distorted octahedral for  $\text{VPO/bulk}$  and  $\text{VPO/SiO}_2$  and tetrahedral for  $\text{VPO/TiO}_2$ . It is, however, interesting to note that the octahedrons are edge-sharing in  $\text{VPO/bulk}$  and corner-sharing in the  $\text{VPO/SiO}_2$  catalyst. Nevertheless, the surface structure of  $\text{VPO/bulk}$  cannot be selectively probed with EXAFS and consequently it is not obvious that the active sites in  $\text{VPO/bulk}$  are edge-sharing  $\text{VO}_6$  units. The high selectivity of the  $\text{VPO/SiO}_2$  catalyst indicates that an edge-sharing geometry is not a prerequisite for optimal catalytic performance in the *n*-butane oxidation reaction. The high selectivity of the  $\text{VPO/SiO}_2$  catalyst and the ESR and EXAFS results for this catalyst indicate that the active surface V-P-O phase probably consists of a V-P-O phase, which is built from the earlier described corner-sharing square planar  $\text{VO}_5$  units.

However, Overbeek has found that the structure of the V-P-O catalyst is affected by the adsorbed reactants and products and the reaction temperature [1]. Therefore, characterisation of the active phase in V-P-O catalysts can only be performed *in-situ*, *i.e.* at reaction temperatures and in the presence of reactants. Furthermore, Overbeek has studied the mechanism of the *n*-butane oxidation reaction to maleic anhydride using a titania-supported V-P-O catalyst with *in-situ* XAFS [1]. In order to study whether *in-situ* XAFS spectroscopy is able to discriminate between the different reaction mechanisms, we have applied *in-situ* XAFS spectroscopy on a model catalyst, *i.e.* 17.5 wt%  $\text{V}_2\text{O}_5$ -on- $\gamma$ - $\text{Al}_2\text{O}_3$ . The loading of this sample amounts to about 80% of the monolayer capacity of this support. The results of this study are represented in chapter 7 of this thesis. In agreement with the literature, the Mars-Van-Krevelen mechanism is operative at 723 K for both CO and *n*-butane oxidation. At 623 K, the catalyst follows the associative mechanism in CO oxidation [2]. XANES, EXAFS and principal component analysis (PCA) revealed that, in agreement with Raman data, the

structure of the supported  $V_2O_5$  phase consists of monomeric tetrahedral  $(Al-O)_3-V=O$  units and an additional contribution in the spectra, which is most probably originating from a small amount of polymeric vanadate species after dehydration in air at 623 K. This structure remains the same during steady state *n*-butane and CO oxidation. However, when oxygen is removed from the feed at 723 K, reduction of the  $V_2O_5$  was observed. It was found that reduction brings about removal of the vanadyl oxygen atom. The  $V^{3+}$  ion is subsequently migrating into the  $\gamma-Al_2O_3$  lattice, where it is positioned at an  $Al^{3+}$  octahedral position. This process was already proposed by van Dillen for vanadium oxide on alumina [3], but until now, experimental evidence was not available. Comparable results for vanadium oxide on silica were obtained by Vogt with FTIR spectroscopy [4]. However, with vanadium oxide on silica, reduction to  $V^{4+}$  occurs and vanadium is possibly located on the  $Si^{4+}$  positions of the support. Our results indicate that the migration process of low-valent vanadium species into the octahedral positions of  $\gamma-Al_2O_3$  is reversible and that the  $(Al-O)_3-V=O$  units have returned after re-oxidation. We have shown that this model is in agreement with our XANES and EXAFS results. To our knowledge, this is the first time that the structure of the  $V^{3+}$  phase has been reported. This is probably caused by the fact that we applied the difference file technique for the analysis of the complex EXAFS data. Without this data analysis procedure, a solution for the problem would not have been found, due to destructive interference of the various components of the Fourier transforms. It was found that XAFS spectroscopy is a powerful tool to study changes in the local environment and the oxidation-state of vanadium centres in the sample.

In chapter 8 of thesis, we have applied *in-situ* Raman spectroscopy and *in-situ* X-ray absorption spectroscopy to investigate the mechanism of the *n*-butane oxidation to MA over VPO/SiO<sub>2</sub> and VPO/TiO<sub>2</sub> catalysts. Raman spectroscopy revealed that VPO/TiO<sub>2</sub> consists of monolayer type species, which is in agreement with ESR and EXAFS results. The Raman spectra did not change upon the application of catalytic conditions. However, when the catalyst was exposed to *n*-butane/helium at 653 K, a small amount of reduction occurred. After re-oxidation, a second reduction was not visible in the Raman spectra. This is in agreement with earlier EXAFS results for a titania-supported V-P-O catalyst and indicates that the Mars-Van-Krevelen mechanism is not operative for VPO/TiO<sub>2</sub>.

VPO/SiO<sub>2</sub> mainly shows the Raman absorption bands of  $\alpha_1$ -VOPO<sub>4</sub>, which must be present as microcrystalline state within VPO/SiO<sub>2</sub>. However,  $\alpha_1$ -VOPO<sub>4</sub> must be a minor component in the VPO/SiO<sub>2</sub> catalyst, because the structure of  $\alpha_1$ -VOPO<sub>4</sub> does not match with the best fit of our EXAFS data for this catalyst. The  $\alpha_1$ -VOPO<sub>4</sub> phase is not affected by the applied catalytic conditions at 653 K. No bands appear or disappear in the Raman spectrum of VPO/SiO<sub>2</sub> under catalytic conditions. However, this does only imply that the  $\alpha_1$ -VOPO<sub>4</sub> phase is inert under the applied conditions. Other, less ordered phases, which are broadened beyond detection in the Raman background, might change, but these changes will remain invisible in the Raman spectra. In contrast to Raman spectroscopy, XAFS probes all vanadium centres in the catalysts. The EXAFS oscillations of the higher shells decreased to zero with the high-temperature experiments. Nonetheless, structural



### Summary and concluding remarks

parameters were not affected, except for the Debye-Waller factors. This is the result of thermal effects. The effects of the catalytic conditions were much smaller for VPO/SiO<sub>2</sub> compared to the V<sub>2</sub>O<sub>5</sub>-on- $\gamma$ -Al<sub>2</sub>O<sub>3</sub> sample. This is probably the result of the much better dispersion of the latter. The *in-situ* XAFS experiments showed that the distorted octahedral geometry of the vanadium sites remained unchanged under reaction conditions. However, small changes in the pre-edge upon steady-state and oxygen free catalytic conditions showed that the Mars-Van-Krevelen is operative for VPO/SiO<sub>2</sub> at 653 K.

In conclusion, we have improved the catalytic performance of the supported V-P-O catalyst, resulting in a maximum yield of 26 % for a (7.5 wt%) VPO/SiO<sub>2</sub> catalyst. The structural characterisation of the supported V-P-O catalysts has revealed remarkable differences between the structure of VPO/TiO<sub>2</sub> on the one and VPO/SiO<sub>2</sub> on the other hand. These structural differences can explain the different catalytic behaviour of the two supported V-P-O catalysts. Furthermore, we have shown that the reaction mechanism for the selective oxidation of *n*-butane to maleic anhydride is different for the supported catalysts. The Mars-Van-Krevelen mechanism is operative for VPO/SiO<sub>2</sub> and VPO/bulk, whereas for VPO/TiO<sub>2</sub> the associative mechanism most probably operative. This can also explain the low selectivity of the VPO/TiO<sub>2</sub> catalysts.

### SUGGESTIONS FOR FURTHER RESEARCH

In the four years of this Ph.D. research project, we have learned a lot about the nature of V-P-O catalysts. Nevertheless, the question remains if we can increase the catalytic yield to MA sufficiently for commercial application with this knowledge. In this thesis, an increase of the yield to 26 % has been reported, which is about 6 % more than the best supported V-P-O sample of Overbeek [1]. Although it is the highest reported value in the literature for supported V-P-O catalysts, 26 % is still too low to consider commercial application. To our opinion, the two-step preparation procedure of Overbeek does not have much more space for improvement. Further improvement calls for a one-step preparation procedure, based on simple and controllable chemistry. Preliminary experiments have shown that vanadium-oxalate-phosphate precursor solutions have interesting properties in this respect. With these solutions, it is possible to install the viscosity, the desired P/V ratio and the vanadium valence state. The precursor solutions can be impregnated or spin-coated on almost any kind of support, which also opens a new field of characterisation techniques, such as AFM and SIMS.

An important parameter that can determine the selectivity of V-P-O catalysts is the V-O bond strength. The vanadyl oxygen atom is found at an almost equal distance of 1.59 Å, 1.62 Å and 1.61 Å for VPO/bulk, VPO/SiO<sub>2</sub> and VPO/TiO<sub>2</sub>, respectively. However, the Debye-Waller factors for this V-O<sub>1</sub> contribution are positive for VPO/bulk and VPO/SiO<sub>2</sub> and negative for the VPO/TiO<sub>2</sub> catalyst, which indicates that the vanadium oxygen bond is much stronger in the latter. Nevertheless, the role of the vanadyl group in the *n*-butane oxidation reaction is still not clear and a more systematic approach with various vanadium oxide based catalysts is necessary to provide more knowledge on this subject. To improve the

knowledge of the V-P-O system, application of molecular modelling in combination with EXAFS would be a powerful tool to validate the models that are obtained from EXAFS data analysis. It is desired that the modelling results are correlated with the catalytic activity and selectivity. Furthermore, molecular modelling could be helpful with the interpretation and understanding of the  $V_2O_5$ -on- $\gamma$ - $Al_2O_3$  data.

## REFERENCES

- 1 R.A. Overbeek, *New aspects of the selective oxidation of n-butane to maleic anhydride: The development of a novel catalyst*, Thesis, Utrecht University, 1994
- 2 J. van den Berg, *Stoichiometry and catalytic activity of vanadia-based oxides for the oxidation of CO and H<sub>2</sub>*, Thesis, Utrecht University, 1984
- 3 A.J. van Dillen, *Catalytic oxidation of carbon monoxide over oxides of indium and vanadium*, Thesis, Utrecht University, 1977
- 4 E. Vogt, *Preparation and properties of catalysts supported on modified silica*, Thesis, Utrecht University, 1988

## SAMENVATTING

---

Drie hoofdonderwerpen vormen de basis van het werk dat in dit proefschrift is beschreven: i) bereiding van gedragen V-P-O katalysatoren met een hoge activiteit en selectiviteit in de selectieve oxidatie van *n*-butaan naar maleïnezuuranhydride, ii) karakterisering van de gedragen V-P-O katalysatoren en bepaling van de aard van de actieve plaatsen en iii) bepaling van het mechanisme van de selectieve oxidatie van *n*-butaan naar maleïnezuuranhydride over de gedragen V-P-O katalysatoren. Dit hoofdstuk geeft een samenvatting van de belangrijkste resultaten.

V-P-O (vanadiumfosfaat) katalysatoren worden sinds 1974 commercieel gebruikt voor de productie van maleïnezuuranhydride uit *n*-butaan of 1-buteen. Ondanks het feit dat het proces al zo'n 25 jaar wordt toegepast, zijn er nog vele mogelijkheden tot verbetering denkbaar. Zo is het heel lastig om de huidige bulk katalysator reproduceerbaar te bereiden en zijn de productiekosten hoog (\$90/kg). Na bereiding volgt een moeilijke activeringsprocedure, waarbij het soms meer dan 2000 uren duurt voor de optimale reactieopbrengst wordt verkregen. Bovendien is deactivering van de katalysator een groot probleem. Een bijkomstig feit is dat, ondanks 30 jaar onderzoek aan het V-P-O systeem, de aard van de actieve plaatsen op de bulk V-P-O katalysator nog steeds niet is opgehelderd.

Wij hebben ervoor gekozen om een gedragen V-P-O katalysator te ontwikkelen om een aantal nadelen van de huidige bulk V-P-O katalysator weg te nemen. Bij een juiste keuze van het drager materiaal ontstaat een slijtvastere katalysator, welke geschikt is voor gebruik in een wervelbed proces. In wervelbedreactoren is een veel betere afvoer van de reactiewarmte mogelijk, waardoor de selectiviteit naar maleïnezuuranhydride hoger is. Daarnaast is het met de toegepaste bereidingsmethoden goed mogelijk om de verschillende parameters van het systeem (belading, dispersie, valentietoestand van het vanadium en P/V verhouding) gecontroleerd in te stellen. Door een drager met een relatief hoog specifiek oppervlak te kiezen kunnen we het aantal actieve plaatsen uitspreiden over een groter oppervlak. Hierdoor neemt de efficiëntie per eenheid V-P-O sterk toe en kan de prijs van de katalysator verder dalen.

Een bijkomend voordeel van een gedragen systeem met goed gedispergeerde V-P-O deeltjes is dat de karakterisering van de monsters niet gehinderd wordt door bijdragen van de bulk in de diverse spectra. Veel karakteriseringstechnieken maken geen onderscheid tussen het oppervlak van het monster, waar de reactie plaats vindt, en de bulk, die niet deelneemt aan de reactie maar wel een dominerende bijdrage in de spectra geeft te zien. Als we in staat zouden zijn om goed gedispergeerde gedragen V-P-O katalysatoren te bereiden met een aanvaardbare katalytische activiteit en selectiviteit zouden we deze katalysatoren kunnen beschouwen als modelsystemen voor het oppervlak van de bulk V-P-O katalysatoren.

In een eerder promotieonderzoek heeft Overbeek laten zien dat silica- en titania-gedragen V-P-O katalysatoren interessante eigenschappen bezitten voor de *n*-butaan oxidatie reactie [1]. Na een grondige bestudering van de bulk V-P-O

## Samenvatting

katalysator werden de belangrijkste eigenschappen van het systeem in kaart gebracht. Op basis van deze gegevens werd een bereidingsprocedure ontwikkeld voor de gedragen V-P-O katalysatoren die goedkoop en eenvoudig op te schalen is. Bovendien resulteerde deze bereidingsmethode in een betere reproduceerbaarheid van de katalysatoren. De katalytische prestaties van de door Overbeek ontwikkelde katalysatoren was echter aanzienlijk minder goed dan die van de bulk V-P-O katalysatoren (opbrengst < 20%). Over het algemeen waren de titania-gedragen V-P-O katalysatoren veel actiever dan de silica-gedragen V-P-O katalysatoren. De silica-gedragen katalysatoren waren echter veel selectiever, hetgeen resulteerde in een hogere opbrengst [1].

Wij hebben de samenstelling en bereiding van de silica-gedragen V-P-O katalysatoren verder geoptimaliseerd, waardoor de katalytische prestaties verbeterden. Onze beste silica-gedragen V-P-O katalysator (7.5 wt% V, P/V 1.1) had een opbrengst aan maleïnezuuranhydride van 26% bij een *n*-butaan conversie van 48% (680 K). De selectiviteit van dit systeem was vergelijkbaar met dat van onze eigen bulk V-P-O katalysator. De gedragen katalysator was echter veel actiever. Wij denken dat dit het gevolg is van een groter aantal actieve plaatsen per oppervlakte eenheid.

Overbeek heeft laten zien dat de actieve fase in bulk V-P-O hoogstwaarschijnlijk amorf is [1]. Met Röntgendiffractie (XRD) en Transmissie Electronen Microscopie (TEM) hebben we laten zien dat het gedragen systeem goed gedispergeerd is en geen kristallijne V-P-O fasen bevat. Dit is een belangrijke voorwaarde voor het gebruik van de VPO/SiO<sub>2</sub> katalysator als model systeem voor de amorfe fase van de bulk V-P-O katalysatoren.

Om te beginnen hebben we VPO/bulk gekarakteriseerd met Electron Spin Resonantie Spectroscopie (ESR) en magnetisatie metingen bij lage temperaturen. De resultaten van dit onderzoek zijn weergegeven in hoofdstuk 3 van dit proefschrift. Uit deze metingen kwam naar voren dat het vanadium in VPO/bulk in drie vormen aanwezig is. Door de resultaten van ESR en magnetisatie metingen te combineren hebben we laten zien dat de relatieve verhouding van deze drie bijdragen 10:7:2 bedraagt. Het grootste deel van de VO<sup>2+</sup> ionen bevindt zich in een fase waarin de vanadyl groepen een zeer sterke interactie vertonen (-65.7 K). Deze bijdrage wordt veroorzaakt door vanadylpyrofosfaat. De tweede vorm vertoont een veel geringere interactie (-4.7 K), die vermoedelijk afkomstig is van een gehydrateerde V-P-O fase, nl. VO(HPO<sub>4</sub>)·4H<sub>2</sub>O. Dit is opmerkelijk, omdat volgens gegevens in de literatuur geen rehydratatie van de monsters plaats kan vinden na de thermische voorbehandeling. Hydratatie experimenten bij kamertemperatuur bevestigden de resultaten uit de literatuur, maar de aanwezigheid van VO(HPO<sub>4</sub>)·4H<sub>2</sub>O is een sterke aanwijzing dat rehydratatie onder reactieomstandigheden (~ 700 K, 1 atm.), waarbij een van de reactieproducten stoom is, wel degelijk plaats kan vinden. De derde bijdrage is afkomstig van V<sup>5+</sup> defecten in de vanadylpyrofosfaat structuur.

Een van de belangrijkste kenmerken van V-P-O katalysatoren, de samenstelling van het oppervlak, staat nog steeds ter discussie in de literatuur. De interpretatie van Röntgen Foto-electron spectroscopie (XPS) data is zeer moeilijk door het ontbreken van geschikte referentieverbindingen. Lage Energie Ionen verstrooiing (LEIS) is een

## Samenvatting

techniek die dit nadeel niet kent. Kwantificering van de data kan met de monsters zelf door het toepassen van de zogenaamde DISC methode. Bovendien is deze techniek alleen gevoelig voor de buitenste atoomlaag van de monsters, in tegenstelling tot XPS dat een doordringdiepte van ongeveer 10-50 Å kent. Daarom hebben wij er voor gekozen om LEIS toe te passen ter karakterisering van onze V-P-O katalysatoren (bulk en gedragen). De resultaten van dit onderzoek zijn weergegeven in hoofdstuk 4 van dit proefschrift. De XPS resultaten laten zien dat er een aanzienlijke hoeveelheid koolstof-verontreiniging aanwezig is op het oppervlak van de VPO/bulk katalysatoren. De hoeveelheid van de kool was onafhankelijk van de bereidingsmethode (organisch of waterig). De kool dekt de vanadium, fosfor en zuurstofatomen aan het oppervlak af en hindert daarmee de kwantitatieve analyse van de LEIS data. Het was mogelijk om de kool te verwijderen door de monsters voor te behandelen in lucht bij 573 K, maar dit veroorzaakte tevens oxidatie van het vanadium, welke meestal gepaard gaat met structurele veranderingen. Op de gedragen V-P-O katalysatoren was veel minder kool aanwezig. Dit komt waarschijnlijk doordat de kool in deze monsters over een veel groter oppervlak kan worden uitgespreid. Echter, door overlap van de  $^{30}\text{Si}$  en  $^{31}\text{P}$  signalen was de kwantitatieve analyse van de LEIS data van VPO/SiO<sub>2</sub> ook onmogelijk. Desalniettemin kunnen we concluderen dat de VPO/SiO<sub>2</sub> katalysator fosfaat heeft verloren onder reactieomstandigheden.

In hoofdstuk 5 van dit proefschrift beschrijven we de katalytische eigenschappen van onze beste monsters. De katalytische activiteit en selectiviteit werden bepaald en vergeleken met de resultaten van VPO/bulk. In overeenstemming met de resultaten van Overbeek waren de titania-gedragen katalysatoren het meest actief, gevolgd door VPO/SiO<sub>2</sub> en VPO/bulk. Als we de opbrengst aan maleïnezuuranhydride uitzetten tegen de conversie blijkt dat de prestaties van VPO/SiO<sub>2</sub> bijna gelijk zijn aan die van VPO/bulk. De katalytische prestaties van beide systemen, bulk en gedragen, zijn echter nog wel minder dan die van een geoptimaliseerde industriële V-P-O katalysator. Desalniettemin denken wij dat de vergelijking van de structuur van onze silica-gedragen V-P-O katalysator met de structuur van ons bulk V-P-O monster interessante informatie op kan leveren, die van belang is voor een beter fundamenteel begrip van het V-P-O systeem in het algemeen.

Vervolgens hebben we de gedragen V-P-O fase uitgebreid gekarakteriseerd met Röntgen Absorptie Spectroscopie (XAFS) in helium bij 77 K. Deze techniek geeft informatie over de geometrie rondom de vanadium atomen en over structurele parameters, zoals coördinatiegetallen en bindingsafstanden. Röntgen Absorptie Nabije Kant Structuur (XANES) en de voorkant van de Vanadium K-absorptie kant hebben ons laten zien dat het vanadium in VPO/TiO<sub>2</sub> tetraëdrisch gecoördineerd is. In VPO/SiO<sub>2</sub> en VPO/bulk daarentegen is sprake van een verstoorde octaëdrische of vierkant-pyramidale coördinatie. De Uitgestrekte Röntgen Absorptie Fijn Structuur (EXAFS) spectra van de silica- and titania-gedragen V-P-O katalysatoren kwamen niet overeen met het spectrum van VPO/bulk. Hieruit hebben we geconcludeerd dat de structuur van de gedragen fasen niet overeenkomt met de structuur van vanadylpyrofosfaat. Bovendien was de structuur van VPO/TiO<sub>2</sub> niet gelijk aan die van VPO/SiO<sub>2</sub>. Bij beide gedragen V-P-O katalysatoren hebben we geen lange afstandsordening waargenomen in de EXAFS spectra.

### Samenvatting

Om de V-V interacties in de gedragen V-P-O katalysatoren te bestuderen hebben we, conform de experimenten met VPO/bulk, ESR metingen uitgevoerd bij lage temperaturen. Bij VPO/TiO<sub>2</sub> hebben we het karakteristieke octet waargenomen dat het gevolg is van de hyperfijn koppeling van de electronen spin ( $S = 1/2$ ) met de <sup>51</sup>V kern ( $I = 7/2$ ). Dit betekent dat in deze katalysator alleen geïsoleerde vanadylgroepen aanwezig zijn. Bij VPO/SiO<sub>2</sub> hebben we geen fijnstructuur waargenomen. De afwezigheid van fijnstructuur impliceert dat er een interactie is tussen de verschillende spins, en dus tussen de verschillende vanadylgroepen in het monster. De lage temperatuur ESR data van VPO/SiO<sub>2</sub> volgen de Curie-Weiss wet voor antiferromagnetische uitwisselingsinteracties. We hebben de data geëxtrapoleerd en de uitwisselingsconstante,  $\theta$ , bepaald op 2 K. Deze waarde is veel lager dan die van de in de literatuur gerapporteerde V-P-O verbindingen en kan naar onze mening alleen worden toegeschreven aan een zeer amorfe V-P-O fase of een V-P-O fase waarin de vanadium atomen zodanig ver van elkaar verwijderd zijn dat de electronen banen van de twee atomen niet of nauwelijks overlappen.

De resultaten van de kwantitatieve analyse van de EXAFS data zijn weergegeven in hoofdstuk 6 van dit proefschrift. Gebleken is dat EXAFS weinig informatie oplevert over de oppervlakte structuur van VPO/bulk, omdat de bijdrage van het oppervlak te verwaarlozen is en wegvalt in de achtergrond. Hierdoor waren we slechts in staat om de spectra van de bulk katalysatoren te simuleren met de parameters van vanadylpyrofosfaat. De simulaties kwamen prima overeen met onze experimentele data, ondanks het feit dat we uit ESR en magnetisatie metingen weten dat slechts 63% van het monster uit deze fase bestaat. We hebben slechts kleine verschillen waargenomen tussen de structuur van de bulk katalysator die in organisch milieu was bereid en de structuur van het monster dat in waterig milieu was bereid.

De analyse van de EXAFS spectra van de gedragen V-P-O katalysatoren was zeer complex. Dit is waarschijnlijk het gevolg van de inhomogeniteit van de monsters of van de enorme wanorde in de aangebrachte V-P-O fase. De ruwe coördinatiegetallen komen aardig overeen met de geometrie die met XANES werd vastgesteld. Voor beide gedragen V-P-O katalysatoren werden redelijk acceptabele simulaties verkregen.

Het model dat we voor VPO/SiO<sub>2</sub> hebben opgesteld bestaat uit een centrale vierkant-pyramidale VO<sub>5</sub> eenheid met een korte V=O binding van 1.59 Å en vier langere V-O bindingen van ongeveer 2 Å. De individuele VO<sub>5</sub> eenheden zijn onderling verbonden via de hoekpunten. De gemiddelde coördinatiegetallen wijzen er op dat de clusters bestaan uit zes VO<sub>5</sub> eenheden. De overige hoekpunten worden gecompenseerd door terminale fosfaat groepen. De resulterende V-V afstand bedraagt 4.32 Å, wat in overeenstemming is met de verwachting op basis van de eerder beschreven ESR experimenten. Daarnaast is de beschreven geometrie in overeenstemming met de eerder beschreven XANES resultaten.

Ook het structuur model dat we voor VPO/TiO<sub>2</sub> hebben opgesteld is in overeenstemming met de ESR en XANES resultaten die we voor dit monster hebben verkregen. De structuur is opgebouwd uit geïsoleerde tetraëdrische VO<sub>4</sub> eenheden, die zijn opgebouwd uit een korte V=O binding van 1.61 Å en drie lange

### Samenvatting

V-O(-Ti) bijdragen van 1.99 Å. Het fosfaat in deze katalysator is niet rechtstreeks gebonden aan de vanadium eenheden, maar aan de titaniumoxide drager. Wel is het waarschijnlijk dat er een interactie is tussen het fosfaat en het vanadium door waterstofbruggen tussen de terminale OH groepen van het fosfaat en het vanadyl zuurstof atoom van de VO<sub>4</sub> eenheden.

Als we de resultaten van de katalytische metingen combineren met de resultaten van de structurele karakterisering van de gedragen V-P-O fase, dan kunnen we niet anders dan concluderen dat de aanwezigheid van vanadylpyrofosfaat geen vereiste is voor een goede selectiviteit naar maleïnezuuranhydride bij de selectieve oxidatie van *n*-butaan over een V-P-O katalysator. Ondanks het feit dat de verkregen simulaties van de EXAFS spectra niet optimaal zijn, hebben ze toch geleid tot aanvaardbare speculaties omtrent de structuur van de verschillende gedragen V-P-O fases. Op basis van onze resultaten is het zeer wel mogelijk dat de actieve oppervlakte fase in V-P-O bestaat uit een amorse mengverbinding van vanadiumoxide en fosforoxide. Echter, het model dat verkregen is op basis van de EXAFS data van VPO/SiO<sub>2</sub> zou een redelijk model van de actieve fase kunnen voorstellen. De geringe katalytische selectiviteit van VPO/TiO<sub>2</sub> zou op basis van het model dat door ons is opgesteld het gevolg zijn van het ontbreken van een directe chemische interactie tussen het vanadium en het fosfaat (V-O-P bindingen). Vanadium oxide is wel actief, maar niet selectief in de selectieve oxidatie van *n*-butaan naar maleïnezuur anhydride, hetgeen in overeenstemming is met onze katalytische resultaten van VPO/TiO<sub>2</sub>.

Het is echter bekend dat de beste methode om katalysatoren te karakteriseren de karakterisering onder reactieomstandigheden is. Overbeek heeft eerder aangetoond dat veel katalysatorsystemen, waaronder V-P-O, veranderen van structuur als er reactanten of producten op het oppervlak aanwezig zijn [1].

Bovendien heeft Overbeek het mechanisme van de *n*-butaan oxidatie reactie naar maleïnezuuranhydride over een titania-gedragen V-P-O katalysator bestudeerd met XAFS [1]. Om de toepasbaarheid van XAFS ter onderscheiding van de verschillende reactiemechanismen te bestuderen hebben wij XAFS toegepast met een model systeem, *i.e.* 17.5 wt% V<sub>2</sub>O<sub>5</sub> op  $\gamma$ -Al<sub>2</sub>O<sub>3</sub>. Dit systeem is uitermate goed gekarakteriseerd en heeft een belading van ongeveer 80% van de monolaag capaciteit van dit dragermateriaal. Onze resultaten zijn weergegeven in hoofdstuk 7 van dit proefschrift en laten zien dat XANES een zeer geschikte techniek is om de veranderingen in de locale geometrie rondom de vanadium atomen en de valentie toestand van de vanadium atomen in de katalysator te bestuderen.

We hebben twee reacties onderzocht, namelijk de oxidatie van CO en van *n*-butaan. In overeenstemming met de literatuur hebben we gevonden dat het Mars-Van-Krevelen mechanisme werkzaam is bij 723 K. Bij 623 K is het associatieve mechanisme van kracht voor de CO oxidatie [2].

Allereerst werd het V<sub>2</sub>O<sub>5</sub> op  $\gamma$ -Al<sub>2</sub>O<sub>3</sub> monster gedehydrateerd in lucht of helium bij 623 K. Dehydratie in lucht had een (partiële) reductie van het vanadium tot gevolg, doordat de aan vanadium gebonden OH-groepen verwijderd worden. Daarom is het in lucht gedehydrateerde monster als aftelpunt voor de overige experimenten gebruikt. Met XANES, EXAFS en hoofd-componenten analyse (PCA) hebben we aangetoond dat de structuur van deze gedragen V<sub>2</sub>O<sub>5</sub> fase bestaat uit

## Samenvatting

monomere  $(\text{Al-O})_3\text{-V=O}$  eenheden (tetraëdrisch) en een klein aantal polymere vanadaat clusters. Dit resultaat is in overeenstemming met de data in de literatuur. Tijdens CO oxidatie bij 623 K verandert deze structuur niet. Ook als de zuurstof uit de voeding werd weggenomen had dit bij 623 K geen gevolgen voor de structuur van het monster. Dit is een sterke aanwijzing dat bij deze temperatuur het associatieve mechanisme van kracht is.

Toen we evenwel de zuurstof uit de voeding verwijderden bij een reactie temperatuur van 723 K, namen we een reductie van het  $\text{V}_2\text{O}_5$  waar. Uit de Temperatuur geprogrammeerde reductie (TPR) experimenten kunnen we opmaken dat hierbij  $\text{V}^{3+}$  ionen worden gevormd. De EXAFS analyse toonde aan dat deze  $\text{V}^{3+}$  ionen vervolgens migreren in het  $\gamma\text{-Al}_2\text{O}_3$  rooster, waar ze preferentieel de  $\text{Al}^{3+}$  octaëder posities bezetten. Dit was in het verleden al eens gesuggereerd door van Dillen voor vanadiumoxide op alumina [3], maar tot op heden was geen experimenteel bewijs beschikbaar. Vogt vond vergelijkbare resultaten voor vanadiumoxide op silica [4]. Met FTIR spectroscopie toonde hij aan dat de reductie van vanadium op dit dragermateriaal meestal niet verder gaat dan  $\text{V}^{4+}$ . Het is zeer goed mogelijk dat deze tetravalente ionen in de  $\text{Si}^{4+}$  posities van het dragermateriaal worden gestabiliseerd.

We hebben sterke aanwijzingen dat het migratieproces van de  $\text{V}^{3+}$  ionen naar de oppervlakte lagen van het  $\gamma\text{-Al}_2\text{O}_3$  reversibel is en dat de  $(\text{Al-O})_3\text{-V=O}$  eenheden na reoxidatie weer zijn terug gevormd. Deze resultaten worden bevestigd door moleculaire simulaties (krachtveld theorie). Naar onze mening is dit de eerste keer dat de structuur van de gedragen  $\text{V}^{3+}$  fase is gerapporteerd. Dit is vermoedelijk het gevolg van het feit dat wij de verschil techniek hebben gebruikt voor het analyseren van onze EXAFS data. Zonder deze analyse methode zouden we geen oplossing voor het probleem hebben gevonden, omdat de diverse bijdragen in de EXAFS spectra sterk met elkaar in tegenfase zijn.

In hoofdstuk 8 van dit proefschrift beschrijven we de karakterisering van de gedragen V-P-O katalysatoren onder reactieomstandigheden. Hiertoe hebben we *in-situ* Raman spectroscopie en *in-situ* XAFS toegepast. Raman spectroscopie aan  $\text{VPO/TiO}_2$  laat zien dat dit monster uit een monolaag fase bestaat, hetgeen in overeenstemming is met onze ESR en EXAFS resultaten. Ook dit Raman spectrum veranderde niet onder de katalytische condities. Echter, toen alleen butaan en helium over het monster werd geleid was een lichte reductie van de intensiteit van de absorptieband waar te nemen, hetgeen duidt op reductie. Na reoxidatie was een nieuwe reductie veel minder duidelijk. Dit is in overeenstemming zijn met eerdere EXAFS resultaten voor een titania-gedragen V-P-O katalysator en toont aan dat het Mars-Van-Krevelen mechanisme niet operatief is over  $\text{VPO/TiO}_2$  onder de door ons gekozen omstandigheden [1].

Het Raman spectrum van  $\text{VPO/SiO}_2$  toont slechts de aanwezigheid van  $\alpha_1\text{-VOPO}_4$ . Gezien de grotere gevoeligheid van Raman spectroscopie voor dergelijke deeltjes bestaat het vermoeden dat slechts een klein deel van de aangebrachte V-P-O fasen in deze vorm bestaat. Dit zou kunnen verklaren waarom de EXAFS simulaties van  $\text{VPO/SiO}_2$  niet overeenkomen met de structuur van  $\alpha_1\text{-VOPO}_4$ . Onder reactieomstandigheden worden geen nieuwe absorptiebanden gevormd in het Raman spectrum en er verdwijnen ook geen banden. Dit betekent echter alleen dat



## Samenvatting

de  $\alpha_1$ -VOPO<sub>4</sub> fase inert is ten opzichte van de aangelegde condities (butaan/lucht, 653 K). De overige aanwezige V-P-O fasen kunnen wel degelijk veranderen onder deze condities, maar zijn niet waar te nemen omdat ze wegvallen in de achtergrond van het  $\alpha_1$ -VOPO<sub>4</sub> spectrum. In tegenstelling tot Raman spectroscopie analyseert XAFS alle vanadium atomen in de katalysatoren. The EXAFS bijdragen van de hogere schillen namen aanzienlijk af in de spectra die bij 653 K werden verkregen. De structurele parameters, met uitzondering van de Debye-Waller factoren, bleven echter gelijk. Dit is hoogstwaarschijnlijk het gevolg van thermische effecten. Het is opvallend dat de effecten van het toepassen van katalytische condities veel kleiner waren voor VPO/SiO<sub>2</sub> dan voor de eerder beschreven V<sub>2</sub>O<sub>5</sub>/Al<sub>2</sub>O<sub>3</sub> katalysator, hetgeen het gevolg is van de betere dispersie van de vanadium oxide katalysator. De XANES experimenten met VPO/SiO<sub>2</sub> laten zien de verstoorde octaëdrische geometrie van de uitgangstoestand gehandhaafd blijft onder reactieomstandigheden. Echter, kleine veranderingen onder *n*-butaan oxidatie condities met en zonder zuurstof in de voeding geven aanwijzing dat het Mars-Van-Krevelen mechanisme operatief is over VPO/SiO<sub>2</sub> bij 653 K.

Resumerend kunnen we vaststellen dat dit onderzoek heeft geleid tot een verbetering van de katalytische prestaties van gedragen V-P-O katalysatoren, waarbij een maximale opbrengst van 26% werd behaald met een (7.5 wt%) VPO/SiO<sub>2</sub> katalysator. De karakterisering van de gedragen V-P-O katalysatoren bracht grote structuur-verschillen aan het licht tussen VPO/TiO<sub>2</sub> en VPO/SiO<sub>2</sub>. De verschillende structuren vormen een mogelijke verklaring voor het verschil in katalytisch gedrag van VPO/TiO<sub>2</sub> en VPO/SiO<sub>2</sub>. Bovendien hebben we laten zien dat het reactiemechanisme van de selectieve oxidatie van *n*-butaan naar maleïnezuuranhydride verschilt. Voor VPO/SiO<sub>2</sub> en VPO/bulk is het Mars-Van-Krevelen mechanisme van kracht, terwijl de reactie over VPO/TiO<sub>2</sub> waarschijnlijk verloopt via het associatieve mechanisme. Dit vormt ook een mogelijke verklaring voor het verschil in katalytische activiteit en selectiviteit tussen de gedragen V-P-O katalysatoren.

## REFERENTIES

- 1 R.A. Overbeek, *New aspects of the selective oxidation of n-butane to maleic anhydride: The development of a novel catalyst*, proefschrift, Universiteit Utrecht, 1994
- 2 J. van den Berg, *Stoichiometry and catalytic activity of vanadia-based oxides for the oxidation of CO and H<sub>2</sub>*, proefschrift, Universiteit Utrecht, 1984
- 3 A.J. van Dillen, *Catalytic oxidation of carbon monoxide over oxides of indium and vanadium*, proefschrift, Universiteit Utrecht, 1977
- 4 E. Vogt, *Preparation and properties of catalysts supported on modified silica*, proefschrift, Universiteit Utrecht, 1988

## DANKWOORD

---

Met de afronding van dit proefschrift is tegelijk een einde gekomen aan een periode van negen jaar aan de Universiteit Utrecht, waarvan ruim vier op de tweede verdieping van het Wentgebouw. Op deze plaats wil ik iedereen bedanken die er voor heeft gezorgd dat ik met erg veel plezier terug kan kijken op een mooie tijd.

Allereerst mijn ouders, Bruus en Janny. Lieve pa en ma, jullie warme belangstelling en geruststellende woorden in tijden van geestelijke nood zijn voor mij altijd heel belangrijk geweest. Ookal hebben jullie van chemie geen kaas gegeten, ik denk dat niemand een grotere bijdrage heeft geleverd aan de uiteindelijke totstandkoming van dit boekwerk. Ik ben er trots op dat mijn proefschrift in 'onze' drukkerij is gemaakt en heb veel plezier beleefd aan jullie enthousiasme over het prachtige resultaat. Soms vind ik het jammer dat ik de chemie nog leuker vind dan het drukkersvak.

In de zomer van 1993 kwam ik op een fietstocht door Frans-Baskenland een wegwijzer tegen die richting het plaatsje Geus wees. Ik heb die weg genomen en heb er geen spijt van gekregen. John Geus wil ik bedanken voor de mogelijkheid die hij me heeft gegeven om aan dit onderzoek te beginnen en het geheel naar eigen inzicht af te ronden. Diek Koningsberger, als twee kleine kinderen reisden we samen door XAFS-land op zoek naar de echte 'science'. Nooit te beroerd voor wat vaderlijk advies, zelfs met betrekking tot mijn sexleven. Last, but not least in het rijtje (co)promotoren, Jos van Dillen. Beste Jos, onze gemeenschappelijke hobby was vanadiumoxide. Ik heb genoten van je enthousiasme toen een aantal stukjes uit een ruim 20 jaar oude puzzel netjes op zijn plaats terecht kwam.

Ik heb het genoeg gehad met een groot aantal practicumstudenten, keuzevakkers, afstudeerders en scriptieschrijvers te mogen samenwerken. Het is verbazingwekkend hoe weinig van jullie werk in dit boekje terecht is gekomen, maar dat heeft zeker niet aan jullie gelegen!

De ondersteunende diensten hebben een grote rol gespeeld bij het op gang brengen en houden van mijn werk. Dames en heren, bedankt voor al het vakwerk. Ik heb regelmatig het gevoel gehad met twee linkerhanden geboren te zijn.

Dan is het nu even tijd voor een sectie Engels: I would like to thank the people from ABB Lummus Global Inc. Technology Development Center in Bloomfield NJ (USA) for having me over twice. I have enjoyed working with you very much. Furthermore, it was a great opportunity to learn how it is to work in an industrial laboratory. Larry, your pronunciation of Matthijs gave an extra dimension to my name. During my time in Bloomfield I was able to visit the Zettlemoyer center for Surface Studies, which is part of Lehigh University in Bethlehem PA. I would like to thank Professor Israel Wachs and his co-workers for their assistance with the Raman and UV-VIS DRS measurements. It is almost unbelievable that a tiny bit of 60 mg of your  $V_2O_5$ -on- $Al_2O_3$  catalyst was sufficient to produce the largest chapter of this thesis.

Furthermore, I would like to thank the Anschuetz family for their hospitality in Montclair. You definitively own the most beautiful pink house I have ever seen.

## Dankwoord

Een apart woordje voor Ruud Overbeek, die mij het vertrouwen heeft gegeven om zijn eigen kindje te adopteren. Was het in het begin nog drie keer in de week, later nam de frequentie van onze long-distance calls wat af. Jouw grenzeloze enthousiasme en chemische intuïtie hebben je geen windeieren gelegd en al is MEC iets anders dan VPO, je belangstelling was er niet minder om. In het verre Bloomfield bleek je soms beter op de hoogte van het reilen en zeilen op de vakgroep dan ik.

Wat ik de afgelopen vier jaar zeker geleerd heb is dat fysici anders denken dan chemici, hetgeen soms tot verrassende inzichten leidt. Desalniettemin heb ik de samenwerking met de mannen van de sectie Atoom en Grenslaagfysica en de TUE zeer gewaardeerd.

Ik wil alle (ex)collega's en studenten bedanken voor hun bijdrage in de feestvreugde. De gezelligheid voor, tijdens en na 'het werk' hebben me altijd met plezier naar Utrecht doen fietsen. Dat neemt niet weg dat ik met net zo veel plezier ook weer terug fietste naar het mooie Doorn. Regelmatig reed er een clubje mee. Ik hoop dat jullie behalve bloed, zweet en tranen ook nog iets van de Utrechtse Heuvelrug hebben gezien.

Mijn kamergenoten, Jeroen en Roger, wil ik bedanken voor het feit dat ik nooit het gevoel heb gehad dat drie teveel is. Met veel plezier deed ik dagelijks een striptease, maar ik heb nooit de indruk gehad dat het jullie kon bekoren. Behalve het feit dat ik soms kriegel werd van de modem van Roger en de luchtjes van Jeroen heb ik niet te klagen gehad met jullie.

Eén van de weinige mensen waarin ik regelmatig mijn meerdere heb moeten erkennen op de fiets is señor Bok. Toch is ook voor hem de Amerongse berg soms te lang, hèhèhè. Ik hoop in de toekomst nog regelmatig wat kilometers met je te maken, evenals met Franis, maar dan op de skates. Heren, bedankt voor de bereidheid om mijn paranimfen te zijn. Net op het moment dat jullie dachten er met een makkie af te komen was er ook nog zoiets als de correctie van het manuscript. Bedankt voor het kritisch doornemen van de door mij geproduceerde teksten. Het was laat, maar wel gezellig. Nu jullie nog.....

In Doorn is het niet alleen mooi wonen, het is er ook goed korfballen. Ondanks alle drukte in de laatste maanden maakte ik met plezier tijd vrij om te spelen in het gezelligste team van KC Doorn, het 4<sup>e</sup>. Ook het trainen en coachen van mijn kiddo's gaf een extra dimensie aan het leven. Jullie wisten regelmatig het bloed onder mijn toch al korte nagels vandaan te halen, maar dat mocht de pret niet drukken. Dit seizoen hebben we toch maar mooi de dubbel gepakt, stelletje kanjers!

Dat het met elf mensen in de ploeg toch niet altijd meevalt om een compleet volleybalteam op de been te krijgen is een ervaring die ik dank aan de dames en heren van 'gereserveerd voor Jacqueline'. Vooralsnog zijn we het Volendam van de D-poule, maar het niveau is stijgende en gezelligheid is veel belangrijker.

Helaas bleken mijn wensen voor de uitvoering van dit proefschrift de grafische techniek soms te boven te gaan. Desalniettemin ben ik best tevreden met het resultaat. Ik ben grote dank verschuldigd aan drukkerij Print 81, de Océ helpdesk, Deutschmann & Roelants papier, drukkerij van Rossum, André van Zwieten, Lex van den Berg en de mannen van Kreon, Brijlant uit Soest, Reprofa en binderij Afco.

## *Dankwoord*

Ik zie dat we al weer bij pagina drie van dit dankwoord zijn aangekomen en ik vrees dat ik nog niet helemaal klaar ben. Een paar mensen wil ik namelijk nog wel even noemen.

Arjan, de andere blonde adonis. Dat we altijd afspreken in 'de vriendschap' zegt genoeg. Een grotere puinhoop dan op jouw kamer heb ik elders nog niet gezien. Misschien wordt het tijd om het studentenhuis eens te gaan verlaten.

Judith, bij jou ga ik zo vaak eten dat ik inmiddels de meeste toetjes al een keer heb meegebracht. Gelukkig weet je mij nog wel altijd te verrassen met het bekende pakket. Zolang er geen tomaten inzitten gaat alles goed.

Roland, van de klok en het vasthouden van de klepel kunnen we alles op het internet lezen, maar ik schaar je toch onder de categorie vrienden. Behalve goede adviezen probeer je me ook altijd die roestbak van je te verkopen. Ik vrees dat dat net zo veel kans heeft als mijn pogingen om je een keer als toeschouwer bij de zaalkorfbalfinale te begroeten. Ik ben benieuwd naar je volgende smoes.

Simone en Victor gaan zo vaak op vakantie dat ik het halve seizoen gratis bij FC Utrecht kan zitten op hun seizoenskaart. Soms gaan we ook samen en ik verbaas me elke keer weer over de enorme metamorfose die jullie ondergaan in vak G in nieuw Galgenwaard. Dat broerlief Coen vroeger misdienaar is geweest is me nog steeds een raadsel. Van Kung-Fu Henry tot &\*\$#@! van Eijkeren, ik vermaak me altijd met de door jullie verzonden bijnamen. Ik ben benieuwd wat de mijne is.

Jacqueline, dat het raar kan lopen in het leven hoef ik jou niet te vertellen. Ik weet niet wat er allemaal gaat gebeuren in de komende acht jaar, maar ik hou je aan onze afspraak. Bedankt voor je gezelligheid. Ik hoop dat we nog lang op deze voet verder kunnen gaan.

Zo, het zit er op. Op naar het volgende feest.....

Matthijs

## CURRICULUM VITAE

---

De auteur van dit proefschrift werd geboren op 2 februari 1972 te Doorn. In 1990 werd het eindexamen gymnasium  $\beta$  met goed gevolg afgelegd aan de toenmalige RSG Schoonoord te Zeist. In dat zelfde jaar werd begonnen met de studie scheikunde aan de Universiteit Utrecht.

In januari 1992 werd het propaedeutisch examen afgelegd, waarna op 23 januari 1995 het doctoraalexamen werd behaald. Tijdens de studie werd een groot bijvak gevolgd bij de vakgroep Anorganische Chemie en Katalyse onder verantwoordelijkheid van Prof. Dr. Ir. J.W. Geus. Het afstuderen vond plaats bij de vakgroep Fysische Organische Chemie bij Prof. Dr. L.W. Jenneskens.

Op 1 februari 1995 trad hij in dienst bij de vakgroep Anorganische Chemie en Katalyse, waar onder begeleiding van Prof. Dr. Ir. J.W. Geus, Prof. Dr. Ir. D.C. Koningsberger en Dr. A.J. van Dillen het in dit proefschrift beschreven onderzoek werd uitgevoerd.

Met financiële ondersteuning van de Universiteit Utrecht, ABB Lummus Global Inc. (Technology Development Center), NWO (SIR beurzenprogramma) en de NAVO (NATO scientific division) is het mogelijk geweest een aantal congressen en symposia te bezoeken. Mede hierdoor zijn delen van het in dit proefschrift beschreven werk gepresenteerd op the ENRAF NONIUS powder diffraction workshop (Delft, 1996), de SON bijeenkomsten van de werkgemeenschap katalyse (Lunteren, 1996, 1997, 1998 en 1999), KNCV katalyse symposia (1996, 1997 en 1998), the NATO Advanced Science Institute: *Catalytic Activation and Functionalisation of Light Alkanes* (Villamoura, Portugal, 1997), the Spring symposium of the Catalysis Society of Metropolitan New York (Bethlehem, USA, 1996 en 1998), the VII<sup>th</sup> International Symposium: *Scientific Bases for the Preparation of Catalysts* (Louvain-La-Neuve, België, 1998) en the 16<sup>th</sup> meeting of the North American Catalysis Society (Boston, USA, 1999).

## LIST OF PUBLICATIONS

---

- Chapter 3 *Evidence for a new type of vanadyl pairs in (VO)<sub>2</sub>P<sub>2</sub>O<sub>7</sub>, an ESR and magnetisation study*, M. Ruitenbeek, A. Barbon, E.E. van Faassen and J.W. Geus, *Catalysis Letters* **54** (1998), 101
- Chapter 4 *Determination of the surface composition of V-P-O catalysts; an XPS and LEIS study*, M. Ruitenbeek, W.P.A. Jansen, A. Dernier van der Gon, H.H. Brongersma and J.W. Geus, manuscript in preparation
- Chapter 5 *Effects of Silica and Titania Supports on the catalytic Performance of Vanadium-Phosphorus-Oxide Catalysts*, M. Ruitenbeek, A.J. van Dillen, D.C. Koningsberger and J.W. Geus, *Studies in Surface Science and Catalysis* **118** (1998), 549
- The selective oxidation of n-butane to maleic anhydride; comparison of bulk and supported V-P-O catalysts*, M. Ruitenbeek, A.J. van Dillen, A. Barbon, E.E. van Faassen, D.C. Koningsberger and J.W. Geus, *Catalysis Letters* **55** (1998), 133
- Chapter 6 *The selective oxidation of n-butane to maleic anhydride; development of silica- and titania-supported V-P-O catalysts*, M. Ruitenbeek, R.A. Overbeek, D.C. Koningsberger and J.W. Geus, in: E.G. Derouane *et al.* (eds.), *Catalytic Activation and Functionalisation of Light Alkanes*, Kluwer Academic Publishers, Dordrecht, 1998, 423
- Chapter 7 *The structure of V<sub>2</sub>O<sub>5</sub> on  $\gamma$ -Al<sub>2</sub>O<sub>3</sub> before, during, and after CO oxidation; an in-situ X-ray absorption spectroscopy study*, M. Ruitenbeek, A.J. van Dillen, J.W. Geus, I.E. Wachs and D.C. Koningsberger, accepted in *Topics in Catalysis*
- The structure of supported vanadium oxide*, M. Ruitenbeek, A.J. van Dillen, J.W. Geus, F.M. de Groot and D.C. Koningsberger, manuscript in preparation
- Chapter 8 *The mechanism of n-butane oxidation; characterisation of titania-supported V-P-O catalysts by pulse flow experiments and in-situ XANES spectroscopy*, M. Ruitenbeek, R.A. Overbeek, A.J. van Dillen, D.C. Koningsberger and J.W. Geus, *Recl. Trav. Chim. des Pays-Bas* **115** (1996), 519
- The mechanism of n-butane oxidation over supported V-P-O catalysts*, M. Ruitenbeek, A.J. van Dillen, J.W. Geus and D.C. Koningsberger, manuscript in preparation